

**OIL-FILLED LIPID NANOPARTICLES CONTAINING DOCETAXEL
CONJUGATES FOR CONTROLLED DRUG RELEASE**

Lan Feng

A dissertation submitted to the faculty of the University of North Carolina at Chapel Hill in partial fulfillment of the requirements for the degree of Doctor of Philosophy in the Division of Molecular Pharmaceutics in the Eshelman School of Pharmacy.

Chapel Hill
2012

Approved by

Russell J. Mumper, Ph.D.

Michael Jay, Ph.D.

Philip C. Smith, Ph.D.

Rudolph Juliano, Ph.D.

Young Whang, M.D., Ph.D.

© 2012
Lan Feng
ALL RIGHTS RESERVED

Abstract

LAN FENG: Oil-filled Lipid Nanoparticles Containing Docetaxel Conjugates for
Controlled Drug Release
(Under the direction of Russell J. Mumper, Ph.D.)

It has always been challenging to deliver anticancer agents effectively, safely and selectively to solid tumors. Taxotere, as the only marketed dosage form of docetaxel (DX), has various drawbacks. The overall objective of this dissertation was to develop oil-filled nanoparticles (NPs) as novel alternative formulation to deliver DX.

Novel oil-filled NPs were developed by sequential simplex optimization. Miglyol 808 was selected as the oil phase due to its high solvation ability for DX. Despite the desirable formulation properties, DX was found to be very quickly released in mouse plasma in-vitro.

To overcome the poor retention of DX in the NPs, three DX lipid conjugates: 2'-lauroyl-docetaxel (C12-DX), 2'-stearoyl-docetaxel (C18-DX) and 2'-behenoyl-docetaxel (C22-DX) were synthesized. The three conjugates showed 10-fold higher solubility in Miglyol 808 than DX. Consequently, the conjugates were entrapped in NPs prepared with reduced surfactant and showed 50-60% entrapment efficiencies. All three conjugates had good retention in mouse plasma. In-vivo, NP-formulated DX conjugates showed 8-450-fold higher $AUC_{0-\infty}$ values than that of Taxotere. More importantly, C12-DX and C18-DX improved DX $AUC_{0-\infty}$ over that of

Taxotere. In addition, these conjugates were significantly less toxic than DX in-vitro.

To further improve the hydrolysis kinetics, a bromoacyl DX-lipid conjugate 2'-(2-bromohexadecanoyl)-docetaxel (2-Br-C16-DX) was synthesized. The conjugate exhibited similar entrapment efficiency and in-vitro release profile in mouse plasma with the other three conjugates without bromine. The NP-formulated 2-Br-C16-DX was slowly hydrolyzed to DX to an extent of 45% in 48 hr by esterases in-vitro. The superior hydrolysis kinetics led to improved cytotoxicity in-vitro with 2-Br-C16-DX NPs. In-vivo, the $AUC_{0-\infty}$ value of NP-formulated 2-Br-C16-DX was about 100-fold higher than Taxotere in mice. Furthermore, 2-Br-C16-DX NP improved DX AUC by 4.3-fold compared to Taxotere. The 2-Br-C16-DX NPs extensively accumulated in solid tumors compared to Taxotere. The 2-Br-C16-DX NPs were well tolerated in mice. In mice bearing metastatic 4T1 tumor, 2-Br-C16-DX NPs showed marked anticancer efficacy as well as survival benefit over all controls. The results of these studies support that the oil-filled NPs containing hydrolyzable lipophilic DX prodrug 2-Br-C16-DX improved the therapeutic index of DX and were efficacious in the treatment of breast cancer in animal models.

To my loving husband Xiaohu Xie and dearest daughter Nora Xie

Acknowledgements

This work could not have been possible without the support of so many people. I would first like to thank my advisor, Dr. Russell Mumper, for his continuous guidance, encouragement and patience in leading me through the completion of this research project and the long journey of my Ph.D. studies. I would like to thank him for giving me the opportunity to explore the fascinating nano-world and having faith in me. Dr. Mumper gave me guidance when I met problems in my research and stimulated my scientific thinking. He also provided invaluable advice about my presentation, writing and communication skills, and always cheered me up when I felt frustrated. I have learned so much and benefited from Dr. Mumper's enthusiasm, optimistic spirit, dedication and extremely organized working style. He has shaped me to be the scientist that I am today. It has been truly a pleasure working with Dr. Mumper, and I could not have asked for a better advisor. I would also like to thank the members of my research committee: Dr. Michael Jay, Dr. Rudy Juliano, Dr. Phil Smith and Dr. Young Whang. Their constructive criticism and invaluable comments have been greatly appreciated. In addition, their guidance helped me make progress and finish the research project in a timely manner.

I would like to thank all current and previous members of Mumper lab as well as Jay lab members, with special thanks to Ping Ma, Lei Peng, Dr. Xiaowei Dong, Dr.

Rahima Benhabbour, and Dr. Xiuling Lu. I sincerely value their helpful discussions and comments, generous support and friendship. It has been a pleasure working with and learning from each of them. I would like to thank those people who provided very important technical support: Mianmian Sun, DLAM staff Charlene Santos, Mark Ross, and Alain Valdivia. Without their help, life would have been much more difficult. I would like to thank Mianmian not only as an analytical specialist, but also as a friend, accompanying me with support and patience through all the struggles with research.

I would like to thank all MOPH faculty for their sharp and helpful discussions and insights in my research. I would like to extend my thanks to all current and previous staff for their diligent work to make all the orders, events, and activities go smoothly. Importantly, I would also like to thank the IT staff in the School of Pharmacy for their technical support. Sincere thanks are extended to many friends I met in the school: Xin Ming, Bo He, Rong Zhao, and Mike Hackett. I have benefited from each of them in so many respects, from coursework to bench work, from research to everyday life.

I am eternally grateful to my family: my husband Xiaohu Xie, my daughter Nora Xie, and my parents. Words cannot express how much I am thankful to my husband for his unconditional love and patience. He not only gave me generous support at home day and night in his already busy schedule, but he also gave me scientific help and opinions. Thank also to my dearest daughter, for being such a good kid and bringing me so much fun and comfort during the past three years. I would also thank my parents for their love, trust, encouragement and unconditional support during this long journey.

Table of Contents

List of Tables.....	xiii
List of Figures	xiv
Chapter 1. Lipid-based nanoparticles for taxane delivery: A review.....	1
1. Overview.....	1
1.1. Introduction of taxanes.....	1
1.2. Currently available formulations in the market.....	4
1.3. Concerns for taxane delivery and clinical difficulties and issues	9
1.4. Criteria for ideal taxane delivery system.....	11
1.5. Nano-formulation and tumor delivery overview.....	13
2. Types of lipid-based nanoparticles to deliver taxanes	19
2.1. Liposomes	19
2.2. Micelles	22
2.3. Nano-emulsions (Emulsions, Micro-emulsions).....	25
2.4. Solid lipid nanoparticles.....	32
2.5. Nanocapsules.....	40
2.6. Core/shell nanoparticles	45
2.7. Prodrug strategy for better lipid nanoparticle encapsulation	46

3. Active targeting of taxane lipid-based nanoparticle	51
4. Advantages and disadvantages of lipid-based nanoparticles compared to other nano-delivery systems	58
5. Future perspective.....	61
6. Research hypotheses	64
References	77
Chapter 2. Development of BTM nanoparticles to deliver docetaxel	94
1. Summary.....	94
2. Introduction.....	95
3. Materials and Methods.....	97
3.1. Materials and cell culture	97
3.2. Methods.....	98
4. Results	106
4.1. Oil lipid screening for DX nanoparticle.....	106
4.2. Sequential simplex optimization of DX BTM NPs.....	107
4.3. Characterization of DX BTM NPs	107
4.4. In-vitro cytotoxicity.....	108
4.5. In-vitro release.....	109
4.6. Re-characterization of DX BTM NPs	109
5. Discussion.....	110
References	127
Chapter 3. Development of lipid nanoparticles containing docetaxel fatty acid conjugates to control the drug release rate in-vitro and in-vivo.....	129

1. Summary.....	129
2. Introduction.....	130
3. Materials and methods	133
3.1. Materials and Animals.....	133
3.2. Methods.....	134
4. Results.....	144
4.1. Synthesis and characterization of DX conjugates	144
4.2. Solubility of DX conjugates in Miglyol 808 and mouse plasma	144
4.3. Optimization of DX conjugate containing NPs by orthogonal design	145
4.4. In-vitro release of DX conjugates from NPs in mouse plasma.....	147
4.5. In-vitro esterase digestion	148
4.6. Esterase activity in plasma samples	149
4.7. In-vitro cytotoxicity.....	149
4.8. In-vivo pharmacokinetics.....	150
5. Discussion.....	151
References.....	172
Chapter 4. Oil-filled lipid nanoparticles containing 2'-(2-bromohexadecanoyl)-docetaxel for the treatment of breast cancer.....	
1. Summary.....	174
2. Introduction.....	175
3. Materials and methods	177

3.1. Materials and Animals.....	177
3.2. Methods.....	178
4. Results.....	188
4.1. Synthesis and characterization of 2-Br-C16-DX.....	188
4.2. Preparation and characterization of 2-Br-C16-DX BTM NPs	189
4.3. In-vitro drug release in mouse plasma	189
4.4. 2-Br-C16-DX digestion.....	190
4.5. In-vitro cytotoxicity.....	191
4.6. In-vivo pharmacokinetics and biodistribution of 2-Br-C16-DX NPs.....	191
4.7. MTD of 2-Br-C16-DX NPs.....	193
4.8. In-vivo antitumor efficacy.....	194
5. Discussion.....	196
References.....	221
Chapter 5. Summary and future directions	223
1. Summary.....	223
2. Future directions	228
References.....	234
Appendix. SiRNA targeting using injectable nano-based delivery systems.....	235
Summary	235
I. Overview	236
1.1. RNAi Mechanisms and siRNA	236
1.2. Therapeutic Target and Applications.....	237

1.3. Delivery Barriers and Challenges	239
1.4. Available Delivery Approaches.....	240
1.5. Differences between siRNA and pDNA Delivery	242
II. Ideal injectable nano-based systems for siRNA delivery.....	245
III. Nano-based delivery systems.....	246
3.1. Complexes.....	246
3.2. Nanoparticles	263
3.3. Nanocapsules	269
3.4. Dendrimers	272
3.5. Other novel carriers	274
IV. Future Perspective.....	276
References	290

List of Tables

Table 1.1.	Similarities and differences between paclitaxel and docetaxel	65
Table 1.2.	Similarities and differences between nano-emulsions and micro-emulsions	66
Table 1.3.	Major advantages and disadvantages of each type of lipid-based nanoparticles.....	67
Table 1.4.	Advantages and disadvantages of lipid-based nanoparticles compared to other nano-based delivery systems	68
Table 2.1.	Physico-chemical properties of Miglyols.....	115
Table 2.2.	Optimization of BTM 808 NPs by Sequential Simplex	116
Table 2.3.	Characterization of DX BTM 808 NPs	117
Table 2.4.	Recovery of DX from plasma from SPE or SEC plus SPE.....	118
Table 3.1.	Solubility of DX and DX conjugates in Miglyol 808 and entrapment efficiency in BTM NPs (N=3)	160
Table 3.2.	Orthogonal design and responses	161
Table 3.3.	Compositions and properties of BTM 808 NPs	162
Table 3.4.	A. Pharmacokinetic parameters of DX conjugates and Taxotere in mice after i.v. bolus administration	163
	B. Pharmacokinetic parameters of DX after i.v. bolus administration of DX conjugates and Taxotere in mice	163
Table 4.1.	Compositions and properties of 2-Br-C16-DX NPs.....	204
Table 4.2.	Pharmacokinetic parameters of 2-Br-C16-DX and DX in mice after i.v. bolus administration of 2-Br-C16-DX NP and Taxotere.....	205
Table 4.3.	Tumor accumulation of 2-Br-C16-DX and DX in mice after i.v. bolus administration of 2-Br-C16-DX NP and Taxotere	206

List of Figures

Figure 1.1.	Structures of (A) paclitaxel and (B) docetaxel	69
Figure 1.2.	Criteria for the ideal taxane delivery system	70
Figure 1.3.	Multi-functional nanoparticles	71
Figure 1.4.	Schematic structures of sterically stabilized micelle (SSM), sterically stabilized mixed micelle (SSMM) and SSMM loaded hydrophobic drug molecules.....	72
Figure 1.5.	Plasma decay curve of [³ H]-paclitaxel-oleate in LDL-resembling nano-emulsion	73
Figure 1.6.	In-vitro temporal release of paclitaxel (PTX) and combretastatin A4 (CA4) from core/shell nanocapsules	74
Figure 1.7.	Plasma concentration-time curves for Taxotere (triangle), docetaxel derivative formulated in Taxotere vehicle (square), and docetaxel derivative formulated in DSPC/Chol liposome.....	75
Figure 1.8.	Antitumor efficacy of targeted SLN (tSLN), non-targeted SLN (nSLN), Taxotere or saline on nude mice bearing hepatoma	76
Figure 2.1.	Morphology of (A) DX BTM 808 NPs and (B) TEM images of DX BTM 808 NPs.	119
Figure 2.2.	Physical stability of DX BTM 808 NPs in 10% lactose stored at 4°C	120
Figure 2.3.	In-vitro cytotoxicity of free DX, DX BTM NPs and blank BTM NPs in (A) DU-145 and PC-3 cells, and (B) DU-145-R and PC-3-R cells.....	121
Figure 2.4.	The expression of P-gp in DU-145 and PC-3 cell lines and their corresponding PX-resistant DU-145-R and PC-3-R cell lines.	122
Figure 2.5.	The separation of NPs with mouse plasma proteins in	

	Sepharose CL-4B column	123
Figure 2.6.	The “release” of DX from BTM 808 NPs in mouse plasma at 37°C.....	124
Figure 2.7.	(A) The entrapment of DX in BTM 808 NPs determined by SEC as compared to (B) free DX dissolved in 10% lactose.	125
Figure 2.8.	The particle size of each fraction from Sepharose CL-4B column after blank BTM NPs were eluted using PBS.	126
Figure 3.1.	Synthesis of 2'-docetaxel conjugates.	164
Figure 3.2.	Solubility of DX conjugates in mouse plasma.	165
Figure 3.3.	3D surface plot for the modeling of the effect of Brij 78 and TPGS concentrations on % drug entrapment.	166
Figure 3.4.	Release of DX conjugates from BTM NPs in mouse plasma at 37°C.	167
Figure 3.5.	The digestion of free DX conjugates and DX conjugate NPs in fresh mouse plasma. (A) The loss of DX conjugates. (B) The formation of DX.....	168
Figure 3.6.	Non-specific esterase activity in fresh mouse plasma, commercial mouse plasma and human plasma samples.	169
Figure 3.7.	In-vitro cytotoxicity of free DX and DX conjugates and their NPs in DU-145 cells.....	170
Figure 3.8.	Plasma concentration-time curves for (A) DX, C12-DX, C18-DX and C22-DX after administration of Taxotere, C12-DX NPs, C18-DX NPs and C22-NPs, and (B) DX as an active metabolite from C12-DX NPs and C18-DX NPs	171
Figure 4.1.	Synthesis of 2'-(2-bromohexadecanoyl)-docetaxel conjugate	207
Figure 4.2.	Physicochemical stability of 2-Br-C16-DX NPs stored at 4°C.	208
Figure 4.3.	Release of 2-Br-C16-DX from BTM NPs in 100% mouse plasma at 37°C.....	209
Figure 4.4.	The digestion of 2-Br-C16-DX in fresh 100% mouse plasma	

	at 37°C.	210
Figure 4.5.	The digestion of 2-Br-C16-DX in 4T1 tumor homogenate at 37°C.	211
Figure 4.6.	In-vitro cytotoxicity of free 2-Br-C16-DX and 2-Br-C16-DX NPs in (A) human prostate cancer cell DU-145 cells and (B) murine breast cancer cell 4T1 cells.	212
Figure 4.7.	Plasma concentration-time curves for (A) DX and 2-Br-C16-DX after administration of Taxotere and 2-Br-C16-DX NPs, and (B) DX as an active metabolite from 2-Br-C16-DX NPs	213
Figure 4.8.	Biodistribution of (A) 2-Br-C16-DX and (B) DX in heart, liver, spleen, lung, kidney and tumor	214
Figure 4.9.	Tumor accumulation of (A) 2-Br-C16-DX from NPs and DX from Taxotere, and (B) DX as an active metabolite from 2-Br-C16-DX NPs	215
Figure 4.10.	Body weight of mice after (A) single i.v. administration of 2-Br-C16-DX NPs, and (B) Q7d × 3 i.v. administration of 2-Br-C16-DX NPs with different doses.	216
Figure 4.11.	The first antitumor efficacy study.	217
Figure 4.12.	The second antitumor efficacy study.	218
Figure 4.13.	The third antitumor efficacy study.	219
Figure 4.14.	Kaplan-Meier survival curves of 4T1 xenografted female BALB/c mice.	220
Figure A.1.	Mechanism of RNA interference	279
Figure A.2.	Challenges for siRNA delivery.	280
Figure A.3.	Structures of (a) CCLA, (b) CDAN, (c) RPR209120, and (d) MVL5	281
Figure A.4.	Dissociation of nucleic acids from ketalized PEI upon hydrolysis.	282

Figure A.5.	Self-assembling of cationic micellar nanoparticles and loading of siRNA	283
Figure A.6.	Schematic structure of H3K8b polymer	284
Figure A.7.	Structure of THCO.....	285
Figure A.8.	Cone-shaped structure of macrocyclic octaamine	286
Figure A.9.	Preparation of PEGylated LPD	287
Figure A.10.	Adsorption of siRNA onto surface-modified QDs	288
Figure A.11.	Schematic structure of engineering pRNA nanoparticle containing siRNA, aptamer and fluorescent label.....	289

Chapter 1.

Lipid-based nanoparticles for taxane delivery: A review

1. Overview

1.1. Introduction of taxanes

In the 1960s, the first taxoid was discovered by the National Cancer Institute.¹ During the massive screening of the antitumor activity of natural products, it was found that the extract from bark of the Pacific yew tree had activity against several murine tumors. Paclitaxel was later identified as the active ingredient of the extract. The early development and application of paclitaxel was limited by the scarcity of the active ingredient in the bark of the tree. Until 1986, docetaxel was semi-synthetically produced from a precursor isolated from European yew tree, 10-deacetylbaccatin III.² At a later time, paclitaxel was also semi-synthetically derived from the precursor.³ The precursor is extracted from the regenerable needles of the plant so that a continuous source of precursor is available for paclitaxel and docetaxel synthesis.

The taxane family includes paclitaxel, docetaxel and analogues with the taxane skeleton. Docetaxel has two structural modifications compared to paclitaxel (Figure 1.1). On the 10-position of baccatin ring, docetaxel has a hydroxyl group instead of an

acetyl group in paclitaxel and in the 3' position of the lateral chain, docetaxel has a $-\text{OC}(\text{CH}_3)_3$ moiety instead of a benzamide phenyl group in paclitaxel. The high lipophilicity and the high lattice energy of paclitaxel and docetaxel which reflect their bulky and fused ring structure with several lipophilic substituents, result in very limited aqueous solubility. The water solubility of paclitaxel has been reported as 0.35-0.7 $\mu\text{g/mL}$.^{4,5} Although both being water-insoluble, the structural differences make docetaxel about 10-fold more soluble in water (3-25 $\mu\text{g/mL}$) than paclitaxel.⁶⁻⁸

In 1979, Schiff et al. discovered the unique pharmacological mechanism of taxanes.⁹ Taxanes inhibit cell growth by binding to microtubules, stabilizing them, and preventing their depolymerization.^{10,11} Since the binding affinity of docetaxel to microtubule is 1.9-fold higher than that of paclitaxel, docetaxel is approximately twice as potent as paclitaxel.^{10,12,13} The in-vitro and in-vivo activities of paclitaxel and docetaxel have been studied and compared in many murine tumor models and human tumor xenografts. Docetaxel was found to be 1.3- to 12-fold more potent than paclitaxel after 96 hr exposure in several murine (P388, SVras) and human tumor cell lines (Calcl8, HCT116, T24, N417, and KB).¹⁴ In another in-vitro study, 2.5-times higher potency of docetaxel over paclitaxel was demonstrated in two murine cell lines J774.2 and P388.¹⁰ In a number of freshly explanted human tumor cells, more than two thirds of the specimens tested, including breast, lung, ovarian, and colorectal cancers and melanomas, were more responsive to docetaxel than to paclitaxel.^{15,16} In six human ovarian-carcinoma cell lines, docetaxel showed an average 4-fold higher potency than

paclitaxel after continuous exposure or after a 2-hour exposure.¹⁷ The superior anticancer potency of docetaxel has been demonstrated in-vivo as well. In a B16 melanoma xenograft model, docetaxel showed 2.7-fold higher potency over paclitaxel.¹⁸

The higher in-vitro and in-vivo anticancer potency of docetaxel may not only be attributed to its higher affinity for microtubules, but also to its superior cellular accumulation. In support of this, an in-vitro study of the uptake and efflux of radiolabeled docetaxel and paclitaxel on P388 leukemia cells demonstrated that intracellular accumulation of docetaxel was 3-fold higher than that of paclitaxel with the same initial extracellular concentration.¹⁹ Conversely, the efflux rate of docetaxel from P388 cells was 3-fold lower than that of paclitaxel.

As analogues in taxane family, paclitaxel and docetaxel share many common properties. They have similar structure and the same antitumor mechanism. Nevertheless, paclitaxel and docetaxel are not simply two of a kind. Their main similarities and differences are summarized in Table 1. Paclitaxel was investigated and delivered for at least a decade prior to docetaxel. Given the earlier introduction and thus larger body of clinical experience, the majority of research in the literature has focused on the formulation and development of paclitaxel. Since the formulation vehicle Cremophor EL (CrEL) used to solubilize paclitaxel presents more pharmacokinetic and pharmacodynamic drawbacks than polysorbate 80 used in the present docetaxel dosage form, an improvement is more likely warranted for paclitaxel. However, considering

the higher antitumor potency, favorable properties for formulation (e.g., higher water solubility) and the cheaper production cost, docetaxel deserves similar attention for development of improved delivery systems. Given the similarity between docetaxel and paclitaxel, the knowledge and experience accumulated from designing paclitaxel delivery systems may facilitate and inspire rationale designs of docetaxel delivery systems. Hence, although the focus of this dissertation is docetaxel formulation and drug delivery, both paclitaxel and docetaxel will be discussed in the present review.

1.2. Currently available formulations in the market

Taxol[®], the first injectable dosage form of paclitaxel is supplied in 50% CrEL (polyoxyethylated castor oil) and 50% dehydrated ethanol.²⁰ In the clinic, it is administered intravenously over a period of 3-24 hr after dilution to a concentration of 1 mg/mL. The most commonly prescribed dosage regimen is 135 mg/m² or 175 mg/m² every 3 weeks. Following intravenous (i.v.) administration of Taxol, paclitaxel is rapidly eliminated from circulation in a biphasic manner. The average distribution half-life of paclitaxel after the administration of Taxol is 0.34 hr and the average elimination half-life is 5.8 hr.^{21,22} The initial rapid decline in blood represents distribution to the peripheral compartment and elimination of the drug. The later phase represents the slow efflux of paclitaxel from the peripheral compartment and elimination. The elimination of paclitaxel is mainly facilitated by CYP-mediated

hepatic metabolism (CYP2C8 and 3A4) and biliary excretion.²³ Paclitaxel is highly bound to plasma protein (89-98%) and the steady-state volume of distribution is large.

The pharmacokinetics of Taxol is nonlinear. It has been concluded that the nonlinear disposition of paclitaxel is due to the formulation vehicle CrEL. Two mechanisms have been proposed to explain the nonlinear pharmacokinetics of Taxol: 1) alteration of hepatic transport function by delivery vehicle,²⁴ and 2) change of erythrocyte accumulation.^{25,26} The large quantity of CrEL in the formulation especially at high dose likely changes hepatic transporter activity, which in turn profoundly influences hepatic uptake and biliary excretion rates of paclitaxel or other co-administered compounds. Another more widely accepted mechanism is that paclitaxel is highly entrapped in CrEL micelles and the free drug fraction available for cellular partitioning is reduced, leading to alteration of paclitaxel accumulation in erythrocytes and thereby dose-dependent disposition. The nonlinear pharmacokinetics of Taxol may raise additional complexities when combination chemotherapy regimens are applied.

The CrEL-related issue is not limited to pharmacokinetics of Taxol. CrEL-related side effects have been reported in clinical practice. It is generally believed that the hypersensitivity reactions associated with Taxol are largely attributed to the CrEL vehicle.²⁷ To minimize the risk of hypersensitivity reactions, patients should be pretreated with a standard regimen containing corticosteroid (e.g., dexamethasone), H1 and H2 blockers, prior to any paclitaxel infusion. However, minor hypersensitivity

reactions still occur in 40% of all patients even with these pretreatments.²⁸ In addition, neurotoxic events such as ganglionopathy, axonopathy and demyelination are also attributable to the CrEL vehicle.²⁹

The only clinically approved alternative to Taxol is Abraxane[®]. This formulation consists of lyophilized cakes of paclitaxel nanoparticles, containing 100 mg of paclitaxel and about 900 mg of human albumin in each 50 mL vial.³⁰ Abraxane is formulated utilizing 130-nanometer albumin-bound technology (nab[™]).³¹ This novel formulation is prepared by high-pressure homogenization of paclitaxel in the presence of human albumin, resulting in a nanoparticle colloidal suspension with a mean particle diameter of 130-150 nm.³² Albumin plays a critical role in binding and delivering many types of hydrophobic molecules including endogenous vitamins, hormones and exogenous drugs. Paclitaxel is hydrophobic and binds to albumin with high affinity. Through binding to a 60 kDa glycoprotein (i.e. gp60, albobin) receptor, albumin initiates transcytosis of albumin-bound cargo across the endothelial cell into the interstitial space.³³ Recent evidence suggests that SPARC (secreted protein, acidic and rich in cysteine), which is overexpressed in about 50-60% of breast cancer may play a role in concentrating albumin in areas of tumor, which, in turn may result in preferential intratumoral accumulation of albumin-bound paclitaxel.³⁴⁻³⁶ Clinical studies have demonstrated that the albumin-bound form of paclitaxel (i.e. nab-paclitaxel) has many clinical advantages over traditional Taxol. First of all, nab-paclitaxel is CrEL-free, so that nab-paclitaxel has markedly reduced the risk of inducing hypersensitivity reactions,

thus premedication is not required. Secondly, due to higher achievable formulation concentration with the nab-paclitaxel formulation, the drug can be administered over a shorter period of time (30 min) without special intravenous tubing needed. The nab-paclitaxel formulation either given weekly or every 3 weeks can achieve >50% higher dose than the typical dose used with CrEL-based paclitaxel formulation. Thirdly, in clinical trials, the response to nab-paclitaxel was shown to be greater than that of Taxol. Last but not the least, nab-paclitaxel was better tolerated than CrEL-paclitaxel. The incidence of grade 4 neutropenia is significantly reduced even with a 49% higher paclitaxel dose administered in nab-paclitaxel as compared to CrEL-paclitaxel.³¹ Overall, nab-paclitaxel increases the therapeutic index of paclitaxel resulting in improved efficacy without increasing overall toxicity.

Currently, the only commercially available dosage form of docetaxel is Taxotere[®]. The Taxotere concentrate is composed of 40 mg/mL docetaxel dissolved in polysorbate 80. Taxotere injection concentrate requires two dilutions before administration. It is firstly diluted with 13% ethanol in water to 10 mg/mL followed by secondary dilution to 0.3-0.74 mg/mL in either saline or 5% dextrose solution.³⁷ The polysorbate 80 in the formulation solubilizes docetaxel into water by forming micelles and entrapping docetaxel inside. However, the resulting micellar solution is supersaturated, therefore, the drug ultimately crystallizes over time. For the purpose of physical stability of the product, Taxotere is provided in two vials (one vial contains docetaxel concentrate and another contains 13% ethanol in water as a diluent). It

requires that the infusion is completed no more than four hours after the dosage preparation. In the clinic, Taxotere is usually administered at a dose of 60 to 100 mg/m² every 3 weeks as a one-hour i.v. infusion.

The pharmacokinetic profile of docetaxel in Taxotere in humans is consistent with a three-compartment model, with half-lives of 4 min, 36 min and 11.1 hr for the α , β and γ phases, respectively.³⁷ Following oxidative metabolism by CYP3A4, docetaxel and metabolites are excreted in both urine and feces, with fecal excretion as the main elimination route. In-vitro studies have demonstrated that about 94% of docetaxel is protein bound, mainly to α_1 -acid glycoprotein, albumin and lipoproteins.³⁷ At clinically relevant concentrations, polysorbate 80 significantly increases the fraction of protein-unbound docetaxel due to the high binding affinity of docetaxel to polysorbate 80.³⁸ As a consequence, polysorbate 80 is associated with alteration of docetaxel pharmacokinetics due to the alteration of docetaxel protein binding profile. Moreover, studies have demonstrated that severe drug-induced hematological toxicity was more closely related to unbound docetaxel than total docetaxel exposure.^{39,40} Despite the fact that polysorbate 80 influences docetaxel pharmacokinetics, the area under the curve (AUC) of docetaxel was proportional to its dose up to 115 mg/m², which is different from Taxol.^{41,42} In addition to the drug-induced toxicity, polysorbate 80 itself causes haemolysis and cholestasis.²⁴

In August 2010, Sanofi-aventis announced that the FDA approved a one-vial formulation of Taxotere (1-vial-Taxotere[®]). For the two-vial formulation

(2-vial-Taxotere[®]), the drug concentrate and the diluent (13% ethanol in water) are packed in two separated blisters, and two dilutions are required before administration. The one-vial formulation eliminates the need for initial dilution step with the diluent and is ready to be added directly into the infusion solution. The new one-vial formulation is composed of 20 mg/mL docetaxel in 50/50 (v/v) polysorbate 80/dehydrated ethanol. The new formulation has the same final drug concentration and the same excipients as the two-vial formulation. The only difference is the alcohol concentration. With 50% dehydrated ethanol, the docetaxel concentrate is physically stable with reduced viscosity so that it can be directly withdrawn and added to the infusion solution.⁴³ The one-vial formulation simplifies the manufacture and clinical preparations but does not solve the issues associated with its excipients polysorbate 80 and ethanol.

1.3. Concerns for taxane delivery and clinical difficulties and issues

First of all, paclitaxel and docetaxel administered in their current dosage forms have undesirable pharmacokinetic profiles. The rapid elimination, short half-lives and large volumes of distribution lead to limited drug accumulation in tumor sites with relatively high drug exposure in normal organs. In addition, the CrEL causes nonlinear pharmacokinetic profile of paclitaxel, which complicates the co-administration of other antitumor agents. Furthermore, rapid elimination of the drugs necessitates inconvenient

dosing schedules to realize optimal efficacy.

Secondly, when administered systemically, adverse effects associated with Taxol and Taxotere include neutropenia, hypersensitivity reactions, fluid retention, peripheral neuropathy, myelosuppression, and gastrointestinal toxicity.^{29,41} Among these adverse effects, some of them are inevitable but controllable, such as neutropenia and gastrointestinal toxicity since paclitaxel and docetaxel are potent cytotoxic agents. While other adverse effects, like hypersensitivity reactions, are clearly vehicle-related and require premedication of corticosteroids or antihistamines. The undesirable pharmacokinetic and biodistribution profiles also make some drug-induced toxicity more severe as discussed above.

The therapeutic index and toxicity of any cytotoxic agent are related to the duration of time that targeted tissues are exposed to a biologically relevant concentration of the drug. The unfavorable pharmacokinetic profile along with high toxicity has a profoundly negative impact on the therapeutic index of paclitaxel and docetaxel. Unfortunately, the excipients in Taxol and Taxotere, namely CrEL, polysorbate 80 and ethanol, not only fail to improve these issues but make them more complicated. Moreover, the limited drug loading in these formulations leads to long clinical infusion time.

The novel CrEL-free Abraxane improved the therapeutic index of Taxol. It almost doubles the response rate and increases the time to progression (TTP).³¹ It is much better tolerated than Taxol due to its decreased systemic toxicity. However, since

the complexity of formulation requires recombinant albumin, the cost of Abraxane is comparatively high. Relative to the significantly higher cost, the antitumor efficacy improvement of Abraxane is only marginal. The TTP and patient survival time with nab-paclitaxel are longer than with Taxol but the benefit is only in the scale of weeks.

In addition to the low therapeutic index, acquired multidrug resistance remains another major obstacle for the successful chemotherapy of taxanes in the clinic. Multidrug resistance (MDR) is a complex phenomenon often involving multiple mechanisms. Taxane resistance has been attributed to differential expression of various tubulin isotypes, decreased microtubule bundle formation, decreased expression of *bcl-2*, and overexpression of membrane efflux transporter P-gp.⁴⁴

1.4. Criteria for ideal taxane delivery system

The ultimate goal of an ideal taxane delivery system is to achieve maximal anticancer efficacy while minimizing adverse effects (Figure 1.2). As was discussed above, paclitaxel and docetaxel are quite insoluble in aqueous solutions due to the high lipophilicity and high lattice energy. An ideal formulation in terms of taxane delivery, first of all needs to solubilize taxanes to a high extent. The solubilization capability is directly related to drug loading, which partly determines the clinical infusion time. Shorter infusion period is favorable to both patients and clinical practitioners. Most importantly, taxanes should maintain a stable therapeutically meaningful concentration

in the tumor sites with minimal accumulation in normal tissues. For systemic administration, a high plasma AUC is a prerequisite but may not be sufficient for high tumor accumulation. Considering the short half-life of paclitaxel and docetaxel, the ideal delivery system should protect the taxanes from being rapidly eliminated from the circulation to gain high AUC. To achieve high blood AUC, the formulation needs to maintain two aspects of stability in-vivo: long circulation of the delivery vehicles and long retention of taxanes in the delivery vehicles. For long circulation, the delivery vehicle must escape from renal, hepatic filtration and reticuloendothelial system (RES) uptake. The long retention in the delivery vehicles requires high affinity of the drug for the carrier and slow drug release. Only with high drug concentration and prolonged exposure in the blood, are these drugs readily available for tumor accumulation over time. Furthermore, to ensure better tumor accumulation, the ideal taxane delivery system should also have some passive or active targeting ability for it to be more specifically distributed to the tumors while minimizing the accumulation in normal organs. Additionally, in terms of adverse effects, the excipients in the formulation should have low toxicity. By optimizing the drug release rate, pharmacokinetics and biodistribution, the delivery vehicle is able to shield or reduce the drug-related systemic toxicity. Another important property of the ideal taxane delivery system is that it could overcome MDR, which remains a significant clinical hurdle for taxane-based chemotherapy.

From the manufacturing perspective, the manufacturing process of the

formulation should be simple, cheap, scalable, and reproducible. The final product should be easy to sterilize with high stability.

From a clinical practice standpoint, the formulation should be easy to prepare for administration, ideally requiring only a bolus injection.

For the sake of patients, low cost, shorter infusion time, and a less frequent dosing schedule is desirable in addition to a high therapeutic index.

1.5. Nano-formulation and tumor delivery overview

The application of nano-formulation to deliver anticancer agents is closely related to the distinct physiological and pathological properties of solid tumors. These properties include: abnormal tumor vasculature, increased tumor vasculature permeability, lack of lymphatic drainage, structural changes in interstitial matrix and high interstitial fluid pressure (IFP).^{45,46} These properties create barriers for efficient drug delivery; on the other hand they provide opportunities for nano-based formulation delivery.

To maintain rapid growth, tumor cells need efficient gas exchange, waste removal, and delivery of nutrients. These rely on the recruitment of new blood vessels caused by a process called angiogenesis. The tumor vessels generated from rapid angiogenesis are often disorganized with loops and trifurcations clearly different from those in normal tissues.⁴⁷ The spatial distribution of tumor vasculature is heterogeneous because angiogenesis is more efficient near the tumor periphery as compared to the

center area.⁴⁵ The insufficient blood supply to the central region of tumors makes it difficult to deliver drug to this area. On the other hand, the fact that tumor development highly depends on angiogenesis allows for the opportunity to starve tumor cells by cutting off their blood supply.

The vasculature permeability is generally higher in tumors than in normal tissues due to large inter-endothelial junctions, increased numbers of fenestrations and abnormal basement membranes. The pore size cutoff in most tumors ranges from 200 nm to 1200 nm, whereas a normal continuous endothelium has pore size no greater than 2 nm.⁴⁸⁻⁵¹ The difference in endothelial pore size between normal tissues and tumors provides the opportunity for nano-formulations to selectively extravasate to tumor sites without penetrating to the normal tissues with tight endothelial junctions. However, the leakiness of tumor vasculature is tumor type dependent and location dependent and therefore the drug delivery counting on this structural feature is often unpredictable with high variance. The leakiness of tumor vasculature is partly attributed to a multifunctional cytokine called vascular permeability factor/vascular endothelial growth factor (VPF/VEGF) secreted by tumors.⁴⁵ The overexpression of VEGF receptors in the tumor and lining the tumor vessels also offers a potential target for active delivering.

Studies have shown that lymphatic systems inside solid tumors are dysfunctional.^{52,53} The absence of lymphatic drainage causes prolonged retention of macromolecules once they extravasate the leaky vasculature and locate inside the

tumors. The enhanced permeability and retention (EPR) effect of macromolecules in solid tumors is a widely accepted concept in nano-formulation delivery research though recently it is argued that EPR effect is overestimated or artificial.⁵⁴ However, despite the fact that the enhanced vessel permeability and impaired lymphatics bring potential benefit to nano-formulation delivery, they cause another major hurdle to tumor drug delivery, which is increased IFP. The IFP in normal tissues is around 0 mmHg whereas it is significantly elevated to around 20-45 mmHg in various tumors.^{55,56} Studies have shown that the IFP elevation strongly correlates with tumor size and tumor regions.⁵⁵ The IFP is lower near the tumor periphery but increases significantly along the tumor cross-section toward tumor central region and the larger tumor is associated with higher IFP. The detrimental outward pressure gradient not only hinders the transvascular drug penetration from blood vessel to the interstitial space but also causes great resistance for transport in the interstitial space with particular difficulties in large tumors.

The tumor interstitial matrix is a space rich in collagen fibers and other additional components, such as proteoglycans and glycosaminoglycans.^{57,58} The mesh-like, tortuous structure of extracellular matrix along with its unique contents leads to high transport resistance to optimal drug delivery. The size, charge and surface properties of macromolecules determine their transport in this space. Apparently, a large particle size is not a favorable property to effectively diffuse through the collagen-rich matrix. The electro-interaction of charged particles with the oppositely charged components in the interstitial space resulting in trapping or aggregation causes

another transport hindrance. Particles with flexible configurations likely transport more efficiently than rigid particles of comparable size. Moreover, the compositions and distribution of components are heterogeneous in tumors and between tumor types. Some tumor (area) contains high collagen type I and fibrillar collagen contents while others are with low fiber concentration.⁵⁸⁻⁶⁰ The heterogeneous structure of tumor interstitial matrix also causes heterogeneous drug delivery and variance in different tumor types.

Nano-based delivery systems have attracted a great deal of attention in the past two decades as a strategy to overcome the low therapeutic index of conventional anticancer drugs and delivery barriers in solid tumors. According to the definition of National Nanotechnology Initiative, nanoparticles are particles with sizes from about 1 to 100 nm. A more commonly used definition in drug delivery research for nanoparticle is particles in the submicron range (1 to 1000 nm). The wide application of nanoparticles in anticancer agent delivery is based on their appealing and unique properties.

Firstly, nano-formulations provide the physical and chemical protection for water insoluble and labile drugs. To date, parenteral administration is still the major administration route for highly cytotoxic anticancer agents. Hence, the low solubility of some agents such as taxanes, vinblastine, and topotecan, limits their optimal clinical application. By utilizing proper nano-materials, the poorly water-soluble drugs could be entrapped in nanoparticles and achieve high concentration in injectable aqueous

vehicles.^{61,62} Nano-formulations also offer protection for chemically unstable drugs by reducing their exposure to water or biological environments. Such examples include camptothecin, SN-38, ATRA, peptides, proteins, and nucleotides.⁶³⁻⁶⁵

Secondly, nano-formulations can improve the pharmacokinetics of anticancer agents. As discussed previously, the improvement of pharmacokinetics relies on the long circulation of delivery vehicles and long retention of anticancer agent in the delivery vehicles. The importance of long circulation of nanoparticles has been widely recognized and extensively demonstrated for decades. It has been demonstrated that nanoparticles with hydrophobic surfaces are more prone to opsonization and uptake by the RES system. To shield the hydrophobic surface and evade the RES clearance, hydrophilic modifications have been made to nanoparticles. The most commonly used strategy is PEGylation, which is a process of decorating the particle surface with polyethylene glycol (PEG)-type polymers. The hydrophilic PEG chains make nanoparticles less visible to the RES system and therefore decrease elimination and increase circulation time in-vivo. Various PEG-coated nano-formulations have shown prolonged circulation time in-vivo.⁶⁶⁻⁶⁹ However, the importance of long retention of anticancer drugs in the nanoparticles is often underappreciated. The widely available materials for nano-formulation engineering enables manipulating release rate either by tuning the affinity of anticancer drug and delivery materials, or by choosing polymers with appropriate properties (e.g., molecular weight). It is worth noting that the correlation of in-vitro and in-vivo release behaviors is often poor due to the

methodology of in-vitro release studies. The slow and sustained release profile in simple aqueous medium such as PBS is misleading in many circumstances. A more biologically relevant release method is crucial to predict the actual in-vivo drug release.

Thirdly, nano-formulations take advantage of the famous EPR effect and improve the biodistribution of anticancer agents. With a high concentration of drug in the circulation with prolonged period of time, the EPR effect plays a key role in passive targeting of nanoparticles. However, although PEGylation reduces the clearance by the RES, significant accumulation in the liver and spleen is still a typical distribution pattern for most nano-formulations. To further increase the selectivity, active targeting is utilized. The flexible surface chemistry of nanoparticles allows covalent or non-covalent incorporation of targeting ligands. The targeted receptor which may be over-expressed in tumor cells or site is expected to “attract” more nanoparticles. To date, it is still controversial about whether active targeting truly causes this “homing” effect; however, the internalization is proven to be evidently increased in tumor cells once the drug-loading nanoparticles reach tumor interstitial space.⁷⁰ The passive and active targeting properties of nanoparticles increase the anticancer agent accumulation in tumors while decrease the penetration to normal tissues. The superior biodistribution ultimately leads to reduced systemic toxicity and increased efficacy.

Finally, nano-formulation is versatile and multifunctional (Figure 1.3). Nano-formulations enable the co-delivery of multiple agents entrapped in the nanoparticles to gain synergistic anticancer effects or multi-functions. Various

modifications have been made to the nanoparticle surface as well. According to the application, the nanoparticles can be engineered to be positively-charged or negatively-charged. Active targeting ligands have been covalently attached to the distal end of PEG chain or directly attached to the lipids or polymers. Nanoparticle surface can be chelated with Ni and incorporate His-tagged antibody/affibody or vaccines.^{71,72}

Myriads of preclinical studies have been focused on developing nano-formulations to effectively deliver taxanes, one of the most important and most prescribed anticancer drug types in the clinic. Some of these nano-based delivery systems utilize natural carriers such as albumin and lipoproteins,^{32,73} while other systems such as polymeric nanoparticles, liposomes, micelles, nanoemulsions, solid lipid nanoparticles, nanocapsules, and dendrimers use synthetic materials. The rest of the review will focus on the advancement on development of lipid-based nanoparticles for taxane delivery.

2. Types of lipid-based nanoparticles to deliver taxanes

2.1. Liposomes

Liposomes may be the earliest nano-carrier applied in pharmaceutical field dating back to the 1960s. They have been extensively investigated for delivering various hydrophobic and hydrophilic drugs including anticancer agents for several decades and vast amounts of data have been generated and reviewed. Liposomal anticancer drugs

were the first nano-formulations being approved for cancer therapy by FDA. The liposomal anticancer drugs approved and marketed for clinical oncology use in the U.S. include Doxil[®] (doxorubicin), DauoXome[®] (daunorubicin) and DepoCyt[®] (cytarabine).

In the development of liposomes to deliver taxanes, increasing drug solubility, decreasing dose-limiting toxicities and altering undesirable pharmacokinetics are the main goals. The most commonly used preparation method of taxane liposome is simple. The drugs dissolved in an organic solvent are mixed with the lipid excipients dissolved in a miscible organic solvent. The thin lipid film produced by rotary evaporation is then hydrated by adding an aqueous solution. The resultant multilamellar liposomes are extruded through membranes with defined pore size or sonicated to form small unilamellar vesicles with size range 20-150 nm. The stability of liposomes remains one of the most important issues in the development of taxane liposomes. To prepare physically stable taxane liposomes, the lipid composition and the drug to lipid ratio have to be considered and balanced.⁷⁴ The most widely utilized lipids in liposome preparation are neutral zwitterionic lipids such as phosphatidylcholine (PC). To minimize aggregation and increase stability, cholesterol or some anionic or cationic phospholipids are often included.^{75,76} The drug-lipid interaction determines the accommodation of water-insoluble taxanes to the lipid bilayer of liposomes. Ideally, a maximal drug to lipid ratio leads to high drug payload and reduces the vehicle-related toxicities. However, increasing the drug/lipid ratio decreases the physical stability of

liposomes in aqueous media.⁷⁵ A drug loading of 3-3.5 mol% (paclitaxel to phospholipid) was physically stable for weeks to months, whereas 4-5 mol% paclitaxel was stable in the time range of just several hours to a day, and an 8% paclitaxel loading only resulted in 15 min of liposome stability. Thereby, to achieve a high drug/lipid ratio while retaining the long-term physical-chemical stability, a freeze-drying method is employed to obtain a dry drug-lipid powder, which is rehydrated in an aqueous solution immediately before use.^{77,78} The physical stability of taxane liposomes can be characterized by measurement of drug retention, circular dichroism spectropolarimetry (CD), differential scanning calorimetry (DSC) and other methods.^{79,80} Besides the physical stability, in-vivo stability is equally important if not more important. The long-circulation of liposomes has been realized by sterically stabilizing liposomes using the PEGylation approach.⁶⁹ However, a decrease of the physical stability of paclitaxel liposomes has been reported by the incorporation of PEG-modified lipids.⁸¹ It also has been demonstrated that repeated injection of PEGylated liposomes caused accelerated blood clearance of the following injected PEGylated liposomes.⁸² The phenomenon is attributed to the abundant IgM secreted by spleen upon first injection. In the clinic, taxanes require repeated doses, therefore this phenomenon may cause potential problems for taxane liposomal formulations. In addition to the stability and drug leakage issues, liposomes have other disadvantages including low loading capacity to lipophilic drugs and the requirement for the use of an organic solvent in the preparation.

Taxane liposomes have shown slower elimination, higher antitumor activity against various murine and human tumors and lower systemic toxic effect compared to Taxol.⁸³⁻⁸⁵ They have also shown antitumor effects in Taxol-resistant tumor models.⁷⁷ Cationic liposomes have been prepared from DOTAP and DOPE to encapsulate paclitaxel and selectively target angiogenic tumor endothelium.⁸⁶ The paclitaxel-containing cationic liposomes remarkably inhibited the growth of A-Mel-3 tumors while control tumors showed exponential growth. A liposomal paclitaxel formulation composed of cardiolipin, egg PC, cholesterol and D- α -tocopheryl acid succinate (Vitamin E) has progressed to a phase-I clinical trial.⁸⁷ Unfortunately, despite the promising pre-clinical results, they failed to provide advantages over Taxol in patients with solid tumors.

2.2. Micelles

Micelles are the simplest colloidal systems formed spontaneously by amphiphilic molecules. Depending on the types of amphiphilic molecules, micelles can be divided into lipid micelles, polymeric micelles and lipid-polymeric hybrid micelles. For lipid micelles, the amphiphilic molecules are usually small molecular surfactants. Different from the lipid bilayer structure of liposomes, the structure of lipid micelles is a monolayer structure with hydrophilic heads facing the outside aqueous environment and lipophilic tails forming the inner core. The shape of micelles can be spherical,

ellipsoidal or rod-like depending on the composition.⁸⁸ At low concentration, the amphiphilic molecules exist in the aqueous media in a separated status. In contrast, when the concentration increases, they start to assemble to micellar structures driven by the decrease of free energy. The lowest concentration at which micelles are formed is called the critical micelle concentration (CMC). As a simple colloidal system, micellar nano-carriers are utilized in drug delivery fields to mainly deliver hydrophobic drugs, whereas hydrophilic or amphipathic agents are sometimes delivered as well.⁸⁹⁻⁹² Improving drug solubility is the major rationale of designing micellar nano-carriers. Hydrophobic drugs like taxanes are entrapped in the lipophilic core of the micelles. The commercial dosage forms of paclitaxel and docetaxel, Taxol and Taxotere, can be classified as micelles. However, lipid micellar nano-carriers have two main limitations: relatively low hydrophobic volume of the interior space and dissociation upon dilution. Due to the small interior hydrophobic space, the drug loading capacity of lipid micelles is often limited. Also, since the CMC of conventional lipid micelles is often high, they are not stable and tend to dissociate when they are diluted in-vitro or in-vivo. To address these issues, several alternative approaches have been pursued. In the case of Taxol and Taxotere, ethanol is incorporated in both dosage forms to facilitate the drug dissolution and stability. Besides the organic solvent related toxicities, for Taxotere, the micellar solutions after dilution with infusion medium are supersaturated and have to be used in 4 hr before docetaxel begins to crystallize.

In the field of micellar nano-carriers development, a larger amount of studies

have focused on the development of polymeric micelles because the CMC of polymeric micelles is extremely low, in the range of 10^{-6} to 10^{-7} M.⁹³ To combine the advantages of lipid micelles and polymeric micelles, a novel sterically stabilized micellar (SSM) system composed of poly (ethylene glycol)-grafted distearoylphosphatidylethanolamine (DSPE-PEG) was developed to deliver water-insoluble drugs including paclitaxel.⁹⁴⁻⁹⁶ These phospholipid micelles are biocompatible and easy to prepare. The long acyl chains of DSPE-PEG creates a large hydrophobic inner core. To further increase the hydrophobic space and improve the solubilization of paclitaxel, another phospholipid, egg PC was incorporated to form sterically stabilized mixed micelles (SSMM) (Figure 1.4).⁹¹ SSMM solubilized 1.5-times more paclitaxel than SSM for the same total lipid concentration. The PEG chains on the surface of these micelles and the strong hydrophobic interactions between the double acyl chains of the phospholipid residues result in lower CMC and higher thermodynamic stability compared to conventional micelles. The particle size and CMC of these micelles highly depend on the length of PEG chains. With the molecular weight of PEG increased from 750 to 5,000 Da, particle sizes increased from 7-15 nm to 10-35 nm, and CMC decreased from 1×10^{-5} to 7×10^{-6} M.^{97,98} The paclitaxel-loaded SSM and SSMM were monodispersed with mean particle sizes of 15 ± 1 nm and 13.1 ± 1.1 nm, respectively. Moreover, the PEG chains are also expected to render protection against RES uptake and thus increase drug circulation time in-vivo. Furthermore, the active targeting property can be obtained by conjugating targeting moieties to the distal

end of PEG chains. The paclitaxel-loaded SSM and SSMM showed similar in-vitro cytotoxicity against human breast cancer MCF-7 with paclitaxel dissolved in 10% DMSO. However, in a more recent study, it was shown that by adding excessive empty micelles (1 μ M), the IC₅₀ value of both formulations was about 7-fold lower than that of paclitaxel dissolved in DMSO.⁹⁵ This phenomenon provides an idea of preventing micelle rapid breakdown in-vivo by mixing empty micelles as a dilution cushion with drug-loading micelles. To date, there is no direct in-vivo evidence of improved pharmacokinetics or antitumor efficacy for the paclitaxel-loaded micelles over Taxol. The radiolabeled SSM showed increasing circulation half-life with the increase in the size of PEG block.⁹⁸ These micelles efficiently and specifically accumulated in Lewis lung carcinoma and EL4 T lymphoma xenografts in mice. It has also been observed that DSPE-PEG2000 and DSPE-PEG5000 micelles retained their size characteristics after 48 hr incubation with blood serum at room temperature. The integrity of micelles is likely associated with the drug retention in the nano-carriers. Collectively, these evidences suggest that the SSM or SSMM loaded with paclitaxel has the potential to prolong the drug circulation and achieve efficient tumor accumulation by the EPR effect.

2.3. Nano-emulsions (Emulsions, Micro-emulsions)

Emulsions are mixtures of oil(s), water, and surfactant(s). The difference between

emulsion and micro-/nano-emulsion is obvious and can be detected by the naked eye: emulsions are cloudy suspensions with droplet sizes over 1 μm , whereas micro-/nano-emulsions are transparent or translucent. However, the misconception about micro-emulsion and nano-emulsions is common in the literature.⁹⁹ Many of the systems referred to micro-emulsions in the literatures are actually nano-emulsions, while micro-emulsions are sometimes erroneously considered as nano-emulsions because they have the same apparent structure as nano-emulsions, which is spherical nano-sized droplets dispersed in a continuous phase. The fundamental difference between micro-emulsion and nano-emulsion is not their droplet sizes as suggested by their names (micro- vs. nano-) but their thermodynamic behaviors. Micro-emulsion is a thermodynamically stable system while nano-emulsion is thermodynamically unstable but kinetically stable. The key differences between micro-emulsion and nano-emulsion are not only critical to their preparation process and characterization, but also influence their applications (Table 2). Micro-emulsion, as a thermodynamic equilibrium system, is formed spontaneously by mixing oil, water and surfactant(s) and no energy is needed. To accelerate the emulsification process, in many cases some energy is input to overcome certain kinetic barriers through mechanical stirring or heating.¹⁰⁰ On the contrary, nano-emulsion is in a non-equilibrium state and is generally formulated through the “high-energy” methods such as high-pressure homogenization, ultrasonication, to recruit high energy to breakdown the large droplets to submicron size.¹⁰¹ Nano-emulsions are also formulated by low-energy methods taking advantage

of the intrinsic physicochemical properties of the components. The phase inversion temperature (PIT) method is the most widely used low-energy method in industry. PIT is the temperature or temperature range at which a nonionic surfactant reaches the hydrophilicity and lipophilicity balance. The method is mainly based on the changes in solubility of the polyoxyethylene-type non-ionic surfactant with temperature. Another low-energy method is “spontaneous” emulsification. Nano-emulsions were formed simply by adding oil/surfactant mixture with an aqueous phase. However, the order in which the different components are mixed is essential for the formation of nano-emulsions in this method. Due to the small size of nano-emulsions, the sedimentation or aggregation rate is slow so that they are considered kinetically stable. The Oswald ripening is the only mechanism of nano-emulsion destabilization. The development of micro-emulsion is assisted by ternary phase diagram. As long as the component ratio is in the micro-emulsion forming domain, the mixing order does not influence the micro-emulsion formation. An important disparity associated with this is that micro-emulsion is not stable upon dilution because with the aqueous phase increasing, the composition of the water/oil/surfactant can reach out of the micro-emulsion forming boundary; in contrast, nano-emulsion is stable upon dilution or concentration once it is formed. Another important difference between micro-emulsion and nano-emulsion is that the phase behavior of micro-emulsion but not nano-emulsion is sensitive to temperature change.

The instability of micro-emulsions toward dilution and temperature limits their

application as parenteral drug delivery carriers although their size may be in the nano-scale range. When administered intravenously, the formulation is largely diluted by blood and body fluids. In addition, the temperature is different as well. The breakdown of micro-emulsion in-vivo may cause a quick release of encapsulated drug or even drug precipitate leading to severe safety issues. The temperature sensitivity also makes sterilization of micro-emulsions by autoclave an invalid option. Overall, despite of the structural similarity, nano-emulsions and micro-emulsions are two different systems. The better stability of nano-emulsions to environmental stress makes them more suitable for parenteral drug delivery, while micro-emulsions have their applications in oral or topical delivery. Since micro-emulsions and nano-emulsions are both nano-sized drug carriers, their application in taxane delivery will both be reviewed.

An early effort to develop CrEL-free paclitaxel dosage form formulated paclitaxel in an emulsion composed of triacetin as oil phase and soybean lecithin, pluronic F68, and ethyl oleate as surfactants.¹⁰² The emulsion was able to accommodate 10-15 mg/mL paclitaxel. But as an emulsion system, the droplet size was large ranging from 0.5 to 5 μm and increased over time and eventually phase separation occurred. With the advance of technology in engineering, later, high-pressure homogenization was utilized to breakdown the droplets of coarse emulsion to smaller than 200 nm. A vitamin E-based nano-emulsion composed of tocopherol (vitamin E) as oil phase, TPGS and Poloxamer 407 as surfactants was prepared by high-shear

homogenization.¹⁰³ The nano-emulsion of paclitaxel developed by Sonus Pharmaceuticals is named TOCOSOLTM. The nano-emulsions had a mean particle size of 62 nm and could load 8-10 mg/mL paclitaxel. In-vitro drug release was slow both in the presence and absence of human serum albumin. In the preclinical studies, the paclitaxel-loaded nano-emulsion was well tolerated with 3-fold higher maximum tolerated dose (MTD) over Taxol. It showed superior antitumor efficacy and survival benefit in B16 melanoma mouse model. In the pharmacokinetic and biodistribution studies, it was found that although the blood AUC of paclitaxel nano-emulsion was similar to that of Taxol in B16 melanoma mouse model, the tumor uptake of paclitaxel in nano-emulsion was significantly higher than that of Taxol.¹⁰⁴ The tumor C_{max} was 1.5-times higher and AUC was 2.2-times higher after administration of paclitaxel nano-emulsion compared to Taxol. Based on the promising preclinical results, TOCOSOL entered a clinical trial. In phase I, patients received doses up to 225 mg/m² every 3 weeks. In phase II studies, the efficacy of TOCOSOL was investigated in patients with ovarian cancer, colorectal cancer, NSCL cancer or bladder cancer. In 2007, TOCOSOL was advanced to a phase III clinical trial. Unfortunately, phase III studies of TOCOSOL in women with metastatic breast cancer failed to show improvement on objective response rate (ORR) compared to the Taxol arm. In addition, the rates of neutropenia and febrile neutropenia in the TOCOSOL arm were significantly higher than the Taxol arm. Consequently, all clinical trials of TOCOSOL were terminated.

A more recent report used high-pressure homogenization to prepare a

nano-emulsion system to deliver docetaxel.¹⁰⁵ The entrapment efficiency determined by ultrafiltration and ultracentrifugation was greater than 90%. The pharmacokinetic study revealed a 3-fold higher AUC with docetaxel formulated in the nano-emulsion over Taxotere. Another nano-emulsion composed of tricaproin/tricaprylin 3:1, egg PC, and Tween 80 in glycerol solution was developed by first identifying an oil phase with high paclitaxel solubility.¹⁰⁶ It was found that the triglycerols (tributyrin, tricaproin, and tricaprylin) generally had higher solubility to paclitaxel than the natural oils (corn oil, soybean oil, cotton seed oil and mineral oil) selected in the study. By sonication, the resultant nano-emulsions had particle size around 150 nm and were stable for at least 3 months when stored at 4°C. The paclitaxel-loaded nano-emulsion showed survival benefit over paclitaxel-free nano-emulsion in ascetic-tumor-bearing mice, but whether the formulation had superior antitumor efficacy than Taxol was not investigated.

Nano-emulsions have also been employed to improve the oral bioavailability of paclitaxel. The nano-emulsion was formulated with pine nut oil and egg lecithin by sonication method.¹⁰⁷ After oral administration, a significantly higher concentration of paclitaxel was observed in the systemic circulation from paclitaxel nano-emulsions over a control paclitaxel solution. Yin et al. also reported enhanced bioavailability of docetaxel using a micro-emulsion.¹⁰⁸ The micro-emulsion developed with the assistance of pseudo ternary phase diagrams was composed of Capryol 90, CrEL and Transcutol. The micro-emulsion significantly improved the bioavailability of docetaxel (34.4%) in rats compared to Taxotere (6.6%) after oral administration. These studies

demonstrated a proof-of-concept that a nano-emulsion/micro-emulsion could enhance the oral bioavailability of hydrophobic drugs such as taxanes. However, as oral delivery systems of taxanes for practical application, important toxicity issues remain to be thoroughly investigated, because as cytotoxic agents, taxanes are especially toxic to the rapid-proliferating intestinal epithelial cells.

A novel cholesterol-rich nano-emulsion resembling low-density lipoprotein (LDL) was developed by Maranhao et al.¹⁰⁹ LDL is the main carrier of plasma cholesterol in human. In some tumor types, LDL receptor was overexpressed in the neoplastic cells to meet the increased need of cholesterol for new membrane synthesis. Therefore, LDL can serve as a potential drug carrier to specifically deliver anticancer agent to cancer cells overexpressing LDL receptors. However, the isolation and handling of native LDL are difficult. It led to the design of a cholesterol-rich nano-emulsion that resembles the structure of LDL as a vehicle to paclitaxel. The nano-emulsion was prepared from a lipid mixture of 20 mg cholesteryl oleate, 40 mg egg PC, 1 mg triolein and 0.5 mg cholesterol. The final nano-emulsion had a mean particle size of 85 nm obtained by ultrasonication. The radiolabeled nano-emulsion was found to be more rapidly cleared from the patients with acute myeloid leukemia (AML) than in the patients with acute lymphocytic leukemia (ALL).¹⁰⁹ The fact that LDL receptor is overexpressed in AML but not ALL suggests that the cholesterol-rich nano-emulsion was taken up by malignant cells with increased LDL receptor. Later, a lipophilic paclitaxel derivative paclitaxel-oleate was encapsulated into the

nano-emulsion. The formulation showed about 2-times higher AUC in both mice and patients with gynecologic cancers.^{110,111} The LD₅₀ dose of the formulation was 9-times higher than that of Taxol in mice. Its therapeutic efficacy in B16F10 tumor bearing mice was remarkably greater than Taxol in terms of tumor growth inhibition, survival rates and % cure of treated mice. Another pilot clinical study in nine breast cancer patients also showed more than 3-fold increase of blood AUC compared to Taxol (Figure 1.5).¹¹² Both studies conducted in patients with gynecologic cancers and breast cancer showed 3-3.5-times higher drug accumulation in the malignant tumor tissues than in the normal tissues. The paclitaxel-oleate nano-emulsion showed great potential for further clinical development. The idea of constructing LDL-like nano-emulsion to target LDL receptor overexpressing cancer cells was also explored by another group.¹¹³ Instead of making the nano-emulsions cholesterol-rich to resemble LDL, they incorporated a 29-amino acid synthetic peptide containing a lipid binding motif and an LDL receptor binding domain. Their in-vitro studies showed that the nano-emulsions containing paclitaxel-oleate inhibited the growth of LDL receptor overexpressing GBM cells and demonstrated that the drug was internalized via the LDL receptor.

2.4. Solid lipid nanoparticles

Compared to the lipid nano-formulations discussed above, solid lipid nanoparticle (SLN) is a relatively new colloidal drug delivery system introduced in early 1990s.

Compared to other lipid nano-systems, SLNs have many advantages including ease of preparation and scale-up with low cost, good physical stability, controlled drug release, and versatile chemistry, in addition to others. SLNs can be prepared by high-pressure homogenization, micro-emulsion method, precipitation method by solvent evaporation, W/O/W double emulsion method, and high speed stirring/ultrasonication method.¹¹⁴

The high-pressure homogenization methods include hot homogenization and cold homogenization. For both techniques the drug is firstly solubilized in the melted lipid. For the hot homogenization technique, the drug-containing lipid melt is dispersed under stirring in a hot aqueous surfactant solution with the same temperature. A hot O/W nano-emulsion is then obtained through high-pressure homogenization. SLNs are formed when the hot O/W nano-emulsion is cooled down to room temperature and the lipid recrystallizes. Different from the hot technique, the drug-containing lipid melt is dispersed in a cold surfactant solution for the cold homogenization technique leading to the formation of microparticles. The microparticles are then directly homogenized to nano-sized SLNs at or below room temperature.¹¹⁵ The high-pressure homogenization method has been scaled up to 2-10 kg batch sizes under GMP.^{116,117} SLNs can also be produced via micro-emulsions. A mixture of lipid, surfactant, co-surfactant and water heated above the melting point of the solid lipid in the micro-emulsion forming region firstly forms a thermodynamically stable micro-emulsion system. SLNs are then formed by dispersing the warm micro-emulsion into a cold aqueous medium under mild mechanical mixing. Mumper et al. developed a warm micro-emulsion precursor

process to manufacture SLNs in a one vessel process.¹¹⁸ The process has been scaled up to 10 liters in the lab and 1 liter under cGMP. For the precipitation method, solid lipid dissolved in an organic solvent is emulsified in a surfactant solution. The lipid precipitates forming SLNs after organic solvent evaporation. The involvement of organic solvent is an obvious disadvantage of this method. The W/O/W double emulsion method is a relatively new method developed recently to encapsulate hydrophilic molecules. The high-pressure homogenization, micro-emulsion method, precipitation method all have been employed to prepare SLNs to encapsulate paclitaxel and docetaxel.¹¹⁹⁻¹²³ A large pool of solid lipids (mono-, di- and tri-glycerides, lipid acids, phospholipids, wax etc.) and surfactants are available for SLN engineering. Among these excipients, some lipids (e.g., glycerides, phospholipids) and surfactants (e.g., Tween 80, lecithin, Poloxamer 188, sodium glycocholate) are acceptable for i.v. injection. The wide availability of i.v.-acceptable solid lipid and surfactant makes SLN a versatile platform for drug delivery readily translational to clinical application although so far no SLN products have been introduced into the market for parenteral use. Due to the solid status of the SLN matrix, the physical stability of optimized SLN is generally more than one year.^{124,125}

The drug loading capacity and drug retention in the SLNs are closely related to the solubility and miscibility of drug with the lipid phase, as well as the physicochemical structure of the solid lipid matrix and the polymorphic state of the lipid material.¹¹⁵ Choosing a lipid with high drug solubility and miscibility is a

prerequisite for forming SLN with high drug loading and slow drug release. A paclitaxel-loaded SLN developed by Cavali et al. showed only 0.1% drug release in PBS in 2 hr following pseudo zero order release.¹²³ Another paclitaxel-loaded SLN prepared from phospholipid and sucrose fatty acid esters released only 12.5-16.5% of paclitaxel within 14 days.¹²⁶ More impressively, Lee et al. studied the release of paclitaxel from a SLN in 80% human plasma at 37°C using dialysis method. They found that only 10% of paclitaxel was released from the SLNs in 24 hr.¹²⁰

However, the solid lipids with highly organized crystal lattice structure are orderly and tightly packed together leaving very limited space to accommodate large amounts of drug molecules, which leads to low drug loading and burst release. It has been demonstrated that the extent of burst release is not only associated with the lipid matrix properties, but also is a function of production temperature and surfactant concentration.^{115,127,128} The initial burst release increases with increasing preparation temperature and increasing surfactant concentration. With higher production temperature and surfactant concentration, the drug solubility in the aqueous phase is higher. During the cooling process of SLN preparation when warm method is used, the drug solubility in the aqueous phase decreases while at the same time the lipid melts solidify and crystallize.¹²⁹ The drug re-partitions into the lipids while the lipids increase structural perfection during the cooling, leading to the embedding of drug molecules onto the particle surface and formation of a drug-enriched shell. This unfavorable drug incorporation mode limits the drug loading capacity, and leads to drug expulsion during

storage and burst release. To overcome this potential issue, Muller et al. proposed a novel lipid nano-system called “nanostructured lipid carriers” (NLC).¹²⁹ The NLC is a modification of the conventional SLN by making the solid lipid core a less organized nanostructure. The lipid cores with imperfect crystal structure can be realized by either using spatially different lipids, such as mono-, di-, tri-glycerides with different chain lengths, or mixing some liquid lipids (oils) with the solid lipid. The space between different fatty acid chains and crystal imperfections provide more accommodation for drug molecules. In addition, some drugs have higher solubility in oils than in solid lipids. Therefore, the NLC as a new generation of SLN increases the drug payload and decreases drug expulsion and burst release. Besides the lipid matrix, it is also possible to tune the release profile by adopting different production method (warm or cool) or modifying surfactant concentration. Finally, it is worth noting that burst release may not be necessarily a bad property for all drugs. When an initial high blood concentration is desirable according to the therapeutic needs, the burst release can be useful under more precise control.

The in-vitro uptake and cytotoxicity of paclitaxel-loaded SLNs have been demonstrated in several cell lines.^{120,121,130,131} The lipid matrix materials seem to not only influence drug release rate but also affect cellular uptake as well. Yuan et al. investigated the cellular uptake of several SLNs composed of different lipid materials including monostearin, stearic acid, glycerol tristearate and Compritol 888 ATO (ATO888).¹³⁰ Their results showed that the cellular accumulation preference was in the

order of glycerol tristearate SLN > monostearin SLN > stearic acid SLN > ATO888 SLN. This is explained by different affinity between fatty acids and cell membrane. Moreover, the PEGylated stearic acid SLN showed the highest cellular uptake among the materials tested. Paclitaxel loaded in these SLNs showed 1.6-10-fold higher cytotoxicity compared to Taxol. SLNs encapsulating paclitaxel not only showed higher anticancer activity in sensitive cell lines, but also overcame MDR in P-gp overexpressing cells. In a P-gp-overexpressing human ovarian carcinoma cell line NCI/ADR-RES, SLN G78 containing paclitaxel showed 9-fold lower IC₅₀ value.¹³¹ The potential mechanism of overcoming P-gp-mediated MDR was also investigated. It was demonstrated that the surfactant Brij 78 used in the SLN G78 temporarily decreased ATP level in resistant cells, thus the energy-dependent P-gp efflux was transiently inhibited. The increased uptake of high drug payload SLNs by endocytosis along with the inhibition of P-gp function resulted in greater cellular uptake and higher cytotoxicity in resistant cells. The blank SLNs themselves were well-tolerated both in-vitro and in-vivo. In-vitro experiments showed that SLN E78 did not cause blood cell lysis at concentration up to 1 mg/mL and did not activate platelets.¹³² In-vivo i.v. bolus injections of cetyl palmitate SLNs into mice at dose up to 1.33 g/kg with 6 repeats did not cause acute toxicity or increase in liver and spleen weight.¹¹⁵

SLN encapsulation improves drug pharmacokinetics and biodistribution. Similar to other nanoparticles, the long-circulation of SLNs can be achieved by modifying the particle surface with more hydrophilic moieties to evade RES clearance.

The most widely used method is PEGylation. As compared to other more well-established nano-systems such as liposomes, the development of stealth SLNs is still in its initial phase. Also due to the great diversity of SLNs, there are no certain rules and approaches that can be universally applied to all or most of the SLNs in terms of coating density, chain length and incorporation method. To date in the literature, stealth SLNs are PEGylated through either PEG-grafted lipids (e.g., DSPE-PEG2000, stearic acid-PEG) or surfactants with certain PEG chains (e.g., Brij 700, TPGS). Two long-circulating SLNs containing paclitaxel were developed and their pharmacokinetics were evaluated in mice by Chen et al.¹¹⁹ Both of the SLNs were composed of stearic acid and lethicin as oil phase, with Brij 78 as surfactant in one formulation (Brij78-SLN) and Poloxamer F68 and DSPE-PEG2000 in another (F68-SLN). Brij78-SLN and F68-SLN increased paclitaxel AUC 1.7-fold and 1.9-fold compared to Taxol, respectively. The longer PEG chain of DSPE-PEG2000 (Mw 2000) compared to Brij 78 (Mw 1200) may be responsible for the slightly longer circulation and higher AUC of F68-SLN. Interestingly, non-stealth SLNs without PEGylation also enhanced systemic circulation of encapsulated drugs.¹³³⁻¹³⁷ The mechanism of this unique characteristic of SLN is not clear. It is possible that some surfactants used in the so-called non-stealth SLNs carry similar properties as PEG. For example, Poloxamer used in the study of Yang et al. is a triblock copolymer composed of a central hydrophobic chain of polyoxypropylene flanked by two hydrophilic chains of polyoxyethylene.¹³⁷ Another example is vitamin E-TPGS (alpha-Tocopheryl

Polyethylene Glycol 1000 succinate) which has a medium PEG chain with molecular weight of 1000. These surfactants may result in a hydrophilic shield on the SLNs to protect them from RES uptake. However, in more cases, this explanation may not apply. Further thorough investigations are needed to fully understand the underlying mechanism. Up until now, a considerable accumulation of SLNs in the organs of RES (liver, spleen, and lung) is still a typical distribution pattern after i.v. injection of either non-stealth or stealth SLNs. With prolonged exposure in the systemic circulation, SLNs deliver more entrapped drugs to solid tumor tissues taking advantage of the EPR effect.¹³⁸ An extraordinary finding by many research groups revealed that SLNs improved the delivery of various drugs to brain.^{134,135,137,138} One potential explanation of the effect is that plasma proteins (e.g., apolipoproteins) bind to particle surfaces and mediate adherence to blood-brain-barrier (BBB) endothelial cells.¹¹⁴ The BBB endothelial cells are famous for their tight junctions and high expression of P-gp. Brain uptake of paclitaxel nanoparticles was evaluated by Koziara et al. using an in-situ rat brain perfusion model.¹³⁹ Their results suggested that entrapment of paclitaxel in SLNs significantly increased the paclitaxel brain uptake. Possible mechanisms of increased brain delivery of these SLNs include: 1) shielding of drug from direct interaction with P-gp by nanoparticle entrapment, 2) modulating BBB P-gp function by the surfactant (Brij 78), and 3) triggering of endocytosis/transcytosis. These data suggest the possibility of brain delivery of chemotherapy with SLNs.

2.5. Nanocapsules

Nanocapsules are defined as nano-scaled particles with an oil core surrounded by a rigid shell. With the liquid oil core as a drug reservoir and rigid shell as a drug leaking barrier, nanocapsules are expected to have high drug encapsulation capacity, good drug retention and high stability. Similar to SLN, nanocapsules are generally stable over a year. They have fewer drug leakage problems associated with liposomes and avoid drug expulsion problems associated with SLNs. There are two types of nanocapsules, based on the structure and components of the shells: polymer-shelled nanocapsule and surfactant-shelled nanocapsule. The preparation of both polymer-shelled nanocapsule and surfactant-shelled nanocapsule is closely related to nano-emulsion/micro-emulsion. Polymer-shelled nanocapsules can be prepared by interfacial polymerization, salting-out, emulsification-diffusion, and nanoprecipitation etc.¹⁰¹ For the interfacial polymerization method, nano-emulsion droplets serve as individual nano-reactors, on the surface of which polymerization of monomers with different mechanisms occur and form polymeric shell encapsulating liquid oil core and drugs.¹⁴⁰⁻¹⁴² Different from interfacial polymerization technique, the latter three methods disperse preformed polymer on nano-emulsion surface. The latter three methods were compared by Galindo-Rodriguez et al.¹⁴³ Methacrylic acid copolymer and poly(vinyl alcohol) (PVA) were selected as polymer and emulsifying agent to prepare nanocapsules utilizing all three methods. The size distribution of nanocapsules prepared by nanoprecipitation was narrower than those by salting-out and emulsification-diffusion methods. The factors

influencing nanocapsule formation by salting-out and emulsification-diffusion methods were PVA chain interactions at the interface and in the bulk solution; while the parameter governing the nanocapsule characteristics from nanoprecipitation method was water-solvent interaction. All the methods for polymer-shelled nanocapsule preparation involve the use of organic solvent. Nanocapsules have been developed to deliver paclitaxel since 20 years ago.¹⁴⁴ Unfortunately, the mice treated with 1.5 mg/kg paclitaxel-loaded nanocapsules died before control mice, suggesting high toxicity of the nanocapsules which was composed of poly(lactic acid), benzyl benzoate and Pluronic F68. Over the past 20 years, the development of nanocapsules for anticancer drug delivery is fairly slow compared to other lipid-based nano-carriers. Until more recently, several polymer-shelled nanocapsules are reported for paclitaxel delivery with only in-vitro studies. Nanocapsules were prepared using a freeze-drying method to directly disperse Pluronic F-127 triblock copolymer to the surface of lipid core composed of lecithin and paclitaxel.¹⁴⁵ The paclitaxel-loaded lipid cores dispersed in 10 wt% F-127 aqueous solution exhibited droplet size of 99 nm. However, after the freeze-drying to induce the formation of polymeric shell, a mean particle size of 267.4 nm and broad distribution were observed. The large particle size and broad distribution may cause potential risks for parenteral application. PEO-PPO-PEO/PEG shell cross-linked nanocapsules were prepared by dissolving an oil (Lipiodol[®]) and an amine-reactive PEO-PPO-PEO derivative in DCM and consequently dispersing in an aqueous solution containing amine-functionalized six-arm-branched PEG by

ultrasonication.¹⁴⁶ The resultant nanocapsules had an average particle size of 110 ± 9.9 nm with paclitaxel-loading efficiency of $46.5 \pm 9.5\%$. Zhang et al. prepared nanocapsules through interfacial polymerization of butylcyanoacrylate (BCA) with PEG as initiator.¹⁴⁷ The particle sizes, paclitaxel entrapment and hemolytic potential of PEG-PBCA nanocapsules were all related to the quantity and molecular weight of mPEG. With longer PEG chain length, mPEG5000 served as a stronger stabilizer and formed smaller nanocapsules compared to mPEG2000. The encapsulation efficiency of paclitaxel also increased with increase of PEG concentration. The 10% (w/v) PEG-PBCA nanocapsules showed about 60% of paclitaxel encapsulation efficiency. With the increase of PEG concentration, the hemolysis rate decreased as well. Generally, the encapsulation efficiency of paclitaxel in polymer-shelled nanocapsules is not very high so far.

The surfactant-shelled nanocapsules are prepared by the PIT method. Both nano-emulsions and nanocapsules can be prepared using the PIT technology. The three basic components are the same for nano-emulsions and nanocapsule; each containing an oil phase, an aqueous phase and surfactant(s). However, the fundamental composition of nanocapsules falls in the microemulsion-forming region (Winsor IV region); while the composition of nano-emulsions is in the Winsor III region. As briefly discussed in nano-emulsion production, the PIT method is based on the changes in solubility of the polyoxyethylene-type non-ionic surfactant with temperature. At temperatures below the PIT, the surfactant monolayer has a positive curvature forming

O/W emulsions; while above the PIT, the curvature becomes negative forming W/O emulsions. During the preparation of nanocapsules, the mixture of all components is heated to above the PIT (T2) then cooled to temperature below the PIT (T1). Several temperature cycles between T1 and T2 were carried out followed by a sudden dilution with cold water to induce an irreversible shock. This method developed by the Benoit group generally uses capric and caprylic acid triglycerides as the oil phase, and a small amount of Lipoid[®] as the hydrophobic surfactant.^{148,149} The leading role is played by the hydrophilic surfactant Solutol[®] HS 15, which is a mixture of free PEG 660 and PEG 660 hydroxystearate. The nonionic surfactants finally crystallize since the final temperature is below their melting point (about 30°C), leading to the formation of a rigid shell. The shell is structured as a combination of hydrophobic surfactant (Lipoid) anchoring in the oil phase and hydrophilic surfactant (Solutol) orienting toward the aqueous phase. The percentage of Solutol and the number of temperature cycles have major influence on particle size and size distribution. With higher percentage of Solutol and more temperature cycles, the particle size decreases and size distribution becomes narrower. Paclitaxel was encapsulated in the surfactant-shelled nanocapsules by the same research group. The entrapment efficiency in these nanocapsules was 99.9%. The pharmacokinetics and biodistribution of radiolabeled blank nanocapsules were studied.¹⁵⁰ The $t_{1/2}$ and MRT values of nanocapsules (2-3 hr) indicated long circulation of the nanocapsules. The pharmacokinetics of paclitaxel-loaded nanocapsule was missing. However, the slow release of paclitaxel from the nanocapsules in-vitro along

with the long-circulation of blank nanocapsules in-vivo suggested the potential of improved paclitaxel pharmacokinetics.¹⁵¹ The antitumoral activity of paclitaxel-loaded nanocapsule was evaluated in a chemically induced hepatocellular carcinoma (HCC) model. Animals treated with $4 \times 70 \text{ mg/m}^2$ of paclitaxel-loaded nanocapsules showed significant increase in the mean survival time compared to the blank nanocapsule and saline groups but with no statistical significance compared to the Taxol group.¹⁵⁰ The antitumoral activity was also studied in a glioma model with MDR.¹⁵¹ Paclitaxel-loaded nanocapsules significantly lowered both the tumor mass and tumor volume growth; whereas Taxol treatment showed no significant effect. The potential mechanisms of overcoming MDR by these nanocapsules were inhibition of MDR efflux pump by PEG-HS and redistribution of intracellular cholesterol. These nanocapsules were also administered orally to enhance the oral bioavailability of paclitaxel.¹⁵² The AUC of paclitaxel-loaded nanocapsule was 3-fold higher in comparison to the AUC of Taxol group, and comparable to the Taxol + verapamil group. The improvement of oral paclitaxel bioavailability when it was loaded in nanocapsules was likely due to the inhibition of P-gp by nanocapsules. Another research group prepared nanocapsules using the same PIT method to deliver docetaxel to solid tumor.¹⁵³ Encapsulation of docetaxel in the nanocapsule increased its AUC in blood and in tumor 4-fold and 5-fold, respectively, compared to Taxotere. The pharmacokinetics and biodistribution profiles were found to depend on PEG density on the particle surface. PEGylation of nanocapsules with DSPE-PEG2000 at 6, 10 and 15 mol% greatly enhanced

nanocapsule circulation time. The highest blood concentration of docetaxel 2 hr post-injection was obtained with 120 nm 15 mol% PEG nanocapsules. Tumor accumulation seemed to increase with PEG density but not statistically significant until 12 hr only between 6% and 15% of PEG groups.

2.6. Core/shell nanoparticles

In contrast to nanocapsules which are nanoparticles with lipid core surrounded by polymers, the so-called core/shell nanoparticles are nanoparticles with polymer core surrounded by lipids although in the literature nanocapsules are sometimes called core/shell nanoparticles. These core/shell nanoparticles are essentially comprised of a hydrophobic poly (lactic-co-glycolic acid) (PLGA) core, a hydrophilic poly (ethylene glycol) (PEG) shell, and a lipid layer in the form of monolayer or bilayer. This type of hybrid nanoparticle combines the beneficial properties of liposomes and polymeric nanoparticles. The hydrophobic polymeric core provides the nanoparticles high drug loading capacity, high stability and controlled drug release. The PEG and lipid shells render the nanoparticles natural property, extra shield against drug leaking, stealth feature for long-circulation, and favorable surface for cellular uptake. The physical stability and particle size were controlled by various formulation parameters such as lipid/polymer mass ratio and lipid/lipid-PEG molar ratio.¹⁵⁴ These factors also showed effects on the docetaxel release rate in water when docetaxel was entrapped into these

core/shell nanoparticles. The nanoparticles with 100% (w/w) lipid/polymer mass ratio released 90% docetaxel in 100 hr. Comparable release profiles were also reported by two other studies encapsulating docetaxel and paclitaxel.^{155,156} The nanoparticles did not cause significant cytotoxicity against HeLa cells and HepG2 cells.¹⁵⁴ These nanoparticles showed good physical stability in 10% (v/v) human plasma or 100% FBS at 37°C.

More interestingly, the core/shell structure enables co-delivery of a secondary drug. Combretastatin A4 (CA4) as a vascular disrupting agent was entrapped in the lipid layer of the core/shell nanoparticles and co-delivered with paclitaxel.¹⁵⁶ The sequential release of these two drugs over a time difference of 36 hr provides an opportunity of sequential anti-angiogenesis and anticancer functions (Figure 1.6). In addition, the arginine-glycine-aspartic acid (RGD) was conjugated to the nanoparticles to render the particles further vascular-targeting properties.

2.7. Prodrug strategy for better lipid nanoparticle encapsulation

Various paclitaxel and docetaxel prodrugs have been designed by conjugating small molecules, polymers, or targeting ligands etc. to realize different goals such as increasing water-solubility, site-specific release and tumor targeting.¹⁵⁷ In this section, we only focus on the prodrug strategies to manipulate the taxane hydrophilicity/hydrophobicity to be better incorporated into different lipid

nano-carriers.

Most lipid-based nanoparticles are designed to be more suitable and efficient for the encapsulation of lipophilic drugs. Paclitaxel and docetaxel are water-insoluble and often used as lipophilic model drugs when developing formulations that serve as lipophilic drug carriers. However, they have appreciable solubility in aqueous solutions and are highly protein bound. In addition, their solubilities in many lipids are limited. Therefore, in a biological environment, especially in-vivo, taxanes are no longer well retained in the nano-carriers. This issue is often neglected or underappreciated because most of the in-vitro release experiments are performed in simple aqueous solutions like PBS and have poor prediction of the in-vivo release behaviors. To address this potential issue, lipophilic taxane prodrugs were synthesized to further increase their lipophilicity and miscibility with lipids. Stevens et al. synthesized paclitaxel-7-carbonyl-cholesterol (Tax-Chol) and evaluated its incorporation into a nano-emulsion formulation.¹⁵⁸ Tax-Chol was incorporated into the nano-emulsion with greater than 90% entrapment efficiency. The release of Tax-Chol or paclitaxel from the nano-emulsions was determined in 45 mg/mL bovine serum albumin (BSA). The release of Tax-Chol was significantly slower than that of paclitaxel from the nano-emulsion. Paclitaxel was modified by attaching an oleoyl group to mimic cholesteryl esters and enhance its incorporation and retention in LDL-resembling nano-emulsions by several groups.^{110,113,159} The paclitaxel-oleate demonstrated significantly greater incorporation into nano-emulsions compared to unmodified paclitaxel.¹¹³ These paclitaxel-oleate

nano-emulsions showed promising in-vitro properties as well as in-vivo pharmacokinetics. To enhance the solubility of docetaxel in LabrafacTM (propylene glycol dicaprylate/dicaprate), a docetaxel prodrug was synthesized by attaching a lauroyl group to docetaxel through an ester link.¹⁶⁰ The 2'-lauroyl docetaxel showed greater than 8-fold solubility in the oil compared to unmodified docetaxel. In a nano-emulsion using Labrafac as the oil phase, 2'-lauroyl docetaxel showed high loading capacity (5.7% w/w) and high entrapment efficiency (97%). Since medium chain glycerides are widely used in formulating various nano-emulsions, micro-emulsions and nanocapsules, this strategy has its potential application in a number of nano-carriers. Ali et al. synthesized a series of paclitaxel prodrugs with 2-bromoacyl chains ranging from 6, 8, 12, 14 to 16 carbons in length.¹⁶¹ For comparison, hydrophobic paclitaxel prodrugs in acyl chain lengths from 6 to 16 without bromine at the 2-position were also synthesized. In-vitro, the cytotoxicity decreased with the increase of acyl chain length. In general, the taxanes lacking bromine were 50- to 250-fold less active than their bromoacyl counterparts indicating that the electron-withdrawing group facilitated the cleavage of active paclitaxel. The 2-bromoacyl taxanes were formulated into liposomes and evaluated for their anticancer efficacy in an ovc3 ovarian mouse model. In-vivo results showed that prodrugs with a longer chain were therapeutically more efficacious than those with a shorter chain, which was opposite to the in-vitro cytotoxicity. The trend was probably explained by slower release and hydrolysis in the systemic circulation leading to higher

accumulation in the tumor site for prodrugs with a longer chain.

Different than other lipid-based nano-carriers, liposomes are capable of directly encapsulating both lipophilic and hydrophilic drugs. However, drug loading of hydrophobic drugs in lipid bilayers of liposome is often limited. It has been demonstrated that paclitaxel and docetaxel are difficult to encapsulate and retain in liposomes. To overcome this issue, paclitaxel and docetaxel for liposomal delivery are modified more water-soluble. Water-soluble paclitaxel prodrug was synthesized by attachment of a methacrylic acid based oligomer with molecular weight of 1657 Da.¹⁶² The optimized liposomal formulation encapsulated 3 mol% of paclitaxel prodrugs with entrapment efficiency of 91%. In 180 hr, 45% prodrug release was observed in saline. However, as a prodrug, it did not release paclitaxel efficiently both in-vitro and in-vivo. In rat plasma, less than 1% of paclitaxel was liberated from the prodrug in 24 hr. Another study developed a weak-base derivative of docetaxel, 2'-O-(N-methyl-piperazinyl butanoyl) docetaxel.¹⁶³ The weak-base prodrug was actively loaded into liposomes using pH gradient loading techniques and achieved stable drug encapsulation and retention. In-vitro cytotoxicity studies in several cancer cell lines showed similar activity as unmodified docetaxel, suggesting efficient converting of prodrug to active parent drug. The prodrug formulated in liposomes extended the circulation half-life to about 10 hr with 50-100-times higher plasma exposure compared to Taxotere or docetaxel derivative formulated in the Taxotere vehicle (Figure 1.7). The MTD of liposomal prodrug was 3-fold higher than that of

Taxotere. In a human breast cancer (MDA-MB-435/LCC6) xenograft model, at equimolar dose (25 mg docetaxel/kg), the liposomes and Taxotere had similar activity; while at dose level of 88 mg docetaxel/kg, the drug-loading liposomes was much more efficacious.

It has been established that 2'-OH of both paclitaxel and docetaxel is more reactive than the 7-OH or other hydroxyl groups and the 2'-OH is critical for microtubule binding and cytotoxic effects.¹⁶⁴ In contrast, 7-OH is not as essential for the cytotoxicity of taxanes as 2'-OH but derivatives at 7-OH position are very stable under physiological conditions.^{165,166} As a result, derivatives of taxanes are almost always carried out at 2'-OH generating less toxic taxane prodrugs. Besides the improvement of drug encapsulation in lipid nano-carriers, taxane prodrugs have other advantages such as reduced systemic toxicity and potential of site-specific release to active drugs depending on the conjugation chemistry. If the conjugation linkage is cleaved by some enzymes specifically expressed or overexpressed in tumor site, it will lend the prodrug formulation extra targeting properties and further enhanced therapeutic index. The prodrug strategies benefit taxane delivery in many aspects, but at the same time complicates taxane delivery in terms of drug release profile. In addition to the drug release from formulations, active drugs need to be liberated from the prodrugs as well. Problems can be caused by either premature cleavage and release of active drugs, or too slow cleavage and inefficient liberation of active drugs. Therefore, when designing taxanes prodrug, a suitable drug cleavage rate is critical.

3. Active targeting of taxane lipid-based nanoparticle

Passive targeting of nanoparticle is based on the unique property of nanoparticles as well as the unique physiology and microenvironment of solid tumors. Nano-scaled particles preferentially accumulate in solid tumors taking advantage of the EPR effect. Different from passive targeting happening in tissue level, active targeting is based on specific molecular recognition, binding and the following endocytosis. The active targeting property can be intrinsic due to the nature of the nanoparticles. For example, cholesterol-rich nanoparticles target LDL receptors due to their components and structure resembling native LDL.¹⁰⁹ Cationic liposomes prepared from DOTAP and DOPE selectively target angiogenic tumor endothelium.⁸⁶ There are only a few examples of “build-in” active targeting, but it represents an inspiring alternative of conventional active targeting strategy. The most commonly used active targeting strategy is to graft targeting ligands such as antibody, peptide, small molecules, or aptamer on the surface of nanoparticles. Because nanoparticles usually carry high payload of anticancer agents, fewer ligands are required to achieve high active targeting efficiency compared to other delivery systems such as drug-ligand conjugate. Choosing a suitable target as well as targeting ligand is critical for the successful active targeting therapeutics. Ideally, the expression of the receptor on the target cells should be highly specific with high expression level in majority of the target cells. In reality, it is almost

impossible that the receptors only express in malignant cells. Higher tumor to normal tissue expression ratio provides higher selectivity. The major molecular targets for active targeting strategy include three types: angiogenesis-associated targeting (e.g., VEGFR), uncontrolled proliferation targeting (e.g., transferring receptors, folate receptors) and tumor cell targeting (e.g., HER-2, asialoglycoprotein receptor).¹⁶⁷ The targeting ligand should have high affinity with the target receptor to ensure sufficient retention time as well as trigger cellular uptake via receptor mediated endocytosis instead of remaining bound to the receptor. Furthermore, the targeting ligand should be amenable to the required chemistries to attach the ligand to the nano-carrier. To avoid spatial shield, targeting ligands are usually conjugated to the distal end of PEG chains. The incorporation method of PEG-ligand includes pre-insertion and post-insertion methods. The pre-insertion method is to mix functionalized lipid-PEG with other components and prepare nanoparticles first, and then covalently graft targeting ligands to the nanoparticle surface. The post-insertion method is to prepare nanoparticles first followed by mixing with preformed lipid-PEG-ligand conjugate. Alternatively, the preformed lipid-PEG-ligand conjugate can be directly mixed with other components and prepare nanoparticles.

During the development of active targeting nanoparticles, several factors must be taken into consideration. From the targeting ligand point of view, the conjugation chemistry and preparation conditions should not alter their binding affinity. The functional group or structure essential for receptor recognition and binding should not

be abolished or shielded due to the coupling to PEG. For some antibodies or peptide ligands, certain configuration must be retained to keep their binding affinity. Thus, depending on their sensitivity to environment, preparation conditions such as high temperature or the involvement of organic solvent should be avoided or used with extra caution. On the other hand, the incorporation of targeting ligand should not negatively change the properties of nanoparticles in terms of particle size, drug loading, drug release profiles and in-vivo elimination rate. Moreover, the targeting ligand should stably associate with the nanoparticles until they reach the targeting site. However, in some types of lipid-based nanoparticle such as liposomes, the lipids are in constant exchange with the environment that they in contact such as cell membranes. Consequently, there is a potential risk of losing active targeting ligands in biological condition. Finally, defining optimal density of targeting ligand on the nanoparticles is another important task. High ligand density in a feasible range may increase target binding, yet higher than optimal density may cause issues like higher cost, or aggregation etc.

The folate receptor is one of the mostly used targets for active targeting therapeutics. The folate receptor is significantly upregulated in many cancer cells including ovarian, lung, brain, head and neck, and breast cancers.^{168,169} What makes the folate receptor an interesting target is that normal cells use the reduced-folate carrier pathway that only transports reduced-folate but not folate conjugates of any type, while folate-conjugated nanoparticles can only use folate receptor pathway which has high

specificity in malignant cells.¹⁶⁸ Folic acid has a very high affinity for folate receptor ($K_d \approx 10^{-10}$). As small molecule, folic acid has many advantages over antibody ligand including small size, nonimmunogenicity, nontoxicity, ease to handle and conjugate to carriers, high stability in preparation, storage and circulation, and low cost. Folic acid has been conjugated to liposomes,¹⁷⁰ SLNs,¹³⁰ nanocapsules,¹⁴⁶ nano-emulsions¹⁵⁸ and core/shell nanoparticles¹⁵⁵ for paclitaxel and docetaxel targeted delivery. Wu et al. developed a folate receptor-targeted liposome and demonstrated efficient uptake by KB cells, which have high folate receptor expression.¹⁷⁰ The targeted liposomes containing paclitaxel showed 3.8-fold greater cytotoxicity compared to non-targeted liposomes in KB cells. The in-vivo half-life of targeted liposomes was comparable to that of non-targeted liposomes and both were much longer than the half-life of Taxol (7- to 8-fold). Studies by Bae et al. revealed significantly enhanced cellular uptake and cytotoxicity of a folate-conjugated nanocapsule in KB cells using confocal microscopy and flow cytometric analysis.¹⁴⁶ Enhanced cellular uptake and cytotoxicity were also observed for a folate-conjugated core/shell nanoparticle containing docetaxel in MCF7 cells.¹⁵⁵ In a folate receptor overexpressing A549 cell line, paclitaxel-loaded SLNs modified with folic acid-stearic acid enhanced the cellular uptake and cytotoxicity 2-fold and 8.8-fold compared to non-targeted SLNs, respectively.¹³⁰ Steven et al. delivered folate-conjugated nano-emulsions containing a paclitaxel lipophilic prodrug to mice bearing M109 tumors. Significantly greater tumor inhibition and animal survival were observed for targeted nano-emulsion treatment group compared to

treatment with non-targeted nano-emulsions or Taxol.¹⁵⁸

Asialoglycoprotein receptor (ASGP-R) is a promising receptor for liver targeting. Xu et al. designed SLNs using a galactose moiety to target ASGP-R.¹⁷¹ In in-vivo efficacy studies, mice bearing hepatoma were treated with 10 mg docetaxel/kg once a week for three weeks with targeted SLNs, non-targeted SLNs or Taxotere. The targeted SLNs demonstrated the most dramatic efficacy with complete tumor regression in all six mice (Figure 1.8). The outstanding antitumor efficacy of targeted SLNs was attributed to both increased accumulation in tumor indicated by biodistribution study and more cellular uptake by hepatoma cells demonstrated by confocal images.

Overexpression of epidermal growth factor receptor (EGFR) has been detected in one third of all solid tumors, in many of which EGFR expression characterizes a more advanced disease stage.¹⁷² Docetaxel nanoparticles modified with recombinant human EGF showed improvement of cell internalization and higher cytotoxicity against MDA-MB-468 cells.¹⁷³ In BALB/c mice bearing MDA-MB-468 tumor xenografts, targeted nanoparticles exhibited stronger inhibition of tumor growth compared to non-targeted nanoparticles or Taxotere. At a dose of 10 mg docetaxel/kg, tumor disappeared completely in the targeted nanoparticle treatment group. The dramatic antitumor activity was also consistent with the 3.6-times higher AUC over that of Taxotere and significantly higher tumor accumulation compared to non-targeted nanoparticles.

Vasoactive intestinal peptide (VIP) receptor is a relatively new target investigated for active pharmaceutical targeting. VIP receptors are found in high densities in human lung and breast cancers.^{174,175} VIP has been grafted to sterically stabilized micelles.^{95,176} The in-vitro internalization of VIP-grafted micelles in human MCF-7 breast cancer cells and increased cytotoxicity in drug resistant BC19/3 cells have been established. So far, in-vivo pharmacokinetics and antitumor efficacy data are still lacking, and a thorough understanding of VIP expression specificity in tumors compared to normal tissues remains to be mapped out.

Nowadays, there are existing controversies about whether the targeting ligands influence nanoparticle tumor localization or uptake. There exist conflict observations in the literature. Some studies being discussed previously in this review as well as others reported enhancement of tumor accumulation, whereas others believe that ligand only increases tumor cellular uptake instead of tumor localization. Pirollo et al. proposed explanations for the conflict observations based on the detailed review of three studies.¹⁷⁷ Their hypothesis is that the presence or absence of PEG makes a difference. In the works of Barlette et al.¹⁷⁸ and Kirpotin et al.¹⁷⁹, they used PEGylated nanoparticles with or without target ligands. PEGylation already achieved great improvement of nanoparticle circulation time which in turn increases tumor accumulation by the EPR effect so that further increase in tumor localization attributed to active ligand is masked. Conversely, when PEG chains are absent as in the reports of Wu et al.,¹⁸⁰ the contrast becomes more apparent. However, the PEG theory does not

apply to many other cases. Hussain et al. reported a 2-fold tumor accumulation of EpCAM-targeted liposomes over non-targeted liposomes loaded with doxorubicin in mice bearing SW2 tumor xenografts.¹⁸¹ In this study, both targeted and non-targeted liposomes are PEGylated. For some nano-delivery systems, active target ligand alters nanoparticle surface property so that the clearance is reduced. It was reported that the transferrin on the surface of positively charged polymeric nanoparticles shielded some charges so that the elimination associated with the non-specific interactions was decreased and passive targeting was increased.¹⁸² It seems that the so-called “active targeting” is not that the ligand on the nanoparticles actively searches for its target in the circulation and directs the localization of its cargo; instead, active targeting is essentially an EPR effect with reinforced retention effect due to the ligand-target binding. Whether targeting ligand truly enhances active targeting nanoparticle tumor localization is a very complicated issue. In addition to PEGylation and nanoparticle surface properties, other factors such as target ligand type and property, ligand-target interaction and tumor type also play critical roles in this issue. To date there is no single theory that can be generalized to all observation conflicts. Comprehensive researches are definitely needed for a more complete understanding. Despite the controversy about target ligand’s essential function, enhanced therapeutic efficacy with targeted nanoparticles is commonly reported. The improvement of anticancer efficacy is explained by 1) active targeting ligand mediates endocytosis thus increases cellular accumulation of anticancer agents, and 2) some active targeting antibodies carry

anticancer activity by their own such as anti-EGFR antibody. The ligand-mediated endocytosis is particularly important for nucleotide (e.g., siRNA, oligonucleotide) delivery.

Inclusion of active targeting moieties in nano-formulations renders enhanced specificity and selectivity for delivery of anticancer agents to tumors. However, a great deal of effort still needs to be made to address many issues such as immunogenicity, toxicity, cost, scale-up difficulties particularly for antibody-based active targeting.

4. Advantages and disadvantages of lipid-based nanoparticles compared to other nano-delivery systems

Polymeric nanoparticles are another major class of nano-based system for taxane delivery. Because polymeric materials are synthetic, they can be designed to offer a more versatile structure and more functionality for linking various ligands to the surface of the colloidal systems. To date in the literature, more active targeting researches use polymeric nanoparticles as compared to lipid-based nanoparticles. One of the potential reasons is the higher stability of the targeting ligands on the polymeric nanoparticles both in-vitro and in-vivo over lipid-based nanoparticles. Polymeric micelles compared to conventional lipid micelles, are more stable due to their lower CMC. However, polymeric nanoparticles still lack a suitable and cost-efficient scale-up production method; while large scale production methods of lipid-based nanoparticles such as liposomes and SLNs are readily available. Lipid nanoparticles are generally

less toxic than polymeric systems attributed to their natural property.¹⁸³ A comparative study demonstrated that the highest toxicity was observed for the faster degrading polymers, low molecular weight PLA and PLGA, and the least toxic effects were observed for SLNs.¹⁸⁴ The toxicity may partly attribute to the acidic degradation products by these polymers.¹⁸⁵ In addition, the preparation of polymeric nanoparticles almost always involves organic solvent which causes more production and toxicity issues. Most of the dendrimer carriers covalently graft taxanes to their surface functional groups.^{186,187} Very few of them physically solubilize taxanes.¹⁸⁸ As a special type of polymer, dendrimers share the disadvantages of other polymers. Moreover, the covalent conjugation makes dendrimer carrier production even more complicated and difficult to scale up.

Natural macromolecules account for another class of taxane delivery nano-carriers. The currently marketed paclitaxel formulation Abraxane employs the most abundant plasma protein albumin as a delivery vehicle. The details of its advantages and disadvantages have been discussed in the previous sections. Lipoproteins including native and synthetic LDL and HDL (high-density lipoprotein) have been used for taxane delivery.¹⁸⁹⁻¹⁹¹ As endogenous carriers for lipids, lipoproteins have high biocompatibility, relatively long circulation half-life and functional capacity to deliver hydrophobic drugs.¹⁹² LDL and HLD also have intrinsic targeting properties to LDL or HDL receptors which are overexpressed in various malignant cells and tumors.^{193,194} Enhanced targeting can also be obtained by conjugating targeting

ligands.¹⁹⁵ However, native paclitaxel-LDL complexes were proven to be unstable in the presence of human plasma.¹⁹¹ More importantly, the availability of lipoproteins is limited because of the difficulty in isolating native LDL/HDL or isolating apolipoproteins for the reconstitution of synthetic lipoproteins. As a result, production scale-up is challenging and cost is too high. The lipoprotein delivery system is still in their early development phase. Important safety issues such as immunogenicity have not been systematically investigated. Alternatively, the LDL-mimicking nano-emulsions without the protein component or using peptides replacing the binding function of apolipoprotein B-100 were developed.^{109,113} These lipid-based nanoparticles can be viewed as an evolution of lipoprotein-based formulations.

In addition to these major types of nanoparticles, there are other minor classes of nanoparticles designed and investigated for the delivery of taxanes as well. One of the examples is inorganic nanoparticles including silica nanoparticles, gold nanoparticles, magnetic nanoparticles, and quantum dots, as well as others.¹⁹⁶ The surface of these nanoparticles is usually physically or chemically modified or functionalized. Except for porous silica nanoparticles which incorporate hydrophobic drug into their interior pores, most of the inorganic nanoparticles covalently conjugate taxane to their functionalized surface.¹⁹⁷⁻²⁰¹ Besides their small, uniform and tunable particle sizes, another major advantage of these nanoparticles is their multi-functionality. The gold nanoparticles, magnetic nanoparticles, and quantum dots are capable of delivering anticancer agents with simultaneous optical imaging and localization of tumors. An obvious drawback of

these inorganic nanoparticles is their relatively low biocompatibility as compared to lipid-based nanoparticles. Researchers are working on the improvement of their biocompatibility by approaches like modifying the nanoparticles with a lipid coating.²⁰²

5. Future perspective

Drug delivery is a highly interdisciplinary research field. The advances in material science, molecular biology and tumor biology facilitate the development of innovative nano-carriers with the potential to achieve the criteria for an “ideal” nano-delivery system.

It has been proposed by clinical oncologists that to achieve the maximal anticancer effect, therapies that hit as many potential targets or pathways as possible are desirable because cancer cells are a population of highly heterogeneous cells. Hence, a delivery system capable of delivering combination of multiple anticancer agents, such as cytotoxic drugs, drugs targeting specific biomarkers, radiotherapeutics, vaccines, and even siRNA, is the future direction that researchers should definitely keep pursuing. Diagnostic probes can also be incorporated either on the surface or entrapped in the nanoparticles to achieve multiple functions. Co-delivery of anticancer agents and highly sensitive diagnostic probe may enable an early detection of drug response or resistance and an early evaluation of benefit/risk ratio of current therapy which makes prompt regimen adjustment and individualized medication possible.

Identifying novel targets and ligands with more specificity relies on the advances in molecular biology and would benefit active taxane targeting delivery. For example, the evolution of antibody-type ligand apparently brings benefits to active targeting. Early development of antibodies derived from animals causes high immunogenicity. Later, chimeric antibodies, completely humanized antibodies, Fab', and single chain variable fragment were developed so that not only the issue of immunogenicity was substantially reduced, but also the size of ligand was significantly smaller which favors nano-formulations as a whole. More recently, a new generation of binding ligands such as monobodies, affibodies, heptameric binding domains have been developed for basic research while at the same time attract increasing interests for the application in active pharmaceutical delivery due to their high binding affinity and potentially low immunogenicity. Moreover, identifying more specifically expressed target such as receptors, integrins and enzymes in pathological tissues is also going to facilitate the development of active targeted therapeutics with more specificity.

To date, parenteral infusion of taxanes is the only administration route used in the clinic. The development of oral dosage form for taxanes is impeded by their toxicity to rapidly proliferating intestinal epithelium. Although several studies have demonstrated enhanced bioavailability of taxanes facilitated by lipid-based nano-formulations, a great deal of efforts is needed to minimize the drug-associated GI toxicity as well as carrier-associated toxicity before oral taxane administration becomes feasible. Central nervous system (CNS) delivery has always been a great challenge due

to the low permeability of BBB. The advances of delivering chemotherapy across BBB for the treatment of brain tumor are still very limited and nanotechnology is holding the promise for a breakthrough in this field.

Environmentally responsive drug delivery systems in response to temperature, pH, ionic strength, enzyme, or oxidative/reductive environment offer great advantages in drug delivery. The unique physiology of solid tumors such as slightly acidic pH, hypoxia in most solid tumors, and overexpression of some enzymes (e.g., sialidase, matrix metalloproteinase) provide great opportunity for the design of environmentally responsive drug delivery systems to specifically release taxanes in tumor site. However, these types of “smart” delivery systems mainly take advantage of unique physico-chemical properties of polymeric materials. Since many lipid-based delivery systems such as nanocapsules and core/shell nanoparticles are hybrid of lipid and polymeric carriers, the idea of environmentally responsive delivery also has the potential to be integrated to lipid-based nano-delivery systems. Alternatively, taxanes themselves can be modified to prodrugs with environmentally responsive linkers.

Taxane, as one of the most potent cytotoxic anticancer agents in clinic, has to be delivered efficiently, specifically and safely. Nano-formulations are a rapid-developing field. All current-reported nano-formulations have improved some aspects of taxane delivery to some extent. However, there are still noticeable gaps and a great deal of efforts has to be devoted to approach the “ideal” taxane delivery system.

6. Research hypotheses

The research was guided by three hypotheses:

Hypothesis #1: Oil-filled NPs prepared from oil-in-water microemulsion precursors can be used to formulate DX efficiently.

Hypothesis #2: DX-lipid conjugate can be stably retained in oil-filled NPs in-vitro and in-vivo.

Hypothesis #3: Bromoacyl DX-lipid conjugate can improve the hydrolysis kinetics and the overall therapeutic index of DX.

Table 1.1. Similarities and differences between paclitaxel and docetaxel

Similarity	Difference
Structure taxane skeleton	Structure Paclitaxel, 10-acetyl group, 3'-benzamide phenyl group Docetaxel, 10-OH, 3'-OC(CH ₃) ₃
Pharmacological mechanism Inhibition of microtubule depolymerization	Water solubility Paclitaxel, 0.35-0.7 µg/mL Docetaxel, 3-25 µg/mL Uptake and efflux Docetaxel 3-fold higher uptake and 3-fold slower efflux than paclitaxel Microtubule binding affinity Docetaxel 1.9-fold higher than paclitaxel Anticancer potency Docetaxel about twice as potent as paclitaxel in-vitro and in-vivo Pharmacokinetics Paclitaxel, nonlinear Docetaxel, linear up to 115 mg/m ²

Table 1.2. Similarities and differences between nano-emulsions and micro-emulsions

	Similarity	
Appearance	Transparent or translucent	
Size	In the nano-scale range	
Structure	Spherical nano-scaled droplets dispersed in a continuous phase	
	Difference	
	Nano-emulsion	Micro-emulsion
Stability	Kinetically stable	Thermodynamically stable
Preparation	Energy is required High-energy methods: high-pressure homogenization, ultrasonication low-energy methods: PIT method, “spontaneous” emulsification	Energy is not required Spontaneously formed in the micro-emulsion forming domain of ternary phase diagram, mechanical stirring or heating may accelerate the equilibrium
Destabilization mechanism	Oswald ripening	Dilution and temperature
Application	Parenteral drug delivery among others	Oral and topical delivery, not suitable for parenteral delivery

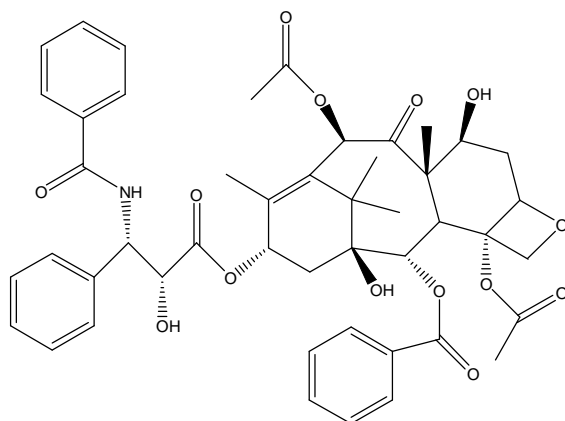
Table 1.3. Major advantages and disadvantages of each type of lipid-based nanoparticles

	Advantages	Disadvantages
Liposomes	Mature production engineering and scale-up techniques, capable of encapsulate both lipophilic and hydrophilic molecules	Drug leakage, low loading capacity to lipophilic drugs
Micelles	Easy production	Relatively low drug loading capacity, potential dissociation upon dilution
Nano-emulsions	High drug loading capacity, versatile chemistry	Relatively low stability and drug retention
Solid lipid nanoparticles	Ease of preparation and scale-up with low cost, good physical stability, controlled drug release, versatile chemistry	Potential of drug expulsion and burst release
Nanocapsules	High drug loading capacity, good drug retention, high stability	Low entrapment efficiency of polymer-shelled nanocapsules
Core/shell nanoparticles	High drug loading capacity, high stability, controlled drug release, temporal co-delivery of a secondary drug	Involvement of organic solvent during preparation, potential toxicity associated with polymers

Table 1.4. Advantages and disadvantages of lipid-based nanoparticles compared to other nano-based delivery systems

	Advantages	Disadvantages
Lipid-based nanoparticles	High biocompatibility	Low CMC of lipid micelles
Polymeric nanoparticles	More versatile chemistry and more functionality, More stable active ligand incorporation	Higher toxicity, organic solvent involvement during preparation, scale-up difficulty
Natural macromolecules	High biocompatibility, functional capacity to deliver hydrophobic drugs, intrinsic targeting property	Production difficulty, high cost
Inorganic nanoparticles	Simultaneous optical imaging	Low biocompatibility

(A)



(B)

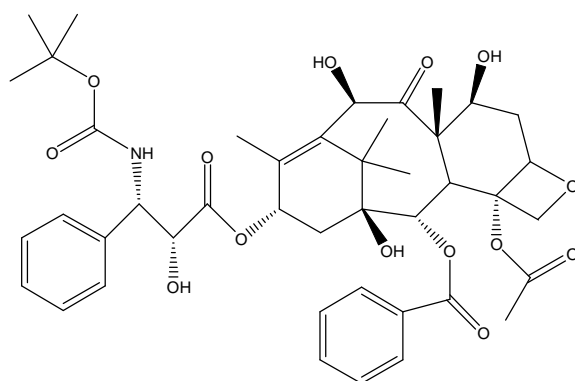


Figure 1.1. Structures of (A) paclitaxel and (B) docetaxel

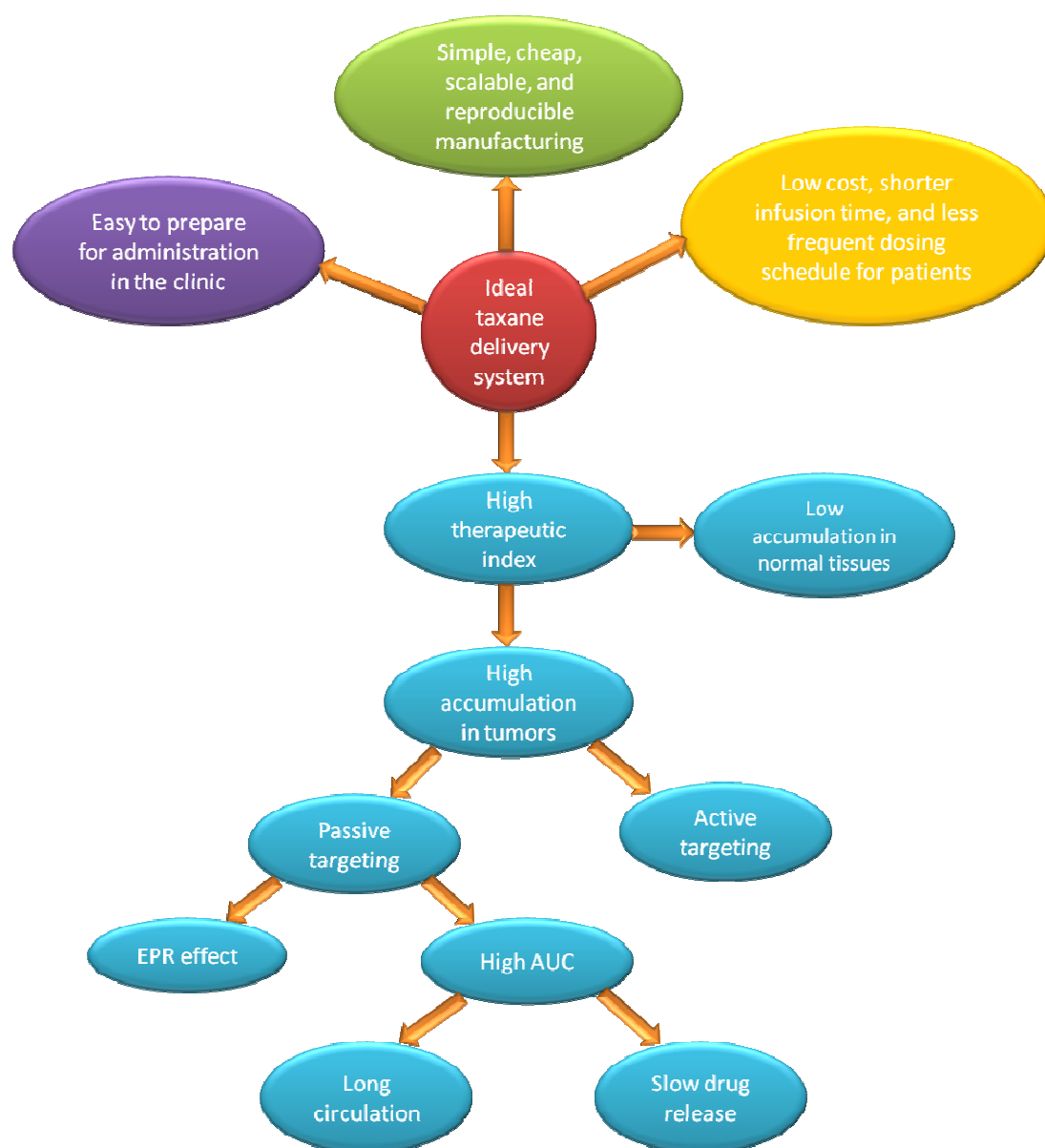


Figure 1.2. Criteria for the ideal taxane delivery system

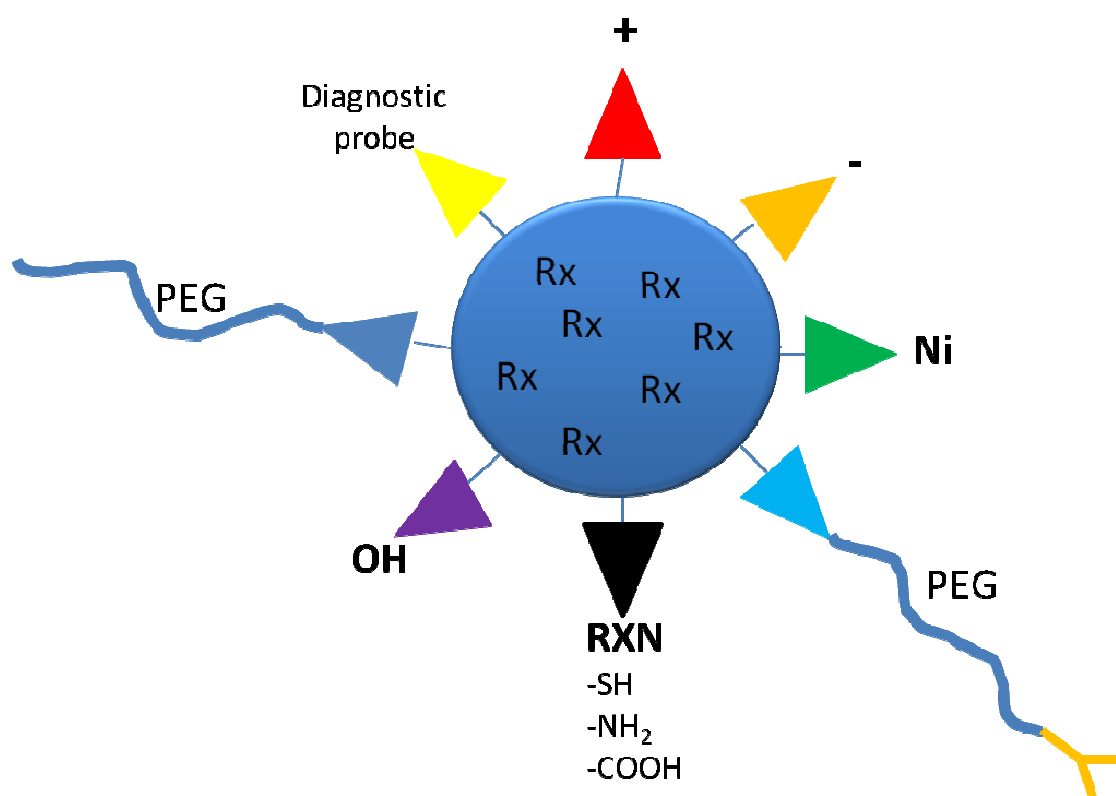


Figure 1.3. Multi-functional nanoparticles

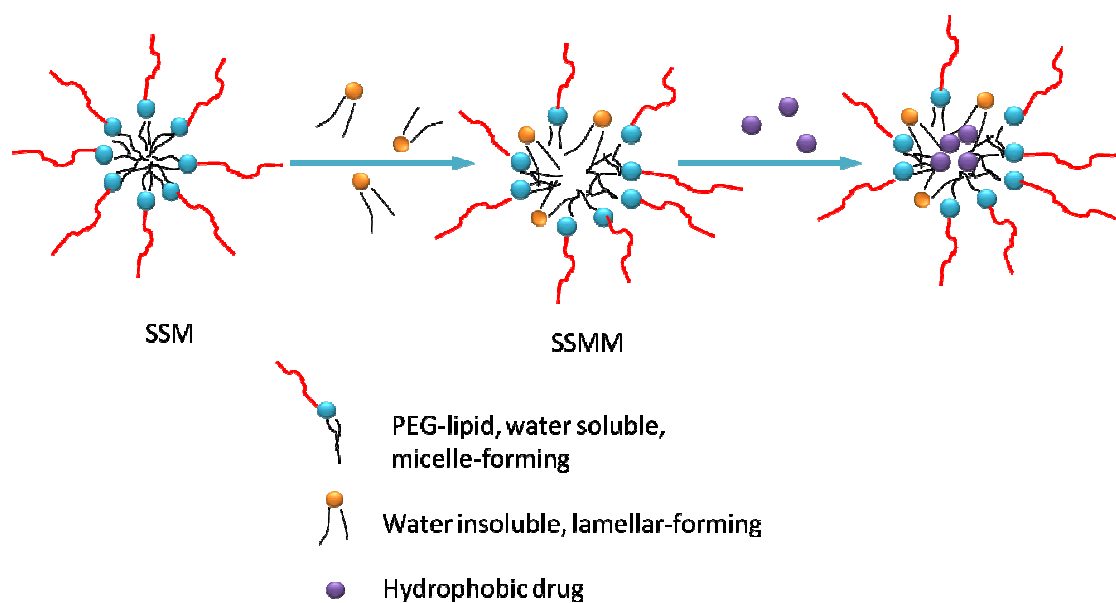


Figure 1.4. Schematic structures of sterically stabilized micelle (SSM), sterically stabilized mixed micelle (SSMM) and SSMM loaded hydrophobic drug molecules

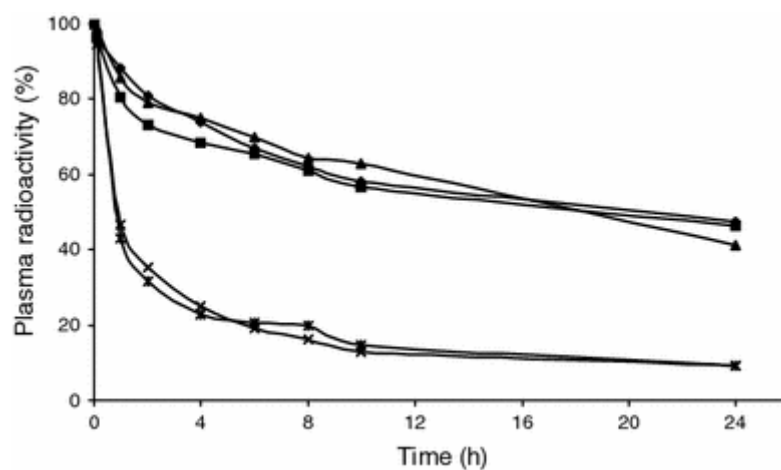


Figure 1.5. Plasma decay curve of [^3H]-paclitaxel-oleate in LDL-resembling nano-emulsion (three patients, filled diamond, triangle and square) and [^3H]-paclitaxel in CrEL (two patients, multi symbol, asterisk) following i.v. bolus injection. Reprinted from Ref [112] with permission.

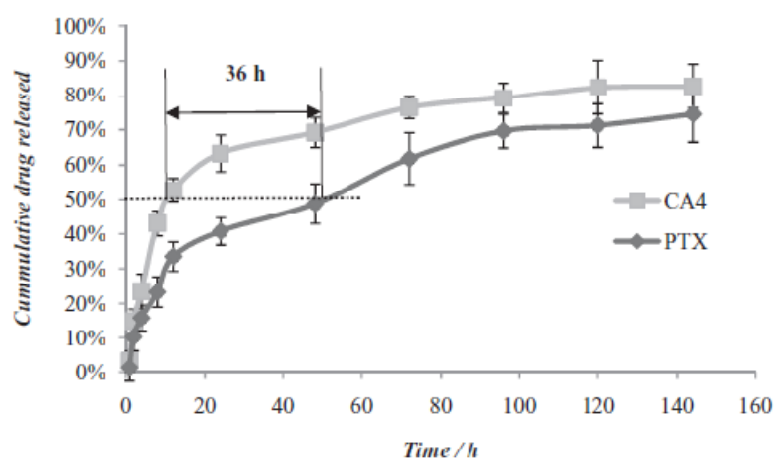


Figure 1.6. In-vitro temporal release of paclitaxel (PTX) and combretastatin A4 (CA4) from core/shell nanocapsules. Reprinted from Ref [156] with permission.

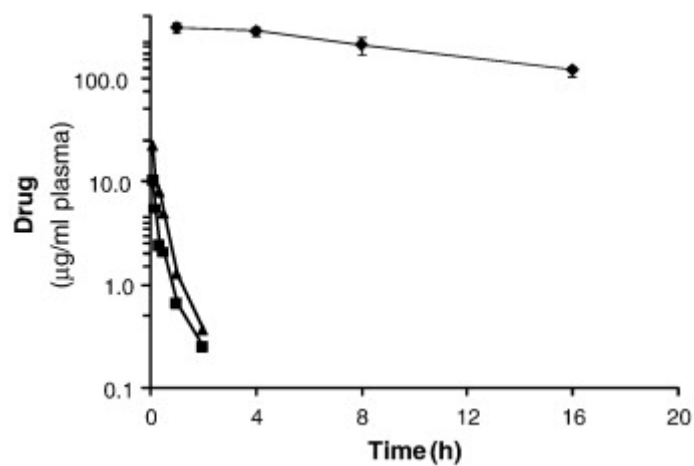


Figure 1.7. Plasma concentration-time curves for Taxotere (triangle), docetaxel derivative formulated in Taxotere vehicle (square), and docetaxel derivative formulated in DSPC/Chol liposome (diamond). Reprinted from Ref [163] with permission.

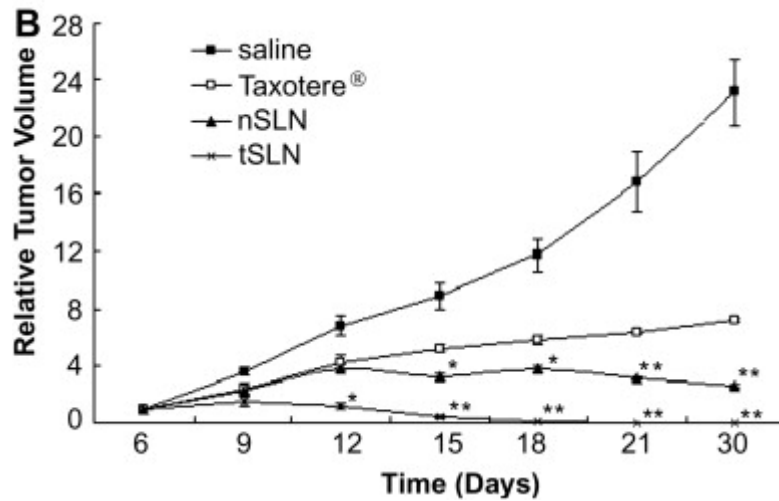


Figure 1.8. Antitumor efficacy of targeted SLN (tSLN), non-targeted SLN (nSLN), Taxotere or saline on nude mice bearing hepatoma after a schedule of multiple doses (10 mg docetaxel/kg once a week for three weeks). Data are presented as mean \pm SD (n=5-6). Reprinted from Ref [171] with permission.

References

1. Cortes JE, Pazdur R. Docetaxel. *J Clin Oncol*. Oct 1995;13(10):2643-2655.
2. Colin M GD, Gueritte-Voegelein F, et al, Inventor. Taxol derivatives, their preparation and pharmaceutical compositions containing them. US patent 48144701986.
3. Guenard D, Gueritte-Voegelein F, Dubois J, Potier P. Structure-activity relationships of Taxol and Taxotere analogues. *J Natl Cancer Inst Monogr*. 1993(15):79-82.
4. Hamada H, Ishihara K, Masuoka N, Mikuni K, Nakajima N. Enhancement of water-solubility and bioactivity of paclitaxel using modified cyclodextrins. *J Biosci Bioeng*. Oct 2006;102(4):369-371.
5. Mathew AE, Mejillano MR, Nath JP, Himes RH, Stella VJ. Synthesis and Evaluation of Some Water-Soluble Prodrugs and Derivatives of Taxol with Antitumor-Activity. *J Med Chem*. Jan 10 1992;35(1):145-151.
6. Du W, Hong L, Yao T, et al. Synthesis and evaluation of water-soluble docetaxel prodrugs-docetaxel esters of malic acid. *Bioorg Med Chem*. Sep 15 2007;15(18):6323-6330.
7. Ali SM, Hoemann MZ, Aube J, Georg GI, Mitscher LA, Jayasinghe LR. Butitaxel analogues: synthesis and structure-activity relationships. *J Med Chem*. Jan 17 1997;40(2):236-241.
8. Zaske L, Perrin MA, Leveiller F. Docetaxel: Solid state characterization by X-ray powder diffraction and thermogravimetry. *J Phys Iv*. Dec 2001;11(Pr10):221-226.
9. Schiff PB, Fant J, Horwitz SB. Promotion of microtubule assembly in vitro by taxol. *Nature*. Feb 22 1979;277(5698):665-667.
10. Ringel I, Horwitz SB. Studies with RP 56976 (taxotere): a semisynthetic analogue of taxol. *J Natl Cancer Inst*. Feb 20 1991;83(4):288-291.
11. Horwitz SB. Mechanism of action of taxol. *Trends Pharmacol Sci*. Apr 1992;13(4):134-136.
12. Guerittevoegelein F, Guenard D, Lavelle F, Legoff MT, Mangatal L, Potier P. Relationships between the Structure of Taxol Analogs and Their Antimitotic

Activity. *J Med Chem.* Mar 1991;34(3):992-998.

13. Diaz JF, Andreu JM. Assembly of Purified Gdp Tubulin into Microtubules Induced by Taxol and Taxotere - Reversibility, Ligand Stoichiometry, and Competition. *Biochemistry-US.* Mar 23 1993;32(11):2747-2755.
14. Riou JF, Naudin A, Lavelle F. Effects of Taxotere on murine and human tumor cell lines. *Biochem Biophys Res Commun.* Aug 31 1992;187(1):164-170.
15. Hanauske AR, Degen D, Hilsenbeck SG, Bissery MC, Von Hoff DD. Effects of Taxotere and taxol on in vitro colony formation of freshly explanted human tumor cells. *Anticancer Drugs.* Apr 1992;3(2):121-124.
16. Vogel M, Hilsenbeck SG, Depenbrock H, et al. Preclinical activity of taxotere (RP 56976, NSC 628503) against freshly explanted clonogenic human tumour cells: comparison with taxol and conventional antineoplastic agents. *Eur J Cancer.* 1993;29A(14):2009-2014.
17. Kelland LR, Abel G. Comparative in vitro cytotoxicity of taxol and Taxotere against cisplatin-sensitive and -resistant human ovarian carcinoma cell lines. *Cancer Chemother Pharmacol.* 1992;30(6):444-450.
18. Bissery MC, Guenard D, Gueritte-Voegelein F, Lavelle F. Experimental antitumor activity of taxotere (RP 56976, NSC 628503), a taxol analogue. *Cancer Res.* Sep 15 1991;51(18):4845-4852.
19. Riou J, Petitgenet O, Combeau C, et al. Cellular uptake and efflux of docetaxel (Taxotere) and paclitaxel (Taxol) in P388 cell line. *Proc Am Ass Cancer Res.* 1994;35:385.
20. Taxol[®] (paclitaxel) Injection. Princeton: Bristol-Myers Squibb; 2011.
21. Sonnichsen DS, Relling MV. Clinical pharmacokinetics of paclitaxel. *Clin Pharmacokinet.* Oct 1994;27(4):256-269.
22. Rowinsky EK, Wright M, Monsarrat B, Donehower RC. Clinical pharmacology and metabolism of Taxol (paclitaxel): update 1993. *Ann Oncol.* 1994;5 Suppl 6:S7-16.
23. Spencer CM, Faulds D. Paclitaxel. A review of its pharmacodynamic and pharmacokinetic properties and therapeutic potential in the treatment of cancer. *Drugs.* Nov 1994;48(5):794-847.
24. Ellis AG, Crinis NA, Webster LK. Inhibition of etoposide elimination in the isolated perfused rat liver by Cremophor EL and Tween 80. *Cancer Chemoth Pharm.* May 1996;38(1):81-87.

25. Sparreboom A, van Zuylen L, Brouwer E, et al. Cremophor EL-mediated alteration of paclitaxel distribution in human blood: clinical pharmacokinetic implications. *Cancer Res.* Apr 1 1999;59(7):1454-1457.
26. van Zuylen L, Karlsson MO, Verweij J, et al. Pharmacokinetic modeling of paclitaxel encapsulation in Cremophor EL micelles. *Cancer Chemother Pharmacol.* Apr 2001;47(4):309-318.
27. Weiss RB, Donehower RC, Wiernik PH, et al. Hypersensitivity reactions from taxol. *J Clin Oncol.* Jul 1990;8(7):1263-1268.
28. Michaud LB. Methods for preventing reactions secondary to Cremophor EL. *Ann Pharmacother.* Nov 1997;31(11):1402-1404.
29. Marupudi NI, Han JE, Li KW, Renard VM, Tyler BM, Brem H. Paclitaxel: a review of adverse toxicities and novel delivery strategies. *Expert Opin Drug Saf.* Sep 2007;6(5):609-621.
30. ABRAXANE® for Injectable Suspension. Los Angeles: Abraxis BioScience, LLC; 2009.
31. Gradishar WJ. Albumin-bound paclitaxel: a next-generation taxane. *Expert Opin Pharmacother.* Jun 2006;7(8):1041-1053.
32. Ibrahim NK, Desai N, Legha S, et al. Phase I and pharmacokinetic study of ABI-007, a Cremophor-free, protein-stabilized, nanoparticle formulation of paclitaxel. *Clin Cancer Res.* May 2002;8(5):1038-1044.
33. Minshall RD, Tiruppathi C, Vogel SM, Malik AB. Vesicle formation and trafficking in endothelial cells and regulation of endothelial barrier function. *Histochem Cell Biol.* Feb 2002;117(2):105-112.
34. Watkins G, Douglas-Jones A, Bryce R, Mansel RE, Jiang WG. Increased levels of SPARC (osteonectin) in human breast cancer tissues and its association with clinical outcomes. *Prostaglandins Leukot Essent Fatty Acids.* Apr 2005;72(4):267-272.
35. Schilling U, Friedrich EA, Sinn H, Schrenk HH, Clorius JH, Maierborst W. Design of Compounds Having Enhanced Tumor Uptake, Using Serum-Albumin as a Carrier .2. In vivo Studies. *Nucl Med Biol.* Aug 1992;19(6):685-695.
36. Sage H. Culture shock. Selective uptake and rapid release of a novel serum protein by endothelial cells in vitro. *J Biol Chem.* May 25 1986;261(15):7082-7092.
37. Taxotere® (docetaxel) Injection. Bridgewater: Sanofi-aventis, LLC; 2010.

38. Loos WJ, Baker SD, Verweij J, Boonstra JG, Sparreboom A. Clinical pharmacokinetics of unbound docetaxel: role of polysorbate 80 and serum proteins. *Clin Pharmacol Ther.* Oct 2003;74(4):364-371.
39. Engels FK, Mathot RA, Verweij J. Alternative drug formulations of docetaxel: a review. *Anticancer Drugs.* Feb 2007;18(2):95-103.
40. Baker SD, Li J, ten Tije AJ, et al. Relationship of systemic exposure to unbound docetaxel and neutropenia. *Clin Pharmacol Ther.* Jan 2005;77(1):43-53.
41. Bissery M, Renard A, Andre S, et al. Preclinical pharmacology and toxicology of Taxotere (RP 56976, NSC 628503). *Ann Oncol.* 1992;3:121.
42. Bissery MC RA, Montay G, et al. Taxotere: Antitumor activity and pharmacokinetics in mice. *Proc Am Ass Cancer Res.* 1991;32:401.
43. Pinguet F, Agustin MJ, Brown P, et al. New formulation Taxotere (R) reduces preparation time and supports the physical stability of the product in infusion bags: data from the RELIUS international observational study. *Ejhp Pract.* 2010;16(3):40-43.
44. Rowinsky EK. The development and clinical utility of the taxane class of antimicrotubule chemotherapy agents. *Annu Rev Med.* 1997;48:353-374.
45. Campbell RB. Tumor physiology and delivery of nanopharmaceuticals. *Anticancer Agents Med Chem.* Nov 2006;6(6):503-512.
46. Jain RK, Stylianopoulos T. Delivering nanomedicine to solid tumors. *Nat Rev Clin Oncol.* Nov 2010;7(11):653-664.
47. Shubik P. Vascularization of tumors: a review. *J Cancer Res Clin Oncol.* 1982;103(3):211-226.
48. Hobbs SK, Monsky WL, Yuan F, et al. Regulation of transport pathways in tumor vessels: role of tumor type and microenvironment. *Proc Natl Acad Sci U S A.* Apr 14 1998;95(8):4607-4612.
49. Takakura Y, Mahato RI, Hashida M. Extravasation of macromolecules. *Adv Drug Deliv Rev.* Oct 5 1998;34(1):93-108.
50. Karakotchian M, Fraser IS. An ultrastructural study of microvascular inter-endothelial tight junctions in normal endometrium. *Micron.* 2007;38(6):632-636.
51. Hashizume H, Baluk P, Morikawa S, et al. Openings between defective endothelial cells explain tumor vessel leakiness. *Am J Pathol.* Apr 2000;156(4):1363-1380.

52. Leu AJ, Berk DA, Lymboussaki A, Alitalo K, Jain RK. Absence of functional lymphatics within a murine sarcoma: A molecular and functional evaluation. *Cancer Research*. Aug 15 2000;60(16):4324-4327.
53. Padera TP, Stoll BR, Tooredman JB, Capen D, di Tomaso E, Jain RK. Pathology: cancer cells compress intratumour vessels. *Nature*. Feb 19 2004;427(6976):695.
54. Maeda H, Wu J, Sawa T, Matsumura Y, Hori K. Tumor vascular permeability and the EPR effect in macromolecular therapeutics: a review. *J Control Release*. Mar 1 2000;65(1-2):271-284.
55. Boucher Y, Kirkwood JM, Opacic D, Desantis M, Jain RK. Interstitial hypertension in superficial metastatic melanomas in humans. *Cancer Res*. Dec 15 1991;51(24):6691-6694.
56. Sevick EM, Jain RK. Geometric resistance to blood flow in solid tumors perfused ex vivo: effects of tumor size and perfusion pressure. *Cancer Res*. Jul 1 1989;49(13):3506-3512.
57. Vijayagopal P, Figueroa JE, Levine EA. Altered composition and increased endothelial cell proliferative activity of proteoglycans isolated from breast carcinoma. *J Surg Oncol*. Aug 1998;68(4):250-254.
58. Pluen A, Boucher Y, Ramanujan S, et al. Role of tumor-host interactions in interstitial diffusion of macromolecules: cranial vs. subcutaneous tumors. *Proc Natl Acad Sci U S A*. Apr 10 2001;98(8):4628-4633.
59. Chauhan VP, Lanning RM, Diop-Frimpong B, et al. Multiscale measurements distinguish cellular and interstitial hindrances to diffusion in vivo. *Biophys J*. Jul 8 2009;97(1):330-336.
60. Alexandrakis G, Brown EB, Tong RT, et al. Two-photon fluorescence correlation microscopy reveals the two-phase nature of transport in tumors. *Nat Med*. Feb 2004;10(2):203-207.
61. Simeonova M, Ilarionova M, Ivanova T, Konstantinov C, Todorov D. Nanoparticles as drug carriers for vinblastine. Acute toxicity of vinblastine in a free form and associated to polybutylcyanoacrylate nanoparticles. *Acta Physiol Pharmacol Bulg*. 1991;17(4):43-49.
62. Souza LG, Silva EJ, Martins AL, et al. Development of topotecan loaded lipid nanoparticles for chemical stabilization and prolonged release. *Eur J Pharm Biopharm*. Sep 2011;79(1):189-196.
63. Yang SC, Zhu JB. Preparation and characterization of camptothecin solid lipid nanoparticles. *Drug Dev Ind Pharm*. 2002;28(3):265-274.

64. Lim SJ, Lee MK, Kim CK. Altered chemical and biological activities of all-trans retinoic acid incorporated in solid lipid nanoparticle powders. *J Control Release*. Nov 5 2004;100(1):53-61.
65. Williams J, Lansdown R, Sweitzer R, et al. Nanoparticle drug delivery system for intravenous delivery of topoisomerase inhibitors. *J Control Release*. Aug 28 2003;91(1-2):167-172.
66. Isacchi B, Arrigucci S, Marca GL, et al. Conventional and long-circulating liposomes of artemisinin: preparation, characterization, and pharmacokinetic profile in mice. *J Liposome Res*. Dec 16 2010.
67. Cole AJ, David AE, Wang J, Galban CJ, Hill HL, Yang VC. Polyethylene glycol modified, cross-linked starch-coated iron oxide nanoparticles for enhanced magnetic tumor targeting. *Biomaterials*. Mar 2011;32(8):2183-2193.
68. Kim CK, Kim JY, Kim JK, Park JS, Byun Y. The use of PEGylated liposomes to prolong circulation lifetimes of tissue plasminogen activator. *Biomaterials*. Oct 2009;30(29):5751-5756.
69. Immordino ML, Dosio F, Cattel L. Stealth liposomes: review of the basic science, rationale, and clinical applications, existing and potential. *Int J Nanomedicine*. 2006;1(3):297-315.
70. Benhabbour SR LJ, Kim D, Jain A, Wadhwa S, Parrott MC, Liu R, Desimone J, Mumper RJ. In vitro and in vivo assessment of targeting lipid-based nanoparticles to the epidermal growth factor-receptor (EGFR) using a novel Heptameric Z(EGFR) domain. *J Control Release*. 2011.
71. Patel JD, O'Carra R, Jones J, Woodward JG, Mumper RJ. Preparation and characterization of nickel nanoparticles for binding to his-tag proteins and antigens. *Pharm Res*. Feb 2007;24(2):343-352.
72. Cui Z, Patel J, Tuzova M, et al. Strong T cell type-1 immune responses to HIV-1 Tat (1-72) protein-coated nanoparticles. *Vaccine*. Jun 30 2004;22(20):2631-2640.
73. McConathy WJ, Nair MP, Paranjape S, Mooberry L, Lacko AG. Evaluation of synthetic/reconstituted high-density lipoproteins as delivery vehicles for paclitaxel. *Anti-Cancer Drug*. Feb 2008;19(2):183-188.
74. Straubinger RM, Balasubramanian SV. Preparation and characterization of taxane-containing liposomes. *Methods Enzymol*. 2005;391:97-117.
75. Sharma A, Straubinger RM. Novel taxol formulations: preparation and characterization of taxol-containing liposomes. *Pharm Res*. Jun 1994;11(6):889-896.

76. Campbell RB, Balasubramanian SV, Straubinger RM. Influence of cationic lipids on the stability and membrane properties of paclitaxel-containing liposomes. *J Pharm Sci.* Aug 2001;90(8):1091-1105.
77. Sharma A, Mayhew E, Straubinger RM. Antitumor effect of taxol-containing liposomes in a taxol-resistant murine tumor model. *Cancer Res.* Dec 15 1993;53(24):5877-5881.
78. Zhang JA, Anyarambhatla G, Ma L, et al. Development and characterization of a novel Cremophor EL free liposome-based paclitaxel (LEP-ETU) formulation. *Eur J Pharm Biopharm.* Jan 2005;59(1):177-187.
79. Balasubramanian SV, Alderfer JL, Straubinger RM. Solvent- and concentration-dependent molecular interactions of taxol (Paclitaxel). *J Pharm Sci.* Oct 1994;83(10):1470-1476.
80. Balasubramanian SV, Straubinger RM. Taxol-lipid interactions: taxol-dependent effects on the physical properties of model membranes. *Biochemistry-Us.* Aug 2 1994;33(30):8941-8947.
81. Crosasso P, Ceruti M, Brusa P, Arpicco S, Dosio F, Cattel L. Preparation, characterization and properties of sterically stabilized paclitaxel-containing liposomes. *J Control Release.* Jan 3 2000;63(1-2):19-30.
82. Ishida T, Ichihara M, Wang X, Kiwada H. Spleen plays an important role in the induction of accelerated blood clearance of PEGylated liposomes. *J Control Release.* Oct 27 2006;115(3):243-250.
83. Sharma A, Mayhew E, Bolcsak L, et al. Activity of paclitaxel liposome formulations against human ovarian tumor xenografts. *Int J Cancer.* Mar 28 1997;71(1):103-107.
84. Sharma A, Sharma US, Straubinger RM. Paclitaxel-liposomes for intracavitary therapy of intraperitoneal P388 leukemia. *Cancer Lett.* Oct 22 1996;107(2):265-272.
85. Cabanes A, Briggs KE, Gokhale PC, Treat JA, Rahman A. Comparative in vivo studies with paclitaxel and liposome-encapsulated paclitaxel. *Int J Oncol.* May 1998;12(5):1035-1040.
86. Schmitt-Sody M, Strieth S, Krasnici S, et al. Neovascular targeting therapy: paclitaxel encapsulated in cationic liposomes improves antitumoral efficacy. *Clin Cancer Res.* Jun 2003;9(6):2335-2341.
87. Soepenbergh O, Sparreboom A, de Jonge MJ, et al. Real-time pharmacokinetics guiding clinical decisions; phase I study of a weekly schedule of liposome encapsulated paclitaxel in patients with solid tumours. *Eur J Cancer.* Mar

2004;40(5):681-688.

88. Arleth L, Ashok B, Onyuksel H, Thiyagarajan P, Jacob J, Hjelm RP. Detailed structure of hairy mixed micelles formed by phosphatidylcholine and PEGylated phospholipids in aqueous media. *Langmuir*. Apr 12 2005;21(8):3279-3290.
89. Mu L, Elbayoumi TA, Torchilin VP. Mixed micelles made of poly(ethylene glycol)-phosphatidylethanolamine conjugate and D-alpha-tocopheryl polyethylene glycol 1000 succinate as pharmaceutical nanocarriers for camptothecin. *Int J Pharmaceut*. Dec 8 2005;306(1-2):142-149.
90. Vakil R, Kwon GS. Effect of cholesterol on the release of amphotericin B from PEG-phospholipid micelles. *Mol Pharm*. Jan-Feb 2008;5(1):98-104.
91. Ashok B, Arleth L, Hjelm RP, Rubinstein I, Onyuksel H. In vitro characterization of PEGylated phospholipid micelles for improved drug solubilization: effects of PEG chain length and PC incorporation. *J Pharm Sci*. Oct 2004;93(10):2476-2487.
92. Lim SB, Rubinstein I, Onyuksel H. Freeze drying of peptide drugs self-associated with long-circulating, biocompatible and biodegradable sterically stabilized phospholipid nanomicelles. *Int J Pharm*. May 22 2008;356(1-2):345-350.
93. La SB, Okano T, Kataoka K. Preparation and characterization of the micelle-forming polymeric drug indomethacin-incorporated poly(ethylene oxide)-poly(beta-benzyl L-aspartate) block copolymer micelles. *J Pharm Sci*. Jan 1996;85(1):85-90.
94. Krishnadas A, Rubinstein I, Onyuksel H. Sterically stabilized phospholipid mixed micelles: in vitro evaluation as a novel carrier for water-insoluble drugs. *Pharm Res*. Feb 2003;20(2):297-302.
95. Onyuksel H, Jeon E, Rubinstein I. Nanomicellar paclitaxel increases cytotoxicity of multidrug resistant breast cancer cells. *Cancer Lett*. Feb 18 2009;274(2):327-330.
96. Dabholkar RD, Sawant RM, Mongayt DA, Devarajan PV, Torchilin VP. Polyethylene glycol-phosphatidylethanolamine conjugate (PEG-PE)-based mixed micelles: some properties, loading with paclitaxel, and modulation of P-glycoprotein-mediated efflux. *Int J Pharm*. Jun 6 2006;315(1-2):148-157.
97. Sawant RR, Torchilin VP. Multifunctionality of lipid-core micelles for drug delivery and tumour targeting. *Mol Membr Biol*. Oct 2010;27(7):232-246.
98. Lukyanov AN, Gao Z, Mazzola L, Torchilin VP. Polyethylene

glycol-diacyllipid micelles demonstrate increased accumulation in subcutaneous tumors in mice. *Pharm Res.* Oct 2002;19(10):1424-1429.

99. Anton N, Vandamme TF. Nano-emulsions and micro-emulsions: clarifications of the critical differences. *Pharm Res.* May 2011;28(5):978-985.
100. Lawrence MJ, Rees GD. Microemulsion-based media as novel drug delivery systems. *Adv Drug Deliver Rev.* Dec 6 2000;45(1):89-121.
101. C. Solans PI, J. Nolla, N. Azemar, M.J. Garcia-Celma. Nano-emulsions. *Current Opinion in Colloid & Interface Science.* 2005;10:102-110.
102. Tarr BD, Sambandan TG, Yalkowsky SH. A new parenteral emulsion for the administration of taxol. *Pharm Res.* Apr 1987;4(2):162-165.
103. Constantinides PP, Lambert KJ, Tustian AK, et al. Formulation development and antitumor activity of a filter-sterilizable emulsion of paclitaxel. *Pharm Res.* Feb 2000;17(2):175-182.
104. Constantinides PP, Tustian A, Kessler DR. Tocol emulsions for drug solubilization and parenteral delivery. *Adv Drug Deliv Rev.* May 7 2004;56(9):1243-1255.
105. K. Gao JS, K. Liu, XH. Liu, and ZG. He. Preparation and Characterization of a Submicron lipid Emulsion of Docetaxel: Submicron Lipid Emulsion of Docetaxel. *Drug Dev Ind Pharm.* 2008;34:1227-1237.
106. Kan P, Chen ZB, Lee CJ, Chu IM. Development of nonionic surfactant/phospholipid o/w emulsion as a paclitaxel delivery system. *J Control Release.* Apr 19 1999;58(3):271-278.
107. Tiwari SB, Amiji MM. Improved oral delivery of paclitaxel following administration in nanoemulsion formulations. *J Nanosci Nanotechnol.* Sep-Oct 2006;6(9-10):3215-3221.
108. Yin YM, Cui FD, Mu CF, et al. Docetaxel microemulsion for enhanced oral bioavailability: preparation and in vitro and in vivo evaluation. *J Control Release.* Dec 3 2009;140(2):86-94.
109. Maranhao RC, Garicochea B, Silva EL, et al. Plasma kinetics and biodistribution of a lipid emulsion resembling low-density lipoprotein in patients with acute leukemia. *Cancer Res.* Sep 1 1994;54(17):4660-4666.
110. Rodrigues DG, Maria DA, Fernandes DC, et al. Improvement of paclitaxel therapeutic index by derivatization and association to a cholesterol-rich microemulsion: in vitro and in vivo studies. *Cancer Chemother Pharmacol.* Jun 2005;55(6):565-576.

111. Dias ML, Carvalho JP, Rodrigues DG, Graziani SR, Maranhao RC. Pharmacokinetics and tumor uptake of a derivatized form of paclitaxel associated to a cholesterol-rich nanoemulsion (LDE) in patients with gynecologic cancers. *Cancer Chemother Pharmacol.* Jan 2007;59(1):105-111.
112. Pires L, Hegg R, Valduga C, Graziani S, Rodrigues D, Maranhao RC. Use of cholesterol-rich nanoparticles that bind to lipoprotein receptors as a vehicle to paclitaxel in the treatment of breast cancer: pharmacokinetics, tumor uptake and a pilot clinical study. *Cancer Chemoth Pharm.* Jan 2009;63(2):281-287.
113. Nikanjarn M, Gibbs AR, Hunt A, Budinger TF, Forte TM. Synthetic nano-LDL with paclitaxel oleate as a targeted drug delivery vehicle for glioblastoma multiforme. *Journal of Controlled Release.* Dec 20 2007;124(3):163-171.
114. Wissing SA, Kayser O, Muller RH. Solid lipid nanoparticles for parenteral drug delivery. *Adv Drug Deliv Rev.* May 7 2004;56(9):1257-1272.
115. Muller RH, Mader K, Gohla S. Solid lipid nanoparticles (SLN) for controlled drug delivery - a review of the state of the art. *Eur J Pharm Biopharm.* Jul 2000;50(1):161-177.
116. Jennings V, Lippacher A, Gohla SH. Medium scale production of solid lipid nanoparticles (SLN) by high pressure homogenization. *J Microencapsul.* Jan-Feb 2002;19(1):1-10.
117. Dingler A, Gohla S. Production of solid lipid nanoparticles (SLN): scaling up feasibilities. *J Microencapsul.* Jan-Feb 2002;19(1):11-16.
118. Oyewumi MO, Mumper RJ. Gadolinium-loaded nanoparticles engineered from microemulsion templates. *Drug Dev Ind Pharm.* Mar 2002;28(3):317-328.
119. Chen DB, Yang TZ, Lu WL, Zhang Q. In vitro and in vivo study of two types of long-circulating solid lipid nanoparticles containing paclitaxel. *Chem Pharm Bull (Tokyo).* Nov 2001;49(11):1444-1447.
120. Lee MK, Lim SJ, Kim CK. Preparation, characterization and in vitro cytotoxicity of paclitaxel-loaded sterically stabilized solid lipid nanoparticles. *Biomaterials.* Apr 2007;28(12):2137-2146.
121. Dong XW, Mattingly CA, Tseng M, Cho M, Adams VR, Mumper RJ. Development of new lipid-based paclitaxel nanoparticles using sequential simplex optimization. *Eur J Pharm Biopharm.* May 2009;72(1):9-17.
122. Shenoy VS, Rajyaguru TH, Gude RP, Murthy RS. Studies on paclitaxel-loaded glyceryl monostearate nanoparticles. *J Microencapsul.* Sep 2009;26(6):471-478.

123. Cavalli R, Caputo O, Gasco MR. Preparation and characterization of solid lipid nanospheres containing paclitaxel. *Eur J Pharm Sci.* 2000;10(4):305-309.
124. Shahgaldian P, Da Silva E, Coleman AW, Rather B, Zaworotko MJ. Para-acyl-calix-arene based solid lipid nanoparticles (SLNs): a detailed study of preparation and stability parameters. *Int J Pharm.* Mar 6 2003;253(1-2):23-38.
125. Westesen K, Bunjes H, Koch MHJ. Physicochemical characterization of lipid nanoparticles and evaluation of their drug loading capacity and sustained release potential. *Journal of Controlled Release.* Oct 13 1997;48(2-3):223-236.
126. Arica Yegin B, Benoit JP, Lamprecht A. Paclitaxel-loaded lipid nanoparticles prepared by solvent injection or ultrasound emulsification. *Drug Dev Ind Pharm.* Oct 2006;32(9):1089-1094.
127. zur Muhlen A, Schwarz C, Mehnert W. Solid lipid nanoparticles (SLN) for controlled drug delivery--drug release and release mechanism. *Eur J Pharm Biopharm.* Mar 1998;45(2):149-155.
128. Muhlen A, Mehnert W. Drug release and release mechanism of prednisolone loaded solid lipid nanoparticles. *Pharmazie.* 1998;53:552.
129. Muller RH, Radtke M, Wissing SA. Nanostructured lipid matrices for improved microencapsulation of drugs. *Int J Pharm.* Aug 21 2002;242(1-2):121-128.
130. Yuan H, Miao J, Du YZ, You J, Hu FQ, Zeng S. Cellular uptake of solid lipid nanoparticles and cytotoxicity of encapsulated paclitaxel in A549 cancer cells. *Int J Pharm.* Feb 4 2008;348(1-2):137-145.
131. Dong X, Mattingly CA, Tseng MT, et al. Doxorubicin and paclitaxel-loaded lipid-based nanoparticles overcome multidrug resistance by inhibiting P-glycoprotein and depleting ATP. *Cancer Res.* May 1 2009;69(9):3918-3926.
132. Koziara JM, Oh JJ, Akers WS, Ferraris SP, Mumper RJ. Blood compatibility of cetyl alcohol/polysorbate-based nanoparticles. *Pharm Res.* Nov 2005;22(11):1821-1828.
133. Wang JX, Sun X, Zhang ZR. Enhanced brain targeting by synthesis of 3',5'-dioctanoyl-5-fluoro-2'-deoxyuridine and incorporation into solid lipid nanoparticles. *European Journal of Pharmaceutics and Biopharmaceutics.* Nov 2002;54(3):285-290.
134. Fundaro A, Cavalli R, Bargoni A, Vighetto D, Zara GP, Gasco MR. Non-stealth and stealth solid lipid nanoparticles (SLN) carrying doxorubicin: pharmacokinetics and tissue distribution after i.v. administration to rats. *Pharmacol Res.* Oct 2000;42(4):337-343.

135. Zara GP, Cavalli R, Bargoni A, Fundaro A, Vighetto D, Gasco MR. Intravenous administration to rabbits of non-stealth and stealth doxorubicin-loaded solid lipid nanoparticles at increasing concentrations of stealth agent: pharmacokinetics and distribution of doxorubicin in brain and other tissues. *J Drug Target.* Jun 2002;10(4):327-335.
136. Zara GP, Cavalli R, Fundaro A, Bargoni A, Caputo O, Gasco MR. Pharmacokinetics of doxorubicin incorporated in solid lipid nanospheres (SLN). *Pharmacol Res.* Sep 1999;40(3):281-286.
137. Yang SC, Lu LF, Cai Y, Zhu JB, Liang BW, Yang CZ. Body distribution in mice of intravenously injected camptothecin solid lipid nanoparticles and targeting effect on brain. *J Control Release.* Jun 2 1999;59(3):299-307.
138. Harivardhan Reddy L, Sharma RK, Chuttani K, Mishra AK, Murthy RS. Influence of administration route on tumor uptake and biodistribution of etoposide loaded solid lipid nanoparticles in Dalton's lymphoma tumor bearing mice. *J Control Release.* Jul 20 2005;105(3):185-198.
139. Koziara JM, Lockman PR, Allen DD, Mumper RJ. Paclitaxel nanoparticles for the potential treatment of brain tumors. *J Control Release.* Sep 30 2004;99(2):259-269.
140. Landfester K. Polyreactions in miniemulsions. *Abstr Pap Am Chem S.* Aug 18 2002;224:U500-U500.
141. Rollot JM, Couvreur P, Roblot-Treupel L, Puisieux F. Physicochemical and morphological characterization of polyisobutyl cyanoacrylate nanocapsules. *J Pharm Sci.* Apr 1986;75(4):361-364.
142. Scott C, Wu D, Ho CC, Co CC. Liquid-core capsules via interfacial polymerization: a free-radical analogy of the nylon rope trick. *J Am Chem Soc.* Mar 30 2005;127(12):4160-4161.
143. Galindo-Rodriguez S, Allemann E, Fessi H, Doelker E. Physicochemical parameters associated with nanoparticle formation in the salting-out, emulsification-diffusion, and nanoprecipitation methods. *Pharm Res.* Aug 2004;21(8):1428-1439.
144. Bartoli MH, Boitard M, Fessi H, et al. In vitro and in vivo antitumoral activity of free, and encapsulated taxol. *J Microencapsul.* Apr-Jun 1990;7(2):191-197.
145. Oh KS, Lee KE, Han SS, Cho SH, Kim D, Yuk SH. Formation of core/shell nanoparticles with a lipid core and their application as a drug delivery system. *Biomacromolecules.* Mar-Apr 2005;6(2):1062-1067.
146. Bae KH, Lee Y, Park TG. Oil-encapsulating PEO-PPO-PEO/PEG shell

cross-linked nanocapsules for target-specific delivery of paclitaxel. *Biomacromolecules*. Feb 2007;8(2):650-656.

147. Zhang Y, Zhu SY, Yin LC, Qian F, Tang C, Yin CH. Preparation, characterization and biocompatibility of poly(ethylene glycol)-poly(n-butyl cyanoacrylate) nanocapsules with oil core via miniemulsion polymerization. *Eur Polym J*. Jun 2008;44(6):1654-1661.
148. Huynh NT, Passirani C, Saulnier P, Benoit JP. Lipid nanocapsules: A new platform for nanomedicine. *Int J Pharmaceut*. Sep 11 2009;379(2):201-209.
149. Heurtault B, Saulnier P, Pech B, Proust JE, Benoit JP. A novel phase inversion-based process for the preparation of lipid nanocarriers. *Pharm Res*. Jun 2002;19(6):875-880.
150. Lacoeyille F, Hindre F, Moal F, et al. In vivo evaluation of lipid nanocapsules as a promising colloidal carrier for paclitaxel. *Int J Pharmaceut*. Nov 1 2007;344(1-2):143-149.
151. Garcion E, Lamprecht A, Heurtault B, et al. A new generation of anticancer, drug-loaded, colloidal vectors reverses multidrug resistance in glioma and reduces tumor progression in rats. *Mol Cancer Ther*. Jul 2006;5(7):1710-1722.
152. Peltier S, Oger JM, Lagarce F, Couet W, Benoit JP. Enhanced oral paclitaxel bioavailability after administration of paclitaxel-loaded lipid nanocapsules. *Pharm Res*. Jun 2006;23(6):1243-1250.
153. Khalid MN, Simard P, Hoarau D, Dragomir A, Leroux JC. Long circulating poly(ethylene glycol)-decorated lipid nanocapsules deliver docetaxel to solid tumors. *Pharm Res*. Apr 2006;23(4):752-758.
154. Chan JM, Zhang L, Yuet KP, et al. PLGA-lecithin-PEG core-shell nanoparticles for controlled drug delivery. *Biomaterials*. Mar 2009;30(8):1627-1634.
155. Liu Y, Li K, Pan J, Liu B, Feng SS. Folic acid conjugated nanoparticles of mixed lipid monolayer shell and biodegradable polymer core for targeted delivery of Docetaxel. *Biomaterials*. Jan 2010;31(2):330-338.
156. Wang Z, Ho PC. Self-assembled core-shell vascular-targeted nanocapsules for temporal antivasculature and anticancer activities. *Small*. Nov 22 2010;6(22):2576-2583.
157. Skwarczynski M, Hayashi Y, Kiso Y. Paclitaxel prodrugs: toward smarter delivery of anticancer agents. *J Med Chem*. Dec 14 2006;49(25):7253-7269.
158. Stevens PJ, Sekido M, Lee RJ. A folate receptor-targeted lipid nanoparticle formulation for a lipophilic paclitaxel prodrug. *Pharm Res*. Dec

2004;21(12):2153-2157.

159. Lundberg BB, Risovic V, Ramaswamy M, Wasan KM. A lipophilic paclitaxel derivative incorporated in a lipid emulsion for parenteral administration. *J Control Release*. Jan 9 2003;86(1):93-100.
160. Huynh L, Leroux JC, Allen C. Enhancement of docetaxel solubility via conjugation of formulation-compatible moieties. *Org Biomol Chem*. Sep 7 2009;7(17):3437-3446.
161. Ali S, Ahmad I, Peters A, et al. Hydrolyzable hydrophobic taxanes: synthesis and anti-cancer activities. *Anticancer Drugs*. Feb 2001;12(2):117-128.
162. Dhanikula AB, Panchagnula R. Preparation and characterization of water-soluble prodrug, liposomes and micelles of Paclitaxel. *Curr Drug Deliv*. Jan 2005;2(1):75-91.
163. Zhigaltsev IV, Winters G, Srinivasulu M, et al. Development of a weak-base docetaxel derivative that can be loaded into lipid nanoparticles. *J Control Release*. Jun 15 2010;144(3):332-340.
164. Parness J, Kingston DG, Powell RG, Harracksingh C, Horwitz SB. Structure-activity study of cytotoxicity and microtubule assembly in vitro by taxol and related taxanes. *Biochem Biophys Res Commun*. Apr 14 1982;105(3):1082-1089.
165. Zhu Q, Guo Z, Huang N, Wang M, Chu F. Comparative molecular field analysis of a series of paclitaxel analogues. *J Med Chem*. Dec 19 1997;40(26):4319-4328.
166. Kingston DG. Recent advances in the chemistry of taxol. *J Nat Prod*. May 2000;63(5):726-734.
167. Byrne JD, Betancourt T, Brannon-Peppas L. Active targeting schemes for nanoparticle systems in cancer therapeutics. *Adv Drug Deliv Rev*. Dec 14 2008;60(15):1615-1626.
168. Low PS, Antony AC. Folate receptor-targeted drugs for cancer and inflammatory diseases. *Adv Drug Deliv Rev*. Apr 29 2004;56(8):1055-1058.
169. Elnakat H, Ratnam M. Distribution, functionality and gene regulation of folate receptor isoforms: implications in targeted therapy. *Adv Drug Deliv Rev*. Apr 29 2004;56(8):1067-1084.
170. Wu J, Liu Q, Lee RJ. A folate receptor-targeted liposomal formulation for paclitaxel. *Int J Pharm*. Jun 19 2006;316(1-2):148-153.

171. Xu Z, Chen L, Gu W, et al. The performance of docetaxel-loaded solid lipid nanoparticles targeted to hepatocellular carcinoma. *Biomaterials*. Jan 2009;30(2):226-232.
172. Ritter CA, Arteaga CL. The epidermal growth factor receptor-tyrosine kinase: a promising therapeutic target in solid tumors. *Semin Oncol*. Feb 2003;30(1 Suppl 1):3-11.
173. Gao Y, Chen L, Gu W, Xi Y, Lin L, Li Y. Targeted nanoassembly loaded with docetaxel improves intracellular drug delivery and efficacy in murine breast cancer model. *Mol Pharm*. Nov-Dec 2008;5(6):1044-1054.
174. Moody TW, Gozes I. Vasoactive intestinal peptide receptors: a molecular target in breast and lung cancer. *Curr Pharm Des*. 2007;13(11):1099-1104.
175. Gespach C, Bawab W, de Cremoux P, Calvo F. Pharmacology, molecular identification and functional characteristics of vasoactive intestinal peptide receptors in human breast cancer cells. *Cancer Res*. Sep 15 1988;48(18):5079-5083.
176. Rubinstein I, Soos I, Onyuksel H. Intracellular delivery of VIP-grafted sterically stabilized phospholipid mixed nanomicelles in human breast cancer cells. *Chem Biol Interact*. Jan 30 2008;171(2):190-194.
177. Pirollo KF, Chang EH. Does a targeting ligand influence nanoparticle tumor localization or uptake? *Trends Biotechnol*. Oct 2008;26(10):552-558.
178. Bartlett DW, Su H, Hildebrandt IJ, Weber WA, Davis ME. Impact of tumor-specific targeting on the biodistribution and efficacy of siRNA nanoparticles measured by multimodality in vivo imaging. *Proc Natl Acad Sci U S A*. Sep 25 2007;104(39):15549-15554.
179. Kirpotin DB, Drummond DC, Shao Y, et al. Antibody targeting of long-circulating lipidic nanoparticles does not increase tumor localization but does increase internalization in animal models. *Cancer Res*. Jul 1 2006;66(13):6732-6740.
180. Wu AM, Yazaki PJ, Tsai S, et al. High-resolution microPET imaging of carcinoembryonic antigen-positive xenografts by using a copper-64-labeled engineered antibody fragment. *Proc Natl Acad Sci U S A*. Jul 18 2000;97(15):8495-8500.
181. Hussain S, Pluckthun A, Allen TM, Zangemeister-Wittke U. Antitumor activity of an epithelial cell adhesion molecule-targeted nanovesicular drug delivery system. *Mol Cancer Ther*. Nov 2007;6(11):3019-3027.
182. Kircheis R, Wightman L, Schreiber A, et al. Polyethylenimine/DNA complexes

- shielded by transferrin target gene expression to tumors after systemic application. *Gene Ther.* Jan 2001;8(1):28-40.
183. Muller RH, Ruhl D, Runge S, SchulzeForster K, Mehnert W. Cytotoxicity of solid lipid nanoparticles as a function of the lipid matrix and the surfactant. *Pharm Res.* Apr 1997;14(4):458-462.
 184. Muller RH, Maassen S, Weyhers H, Specht F, Lucks JS. Cytotoxicity of magnetite-loaded polylactide, polylactide/glycolide particles and solid lipid nanoparticles. *Int J Pharmaceut.* Jul 12 1996;138(1):85-94.
 185. Fu K, Pack DW, Klibanov AM, Langer R. Visual evidence of acidic environment within degrading poly(lactic-co-glycolic acid) (PLGA) microspheres. *Pharm Res.* Jan 2000;17(1):100-106.
 186. Majoros IJ, Myc A, Thomas T, Mehta CB, Baker JR, Jr. PAMAM dendrimer-based multifunctional conjugate for cancer therapy: synthesis, characterization, and functionality. *Biomacromolecules.* Feb 2006;7(2):572-579.
 187. Lim J, Simanek EE. Synthesis of water-soluble dendrimers based on melamine bearing 16 paclitaxel groups. *Org Lett.* Jan 17 2008;10(2):201-204.
 188. Ooya T, Lee J, Park K. Hydrotropic dendrimers of generations 4 and 5: synthesis, characterization, and hydrotropic solubilization of paclitaxel. *Bioconjug Chem.* Nov-Dec 2004;15(6):1221-1229.
 189. Lacko AG, Nair M, Prokai L, McConathy WJ. Prospects and challenges of the development of lipoprotein-based formulations for anti-cancer drugs. *Expert Opin Drug Deliv.* Nov 2007;4(6):665-675.
 190. McConathy WJ, Nair MP, Paranjape S, Mooberry L, Lacko AG. Evaluation of synthetic/reconstituted high-density lipoproteins as delivery vehicles for paclitaxel. *Anticancer Drugs.* Feb 2008;19(2):183-188.
 191. Masquelier M, Vitols S, Palsson M, Mars U, Larsson BS, Peterson CO. Low density lipoprotein as a carrier of cytostatics in cancer chemotherapy: Study of stability of drug-carrier complexes in blood. *Journal of Drug Targeting.* 2000;8(3):155-164.
 192. Eisenberg S, Windmueller HG, Levy RI. Metabolic fate of rat and human lipoprotein apoproteins in the rat. *J Lipid Res.* Jul 1973;14(4):446-458.
 193. Ho YK, Smith RG, Brown MS, Goldstein JL. Low-density lipoprotein (LDL) receptor activity in human acute myelogenous leukemia cells. *Blood.* Dec 1978;52(6):1099-1114.

194. Fiorenza AM, Branchi A, Sommariva D. Serum lipoprotein profile in patients with cancer. A comparison with non-cancer subjects. *Int J Clin Lab Res.* 2000;30(3):141-145.
195. Mooberry LK, Nair M, Paranjape S, McConathy WJ, Lacko AG. Receptor mediated uptake of paclitaxel from a synthetic high density lipoprotein nanocarrier. *J Drug Target.* Jan 2010;18(1):53-58.
196. Yezhelyev M, Yacoub R, O'Regan R. Inorganic nanoparticles for predictive oncology of breast cancer. *Nanomedicine (Lond).* Jan 2009;4(1):83-103.
197. Lu J, Liong M, Sherman S, et al. Mesoporous Silica Nanoparticles for Cancer Therapy: Energy-Dependent Cellular Uptake and Delivery of Paclitaxel to Cancer Cells. *Nanobiotechnology.* May 1 2007;3(2):89-95.
198. Paciotti GF, Kingston DGI, Tamarkin L. Colloidal gold nanoparticles: A novel nanoparticle platform for developing multifunctional tumor-targeted drug delivery vectors. *Drug Develop Res.* Jan 2006;67(1):47-54.
199. Hwu JR, Lin YS, Josephrajan T, et al. Targeted Paclitaxel by conjugation to iron oxide and gold nanoparticles. *J Am Chem Soc.* Jan 14 2009;131(1):66-68.
200. Hua MY, Yang HW, Chuang CK, et al. Magnetic-nanoparticle-modified paclitaxel for targeted therapy for prostate cancer. *Biomaterials.* Oct 2010;31(28):7355-7363.
201. Gibson JD, Khanal BP, Zubarev ER. Paclitaxel-functionalized gold nanoparticles. *J Am Chem Soc.* Sep 19 2007;129(37):11653-11661.
202. van Schooneveld MM, Vucic E, Koole R, et al. Improved biocompatibility and pharmacokinetics of silica nanoparticles by means of a lipid coating: a multimodality investigation. *Nano Lett.* Aug 2008;8(8):2517-2525.

Chapter 2.

Development of BTM nanoparticles to deliver docetaxel

1. Summary

To develop a lipid-based nanoparticle (NP) formulation for efficient docetaxel (DX) delivery, liquid Miglyols (the lipid) were screened for their solvation ability for DX. Miglyol 808 was identified as the Miglyol with the highest solvation ability for DX that was capable of forming NPs. To facilitate the optimization of novel BTM NPs using Miglyol 808 as the oil phase, sequential simplex optimization was utilized. After 16 trials, the optimal NP composition was identified as Miglyol 808 (2.8 mg/mL), Brij 78 (3.7 mg/mL) and Vitamin E TPGS (1.2 mg/mL). The final optimized BTM 808 NPs successfully entrapped DX (0.3 mg/mL) with 85% entrapment efficiency as determined by ultrafiltration. The cytotoxicity studies showed that DX NPs significantly reduced IC_{50} values in PX-resistant cells over free DX, while in sensitive cells the IC_{50} values of free DX and DX NPs were comparable. A novel “ex-vivo” release method was developed to study the DX release from NPs in mouse plasma. Despite the desirable formulation properties, DX was found to be quickly released in mouse plasma in-vitro. To understand the rapid drug release in mouse plasma, the entrapment efficiency of DX

in NPs was re-characterized by size exclusion chromatography (SEC). The new entrapment efficiency results demonstrated that DX was not actually “released” from the NPs upon spiking into mouse plasma, but was not truly entrapped into the NPs during preparation.

2. Introduction

DX is a potent anticancer drug used to treat various cancers including metastatic androgen-independent prostate cancer, breast cancer, and advanced non-small cell lung cancer.¹⁻³ DX inhibits cell growth by binding to microtubules, stabilizing them, and preventing their depolymerization.⁴ Currently, Taxotere[®] is the only commercial formulation of DX on the market. The formulation contains a solvent system of polysorbate 80 and ethanol. Adverse effects related to these excipients have been reported such as hypersensitivity and fluid retention.⁵⁻⁹ Great effort has been made to develop safer formulations to effectively deliver DX, including micelles, liposomes, nanoemulsions, solid lipid NPs, nanocapsules and polymeric NPs.¹⁰⁻¹⁵ Given the hydrophobic property of DX, lipid-based NPs, especially liquid oil-filled NPs, serve as a viable alternative delivery system. Lipid-based NPs have the advantages of low toxicity, the capability of drug control release, and the potential to penetrate leaky vasculature of tumors.

In early 1990s, solid lipid NPs started to attract extensive attention as a novel nanoparticulate delivery system. However, during the cooling process of solid lipid NP

preparation, the melting lipids solidify and crystallize. The increase in structural perfection during the process leads to the formation of a drug enriched shell, which limits the drug loading capacity, and leads to the burst drug release and drug expulsion during storage.¹⁶ In the light of this concept, novel liquid oil-filled BTM NPs were developed in our laboratory. The BTM NPs were composed of Brij 78, Vitamin E TPGS, and Miglyol 812.¹⁷ Miglyol[®] is the trade mark of a family of medium-chain triglycerides that differ in fatty acid content and extent on the R1, R2, and R3 of the glycerol backbone extracted from coconut and palm kernel. They are GRAS listed by the FDA and several have been shown to be safe after parenteral administration at levels of 0.5 g/kg, and the LD₅₀ in mice by i.v. injection has been reported to be 3.7 g/kg.¹⁸ Thus, the relatively non-toxic Miglyol could serve as a good oil phase to accommodate DX due to the high partition co-efficiency of DX in medium chain triglycerides.¹⁹ During the initial development of paclitaxel (PX) NPs, Miglyol 812 was selected as the oil phase arbitrarily since there about nine other Miglyols available in the market that were not fully screened. The oil phase with the highest drug solvation ability represents better compatibility and affinity of the drug with the inner liquid oil core of the delivery vehicles thereby leading to higher drug loading capacity and longer retention of drugs in the NPs.

The objective of these present studies was to develop a new generation of BTM NPs using the Miglyol with the highest solvation ability for DX with the goal to achieve high drug loading, high entrapment efficiency and slow drug release.

3. Materials and Methods

3.1. Materials and cell culture

DX and PX were purchased from Sigma-Aldrich (St. Louis, MO). Miglyol 612, 808, 810, 812, 8108, 818, 829, 840, and 8810 were obtained from Sasol (Witten, Germany). Polyoxyl 20-stearyl ether (Brij 78) was obtained from Uniqema (Wilmington, DE). D-alpha-tocopheryl polyethylene glycol succinate (Vitamin E TPGS) was purchased from Eastman Chemicals (Kingsport, TN). BALB/c mouse plasma was purchased from Innovative Research Inc. (Novi, MI). Sepharose CL-4B was purchased from GE Healthcare (Uppsala, Sweden). Oasis HLB SPE cartridge was purchased from Waters (Milford, MA).

The human prostate cancer cell lines, DU-145 and PC-3, were obtained from American Type Culture Collection (ATCC) and were maintained in RPMI-1640 medium with 10% fetal bovine serum (FBS). The corresponding PX-resistant cell lines, DU-145-R and PC-3-R, were generously provided by Dr. Evan T. Keller's laboratory (Unit for Laboratory Animal Medicine and Department of Pathology, University of Michigan). They were maintained in RPMI-1640 medium with 10% FBS and 5 nM DX upon arrival.

3.2. Methods

3.2.1. Liquid lipid screening for DX NP development

3.2.1.1 Semi-quantitative estimation of DX solubility in Miglyols

Five (5) mg of each type of Miglyol (612, 808, 810, 812, 8108, 818, 829, 840, and 8810) was weighed accurately into 1 mL glass vials. Various amounts of DX (0.25-2.5 mg) dissolved in ethanol were added to the vials containing Miglyols. The vials were heated to 65°C on a hotplate. During mixing at 65°C, ethanol was evaporated with a nitrogen stream. The mixture was allowed to cool down to room temperature. The dissolution and dispersion of DX in each Miglyol were visually assessed.

3.2.1.2 Preparation of blank BTM NPs

Blank NPs were prepared using a warm oil-in-water (o/w) microemulsion precursor method previously developed in our laboratory. Briefly, 2.5 mg of the chosen Miglyol, 3.5 mg Brij 78 and 1.5 mg Vitamin E TPGS were accurately weighed into glass vials and heated to 65°C. One (1) mL of pre-heated 10% lactose in water was added into the mixture of oil and melted surfactants. The mixture was stirred for 20 min at 65°C then cooled to room temperature. The resultant NPs were monitored for their appearance and particle size right after preparation and after 24 hr storage at 4°C.

3.2.1.3 Quantification of DX solubility in Miglyol 808 and 812

Approximately 5 mg of DX was added to individual vials containing 50 μ L of Miglyol 808 or Miglyol 812. The mixtures were stirred at room temperature for 24 hr. The samples were then centrifuged for 1 hr at 14,000 rpm to remove undissolved drug. After centrifugation, the saturated supernatant was diluted with acetonitrile (ACN) and analyzed by HPLC.

The DX concentrations were quantified by HPLC using a Finnigan Surveyor HPLC system with a Photodiode Array (PDA) plus detector, autosampler and LC pump plus with a Inertsil[®] ODS-3 column (4 μ m, 4.6 \times 150 mm, GL Sciences) at 25°C. Chromatographic separation was achieved by gradient elution using a mobile phase of 2-propanol, ACN and water (5: 50: 45 v/v/v). The flow rate was 1.0 mL/min and the total run time was 25 min for each 25 μ L injection. The wavelength was 230 nm.

3.2.2. Optimization of DX BTM NPs by sequential simplex

Miglyol 808 was selected as oil phase, and Brij 78 and Vitamin E TPGS were used as the surfactants to prepare the BTM 808 NPs. Sequential simplex optimization was performed to prepare BTM 808 NPs with desirable properties using MultiSimplex Software (CambridgeSoft Corporation, Cambridge, MA). The three control variables were Miglyol concentration, Brij 78 concentration and TPGS concentration. The four response variables were particle size, polydispersity index (P.I.) value, peak number

and % dust. The target response was set as: particle size 150 nm, P.I. value 0.15, peak number 1, and % dust 0. The starting simplex was based on our previously optimized BTM 812 NP composition (2.5 mg/mL Miglyol 812, 3.5 mg/mL Brij 78 and 1.5 mg/mL Vitamin E TPGS). The sequential simplex optimization was performed following the variable-size simplex rules.¹⁷

3.2.3. Characterization of DX BTM NPs

3.2.3.1. Particle size and zeta potential measurements

Particle size and size distribution of NPs were determined using an N5 Submicron Particle Size Analyzer (Beckman). Five (5) μ L of NPs was diluted with 1 mL of water to reach the intensity required by the instrument. Particle size was determined at 90° light scattering at 25°C. The zeta potential of NPs was determined using the Zetasizer Nano Z (Malvern Instruments, Southborough, MA).

3.2.3.2. Drug entrapment efficiency

Drug entrapment efficiency was determined by separating free DX from DX-loaded NPs using a Microcon Y-100 column. Briefly, 100 μ L of DX BTM NPs was applied to the Microcon Y-100 column and centrifuged at 14,000 rpm for 20 min. DX concentrations in filtrate and retained above filter were measured by HPLC respectively. The % drug entrapment efficiency was defined as $100\% \times$ the ratio of the

drug retained above filter to the total drug added.

3.2.3.3. Morphology

The morphology of BTM NPs was examined using a Zeiss EM 900 Transmission Electron Microscope (TEM). Briefly, a drop of diluted NP suspension was placed onto standard copper microscopy grids, examined and photographed with TEM at an accelerating voltage of 60 kV (Carl Zeiss, Thornwood, NY, USA).

3.2.3.4. Physical stability of NPs

The DX BTM NP suspension was stored at 4°C. At designated time points, the particle size was measured after the NP suspension being allowed to equilibrate to room temperature.

3.2.4. In-vitro cytotoxicity of drug BTM NPs

3.2.4.1. In-vitro cytotoxicity in sensitive and resistant cells

The MTT assay was utilized to assess the cytotoxicity of free DX and DX NPs. Serial dilutions of free DX or DX-containing NPs were added to the testing cells and incubated for 48 hr. The cells were then incubated with the MTT solution for 4 hr and the formazan dyes were solubilized by DMSO. The absorbance was measured using the Synergy 2 Multi-Detection Microplate Reader at 570 nm, and the concentration of drug that inhibited cell survival by 50% (IC₅₀) was determined from cell survival plots.

3.2.4.2. Expression of P-gp in sensitive and resistant cells

Cells (DU-145, PC-3, DU-145-R and PC-3-R) cultured in T75 flask were washed twice with ice-cold PBS and lysed in RIPA lysis buffer. Total protein content of samples was quantified by BCA assay with BSA as the reference standard. All samples were diluted in sample buffer to the same protein concentration and subjected to SDS-PAGE, electrophoretically separated. Proteins were transferred to a nitrocellulose membrane in the presence of a transfer buffer. The membrane was blocked with 6% milk in Tris-buffered saline with Tween 20 (TBS-T) for 1 hr at room temperature. The target protein (P-gp or beta-actin) was detected with a primary antibody and a horseradish peroxidase conjugated secondary antibody at the desired dilution. The membrane was exposed to chemiluminescence reagents. The Chemi-Doc Imaging System was used to visualize the target protein.

3.2.5. In-vitro release in mouse plasma

3.2.5.1. Development of in-vitro release method in mouse plasma

To study the separation of NPs with plasma proteins, 200 μ L of blank BTM NPs were mixed with 300 μ L of BALB/c mouse plasma and applied to a Sepharose CL-4B column (15 cm, gravity-packed) and eluted using PBS pH 7.4. The dynamic light scattering intensity in each fraction (1 mL/fraction) was determined using an N5 Submicron Particle Size Analyzer. The protein concentration in each fraction was

quantified by BCA assay with BSA as the reference standard.

To study the extraction recovery of DX from plasma proteins by solid phase extraction (SPE) method, 10 μ L, 50 μ L and 100 μ L of 50 μ g/mL DX stock solution in methanol was aliquoted to individual tubes. Methanol was dried in a nitrogen stream and 0.5 mL of BALB/c mouse plasma was added to each tube to dissolve the drug. The DX was extracted from plasma proteins by SPE method. Briefly, HLB SPE cartridge was first activated and equilibrated by 20% methanol in DCM, 100% methanol and water successively. The DX-dissolved plasma samples were then applied to the cartridge. The cartridge was rinsed with 5% methanol in water and 55% methanol in water. Finally, DX was eluted by 20% methanol in DCM. The samples were dried in nitrogen stream and reconstituted in mobile phase followed by LC/MS/MS analysis. To study the recovery of SEC plus SPE, the same DX-dissolved plasma samples were firstly applied to a Sepharose CL-4B column and eluted using PBS. Fractions 1-20 were collected and subjected to SPE extraction as described above. The samples were analyzed by LC/MS/MS.

The DX concentration was quantified by LC/MS/MS using a Finnigan Surveyor Autosampler Plus and Finnigan Surveyor MS Pump Plus. Chromatographic separations were achieved by gradient separation using a SunFire™ C18 column (2.1 \times 30 mm, 3.5 μ m particle size, Waters) at 25°C. The mobile phase consisted of 0.1% formic acid in water and methanol. The flow rate was 0.5 mL/min and the total run time was 8 min for each 25 μ L injection. Mass spectrometric analysis was performed using a Thermo

Scientific TSQ Quantum Access with positive ionization. The capillary temperature was set up to 390°C, and the spray voltage was 4000V. For DX analysis, m/z 830.0 \rightarrow 549.0 was monitored with PX (m/z 876.3 \rightarrow 308.0) as an internal standard. The recovery was calculated as $100\% \times$ the ratio of total DX weight detected after SPE or SEC+SPE to the DX weight spiked in the plasma.

3.2.5.2. In-vitro release in mouse plasma

Before a release study, 0.5 mL of DX NPs were purified using a Microcon Y-100 column and resuspended in 0.5 mL 10% lactose. The concentration of DX in the resuspended NPs was measured by HPLC. About 30 μ L of purified DX NPs was mixed with 870 μ L of BALB/c mouse plasma and the release mixture was incubated at 37°C under constant shaking. At pre-determined time points, 100 μ L of the release mixture was removed and immediately applied to a Sepharose CL-4B column and eluted using PBS. Fractions 9 to 22 of the eluent (1 mL/fraction) were collected. DX was extracted from the plasma proteins by SPE method as described above. The concentration of DX reconstituted in mobile phase was determined by LC/MS/MS. The % DX released at any time point was calculated as $100\% \times (\text{Drug weight detected in fraction 9-22} / \text{Total drug weight})$.

3.2.6. Re-characterization of DX BTM NPs

3.2.6.1. Entrapment efficiency determined by SEC

DX NPs were separated with the free drugs using a Sepharose CL-4B column. NPs were eluted using PBS in fraction 5-8 (1 mL/fraction). Each fraction was evaporated to dryness in vacuo, resuspended in 1 mL ACN and analyzed by HPLC to determine the concentration of DX in each fraction. The % drug entrapment efficiency was defined as $100\% \times (\text{Weight of drug detected in fraction 5-8} / \text{Total drug weight detected in all fractions collected})$. Free DX solution in water was also applied to the SEC column as a control.

3.2.6.2. Particle size analysis of fractions from SEC

Five hundred (500) μL of blank BTM NPs were applied to a Sepharose CL-4B column and eluted using PBS. The particle size in each fraction (1 mL/fraction) was determined using an N5 Submicron Particle Size Analyzer (Beckman).

3.2.7. Statistical analysis

Statistical comparisons were performed using one-way analysis of variances (ANOVA) ($\text{©1992-2007 GraphPad Prism Software, Inc.}$). Results were considered significant at 95% confidence interval ($p < 0.05$).

4. Results

4.1. Oil lipid screening for DX nanoparticle

The concentrations in vials with visible white specks were defined “insoluble” and the concentrations in vials with clear and transparent appearance were defined as “soluble”. Based on the maximal soluble concentrations of DX in each Miglyol, the Miglyols were divided into 3 groups: high (> 0.2 mg/mg oil), medium (0.05 - 0.1 mg/mg oil) and low (< 0.05 mg/mg oil) solubility of DX as shown in Table 2.1. They were listed in the order of solubility from the highest to the lowest. In the same table, the chemical composition(s) of each Miglyol was also listed.

Based on the semi-quantification results, the Miglyols in the category of “high solubility” were used to prepare NPs based on the previously developed BTM 812 NP composition (Miglyol 812, Brij 78 and Vitamin E TPGS). However, the efforts to develop NPs using all three Miglyols with high solubility did not achieve desirable results. Miglyol 829 formed turbid suspensions with particle size over 250 nm and high % dust. Miglyol 840 and 612 formed acceptable NPs right after preparation but phase separation was observed for both after the storage at 4°C overnight. It was speculated that the difficulty of formulating NPs using these Miglyols may be due to their unfavorable properties, such as high viscosity (Miglyol 829) or volatility (Miglyol 612, 840). Fortunately, Miglyol 808, the Miglyol with solubility right after the highest three Miglyols was capable of formulating NPs with desirable particle size using Brij 78 and Vitamin E TPGS as surfactant and co-surfactant.

To confirm the semi-quantification results of DX solubility, the solubility of DX in Miglyol 808 and 812 was quantitatively determined. The quantitative result showed that the solubility of DX in Miglyol 808 (52.07 ± 0.84 mg/mL) was significantly higher compared to that in Miglyol 812 (36.11 ± 0.10 mg/mL, $p < 0.01$). As a result, Miglyol 808 was chosen as the oil phase for further formulation development.

4.2. Sequential simplex optimization of DX BTM NPs

Sequential simplex optimization was performed as summarized in Table 2.2. A comparison of each trial was based on the membership value which represented the proximity of current trial to the optimum considering the four response variables (particle size, P.I. value, peak number and % dust) of the trial. The higher membership means that the responses were closer to the optimum. After 16 trials, four leading formulations were selected. In comparison, NPs of trial 6 and 8 were less stable than NPs of trial 13 and 15 after storage at 4°C for a week. As a result, trial 15 (Miglyol 808 2.8 mg/mL, Brij 78 3.7 mg/mL and Vitamin E TPGS 1.2 mg/mL) was finally chosen as the optimal formulation to be further studied.

4.3. Characterization of DX BTM NPs

The resultant blank BTM 808 NPs had a mean particle size of 190 nm with low P.I. value and a zeta potential of -5.78 mV (Table 2.3). Surprisingly, after loading 0.3

mg/mL of DX, the particle size decreased to around 160 nm. The image of the NPs observed by TEM showed consistent particle size with that determined by photon correlation spectroscopy (PCS) (Figure 2.1B). The entrapment efficiency of DX in the NPs determined by ultrafiltration was 85.3%. The physical stability of DX NP was evaluated by monitoring changes of particle sizes at 4°C upon long-term storage. The particle size of DX BTM NPs did not significantly change at 4°C for three months (Figure 2.2).

4.4. In-vitro cytotoxicity

The cytotoxicity of DX NPs was tested in DU-145 and PC-3 cells as well as their corresponding PX-resistant lines (Figure 2.3). DX NPs showed dose-dependent cytotoxicity against all cells tested. In sensitive cell lines, the IC_{50} values of free DX and DX BTM NP were comparable. While in resistant cell lines, the IC_{50} values of free DX in DU-145-R and PC-3-R were 200-fold and 60-fold higher than those in sensitive lines respectively, showing that the PX-resistant cells were also cross-resistant to DX. In resistant cell lines, the IC_{50} value of DX NPs was about 3-fold lower compared to free DX. Blank NPs did not cause significant cytotoxicity in all cell lines in the equivalent concentration. Western blotting results showed that P-gp in resistant cells was overexpressed but not in the sensitive cells (Figure 2.4). Moreover, the P-gp expression level in DU-145-R was higher than in PC-3-R cells.

4.5. In-vitro release

A novel “ex-vivo” release method was developed to study the release of DX from the NPs in 100% mouse plasma. In the “ex-vivo” release method, NPs were spiked directly into 100% mouse plasma. Drug-containing NPs were separated from protein-bound DX and free DX by a Sepharose CL-4B column. The 15 cm, gravity-packed Sepharose CL-4B column was able to achieve baseline separation of the NPs with plasma proteins and free drugs, validated by dynamic light scattering intensity, BCA assay and HPLC analysis (Figure 2.5 and Figure 2.7B). The SPE method and SEC plus SPE showed 90 – 110% recovery (Table 2.4).

For the release studies, the DX-containing NPs were first purified by a Microcon Y-100 column. Unfortunately, upon spiking into the mouse plasma, DX was almost immediately released from the NPs (Figure 2.6).

4.6. Re-characterization of DX BTM NPs

The entrapment efficiency of DX BTM NP was characterized again by another method, SEC. As indicated by dynamic light scattering intensity (Figure 2.5), NPs were eluted from Sepharose CL-4B column in fraction 5-8. However, DX was not detected in fraction 5-8 (Figure 2.7A). As shown in control, free DX was mainly eluted after fraction 13 (Figure 2.7B). For DX BTM NPs, about 70% of the drug was eluted in fraction 13-20, and another 30% in fraction 9-12, indicating that DX was not truly

entrapped in the NPs.

Particle sizing of each fraction from SEC showed that fraction 5-8 contained particles with size 100-180 nm while fraction 9-12 was another population of smaller particles with particle size around 50 nm (Figure 2.8).

5. Discussion

A novel liquid oil-filled NP BTM was previously developed in our laboratory, which was composed of Miglyol 812, Brij 78 and Vitamin E TPGS.¹⁷ During the initial development, Miglyol 812 was selected arbitrarily from a family of Miglyols available. For more rational formulation development, the oil phase was first screened in the Miglyol family in terms of their solvation ability for DX. To make a quick estimation, a semi-quantification method was first utilized. The higher solubility of some oils (e.g., Miglyol 829 and 840) may be attributed to their structural uniqueness. Other than these oils, the data showed a general trend that DX favored triglycerides with shorter alkyl chain ($C_6 > C_8 > C_{10}$) within the range of the medium-chain triglycerides tested, probably due to the structural miscibility. Unfortunately, the three Miglyols with highest solubility of DX failed to form homogeneous and stable NPs. It should be noted that the results were merely based on limited combinations of surfactants and concentrations. The potential of these Miglyols to formulate NPs was worth further and more thorough investigations. For the present studies, Miglyol 808 was chosen for further development. In addition, the result of quantification was consistent with the

semi-quantification observation, suggesting that the semi-quantification observation as a preliminary estimation method is reliable and has the potential to be applied to future formulation development. To facilitate the NP formulation optimization, sequential simplex was used. Sequential simplex optimization is a powerful experimental design method. In this method, a simplex is a triangle in a hyperplane with three trials as its three vertices. The trial with the response furthest from optimum is reflected in the hyperplane to form a new simplex. New simplices are continually formed until the optimum is reached. Sequential simplex optimization is a step-wise strategy that helps to achieve optimal results with minimal number of experimental trials. Also, it takes inter-factorial interactions into consideration. Based on particle size, P.I. value, peak number and % dust, the optimal NP composition was identified as Miglyol 808 (2.8 mg/mL), Brij 78 (3.7 mg/mL) and Vitamin E TPGS (1.2 mg/mL). The final optimized BTM 808 NPs successfully entrapped DX (0.3 mg/mL) with 85% entrapment efficiency as determined by ultrafiltration.

The results of cytotoxicity studies indicated that DX NPs significantly reduced IC_{50} values in PX-resistant cells over free DX. The mechanisms of PX-resistance in DU-145-R and PC-3-R cells have been extensively investigated by the group who established them.²⁰ They demonstrated that P-gp overexpression was the major mechanism of PX-resistance in these cells. Our western blotting results of P-gp expression in these cells were in agreement with their findings. Since DX is a P-gp substrate, it is not surprising that the P-gp overexpressing cells were cross-resistant to

DX. It has been reported that the BTM 812 NPs were able to overcome P-gp-mediated multidrug resistance by inhibiting P-gp and depleting ATP.²¹ It has been demonstrated that Brij 78, and not TPGS decreased ATP levels in resistant cells. Because P-gp efflux is an energy-dependent process, ATP depletion led to decreased drug efflux thus higher intracellular drug accumulation. In addition, the increased uptake of NPs by endocytosis could partially bypass P-gp. Current studies have not focused on the mechanism(s) of DX NPs overcoming multidrug resistance, however, due to the similarity between BTM 812 and BTM 808 NPs including Brij 78 as a component with comparable concentration and high drug loading, the mechanisms of BTM 812 NPs overcoming P-gp are likely to be logically extended to BTM 808 NPs as well.

Previously, the release of PX from BTM 812 NPs was studied in PBS with 0.1% Tween 80 by dialysis.¹⁷ The cumulative release of PX was only 50% after 72 hr. However, in in-vivo pharmacokinetic study, PX BTM 812 NPs showed superimposable pharmacokinetic profile with Taxol (data not shown). The superimposable pharmacokinetic profile suggests that PX was very quickly released from NPs in-vivo so that it failed to take advantage of the long-circulating vehicle. The in-vitro drug release of nano-formulation is usually studied in aqueous buffer using a dialysis method. However, the correlation between the in-vitro release and in-vivo pharmacokinetic profile is often poor due to the more complex in-vivo environment, such as the presence of large amounts of proteins and enzymes in the plasma. The poor correlation in this case and many others certainly demands a more predictive in-vitro release method. In

the present studies, we developed a novel “ex-vivo” release method to better mimic the in-vivo environment. By using this “ex-vivo” release method, it was found that DX was very quickly released from the NPs. Although in-vivo pharmacokinetic study was not performed for DX BTM 808 NPs, based on the “ex-vivo” release results, it is fair to predict that DX BTM 808 NPs would have a very similar pharmacokinetic profile as with Taxotere.

Previously, in our laboratory, drug entrapment in NPs was routinely determined by ultrafiltration. The entrapment efficiency of DX in BTM NPs measured by this ultrafiltration method was $85.3 \pm 1.4\%$. However, different methods (e.g., dialysis) have been employed to determine the drug entrapment efficiency in solid NPs, liposomes and other nano-formulations. As the result of different separation methods, the entrapment efficiencies in these systems varied widely. For the purpose of comparison and to understand the rapid drug release in mouse plasma, the entrapment efficiency of DX in NPs was characterized again by separating free DX from DX NPs using Sepharose CL-4B column. Surprisingly, no DX was detected in NP fractions. It is speculated that the DX eluted from latter fractions included free DX dissolved in aqueous phase, DX loosely associated with surfactants and DX entrapped in micelles formed by excessive surfactants. Although the particle size of DX-containing BTM 808 NPs was regarded homogeneous based on the PCS result, the less light reflected micelles are often underestimated or neglected in this method. Figure 2.8 supports the hypothesis that another population of particles with smaller size existed in the NP

suspension. However, the ultrafiltration method could not differentiate the drug in the latter two forms with the drugs truly entrapped in the NPs. Thus, it is apparent that the inability to discriminate these different forms led to an overestimation of the entrapment efficiency in the BTM NPs. The structure and the exact composition of these smaller particles remain unknown. However, regardless of their structure and composition, drugs in these systems in the latter fractions are expected to be eliminated from systemic circulation more quickly than desired in-vivo. Although DX is generally considered a water-insoluble drug, it has measurable solubility in aqueous solutions, which causes low drug entrapment and poor drug retention in the NPs using Miglyol 808 as oil core. Collectively, it is clear that DX was not “released” from the NPs upon spiking into mouse plasma, but was not truly entrapped in the NPs in the first place. Strategies have to be taken not only to entrap the drug into the NPs but also to retain the drug in the NPs in the biologically relevant environment.

Table 2.1. Physico-chemical properties of Miglyols

Miglyol	Chemical composition	Solubility of DX	Viscosity mPa.s at 20°C	Volatility	Ability to form NP
612	Glyceryl trihexanoate	High > 0.2 mg/mg oil	15	+	Bad
829	Caprylic/capric/succinic triglyceride		300	-	Bad
840	Propylene glycol dicaprylate/dicaprate		10	+	Bad
808	Caprylic triglyceride	Medium 0.05-0.1 mg/mg oil	23	-	Good
8108	Caprylic/capric triglyceride		25	N/A	N/A
8810	Butylene glycol dicaprylate/dicaprate		11	N/A	N/A
810	Caprylic/capric triglyceride		26	N/A	N/A
818	Caprylic/capric/linoleic triglyceride	Low < 0.05 mg/mg oil	33	N/A	N/A
812	Caprylic/capric triglyceride		28	-	Good

Table 2.2. Optimization of BTM 808 NPs by Sequential Simplex

Trial No	Miglyol 808 mg/ml	Brij 78 mg/ml	TPGS mg/ml	Particle Size nm	P.I.	Peak number	% Dust	Current Membership
1	2.5	3.5	1.5	191.1	0.380	1	2.5	0.59
2	2	3	2	147.9	0.810	2	1.3	0
3	3	3	1	183.2	0.198	2	1.2	0.37
4	3	4	2	206.5	0.310	1	0	0.57
5	3.7	4	1	186.5	0.192	2	2	0.35
6	3.3	3.8	1.3	182.8	0.336	1	4	0.62
7	2.9	4.5	2.2	112.3	1.04	2	3.8	0
8	3	3.4	1.3	187.5	0.279	1	4	0.62
9	2.9	3.1	0.7	192.9	0.170	2	1.9	0.34
10	3	3.8	1.7	203.2	0.262	2	2.5	0.28
11	2.6	3.8	1.4	196.3	0.322	1	8	0.44
12	2.9	3.5	1	199.7	0.202	1	2.7	0.61
13	2.8	3.8	1.2	185.6	0.282	1	4.4	0.62
14	3.2	3.8	1.5	198.8	0.263	1	2.9	0.59
6RE1	3.3	3.8	1.3	178.9	0.234	2	0	0.38
15*	2.8	3.7	1.2	184.1	0.359	1	3.7	0.61
16	3	3.5	1.2	190.6	0.313	2	0	0.33

* Bold font indicates leading formulations

Table 2.3. Characterization of DX BTM 808 NPs

Formulation	Particle size (nm)	P.I.	Zeta potential (mV)	Drug loading	% Drug entrapment efficiency
DX BTM 808	167.8 ± 1.7	0.19 ± 0.05	-3.08 ± 0.68	0.3 mg/ml w/w drug/oil 10.7%	$85.3 \pm 1.4^*$
Blank BTM 808	191.7 ± 3.9	0.19 ± 0.1	-5.78 ± 1.36		

* The data are presented as the mean of the particle size of NPs in different batches \pm SD (n = 5).

Table 2.4. Recovery of DX from plasma from SPE or SEC plus SPE

DX concentration in plasma (µg/ml)	Low	Medium	High
	1	5	10
Recovery of SPE (%)	111.9	106.4	109.9
Recovery of SEC + SPE (%)	114.4	101.9	89.9

A.



B.

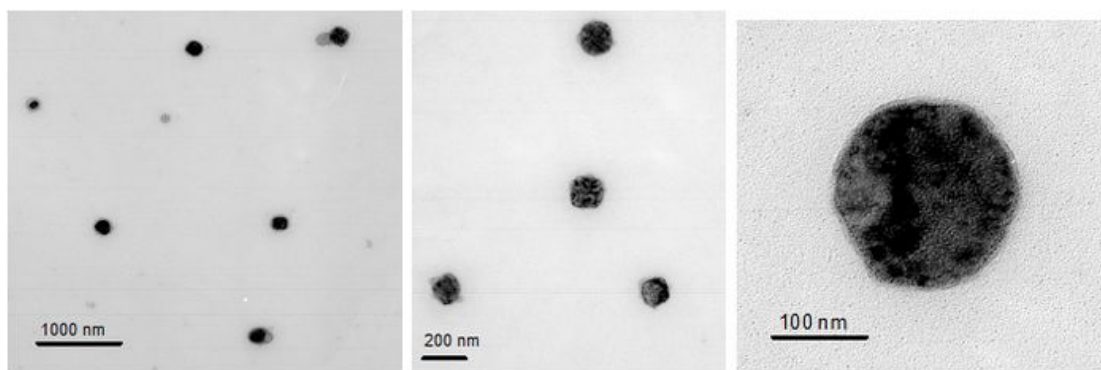


Figure 2.1. Morphology of (A) DX BTM 808 NPs and (B) TEM images of DX BTM 808 NPs.

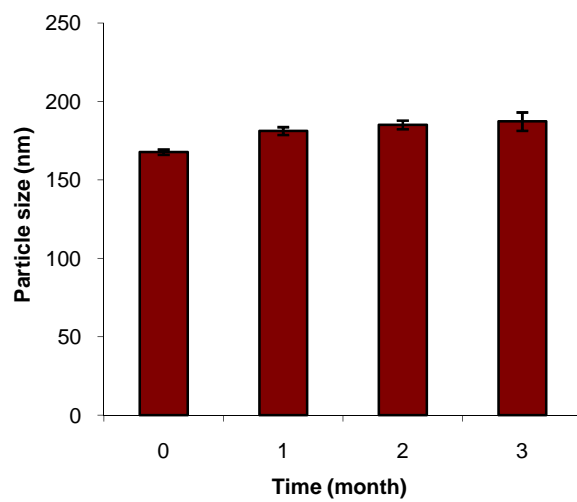
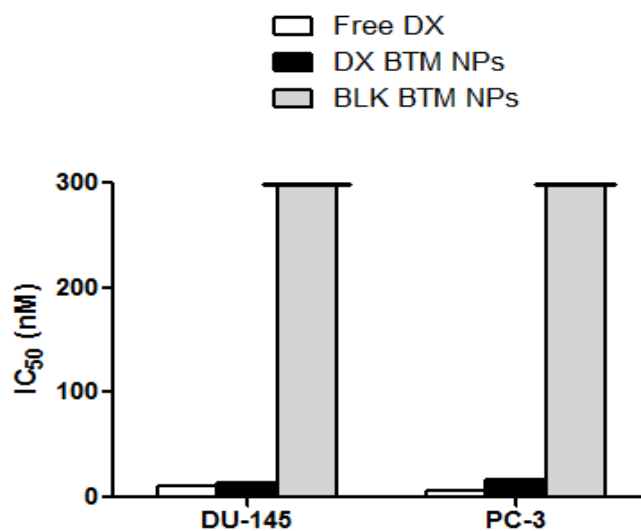


Figure 2.2. Physical stability of DX BTM 808 NPs in 10% lactose stored at 4°C

A.



B.

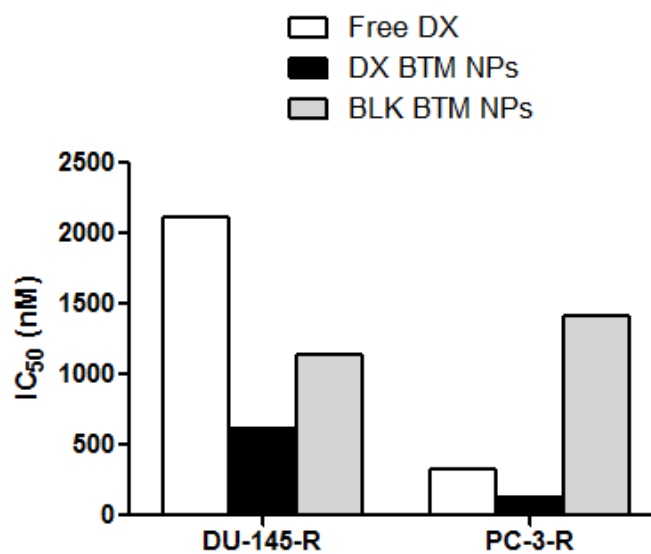
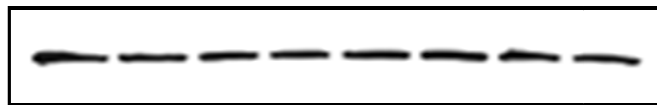


Figure 2.3. In-vitro cytotoxicity of free DX, DX BTM NPs and blank BTM NPs in (A) DU-145 and PC-3 cells, and (B) DU-145-R and PC-3-R cells after 48 hr incubation. Blank NPs were dosed at drug equivalent dose. Drug equivalent dose of NPs are calculated from the NP compositions.

P-gp 170 kDa



Beta-actin 42kDa



Lane	1	2	3	4	5	6	7	8
	DU-145	DU-145-R	PC-3	PC-3-R				

Figure 2.4. The expression of P-gp in DU-145 and PC-3 cell lines and their corresponding PX-resistant DU-145-R and PC-3-R cell lines.

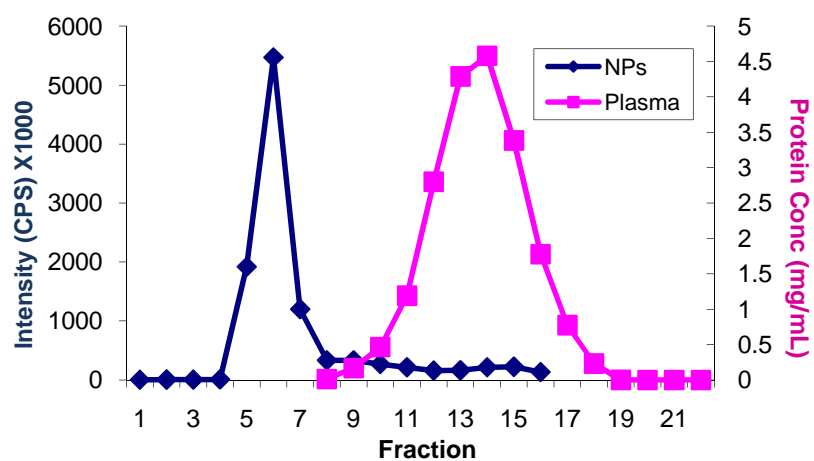


Figure 2.5. The separation of NPs with mouse plasma proteins in Sepharose CL-4B column (15-cm, gravity-packed).

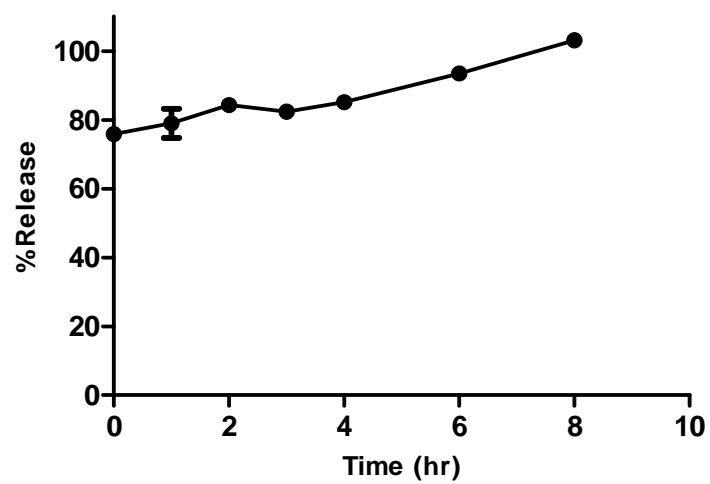


Figure 2.6. The “release” of DX from BTM 808 NPs in mouse plasma at 37°C.

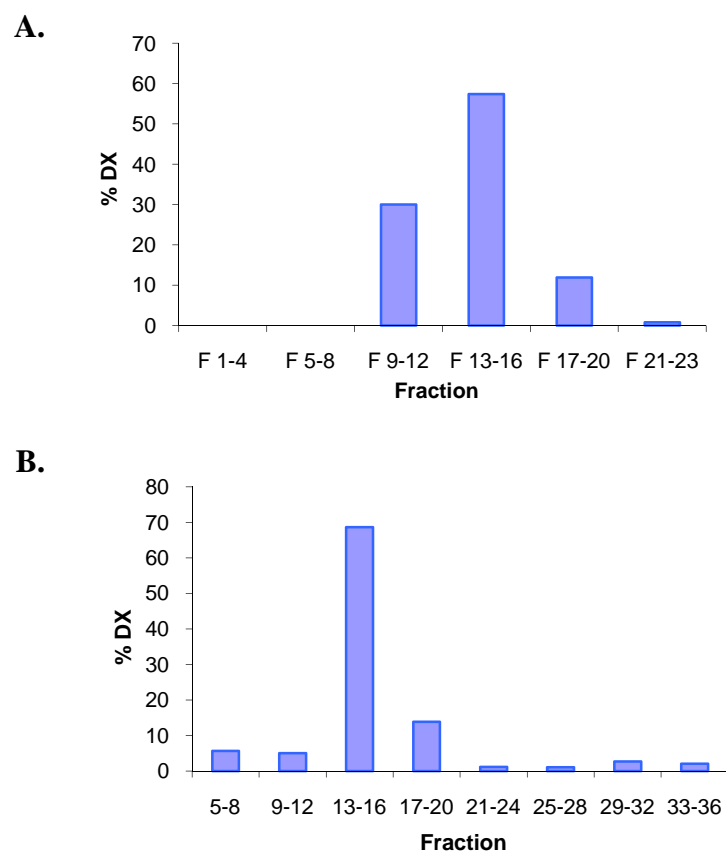


Figure 2.7. (A) The entrapment of DX in BTM 808 NPs determined by SEC as compared to (B) free DX dissolved in 10% lactose.

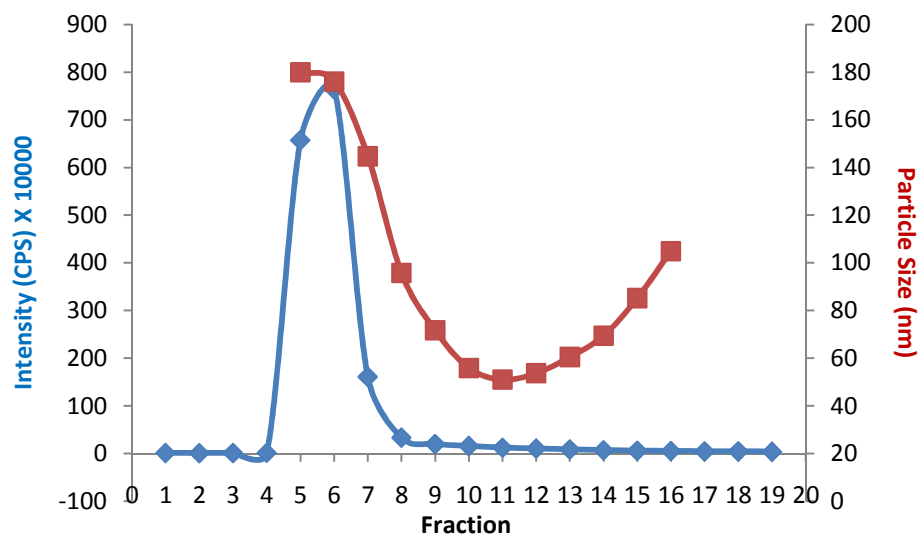


Figure 2.8. The particle size of each fraction from Sepharose CL-4B column after blank BTM NPs were eluted using PBS.

References

1. Goldspiel BR. Clinical overview of the taxanes. *Pharmacotherapy*. Sep-Oct 1997;17(5 Pt 2):110S-125S.
2. van Oosterom AT, Schrijvers D, Schriivers D. Docetaxel (Taxotere), a review of preclinical and clinical experience. Part II: Clinical experience. *Anticancer Drugs*. Jun 1995;6(3):356-368.
3. Cortes JE, Pazdur R. Docetaxel. *J Clin Oncol*. Oct 1995;13(10):2643-2655.
4. Ringel I, Horwitz SB. Studies with RP 56976 (taxotere): a semisynthetic analogue of taxol. *J Natl Cancer Inst*. Feb 20 1991;83(4):288-291.
5. Extra JM, Rousseau F, Bruno R, Clavel M, Le Bail N, Marty M. Phase I and pharmacokinetic study of Taxotere (RP 56976; NSC 628503) given as a short intravenous infusion. *Cancer Res*. Mar 1 1993;53(5):1037-1042.
6. Bissett D, Setanoians A, Cassidy J, et al. Phase I and pharmacokinetic study of taxotere (RP 56976) administered as a 24-hour infusion. *Cancer Res*. Feb 1 1993;53(3):523-527.
7. Burris H, Irvin R, Kuhn J, et al. Phase-I Clinical-Trial of Taxotere Administered as Either a 2-Hour or 6-Hour Intravenous-Infusion. *Journal of Clinical Oncology*. May 1993;11(5):950-958.
8. Pazdur R, Newman RA, Newman BM, et al. Phase I trial of Taxotere: five-day schedule. *J Natl Cancer Inst*. Dec 2 1992;84(23):1781-1788.
9. Tomiak E, Piccart MJ, Kerger J, et al. Phase-I Study of Docetaxel Administered as a 1-Hour Intravenous-Infusion on a Weekly Basis. *Journal of Clinical Oncology*. Jul 1994;12(7):1458-1467.
10. Cui ZR, Yanasarn N, Sloat BR. Nanoparticles engineered from lecithin-in-water emulsions as a potential delivery system for docetaxel. *Int J Pharmaceut*. Sep 8 2009;379(1):174-180.
11. Khalid MN, Simard P, Hoarau D, Dragomir A, Leroux JC. Long circulating poly(ethylene glycol)-decorated lipid nanocapsules deliver docetaxel to solid tumors. *Pharm Res*. Apr 2006;23(4):752-758.
12. Xu Z, Chen L, Gu W, et al. The performance of docetaxel-loaded solid lipid nanoparticles targeted to hepatocellular carcinoma. *Biomaterials*. Jan 2009;30(2):226-232.

13. Elsabahy M, Perron ME, Bertrand N, Yu GE, Leroux JC. Solubilization of docetaxel in poly(ethylene oxide)-block-poly(butylene/styrene oxide) micelles. *Biomacromolecules*. Jul 2007;8(7):2250-2257.
14. Immordino ML, Brusa P, Arpicco S, Stella B, Dosio F, Cattel L. Preparation, characterization, cytotoxicity and pharmacokinetics of liposomes containing docetaxel. *J Control Release*. Sep 4 2003;91(3):417-429.
15. Straubinger RM, Balasubramanian SV. Preparation and characterization of taxane-containing liposomes. *Methods Enzymol*. 2005;391:97-117.
16. Muller RH, Radtke M, Wissing SA. Nanostructured lipid matrices for improved microencapsulation of drugs. *Int J Pharm*. Aug 21 2002;242(1-2):121-128.
17. Dong X, Mattingly CA, Tseng M, Cho M, Adams VR, Mumper RJ. Development of new lipid-based paclitaxel nanoparticles using sequential simplex optimization. *Eur J Pharm Biopharm*. May 2009;72(1):9-17.
18. *Handbook of Pharmaceutical Excipients*: Pharmaceutical Press; 2009.
19. Dhanikula AB, Khalid NM, Lee SD, et al. Long circulating lipid nanocapsules for drug detoxification. *Biomaterials*. Feb 2007;28(6):1248-1257.
20. Takeda M, Mizokami A, Mamiya K, et al. The establishment of two paclitaxel-resistant prostate cancer cell lines and the mechanisms of paclitaxel resistance with two cell lines. *Prostate*. Jun 15 2007;67(9):955-967.
21. Dong X, Mattingly CA, Tseng MT, et al. Doxorubicin and paclitaxel-loaded lipid-based nanoparticles overcome multidrug resistance by inhibiting P-glycoprotein and depleting ATP. *Cancer Res*. May 1 2009;69(9):3918-3926.

Chapter 3.

Development of lipid nanoparticles containing docetaxel fatty acid conjugates to control the drug release rate in-vitro and in-vivo

1. Summary

Three docetaxel (DX) lipid conjugates: 2'-lauroyl-docetaxel (C12-DX), 2'-stearoyl-docetaxel (C18-DX) and 2'-behenoyl-docetaxel (C22-DX) were synthesized to enhance the drug loading, entrapment and retention in liquid oil-filled lipid nanoparticles (NPs). The three conjugates showed 10-fold higher solubility in the liquid oil phase, Miglyol 808, than DX. To further increase the drug entrapment efficiency in NPs, orthogonal design was performed. The optimized formulation was composed of Miglyol 808 (2.5 mg/mL), Brij 78 (1.7 mg/mL) and Vitamin E TPGS (0.8 mg/mL). The conjugates were successfully entrapped in the reduced-surfactant NPs with entrapment efficiencies about 50-60% as measured by size exclusion chromatography (SEC) at a final concentration of 0.5 mg/mL. All three conjugates

L Feng, H Wu, P Ma, RJ Mumper, and SR Benhabbour, "Development of Lipid Nanoparticles Containing Docetaxel Conjugates Designed to Control the Drug Release Rate In-vitro and In-vivo." *International Journal of Nanomedicine*, 2011 (6): 2545-2556.

showed 45% initial burst release in 100% mouse plasma. Whereas C12-DX showed another 40% release over the next 8 hr, C18-DX and C22-DX in NPs showed no additional release after the initial burst of drug. All conjugates showed significantly lower cytotoxicity than DX in human DU-145 prostate cancer cells. The IC_{50} values of free conjugates and conjugate NPs were comparable except for C22-DX, which was non-toxic in the tested concentration range and showed only vehicle toxicity when entrapped in NPs. In-vivo, the $AUC_{0-\infty}$ values of all DX conjugate NPs were significantly greater than that of Taxotere, demonstrating prolonged retention of drug in the blood. The $AUC_{0-\infty}$ value of DX in Taxotere was 8.3-fold, 358.0-fold and 454.5-fold lower than that of NP-formulated C12-DX, C18-DX and C22-DX, respectively. The results of these studies strongly support that the physical/chemical properties of DX conjugates may be fine-tuned to influence the affinity and retention of DX in oil-filled lipid NPs which leads to very different pharmacokinetic profiles and blood exposure of an otherwise potent chemotherapeutic agent. These studies and methodologies may allow for improved and more potent NP-based formulations.

2. Introduction

The enhanced permeability and retention (EPR) effect is the major mechanism for passive targeting of nano-formulations to accumulate in the tumor site. To ensure that the NPs take advantage of the EPR effect, the NPs need to maintain two aspects of

stability in-vivo: long circulation of delivery vehicles and long retention of anticancer agents in the NPs. The importance of long circulation of NPs has been widely recognized and extensively demonstrated for decades. Various polyethylene glycol (PEG)-coated nano-formulations have shown prolonged circulation time in-vivo.¹⁻⁴ On the other hand, the importance of long retention of anticancer agent in the nano-carriers is often underappreciated. The enhancement of drug retention in long circulating NPs increases drug uptake and accumulation in the tumor tissue. To study the retention of drugs in the NPs, many in-vitro release studies have been conducted in aqueous buffers (e.g., PBS) and are expected to predict the in-vivo retention behavior of the nano-formulation. However, the correlation between the in-vitro release in PBS and in-vivo release behavior is often poor, especially when the entrapped drug has extremely low aqueous solubility and/or high protein binding affinity. Given that DX has poor water solubility and high protein binding,⁵ we developed a more predictive “ex-vivo” release method to better mimic the in-vivo environment with the goal to achieve better correlation with the in-vivo pharmacokinetic profiles.

Previously, we developed liquid oil-filled BTM 808 NPs by sequential simplex optimization to deliver DX. However, despite the desirable formulation properties (e.g., monodispersed particle size, apparent drug entrapment efficiency, etc.), DX was found to be very rapidly released in mouse plasma in-vitro. Further investigation revealed that DX was not truly entrapped into the NPs during preparation. Despite that DX is a poorly water-soluble drug, DX has appreciable solubility in aqueous solutions and the

affinity of DX with the oil core was not high enough to prevent its rapid diffusion from the oil core to the aqueous phase. Strategies have to be taken to overcome the poor retention of DX in the NPs in aqueous phase and in biologically relevant medium. Most lipid-based NPs are more efficient for the encapsulation of lipophilic drugs. In the literature, lipophilic taxane prodrugs have been synthesized to further increase their lipophilicity and miscibility with lipids which in turn increases their entrapment in the lipid-based NPs by several research groups.⁶⁻¹⁰

The objective of these present studies was to improve the affinity and retention of DX in the NPs to thereby achieve prolonged in-vivo blood exposure. To this end, we synthesized three lipid-DX prodrugs with different fatty acid chain lengths. The chain lengths (12, 18 and 22) were chosen to be compatible with the liquid oil core, Miglyol 808, which is composed of caprylic acid triglycerides. By utilizing the new release method to investigate the in-vitro release of the conjugates from these NPs, a correlation between the in-vitro release and in-vivo pharmacokinetics was achieved. The superior pharmacokinetic profiles of the three conjugates in NPs compared to Taxotere makes these NPs promising candidates for preclinical anticancer efficacy studies.

3. Materials and methods

3.1. Materials and Animals

DX, paclitaxel (PX), lauroyl chloride (98%), stearyl chloride (97%), behenoyl chloride (>99%), 4-(dimethylamino)pyridine (DMAP) and *p*-nitrophenylacetate (PNPA) were purchased from Sigma-Aldrich (St. Louis, MO). Miglyol 808 was obtained from Sasol (Witten, Germany). Polyoxyl 20-stearyl ether (Brij 78) was obtained from Uniqema (Wilmington, DE). D-alpha-tocopheryl polyethylene glycol succinate (Vitamin E TPGS) was purchased from Eastman Chemicals (Kingsport, TN). BALB/c mouse plasma was purchased from Innovative Research Inc. (Novi, MI). Sepharose CL-4B was purchased from GE Healthcare (Uppsala, Sweden). Hybrid-SPE[®] cartridge was purchased from Sigma-Aldrich Supelco (St. Louis, MO).

The human prostate cancer cell line, DU-145, was obtained from American Type Culture Collection (ATCC) and was maintained in RPMI-1640 medium with 10% fetal bovine serum (FBS). Male athymic nude (nu/nu) mice, 4 to 5 weeks old, were obtained from the University of North Carolina, Division of Laboratory Animal Medicine (DLAM) and housed in a pathogen-free room. All experiments involving mice were conducted according to an approved animal protocol by the University of North Carolina Institutional Animal Care and Use Committee.

3.2. Methods

3.2.1. Synthesis

3.2.1.1. General procedure for the synthesis of 2'-lauroyl-docetaxel (1, C12-DX)⁸

A flame-dried round-bottom flask was charged with DX (0.2 g, 2.48×10^{-4} mol, 1 equiv) and DMAP (0.06 g, 4.95×10^{-4} mol, 2 equiv) in dry CH_2Cl_2 (8 mL) under argon. The solution was stirred for 10 min at 0°C. Lauroyl chloride (57.2 μl , 2.48×10^{-4} mol, 1 equiv) was added, and the reaction mixture was stirred for 6 hr at 0°C. The reaction was monitored by thin layer chromatography (TLC) (CH_2Cl_2 : MeOH 9:1 v/v; $R_f = 0.7$) for completion. After completion, the solvent was removed by rotary evaporation in vacuo and the crude product was dissolved in diethylether (50 mL) and washed with 5% HCl (3×40 mL), and finally with brine (40 mL) to remove the salt byproducts. The organic phase was dried over anhydrous sodium sulfate, and the solvent was evaporated in vacuo. The product was purified by silica-packed column chromatography (9:1 CH_2Cl_2 :MeOH) to give the desired DX derivative as a white solid (0.21 g, yield 85%).

^1H NMR (400 MHz, CDCl_3): δ (ppm) = 1.12 (t, 3H, $-\text{CH}_3(\text{CH}_2)_{10}$), 1.23 (s, 6H, $-\text{H}_{16,17}$), 1.34 (s, 9H, $-\text{H}_{7-9}$), 1.72 (s, 3H, $-\text{H}_{19}$), 1.75 (m, 14H, $-(\text{CH}_2)_7\text{CH}_2\text{CH}_3$), 1.81 (m, 2H, $-\text{CH}_2\text{CH}_2\text{C}_1$), 1.84 (s, 3H, $-\text{H}_{18}$), 1.87 (m, 2H, $-\text{H}_{14}$), 2.26 (d, 2H, $-\text{CH}_2\text{C}_1$), 2.36 (s, 3H, $-\text{H}_{22}$), 2.67 (m, 1H, $-\text{H}_3$), 3.43 (s, 1H, $-\text{H}_7$), 3.9 (d, 1H, $-\text{H}_4$), 4.17 (d, 1H, $-\text{H}_6$), 4.24 (m, 1H, $-\text{H}_5$), 4.3 (d, 1H, $-\text{H}_{20}$), 4.61 (s, 1H, $-\text{H}_{10}$), 4.93 (d, 1H, $-\text{H}_{13}$), 5.21 (d, 1H, $-\text{H}_{10}$), 5.67 (d, 1H, $-\text{H}_2$), 6.21 (t, 1H, $-\text{H}_2$), 7.31 (m, 1H, $-\text{H}_3$), 7.36-7.61 (m, 8H,

–Ar- H_{26-28} and Ar- H_{30-35}), 8.1 (d, 2H, –Ar- $H_{25,29}$). ^{13}C NMR (100 MHz, CD_3OD): δ (ppm) = 9.9 (– C_{19}), 14.4 (– $\text{CH}_3(\text{CH}_2)_{10}$), 20.6 (– C_{18}), 22.5 (– C_{22}), 24.8 (– $(\text{CH}_2)_9\text{CH}_2\text{CH}_3$), 26.44 (– $\text{C}_{16,17}$), 28.2 (– $\text{C}_{7'-9'}$), 31.9 (– $(\text{CH}_2)_8\text{C}_{1''}$), 34.4 (– $\text{C}_{6,14}$), 43.1 (– C_{15}), 46.4 (– C_3), 56.4 (– $\text{C}_{3'}$), 57.6 (– C_8), 72 (– C_{13}), 72.4 (– C_7), 74.5 (– C_2), 74.8 (– C_{10}), 76.6 (– C_{20}), 78.8 (– $\text{C}_{6'}$), 80.2 (– C_1), 81.1 (– C_4), 84.1 (– C_5), 126.7 (– $\text{C}_{31,33,35}$), 128 (– $\text{C}_{32,34}$), 128.7 (– $\text{C}_{26,28}$), 130.2 (– $\text{C}_{24,25,29}$), 133.7 (– C_{27}), 135.9 (– C_{11}), 138.5 (– C_{12}), 155.3 (– $\text{C}_{5'}$), 167.1, 167 (– C_{23}), 172.7 (– C_{21}), 174 (– C_1), 177.8 (– $\text{C}_{1''}$), 211.6 (– C_9).

3.2.1.2. General procedure for the synthesis of 2'-stearoyl-docetaxel (2, C18-DX)

2'-stearoyl-docetaxel was synthesized following the same procedure outlined above for 2'-lauroyl-docetaxel using stearoyl chloride to give the final conjugate as a white solid (0.17 g, yield 65%). ^1H NMR (400 MHz, CDCl_3): δ (ppm) = 0.8 (t, 3H, – $\text{CH}_3(\text{CH}_2)_{16}$), 1.05 (s, 6H, – $H_{16,17}$), 1.14 (s, 9H, – $H_{7'-9'}$), 1.16 (s, 3H, – H_{19}), 1.26 (m, 14H, – $(\text{CH}_2)_{13}\text{CH}_2\text{CH}_3$), 1.45 (m, 2H, – $\text{CH}_2\text{CH}_2\text{C}_{1''}$), 1.68 (s, 3H, – H_{18}), 1.88 (m, 2H, – H_{14}), 2.25 (d, 2H, – $\text{CH}_2\text{C}_{1''}$), 2.37 (s, 3H, – H_{22}), 2.38 (m, 1H, – H_3), 3.43 (s, 1H, – H_7), 3.85 (d, 1H, – H_4), 4.12 (d, 1H, – H_6), 4.24 (m, 1H, – H_5), 4.3 (d, 1H, – H_{20}), 4.88 (d, 1H, – H_{13}), 5.14 (s, 1H, – H_{10}), 5.3 (d, 1H, – H_{10}), 5.61 (d, 1H, – H_2), 6.2 (t, 1H, – $H_{2'}$), 7.2 (m, 1H, – $H_{3'}$), 7.25-7.53 (m, 8H, –Ar- H_{26-28} and Ar- H_{30-35}), 8.05 (d, 2H, –Ar- $H_{25,29}$). ^{13}C NMR (100 MHz, CD_3OD): δ (ppm) = 8.9 (– C_{19}), 13.2 (– $\text{CH}_3(\text{CH}_2)_{16}$), 19.9 (– C_{18}), 21.6 (– C_{22}), 23.7 (– $(\text{CH}_2)_{15}\text{CH}_2\text{CH}_3$), 25.3 (– $\text{C}_{16,17}$), 27.1 (– $\text{C}_{7'-9'}$), 30.9 (– $(\text{CH}_2)_{14}\text{C}_{1''}$), 32.7 (– $\text{C}_{6,14}$), 42.1 (– C_{15}), 45.4 (– C_3), 56.4 (– $\text{C}_{3'}$), 57.6 (– C_8), 70.8 (– C_{13}), 73.1 (– C_7), 73.5

(-C₂), 74 (-C₁₀), 77.9 (-C₂₀), 79.4 (-C_{6'}), 79.9 (-C₁), 83.2 (-C₄), 84.1 (-C₅), 125.3 (-C_{31,33,35}), 127.1 (-C_{32,34}), 127.8 (-C_{26,28}), 129.2 (-C_{24,25,29}), 132.6 (-C₂₇), 134.5 (-C₁₁), 138.2 (-C₁₂), 154.1 (-C_{5'}), 166.1 (-C₂₃), 167.2 (-C₂₁), 168.7 (-C₁), 171.8 (-C_{1''}), 210.6 (-C₉).

3.2.1.3. General procedure for the synthesis of 2'-behenoyl-docetaxel (3, C22-DX)

2'-behenoyl-docetaxel was synthesized following the same procedure outlined above for 2'-lauroyl-docetaxel using behenoyl chloride to give the final conjugate as a white solid (0.26 g, yield 95%). ¹H NMR (400 MHz, CDCl₃): δ (ppm) = 0.81 (t, 3H, -CH₃(CH₂)₂₀), 1.05 (s, 6H, -H_{16,17}), 1.14 (s, 9H, -H_{7',9'}), 1.16 (s, 3H, -H₁₉), 1.23 (m, 36H, -(CH₂)₁₈CH₂CH₃), 1.26 (m, 2H, -CH₂CH₂C_{1''}), 1.45 (s, 3H, -H₁₈), 1.62 (m, 2H, -H₁₄), 1.67 (d, 2H, -CH₂C_{1''}), 1.9 (s, 3H, -H₂₂), 2.26 (m, 1H, -H₃), 2.4 (s, 1H, -H₇), 3.86 (d, 1H, -H₄), 4.12 (d, 1H, -H₆), 4.23 (m, 1H, -H₅), 4.26 (d, 1H, -H₂₀), 4.61 (s, 1H, -H₁₀), 4.9 (d, 1H, -H₁₃), 5.14 (d, 1H, -H₁₀), 5.62 (d, 1H, -H₂), 6.2 (t, 1H, -H_{2'}), 7.2 (m, 1H, -H_{3'}), 7.22-7.53 (m, 8H, -Ar-H₂₆₋₂₈ and Ar-H₃₀₋₃₅), 8.05 (d, 2H, -Ar-H_{25,29}). ¹³C NMR (100 MHz, CD₃OD): δ (ppm) = 8.9 (-C₁₉), 13.2 (-CH₃(CH₂)₂₀), 19.9 (-C₁₈), 21.6 (-C₂₂), 23.7 (-CH₂)₁₉CH₂CH₃), 25.3 (-C_{16,17}), 27.1 (-C_{7',9'}), 30.9 (-CH₂)₁₈C_{1''}), 32.7 (-C_{6,14}), 42.1 (-C₁₅), 45.4 (-C₃), 56.5 (-C_{3'}), 57.2 (-C₈), 70.8 (-C₁₃), 73.1 (-C₇), 73.5 (-C₂), 74.0 (-C₁₀), 76.3 (-C₂₀), 77.9 (-C_{6'}), 79.9 (-C₁), 83.2 (-C₄), 84.1 (-C₅), 125.3 (-C_{31,33,35}), 127.1 (-C_{32,34}), 127.8 (-C_{26,28}), 129.2 (-C_{24,25,29}), 132.6 (-C₂₇), 134.5 (-C₁₁), 138.2 (-C₁₂), 154.2 (-C_{5'}), 166.1, 167.2 (-C₂₃), 168.4 (-C₂₁), 171.8 (-C₁), 177.8 (-C_{1''}),

210.6 ($-C_9$).

3.2.2. Characterization of DX and DX conjugates

3.2.2.1. Mass spectrometry

Electrospray Ionization (ESI) coupled with direct injection was employed to determine the m/z of the final synthetic conjugate products by Thermo Scientific TSQ Quantum Access with positive ionization. The mass of the observed molecular ions were $m/z = 1012.6$, 1096.7 and 1152.8 , which clearly corresponded to the Na^+ adducts of C12-DX, C18-DX and C22-DX, respectively.

3.2.2.2. High performance liquid chromatography (HPLC)

The DX conjugate concentrations were quantified by HPLC using a Finnigan Surveyor HPLC system with a Photodiode Array (PDA) detector, autosampler and LC pump plus with a Inertsil[®] ODS-3 column (4 μm , 4.6 \times 150 mm, GL Sciences) at 25°C. Chromatographic separation was achieved by gradient elution using a mobile phase of 2-propanol, acetonitrile (ACN) and water (5: 55: 40 v/v/v). The flow rate was 1.0 mL/min and the total run time was 25 min for each 25 μL injection. The wavelength was 230 nm.

The DX concentration was quantified by LC/MS/MS using a Finnigan Surveyor Autosampler Plus and Finnigan Surveyor MS Pump Plus. Chromatographic separations

were achieved using a SunFire™ C18 column (2.1 × 30 mm, 3.5 µm particle size, Waters) at 25°C. The mobile phase consisted of 0.1% formic acid in water and methanol using gradient separation. The flow rate was 0.5 mL/min and the total run time was 8 min for each 25 µL injection. Mass spectrometric analysis was performed using a Thermo Scientific TSQ Quantum Access with positive ionization. The capillary temperature was set up to 390°C, and the spray voltage was 4000V. For DX analysis, m/z 830.0 → 549.0 was monitored with PX (m/z 876.3 → 308.0) as an internal standard.

3.2.3. Evaluation of DX conjugate solubility in Miglyol 808 and mouse plasma

Approximately 50 mg of each DX conjugate was added to individual vials containing 50 µL of Miglyol 808. For the evaluation of DX conjugate solubility in mouse plasma, around 1 mg of each DX conjugate was added to a vial containing 1 mL of BALB/c mouse plasma. The mixtures were stirred at room temperature for 24 hr. The samples were then centrifuged for 1 hr at 14,000 rpm to remove undissolved drug. After centrifugation, the saturated supernatant was diluted with ACN and analyzed by HPLC.

3.2.4. Preparation and characterization of BTM NPs

3.2.4.1. Preparation of BTM NPs containing DX conjugates

DX conjugates containing NPs were prepared using a warm oil-in-water (o/w) microemulsion precursor method previously developed in our laboratory.¹¹ Briefly, Miglyol 808 and surfactants (Brij 78 and Vitamin E TPGS) were accurately weighed into glass vials and heated to 50-60°C. Drugs dissolved in ACN were added and the organic solvent was removed by nitrogen flow. One (1) mL of pre-heated 10% lactose in water was added into the mixture of melted oil, surfactants and drugs. The mixture was stirred for 20 min at 50-60°C then cooled to room temperature. Orthogonal design was performed to optimize NPs with desirable properties, including particle size and drug entrapment efficiency.

For in-vivo studies, NPs were concentrated and PEGylated. The formulation was concentrated four-fold by adding four-fold less 10% lactose continuous phase while keeping the other components of the formulation unchanged. The NPs were PEGylated by adding 8% Brij 700 during the preparation wherein 8% was the w/w ratio of Brij 700 to Miglyol 808.

3.2.4.2. Characterization of BTM NPs containing DX conjugates

3.2.4.2.1. Particle size and zeta potential

Particle size and size distribution of NPs were determined using an N5 Submicron Particle Size Analyzer (Beckman). Five (5) µL of NPs was diluted with 1 mL of water

to reach the intensity required by the instrument. Particle size was determined at 90° light scattering at 25°C. The zeta potential of NPs was determined using the Zetasizer Nano Z (Malvern Instruments, Southborough, MA).

3.2.4.2.2. Drug entrapment efficiency

Drug entrapment efficiency was determined by SEC. DX conjugate NPs were separated with the free drugs using a Sepharose CL-4B column (15 cm). NPs were eluted using PBS in fraction 5-8 (1 mL/fraction, confirmed by dynamic light scattering intensity). Each fraction was evaporated to dryness in vacuo, resuspended in 1 mL ACN and analyzed by HPLC to determine the concentration of DX conjugate in each fraction. The % drug entrapment efficiency was defined as $100\% \times \text{the ratio of the weight of drug detected in fraction 5-8 to the total drug weight detected.}$

3.2.5. In-vitro drug release in mouse plasma

In-vitro release studies were performed in 100% plasma from BALB/c mice. Briefly, 100 µL of purified DX conjugate NPs were spiked into 2 mL of mouse plasma. The release mixture was incubated at 37°C in a water bath shaker. At designated time points from 0 hr to 8 hr, two aliquots of release mixture were removed. One aliquot (100 µL) was used to determine the total drug concentration by solid phase extraction (SPE) using Hybrid-SPE precipitate method. Briefly, one volume of release mixture was

mixed with three volumes of 2% formic acid in ACN. Following vortex and centrifugation, the supernatant was applied to a Hybrid-SPE cartridge. The eluate was collected for HPLC analysis. Another aliquot (100 μ L) was used to determine the drug remained in the NPs using the method described above. The % DX released at any time point was calculated as $100\% \times [(\text{Total drug detected} - \text{drug remaining in the NPs}) / \text{Total drug detected}]$.

3.2.6. In-vitro esterase digestion

3.2.6.1. DX conjugate digestion in fresh mouse plasma

The esterase digestion study was performed in fresh mouse plasma. The DX conjugate DMSO stock solutions (5 mg/mL) or DX conjugate NPs (0.5 mg/mL) were spiked into the plasma to make a final concentration of 10 μ g/mL. The mixture was incubated at 37°C in a water bath shaker. At designated time points, 100 μ L of digestion mixture was removed. The concentration of DX conjugates was determined by Hybrid-SPE precipitate method as described above followed by HPLC analysis. The % DX conjugate remaining at any time point was calculated as $100\% \times$ the ratio of remaining drug amount to the total drug spiked into this volume of plasma. The concentration of DX in the same sample was determined by LC/MS. The % DX conjugate hydrolyzed to DX at any time point was calculated as $100\% \times [(\text{DX amount detected} \times \text{conjugate Mw} / 807) / \text{the total drug spiked into this volume of plasma}]$.

3.2.6.2. Esterase activity in plasma samples

Fresh mouse plasma, commercial mouse plasma or human plasma was diluted in PBS to a protein concentration of about 0.3 mg/mL and incubated with PNPA (400 μ M) at 37°C for 15 min. After incubation, equal volume of ice-cold ACN was added to terminate the reaction. The suspension was centrifuged for 5 min at 14,000 rpm at 4°C. The liberated *p*-nitrophenol was determined ($\epsilon = 1.62 \times 10^4 \text{ M}^{-1} \text{ cm}^{-1}$) by measuring the absorbance at 405 nm using the Synergy 2 Multi-Detection Microplate Reader. One unit of esterase activity was defined as the quantity of enzyme required to release 1 μ mol of *p*-nitrophenol per minute under assay conditions.

3.2.7. Evaluation of in-vitro cytotoxicity

The MTT assay was utilized to assess the cytotoxicity of free DX conjugates and the DX conjugate NPs. Serial dilutions of free drugs or drug containing NPs were added to the DU-145 cells and incubated for 48 hr, 72 hr or 96 hr. The cells were then incubated with MTT solution for 4 hr and the formazan dyes were solubilized by DMSO. The absorbance was measured using the Synergy 2 Multi-Detection Microplate Reader at 570 nm, and the concentration of drug that inhibited cell survival by 50% (IC_{50}) was determined from cell survival plots.

3.2.8. In-vivo pharmacokinetic studies

Male athymic nude mice were randomly divided into four groups. The mice (n=3/time point) were injected via tail vein with test samples (Taxotere, C12-DX NPs, C18-DX NPs and C22-DX NPs), all at a DX dose of 10 mg/kg. At designated time points from 3 min to 24 hr, the mice were given an overdose of ketamine (100 mg/kg) and Domitor (0.5 mg/kg) for deep anesthesia prior to cardiac puncture to collect blood and a cervical dislocation was then performed to euthanize the mice. For plasma separation, the blood collected in heparin-coated tubes was centrifuged at 12,300 rpm for 15 min. The obtained plasma was processed with Hybrid-SPE precipitate method as described above. The concentrations of DX conjugates in plasma were determined by HPLC, and the DX concentrations were quantified by LC-MS. Pharmacokinetic analysis and modeling was performed by WinNonlin (version 5.2.1; Pharsight Corp, Mountain View, CA).

3.2.9. Statistical analysis

Statistical comparisons were performed using one-way analysis of variances (ANOVA) (©1992-2007 GraphPad Prism Software, Inc.). Results were considered significant at 95% confidence interval ($p < 0.05$). Orthogonal experimental design for formulation optimization was performed and statistically analyzed using Design Expert® (Version 7.1 Trial; Stat-Ease, Minneapolis, MN).

4. Results

4.1. Synthesis and characterization of DX conjugates

The DX-lipid conjugates in these studies were prepared by a one-step esterification reaction using acid chloride derivatives of various chain length fatty acids (Figure 3.1). Although there are multiple hydroxyl groups in DX molecule, the 2'-OH is the most reactive and accessible one, followed by 7-OH.⁸ It has been previously reported that the conjugation of fatty acids to DX and PX occurred preferentially on 2'-OH.^{8,9,12} By controlling the molar ratio of the fatty acid chloride to DX carefully, 2'-mono substituted DX conjugates were obtained with minimal formation of 2',7-disubstituted byproducts and unreacted DX. In the case of C22-DX, only 2'-OH ester derivative was obtained after washing with 5% HCL and brine as determined by TLC and NMR without further chromatography required. The yield for this reaction was as high as 95%.

4.2. Solubility of DX conjugates in Miglyol 808 and mouse plasma

To enhance the drug loading capacity and retention of drug in the NPs, DX conjugates were synthesized and investigated for their solubility in Miglyol 808 (Table 3.1). The solubility of all three DX conjugates in Miglyol 808 was about 10-fold higher than the

solubility of DX in Miglyol 808. The solubility showed no chain-length dependency. The chemical composition of Miglyol 808 is caprylic acid triglyceride, so DX conjugates with a 12-22 carbon chain are more compatible than DX with Miglyol 808 due to the similarity of the chemical structure.

Since the in-vitro release of DX conjugates from NPs was studied in mouse plasma, the solubility of DX conjugates in BALB/c mouse plasma was determined and compared as well (Figure 3.2). In contrast to solubility in Miglyol 808, the solubility of DX conjugates in plasma showed significant chain-length dependency. With an increase in lipid chain, the solubility of the conjugate in plasma decreased. The solubility of C12-DX (377.0 ± 21.5 $\mu\text{g/mL}$) was about 10-fold higher than that of C22-DX (34.4 ± 0.6 $\mu\text{g/mL}$) and 6.5-fold higher than that of C18-DX (57.5 ± 2.6 $\mu\text{g/mL}$). Given the extremely low water solubility of the DX conjugates, the solubility of the conjugates in plasma was attributed almost entirely to their binding with plasma proteins.

4.3. Optimization of DX conjugate containing NPs by orthogonal design

The orthogonal design was based on the NP previously developed to formulate DX, which was composed of Miglyol 808 (2.8 mg/mL), Brij 78 (3.7 mg/mL), TPGS (1.2 mg/mL) and DX (0.3 mg/mL). In the present study, the particle size and drug entrapment efficiency were chosen as responses in the optimization process. A criterion

in the orthogonal design strategy was to reduce the total amount of surfactant used in the formulation, as it had been previously observed that increased level of surfactants in the formulation decreased drug entrapment, especially for drugs that have amphipathic properties.

Based on the preliminary studies, a 3 level-3 variable orthogonal experiment ($L_9 3^3$) was designed as shown in Table 3.2. The two responses selected were particle size and % entrapment efficiency. In this experiment, C12-DX was used as a representative DX conjugate. The resulting NP compositions based on the optimization using C12-DX were applied to other conjugates. Nine (9) batches of C12-DX NPs were prepared and characterized. The results are also shown in Table 3.2. Statistical analysis showed that temperature as a variable was not significant to the model ($p > 0.05$). The particle size, as a defined model response, was not responsive to the variables ($p > 0.05$). It should be noted that the general placebo composition for this formulation was previously optimized. Thus, it was anticipated that continued optimization with DX conjugates would lead to a relatively narrow response range. When the model focused on the effect of surfactant concentrations on the % entrapment efficiency, it was clear that decreasing the surfactant concentrations increased drug entrapment in the NPs (Figure 3.3). Although the % entrapment efficiency of batch 2 was slightly higher than batch 5, batch 5 was more stable over long-term (one month) storage in 4°C refrigerator (data not shown). The final composition was selected as shown in Table 3.3. Due to the enhanced solubility of drugs in the oil core, the newly developed formulation was

capable of loading more DX conjugate (0.5-1 mg/mL conjugates versus 0.3 mg/mL DX) without significantly changing the physical properties of the resultant NPs. The optimal NPs had a mean particle size of 200 nm with a zeta potential around 0 mV (Table 3.3). The entrapment efficiencies of the three DX conjugates were $55.2 \pm 2.3\%$, $56.3 \pm 7.6\%$ and $59.6 \pm 1.6\%$ for C12-DX, C18-DX and C22-DX, respectively. The similar entrapment efficiency of three DX conjugates was predicted by their comparable solubility in Miglyol 808 as shown in Table 3.1.

4.4. In-vitro release of DX conjugates from NPs in mouse plasma

In this study, the release of DX conjugates from the NPs was studied by the novel “ex-vivo” method in 100% mouse plasma. For the release studies, the DX conjugate containing NPs were first purified by SEC and only NPs with size around 200 nm (fraction 5-8) were collected. For all three DX conjugate NPs, an initial 45% burst release was observed upon spiking into the mouse plasma (Figure 3.4). After the initial burst release, C12-DX was slowly released to 86% in 8 hr, while no additional C18-DX and C22-DX was released from the NPs within 8 hr. A longer time point (96 hr) release study was carried out for the C18-DX NPs; however, no drug was released from the NPs after the burst (data not shown).

4.5. In-vitro esterase digestion

The digestion rate of both free DX conjugates and DX conjugate formulated in NPs in fresh mouse plasma was chain-length dependent (Figure 3.5A). C12-DX with the shortest fatty acid chain length showed 100% parent drug loss within 4-8 hr in free form and in NPs; while about 80% and 90% of C18-DX and C22-DX in their free forms were detected after 48 hr incubation, respectively. Surprisingly, when entrapped in NPs, the loss of C18-DX and C22-DX was more rapid than their free forms. After 48 hr incubation, only 43.7% and 66.5% of C18-DX and C22-DX remained intact, respectively.

The DX liberation rate in fresh mouse plasma was consistent with the digestion rate of each DX conjugate (Figure 3.5B). In 48 hr, 60% and 45% of NP-entrapped C12-DX and free C12-DX were cleaved to DX, respectively. Whereas only 14% of NP-entrapped C18-DX was hydrolyzed to DX and negligible DX was hydrolyzed from free C18-DX, free C22-DX and NP-entrapped C22-DX. It is worth noting that the fraction of remaining DX conjugate plus the fraction of DX conjugate transferred to DX did not reach 100% for all three conjugates. The recovery of free conjugates was 44%, 82% and 90% for C12-DX, C18-DX and C22-DX in 48 hr, respectively. The recovery of NP-entrapped conjugates was 52%, 57% and 68% for C12-DX, C18-DX and C22-DX in 48 hr, respectively. It suggests that besides hydrolysis to DX, DX conjugates have other transfer pathways and the reactivity decreases with the chain-length increases.

4.6. Esterase activity in plasma samples

The non-specific esterase activity of different plasma samples is shown in Figure 3.6. The fresh mouse plasma without freezing-thawing cycle showed the highest esterase activity. The esterase activity in human plasma was over 2-times lower than that in fresh mouse plasma. The commercial mouse plasma used in the drug release studies had the lowest esterase activity, which was 6-times lower compared to that in fresh mouse plasma.

4.7. In-vitro cytotoxicity

The cytotoxicity of DX conjugate NPs was studied in human prostate cancer DU-145 cells using the MTT assay (Figure 3.7). Both free DX conjugates and DX conjugate NPs showed a dose-dependent and time-dependent cytotoxicity in DU-145 cells. In general, all three DX conjugates had significantly lower cytotoxicity than unmodified DX in DU-145 cells. The decrease in cytotoxicity was chain-length dependent. As shown in Figure 3.7A, free C12-DX was 20.6-fold less active than DX, and free C18-DX was 36.5-fold less active than DX after 48 hr incubation. Free C22-DX was almost non-toxic to DU-145 cells. For 48 hr incubation, C12-DX and C18-DX NPs showed comparable IC_{50} values with their free forms, while C22-DX NPs only showed similar toxicity to the blank NPs. The blank NP IC_{50} was 1842 ± 287 nM in DX

conjugate equivalent dose.

Figure 3.7B and C demonstrated the time-dependent cytotoxicity of free DX conjugates and NPs. For free C12-DX, the IC_{50} value decreased about 3-fold from 48 hr to 72 hr incubation and 2-fold from 72 hr to 96 hr. Free C18-DX and C22-DX did not show increased cytotoxicity in 72 hr over 48 hr; while from 72 hr to 96 hr, the IC_{50} values of both C18-DX and C22-DX decreased 2-fold. The IC_{50} value of C12-DX NP decreased 8-fold from 48 hr to 72 hr incubation but only 1.7-fold from 72 hr to 96 hr. For both C18-DX NP and C22-DX NP, the IC_{50} values sequentially decreased 2-fold from 48 hr to 72 hr to 96 hr incubation.

4.8. In-vivo pharmacokinetics

The plasma concentration-time curves in mice receiving i.v. bolus injections of Taxotere, C12-DX NPs, C18-DX NPs and C22-DX NPs at a dose of 10 mg DX/kg are shown in Figure 3.8A. Pharmacokinetic parameters obtained using a noncompartmental model of analysis are listed in Table 3.4A. The $AUC_{0-\infty}$ values of all NP-formulated DX conjugates were significantly higher than that of Taxotere. The AUCs increased as the conjugate chain lengths increased. The $AUC_{0-\infty}$ values of DX were 8.3-fold, 358-fold and 454.5-fold lower than that of NP-formulated C12-DX, C18-DX and C22-DX, respectively. The terminal half-lives of NP-formulated C18-DX and C22-DX were 1.9-fold and 3.4-fold longer than that of DX respectively. The

terminal half-life of NP-formulated C12-DX was shorter than that of DX. The volume of distribution of DX conjugates after administration of C12-DX NPs, C18-DX NPs, and C22-DX NPs were comparable. Overall, the volume of distribution of DX conjugate NPs was 20-fold lower than that of Taxotere.

The plasma concentrations of DX as an active metabolite hydrolyzed from C12-DX, C18-DX and C22-DX were determined and shown in Figure 3.8B. DX concentrations of Taxotere are also shown as a reference for comparison. The pharmacokinetic parameters of noncompartmental model are shown in Table 3.4B. The plasma concentrations of DX from C22-DX NP were below the lower limit of quantification. C12-DX NPs and C18-DX NPs improved DX AUC about 3-fold compared to Taxotere. The AUC of DX from C12-DX NP was slightly higher than that of C18-DX NP and the C_{\max} of DX from C12-DX NPs was 16.7-fold higher than that of C18-DX NPs. However, the terminal half-life of DX from C18-DX NPs was 5-fold higher than that of C12-DX NPs. The DX from C12-DX NPs decreased promptly below the level of DX from C18-DX NPs 4 hr post injection. Eight (8) hr post administration, the DX concentration from C12-DX NP decreased to the same level as Taxotere, whereas DX from C18-DX NP could be detected until 24 hr.

5. Discussion

In the present studies, three DX-lipid conjugates, C12-DX, C18-DX and C22-DX were

synthesized and characterized. The solubility of all three DX-lipid conjugates in Miglyol 808 was enhanced >10-fold over that of DX. Following optimization of the DX conjugate NP using orthogonal design, the final optimized NPs contained significantly reduced surfactant concentrations and increased drug entrapment. The improved retention of DX conjugates in the oil-filled NPs led to very different pharmacokinetic profiles and blood exposure of DX.

A novel liquid oil-filled NP was previously developed in our laboratory, which was composed of Miglyol 812, Brij 78 and Vitamin E TPGS.¹³ During the initial development of NP to formulate DX, Miglyol 808 was selected over Miglyol 812 due to the significant higher solubility of DX in Miglyol 808 (52.07 ± 0.84 mg/mL) compared to in Miglyol 812 (36.11 ± 0.10 mg/mL, $p < 0.01$). The oil phase with higher drug solubility represents better compatibility and affinity of the drug with the inner liquid oil core of the delivery vehicles thereby leading to higher drug loading capacity and longer retention of drugs in the NPs. The high drug loading capacity allows formulating more drugs with less vehicle components so that the potential toxicity of the delivery vehicle could be minimized. The >10-fold increase in the solubility of DX conjugates in Miglyol 808 compared to DX allowed for a significant increase in drug loading and entrapment. The comparable entrapment efficiency of the three DX conjugates in BTM 808 NPs was consistent with solubility of the conjugates in the Miglyol 808 liquid oil core.

While the solubility of DX conjugates in Miglyol 808 strongly influenced the

drug loading and entrapment efficiency in the NP formulation, the partition of DX conjugates in plasma was the driving force of their release in-vivo. Results from the in-vitro release studies showed that after an initial burst, an additional 40% of C12-DX having a relatively higher solubility in plasma was released from the NPs in 8 hr. In contrast, the C18-DX and C22-DX were extensively retained in the NPs after the initial burst release. It should be noted that all three DX-lipid conjugates showed an initial 45% burst release in mouse plasma using this “ex-vivo” method, which suggests that the burst release was not related to the lipid chain length in this range. It is likely that the relatively more hydrophilic head group of the DX-lipid conjugates resided on the surface of NPs and promptly partitioned to plasma proteins upon mixing with plasma. The burst release may not be a desirable property of NPs; however, it almost certainly reflects the true release behavior in-vivo.

In fresh mouse plasma bearing high esterase activity, the digestion rate of DX conjugates showed clear chain-length dependency. C12-DX, with a shorter acyl chain, likely has less steric hindrance and was more rapidly cleaved to release DX. In contrast, the longer acyl chains of C18-DX and C22-DX make them less susceptible to hydrolysis. A surprising finding in this experiment is that when entrapped in NPs, DX conjugates were more quickly hydrolyzed to DX than in their free forms. Nano-formulations are designed in many studies to protect chemically labile compounds. However in this case, oppositely, NP-encapsulation accelerated the digestion kinetics of DX conjugates. A hypothesis to explain this effect is that the

amphiphilic DX conjugates locate on the surface of the oil-filled NPs with relatively hydrophilic head orienting toward the aqueous phase and the lipid tail anchoring in the oil core. The huge specific surface area of NPs makes DX conjugates readily accessible to enzymes including esterases in the aqueous phase to transfer DX conjugates to DX and others. On the contrary, free DX conjugates, once spiked into plasma, tightly bind to the plasma proteins (e.g., albumin) leading to the shield of cleavage site.

The chain-length dependent and NP-accelerated hydrolysis of DX conjugates is consistent with their in-vitro cytotoxicity patterns. C12-DX, with the highest hydrolysis rate/extent exhibited the highest cytotoxicity, whereas free C22-DX and NP-encapsulated C22-DX with no liberation of DX in 48 hr exhibited no cytotoxicity and only vehicle-related toxicity, respectively. When the incubation time was extended to 72 hr and 96 hr, the cytotoxicity of all conjugates and their NPs increased. The time-dependent cytotoxicity increase is more obvious in DX conjugate NPs compared to their free forms especially for C18-DX and C22-DX. In addition, at 72 hr and 96 hr, the cytotoxicity of C18-DX NP and C22-DX NP was significantly higher than their free forms while this effect was less remarkable for C12-DX. It is likely that after 48 hr, DX was slowly hydrolyzed from C18-DX and C22-DX, with even lower hydrolysis rate and/or extent in their free forms. From the digestion study, it is clear that the hydrolysis rate of C12-DX was much faster than the other two and the difference between free and NP was not as significant as the others. It is consistent with its less remarkable time-dependent and NP-enhanced cytotoxicity.

It should be noted that the commercially bought mouse plasma is different from the fresh mouse plasma in terms of esterase activity as indicated in Figure 3.6. The reason of low esterase activity in commercial mouse plasma is unknown. It is possible that the handling process and/or storage of commercial plasma compromised its enzymatic activity. In contrast to the digestion of NP-formulated DX conjugates in fresh plasma (except for C22-DX), all DX conjugates were kept intact in commercial plasma and no DX was detected from any of the conjugates in at least 8 hr in the in-vitro release studies (data not shown). The release profiles obtained in the plasma lack of esterase activity may not reflect the overall behavior of DX conjugate NPs in-vivo, however, the presence of physiologically relevant concentration of proteins still makes commercial plasma a more relevant release medium over simple aqueous solutions. Even better, the lack of esterase activity simplifies the system and enables the study to focus only on the “release” behavior without entangling with the hydrolysis at the same time. The enzyme expression and activity in plasma have species difference. The lower esterase activity in human plasma compared to mouse plasma found in this study is consistent with other reports.^{14,15} It has been reported that butyrylcholinesterase, paraoxonase, and albumin esterase but not carboxylesterase are present in human plasma.¹⁶ The lower esterase activity in human plasma may potentially influence the prodrug activation in human systemic circulation. It remains possible that the esterases in tumors cleave the prodrug and release active DX after DX conjugate NPs passively accumulate in the tumor site via the EPR effect.

In-vivo, NP-formulated C12-DX, C18-DX and C22-DX achieved much higher AUCs compared to Taxotere, which was expected due to their better anchoring in the long circulating NPs. The low volume of distribution of DX conjugates was attributed to the size of NPs which limited their distribution to the normal tissues.¹⁷ In addition to the elimination of conjugate containing NPs by the reticuloendothelial system (RES), the elimination of the conjugates was also attributed to two other possible mechanisms including release of the conjugate from the NPs and hydrolysis of the conjugates. The elimination routes and the relative contribution of each route varied for each conjugate. The DX plasma concentration-time curves indicated that C12-DX was more quickly hydrolyzed to DX in-vivo than the other two conjugates, which is consistent with the in-vitro digestion results. C12-DX in NPs was either released from the NPs followed by hydrolysis to DX or was hydrolyzed to DX first followed by quick release as DX. Regardless of the mechanism, C12-DX had the shortest terminal half-life in-vivo, which was even shorter than Taxotere; however, the plasma exposure of DX was the highest after C12-DX NP injection. In contrast, C18-DX is more slowly hydrolyzed and better anchored in the NPs in-vivo resulting in a significant increase of the plasma exposure of the conjugate. As a result, the AUC of NP-formulated C18-DX was 43-fold higher than that of C12-DX. Because of the slower hydrolysis, the DX AUC from C18-DX NPs was lower compared to C12-DX NPs. However, as shown in Figure 3.8B, the duration of DX exposure after C18-DX NP administration was much longer than C12-DX NPs. C18-DX NPs served as a drug reservoir and released DX in a sustained

manner. It has been reported that prolonged time above a threshold concentration is ideal for cell cycle-specific drugs.¹⁸ Although DX was not detected after C22-DX NPs were injected into the blood, it is possible that the hydrolysis kinetics of C22-DX was too slow and the released DX was too quickly eliminated to be detected. It is worth noting that in the tumor site the overall anti-tumor toxicity comes from three forms: DX taken up by the tumors from the systemic circulation, the accumulating DX conjugates by their own, and the DX hydrolyzed from the accumulating conjugates in the site. It is possible that C22-DX is hydrolyzed to DX slowly after accumulating in the tumors.

While conjugating fatty acid chains to DX decreased its cell growth inhibitory activity in-vitro, the activity in-vivo may actually be enhanced. Many studies have reported the reduction of PX or DX activity in-vitro by conjugating fatty acid chains to 2'-OH.^{8,9,12} This study is consistent with the previous reports that in general, all three DX-lipid conjugates were less potent than DX against DU-145 cells, and increasing the lipid chain length decreased the cell growth inhibitory activity in-vitro. It has been previously demonstrated that esterification at 2'-OH abolished the microtubule binding affinity of the conjugates but not the total toxicity.¹⁹ The DX conjugates as ester prodrugs are expected to be cleaved to release free DX and exert its antitumor toxicity after cleavage. In addition, it is possible that DX conjugates as intact prodrugs are with alternative cytotoxic mechanisms other than microtubule binding. These additional mechanisms, if any, still remain to be investigated. The chain length dependent cytotoxicity reduction may be explained by their different rate/extent of cellular uptake,

different cellular compartmental sequester, and/or different rate/extent of hydrolysis/degradation. However, many studies have reported that the in-vivo efficacy does not necessarily correlate with their in-vitro cytotoxicity. In a previous study,¹² a series of PX prodrugs with various linkers and lipid anchors were synthesized. Among the lipophilic prodrugs of PX, the most potent compound (compound 7) in-vivo only showed moderate in-vitro cytotoxicity. Another study showed that the 2'-(2-bromo)-hexadecanoyl PX with the lowest in-vitro cytotoxicity in its kind was most effective in-vivo, showing 100% survival at day 300 for ovc3-bearing SCID mice.⁹ The DHA-PX on clinical trial III prepared by linking PX to docosahexaenoic acid (DHA) was less toxic than PX in-vitro but cured 10/10 M109 tumor-bearing mice, whereas PX cured 0/10.²⁰ In the present studies, the pharmacokinetics of the DX-lipid conjugate NPs provided the basis for enhanced in-vivo efficacy.

In conclusion, the NP developed in these studies have low toxicity, long circulation in the blood, and released DX-lipid conjugates in a slow and sustained manner in the plasma. Thus, the NPs have the potential to exert superior anti-tumor efficacy and less systemic toxicity in-vivo. The results of these studies strongly support that the physical/chemical properties of DX conjugates may be fine-tuned to influence the affinity and retention of DX in oil-filled lipid NPs which therefore leads to very different pharmacokinetic profiles and blood exposure of DX. These studies demonstrate that the affinity of a drug for the core NP material may influence the retention and release rate of a drug from these NPs. In addition, the new “ex-vivo”

release method along with the digestion study provided good correlation and prediction of the in-vivo pharmacokinetic profile. These studies and methodologies may allow for improved and more potent NP-based formulations.

Table 3.1. Solubility of DX and DX conjugates in Miglyol 808 and entrapment efficiency in BTM NPs (N=3)

Drug	DX	C12-DX	C18-DX	C22-DX
Solubility in Miglyol 808 (mg/mL)	52.1 ± 1.5	523.0 ± 18.2	550.5 ± 23.5	553.0 ± 21.0
Entrapment efficiency (%)	0	55.2 ± 2.3	56.3 ± 7.6	59.6 ± 1.6

Table 3.2. Orthogonal design and responses

Run	Brij 78 (mg/mL)	TPGS (mg/mL)	Temperature (°C)	Entrapment (%)	Size (nm)
1	3.7	1.2	50	36.25	219.7
2	1.7	0.4	55	66.66	202.4
3	3.7	0.8	55	44.44	198.2
4	2.7	0.8	60	54.88	198.4
5	1.7	0.8	50	65.12	202.9
6	2.7	0.4	50	51.46	189.3
7	2.7	1.2	55	52.15	204.0
8	1.7	1.2	60	46.49	198.0
9	3.7	0.4	60	45.89	184.0

Note: Miglyol 808 concentration was 2.5 mg/mL for all 9 runs.
C12-DX concentration was 0.5 mg/mL for all 9 runs.

Table 3.3. Compositions and properties of BTM 808 NPs

Miglyol 808 (mg/mL)	Brij 78 (mg/mL)	TPGS (mg/mL)	DX conjugate (mg/mL)	Temperature (°C)	Particle size (nm)	Zeta potential (mV)
2.5	1.7	0.8	0.5	55 ^a	204.3 ± 8.9	-0.97 ± 0.08

Note: a. Temperature was not a significant variable so that average temperature of orthogonal design was utilized.

Table 3.4. A. Pharmacokinetic parameters of DX conjugates and Taxotere in mice after i.v. bolus administration

	Taxotere	C12-DX NP	C18-DX NP	C22-DX NP
$t_{1/2}$ (hr)	3.63	0.99	6.80	12.4
AUC ₀₋₂₄ (h*mg/L)	1.51	12.8	509	505
AUC _{0-∞} (h*mg/L)	1.55	12.9	555	704
V _d (L/kg)	5.61	0.22	0.17	0.26
K _{el} (1/hr)	0.19	0.70	0.10	0.06
CL (L/hr/kg)	6.43	0.77	0.02	0.01
C _{max} (mg/L)	7.21	71.6	108	108
MRT (hr)	0.87	0.29	9.27	18.3

B. Pharmacokinetic parameters of DX after i.v. bolus administration of DX conjugates and Taxotere in mice

	Taxotere	C12-DX NP	C18-DX NP	C22-DX NP
$t_{1/2}$ (hr)	3.63	1.09	5.42	
AUC ₀₋₂₄ (h*mg/L)	1.51	4.64	3.51	
AUC _{0-∞} (h*mg/L)	1.55	4.66	3.66	-- ^a
K _{el} (1/hr)	0.19	0.63	0.13	
C _{max} (mg/L)	7.21	12.3	0.74	
MRT (hr)	0.87	0.89	6.98	

Note: ^a. Below lower limit of quantification.

Abbreviations: AUC, area under the curve; MRT, mean retention time.

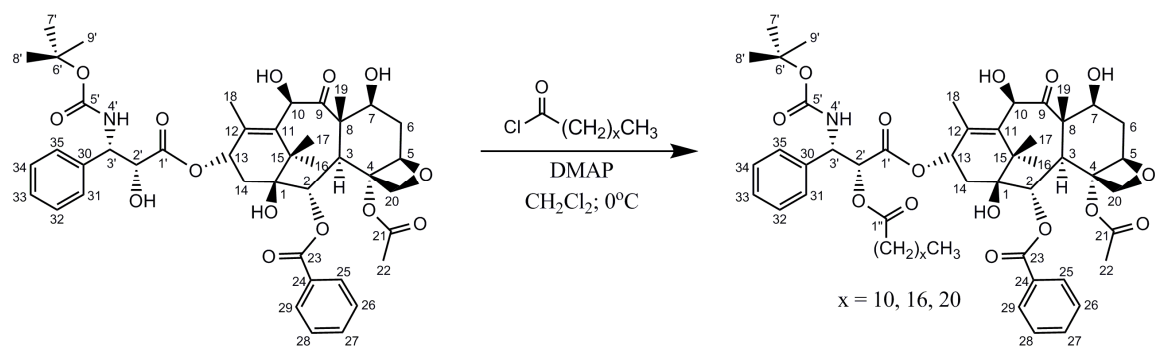


Figure 3.1. Synthesis of 2'-docetaxel conjugates.

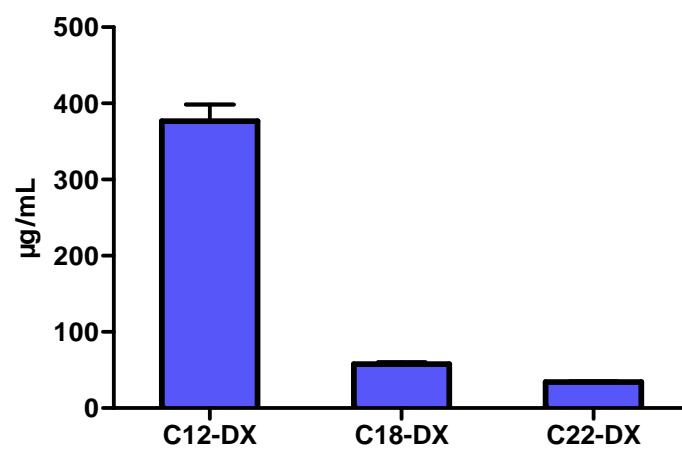


Figure 3.2. Solubility of DX conjugates in mouse plasma.

Design-Expert® Software
Entrapment

X1 = A: Brij 78
X2 = B: TPGS

Actual Factor
C: Temperature = Average

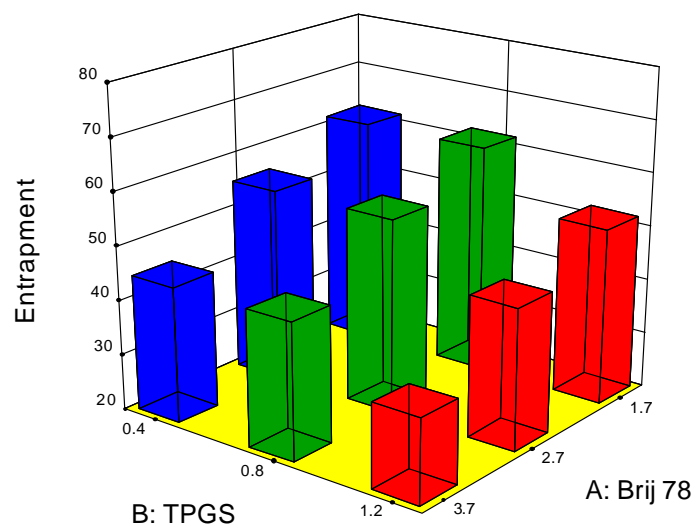


Figure 3.3. 3D surface plot for the modeling of the effect of Brij 78 and TPGS concentrations on % drug entrapment.

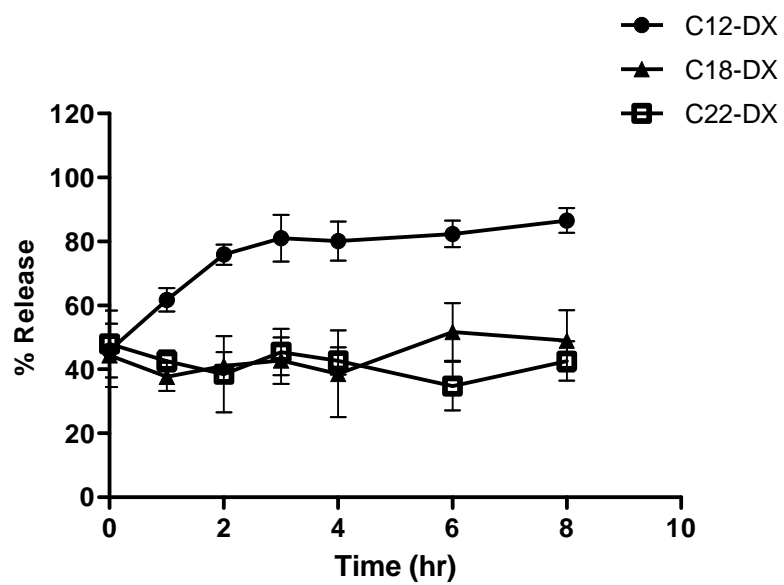
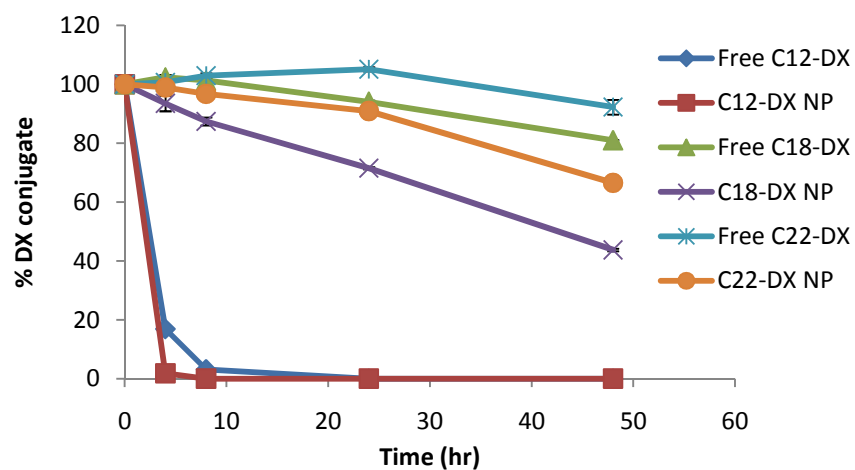


Figure 3.4. Release of DX conjugates from BTM NPs in mouse plasma at 37°C.

A



B

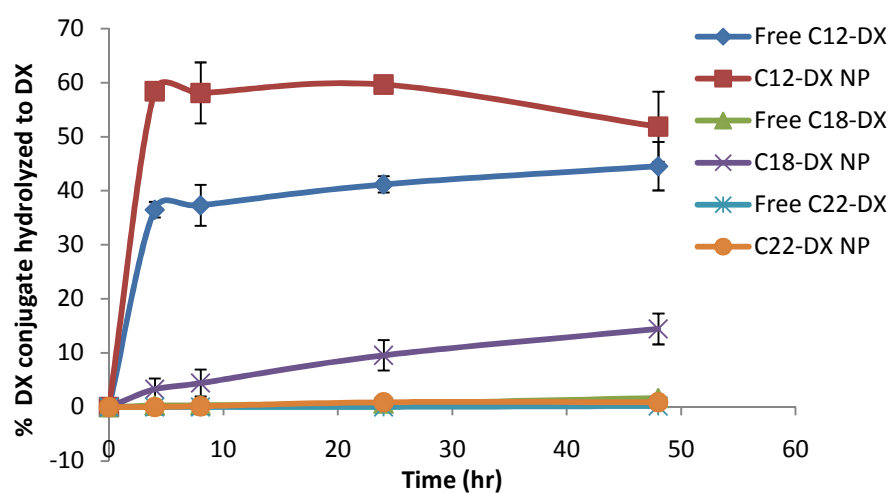


Figure 3.5. The digestion of free DX conjugates and DX conjugate NPs in fresh mouse plasma. (A) The loss of DX conjugates. (B) The formation of DX. Data are shown as mean \pm SD (n = 3).

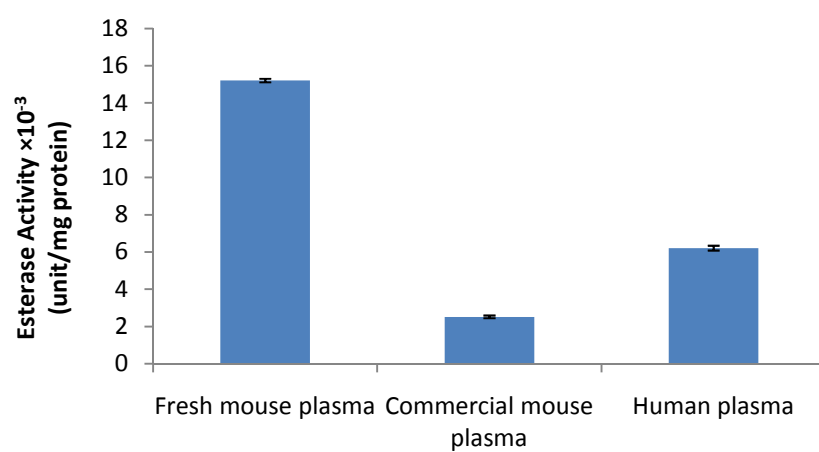
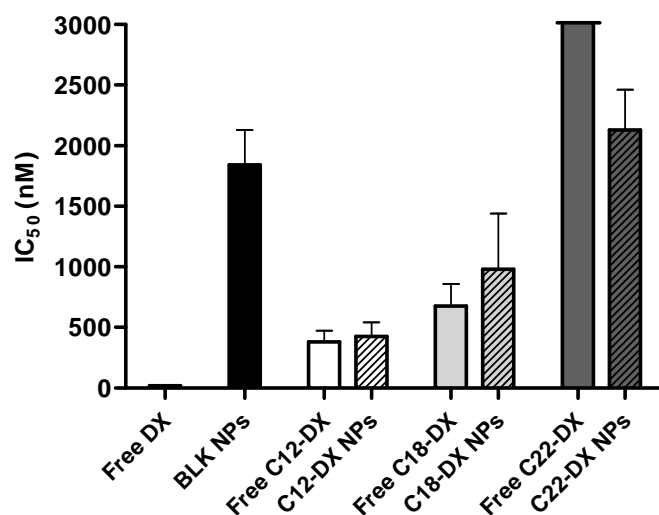
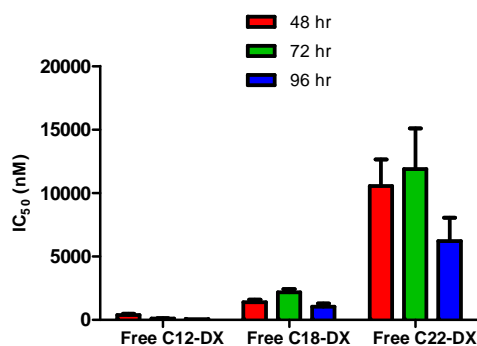


Figure 3.6. Non-specific esterase activity in fresh mouse plasma, commercial mouse plasma and human plasma samples.

A



B



C

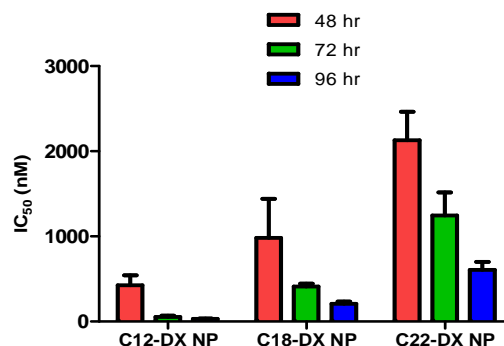
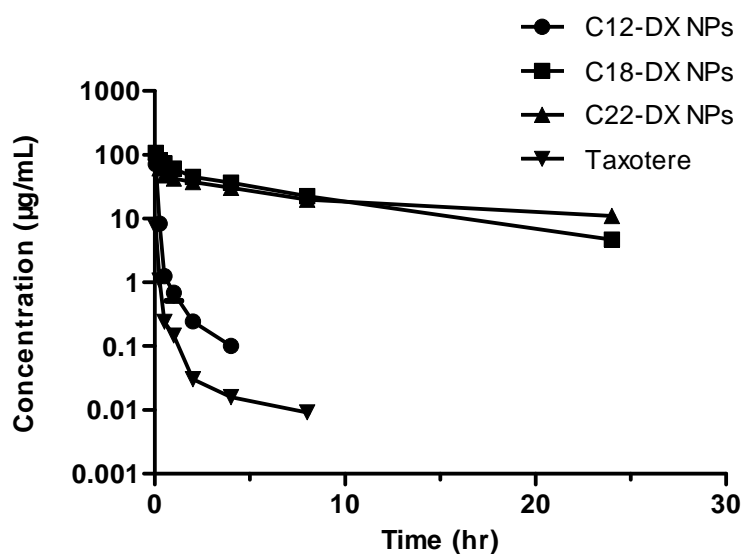


Figure 3.7. In-vitro cytotoxicity of free DX and DX conjugates and their NPs in DU-145 cells (A) after 48 hr incubation. The time-dependent cytotoxicity of (B) free conjugates and (C) conjugate NPs with different incubation time (48, 72, and 96 hr) in DU-145 cells. Blank NPs were dosed at drug equivalent dose. Drug equivalent dose of NPs are calculated from the NP compositions.

A



B

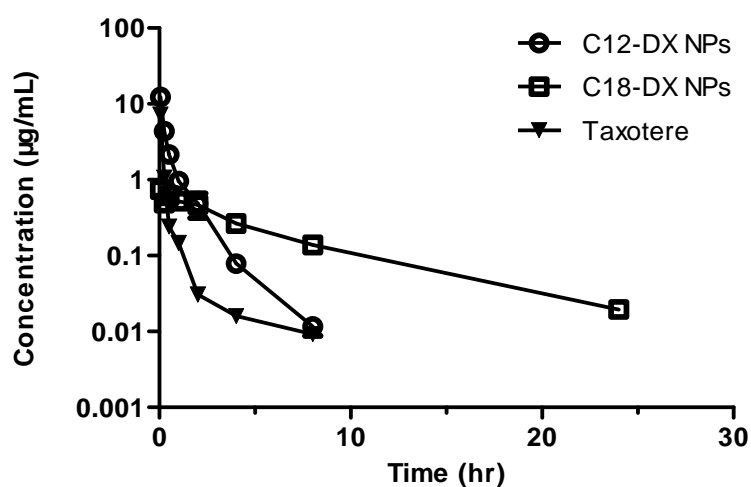


Figure 3.8. Plasma concentration-time curves for (A) DX, C12-DX, C18-DX and C22-DX after administration of Taxotere, C12-DX NPs, C18-DX NPs and C22-NPs (10 mg DX/kg), and (B) DX as an active metabolite from C12-DX NPs and C18-DX NPs using Taxotere as a reference. The plasma concentrations of DX from C22-DX NP were below the lower limit of quantification. Data are shown as mean \pm SD (n = 3).

References

1. Isacchi B, Arrigucci S, Marca GL, et al. Conventional and long-circulating liposomes of artemisinin: preparation, characterization, and pharmacokinetic profile in mice. *J Liposome Res.* Dec 16 2010.
2. Cole AJ, David AE, Wang J, Galban CJ, Hill HL, Yang VC. Polyethylene glycol modified, cross-linked starch-coated iron oxide nanoparticles for enhanced magnetic tumor targeting. *Biomaterials.* Mar 2011;32(8):2183-2193.
3. Kim CK, Kim JY, Kim JK, Park JS, Byun Y. The use of PEGylated liposomes to prolong circulation lifetimes of tissue plasminogen activator. *Biomaterials.* Oct 2009;30(29):5751-5756.
4. Immordino ML, Dosio F, Cattel L. Stealth liposomes: review of the basic science, rationale, and clinical applications, existing and potential. *Int J Nanomedicine.* 2006;1(3):297-315.
5. Devaleriola D. Study of excretion balance, metabolism and protein binding of ¹⁴C-radiolabelled Taxotere (RP56976, NSC628503) in cancer patients. *P Am Assoc Canc Res.* 1993;34:373.
6. Stevens PJ, Sekido M, Lee RJ. A folate receptor-targeted lipid nanoparticle formulation for a lipophilic paclitaxel prodrug. *Pharm Res.* Dec 2004;21(12):2153-2157.
7. Lundberg BB, Risovic V, Ramaswamy M, Wasan KM. A lipophilic paclitaxel derivative incorporated in a lipid emulsion for parenteral administration. *J Control Release.* Jan 9 2003;86(1):93-100.
8. Huynh L, Leroux JC, Allen C. Enhancement of docetaxel solubility via conjugation of formulation-compatible moieties. *Org Biomol Chem.* Sep 7 2009;7(17):3437-3446.
9. Ali S, Ahmad I, Peters A, et al. Hydrolyzable hydrophobic taxanes: synthesis and anti-cancer activities. *Anticancer Drugs.* Feb 2001;12(2):117-128.
10. Nikanjarn M, Gibbs AR, Hunt A, Budinger TF, Forte TM. Synthetic nano-LDL with paclitaxel oleate as a targeted drug delivery vehicle for glioblastoma multiforme. *Journal of Controlled Release.* Dec 20 2007;124(3):163-171.
11. Mumper RJ, Dong XW, Mattingly CA, Tseng M, Cho M, Adams VR. Development of new lipid-based paclitaxel nanoparticles using sequential simplex optimization. *European Journal of Pharmaceutics and*

Biopharmaceutics. May 2009;72(1):9-17.

12. Ansell SM, Johnstone SA, Tardi PG, et al. Modulating the therapeutic activity of nanoparticle delivered paclitaxel by manipulating the hydrophobicity of prodrug conjugates. *J Med Chem*. Jun 12 2008;51(11):3288-3296.
13. Mumper RJ, Dong XW, Mattingly CA, et al. Doxorubicin and Paclitaxel-Loaded Lipid-Based Nanoparticles Overcome Multidrug Resistance by Inhibiting P-Glycoprotein and Depleting ATP. *Cancer Research*. May 1 2009;69(9):3918-3926.
14. Liederer BM, Borchardt RT. Enzymes involved in the bioconversion of ester-based prodrugs. *J Pharm Sci*. Jun 2006;95(6):1177-1195.
15. Lu XL, Howard MD, Talbert DR, et al. Nanoparticles Containing Anti-inflammatory Agents as Chemotherapy Adjuvants II: Role of Plasma Esterases in Drug Release. *Aaps J*. Mar 2009;11(1):120-122.
16. Li B, Sedlacek M, Manoharan I, et al. Butyrylcholinesterase, paraoxonase, and albumin esterase, but not carboxylesterase, are present in human plasma. *Biochem Pharmacol*. Nov 25 2005;70(11):1673-1684.
17. Allen TM, Cullis PR. Drug delivery systems: entering the mainstream. *Science*. Mar 19 2004;303(5665):1818-1822.
18. Gardner SN. A mechanistic, predictive model of dose-response curves for cell cycle phase-specific and -nonspecific drugs. *Cancer Res*. Mar 1 2000;60(5):1417-1425.
19. Deutsch HM, Glinski JA, Hernandez M, et al. Synthesis of congeners and prodrugs. 3. Water-soluble prodrugs of taxol with potent antitumor activity. *J Med Chem*. Apr 1989;32(4):788-792.
20. Bradley MO, Swindell CS, Anthony FH, et al. Tumor targeting by conjugation of DHA to paclitaxel. *J Control Release*. Jul 6 2001;74(1-3):233-236.

Chapter 4.

Oil-filled lipid nanoparticles containing 2'-(2-bromohexadecanoyl)-docetaxel for the treatment of breast cancer

1. Summary

A docetaxel (DX) lipid conjugate 2'-(2-bromohexadecanoyl)-docetaxel (2-Br-C16-DX) was synthesized to enhance the drug loading, entrapment and retention in liquid oil-filled lipid nanoparticles (NPs). The conjugate was successfully entrapped in the previously optimized NPs with an entrapment efficiency of 56.8% as measured by size exclusion chromatography (SEC). In-vitro release study in 100% mouse plasma showed an initial 45% burst release with no additional release within 8 hr. The conjugate was able to be hydrolyzed to release DX by esterases in-vitro and the hydrolysis rate was accelerated by encapsulation in NPs. The conjugate was less potent than unmodified DX in DU-145 and 4T1 cells. However, NPs containing the conjugate showed significantly higher cytotoxicity compared to its free form especially in 4T1 cells. In-vivo, the $AUC_{0-\infty}$ value of NP-formulated 2-Br-C16-DX was about 100-fold higher than DX in Taxotere. Furthermore, 2-Br-C16-DX NP improved DX AUC 4.3-fold compared to Taxotere. The high concentration and prolonged exposure of both

2-Br-C16-DX and DX from 2-Br-C16-DX NPs in circulation caused a 10-fold and 1.5-fold higher accumulation of 2-Br-C16-DX and DX, respectively, in tumors compared to Taxotere. The 2-Br-C16-DX NPs were well tolerated in mice with a 5-fold and 2.5-fold increase in the single-dose and multiple-dose maximum tolerated dose (MTD), respectively, over Taxotere. In mice bearing 4T1 xenograft tumors, 2-Br-C16-DX NPs showed marked anticancer efficacy as well as survival benefit over all controls. The results of these studies support that the oil-filled NPs containing hydrolyzable lipophilic DX prodrug 2-Br-C16-DX improved the therapeutic index of DX and were more efficacious in the treatment of breast cancer. The formulation may have broad applications in other tumors and the prodrug approach may be potentially applied to other anticancer agents.

2. Introduction

Previously, we developed oil-filled BTM 808 NPs by sequential simplex optimization to deliver DX. However, despite the desirable formulation properties (e.g., monodispersed particle size, apparent drug entrapment efficiency, etc.), DX was found to be very quickly released in mouse plasma in-vitro. Further investigation revealed that DX was not truly entrapped into the NPs during preparation. To overcome the poor retention of DX in the BTM 808 NPs in simple aqueous phase and in biologically relevant medium, DX was modified by attaching fatty acid chains with different chain

lengths to the 2'-position of DX via an ester bond. The three DX-lipid conjugates synthesized in Chapter 3 increased the solubility in Miglyol 808 by 10-fold. Consequently, the actual entrapment efficiency determined by SEC increased from zero for DX to about 50-60% for the DX-lipid conjugates. The DX-lipid conjugates were well retained in the NPs even in 100% plasma. The retention of DX conjugates in the long-circulating NPs resulted in significantly reduced elimination, high and prolonged in-vivo drug exposure.

However, in-vitro cytotoxicity studies revealed that these DX conjugates were much less potent than the unmodified DX. Similar results have been reported by other groups.¹ It has been long recognized that the 2'-OH is critical for the microtubule binding and cytotoxic effect of DX.² Hence, the biological activity of these ester prodrugs mostly depends on the liberation of active DX. The compromised cytotoxicity suggests inefficient release of DX in cell culture. The in-vitro hydrolysis and in-vivo pharmacokinetics also revealed sub-optimal hydrolysis kinetics of these conjugates.

Ali et al. synthesized a series of lipid paclitaxel (PX) prodrugs with or without a bromine atom at the 2-position on the fatty acid chain.³ In general, the prodrugs lacking bromine were 50- to 250-fold less active than their bromoacyl counterparts indicating that the electron-withdrawing group facilitated the cleavage of active PX. The bromoacylated PX showed higher anticancer efficacy against OVCAR-3 tumor in-vivo.^{3,4} Their findings suggest that a straightforward modification has the potential to favorably change the physicochemical and biological properties of the current DX

conjugates.

The objective of these present studies was to further tune the prodrug hydrolysis kinetics while retaining the high drug entrapment and retention in the oil-filled NPs. With optimized activation kinetics, the new prodrug containing NPs are expected to achieve sustained release of active drug, low systemic toxicity, and enhancement of antitumor efficacy in-vivo.

3. Materials and methods

3.1. Materials and Animals

DX, PX, 2-bromohexadecanoic acid (>99%), 4-(dimethylamino) pyridine (DMAP) and *N,N'*-dicyclohexyl-carboiimide (DCC, 99%) were purchased from Sigma-Aldrich (St. Louis, MO). Miglyol 808 was obtained from Sasol (Witten, Germany). Polyoxyl 20-stearyl ether (Brij 78) was obtained from Uniqema (Wilmington, DE). D-alpha-tocopheryl polyethylene glycol succinate (Vitamin E TPGS) was purchased from Eastman Chemicals (Kingsport, TN). BALB/c mouse plasma was purchased from Innovative Research Inc. (Novi, MI). Sepharose CL-4B was purchased from GE Healthcare (Uppsala, Sweden). Hybrid-SPE[®] cartridge was purchased from Sigma-Aldrich Supelco (St. Louis, MO).

The human prostate cancer cell line DU-145, and murine breast cancer cell line 4T1 were obtained from American Type Culture Collection (ATCC) and were

maintained in RPMI-1640 medium with 10% fetal bovine serum (FBS). Female BALB/c mice, 4 to 5 weeks old, were purchased from Charles River (Wilmington, MA) and housed in a pathogen-free room. All experiments involving mice were conducted according to an approved animal protocol by the University of North Carolina Institutional Animal Care and Use Committee.

3.2. Methods

3.2.1. General procedure for the synthesis of 2'-(2-bromohexadecanoyl)-docetaxel (2-Br-C16-DX)³

A flame-dried round-bottom flask was charged with (\pm)-2-bromohexadecanoic acid (0.62 g, 1.85×10^{-3} mol, 1.5N) and DCC (0.5 g, 2.47×10^{-3} mol, 2N) in dry CH_2Cl_2 (200 mL) under argon. The solution was stirred for 10 min at room temperature. DX (1.0 g, 1.24×10^{-3} mol, 1N) was added along with a catalytic amount of DMAP (0.15 g, 1.24×10^{-3} mol, 1N) and the reaction mixture was stirred at room temperature for an extra 5 min. The reaction was monitored by TLC (CH_2Cl_2 : MeOH 95:5 v/v; $R_f = 0.58$) for completion. The white precipitate of dicyclohexylurea byproduct was filtered through a fritted funnel, and the filtrate was evaporated under vacuo. The crude product was purified by preparative TLC in CHCl_3 : MeOH (95:5). The silica gel was removed by filtration through a fine fritted funnel and the filtrate was evaporated under vacuo to give the desired product as a white powder (0.4 mg, 86%). ^1H NMR (400 MHz,

CDCl₃): δ (ppm) = 0.8 (t, 3H, $-\text{CH}_3(\text{CH}_2)_{14}$), 1.05 (s, 6H, $-\text{H}_{16,17}$), 1.16 (s, 9H, $-\text{H}_{7',9'}$), 1.19 (s, 3H, $-\text{H}_{19}$), 1.23 (m, 28H, $-(\text{CH}_2)_{14}\text{CH}_3$), 1.68 (s, 3H, $-\text{H}_{18}$), 1.78 (m, 2H, $-\text{H}_{14}$), 1.67 (d, 2H, $-\text{CH}_2\text{C}_{1''}$), 1.87 (s, 3H, $-\text{H}_{22}$), 2.24 (m, 1H, $-\text{H}_3$), 2.38 (s, 1H, $-\text{H}_7$), 3.86 (d, 1H, $-\text{H}_4$), 4.12 (d, 1H, $-\text{H}_2$), 4.2 (t, 1H, $-\text{CHBrC}_{1''}$), 4.26 (t, 2H, $-\text{H}_{13}$), 4.88 (d, 1H, $-\text{H}_{10}$), 5.2 (d, 2H, $-\text{H}_{20}$), 5.22 (d, 1H, $-\text{H}_{2'}$), 5.62 (d, 1H, $-\text{H}_{3'}$), 7.22-7.53 (m, 8H, $-\text{Ar-H}_{26-28}$ and Ar-H_{30-35}), 8.05 (d, 2H, $-\text{Ar-H}_{25,29}$). ¹³C NMR (100 MHz, CD₃OD): δ (ppm) = 8.9 ($-\text{C}_{19}$), 14.1 ($-\text{CH}_3(\text{CH}_2)_{20}$), 20.9 ($-\text{C}_{18}$), 22.6 ($-\text{C}_{22}$), 23.7 ($-(\text{CH}_2)_{19}\text{CH}_2\text{CH}_3$), 27 ($-\text{C}_{16,17}$), 28.1 ($-\text{C}_{7'-9'}$), 29.6 ($-(\text{CH}_2)_{14}\text{C}_{1''}$), 31.9 ($-\text{C}_{6,14}$), 43.1 ($-\text{C}_{15}$), 44.5 ($-\text{C}_3$), 45 ($-\text{CHBr}$), 46.4 ($-\text{C}_{3'}$), 57.5 ($-\text{C}_8$), 71.8 ($-\text{C}_{13}$), 72.1 ($-\text{C}_7$), 74.4 ($-\text{C}_2$), 75 ($-\text{C}_{10}$), 75.3 ($-\text{C}_{20}$), 78.9 ($-\text{C}_{6'}$), 79.9 ($-\text{C}_1$), 80.9 ($-\text{C}_4$), 84.2 ($-\text{C}_5$), 126.3 ($-\text{C}_{31,33,35}$), 128.9 ($-\text{C}_{32,34}$), 129.2 ($-\text{C}_{26,28}$), 130.2 ($-\text{C}_{24,25,29}$), 133.6 ($-\text{C}_{27}$), 135.5 ($-\text{C}_{11}$), 138.9 ($-\text{C}_{12}$), 154.2 ($-\text{C}_{5'}$), 167 ($-\text{C}_{23}$), 167.3 ($-\text{C}_{21}$), 169 ($-\text{C}_1$), 169.7 ($-\text{C}_{1''}$), 211.5 ($-\text{C}_9$).

3.2.2. Characterization of DX and DX conjugates

3.2.2.1. Mass spectrometry

Electrospray Ionization (ESI) coupled with direct injection was employed to determine the m/z of the final synthetic conjugate product by Thermo Scientific TSQ Quantum Access with positive ionization. The m/z of the observed molecular ion was 1125, which clearly corresponded to the H^+ adduct of 2-Br-C16-DX.

3.2.2.2. High performance liquid chromatography (HPLC)

The 2-Br-C16-DX concentrations were quantified by HPLC using a Finnigan Surveyor HPLC system with a Photodiode Array (PDA) detector, autosampler and LC pump plus with an Inertsil[®] ODS-3 column (4 μ m, 4.6 \times 150 mm, GL Sciences) at 25°C. Chromatographic separation was achieved by gradient elution using mobile phase 2-propanol, acetonitrile (ACN) and water (5: 55: 40 v/v/v). The flow rate was 1.0 mL/min and the total run time was 25 min for each 25 μ L injection. The wavelength was 230 nm.

The DX concentration was quantified by LC/MS/MS using a Finnigan Surveyor Autosampler Plus and Finnigan Surveyor MS Pump Plus. Chromatographic separations were achieved using a SunFire[™] C18 column (2.1 \times 30 mm, 3.5 μ m particle size, Waters) at 25°C. The mobile phase consisted of 0.1% formic acid in water and methanol using gradient separation. The flow rate was 0.5 mL/min and the total run time was 8 min for each 25 μ L injection. Mass spectrometric analysis was performed using a Thermo Scientific TSQ Quantum Access with positive ionization. The capillary temperature was set up to 390°C, and the spray voltage was 4000V. For DX analysis, m/z 830.0 \rightarrow 549.0 was monitored with PX (m/z 876.3 \rightarrow 308.0) as an internal standard.

3.2.3. Preparation and characterization of BTM NPs

3.2.3.1. Preparation of BTM NPs containing 2-Br-C16-DX

NPs containing 2-Br-C16-DX were prepared using a warm oil-in-water (o/w) microemulsion precursor method previously developed and later optimized in our laboratory.⁵ Briefly, Miglyol 808 (2.5 mg), Brij 78 (1.7 mg) and Vitamin E TPGS (0.8 mg) were accurately weighed into glass vials and heated to 60°C. Drugs (0.5-1 mg) dissolved in ACN were added and the organic solvent was removed by nitrogen flow. One (1) mL of pre-heated 10% lactose in water was added into the mixture of melted oil, surfactants and drugs. The mixture was stirred for 20 min at 60°C then cooled to room temperature.

For in-vivo studies, NPs were concentrated and PEGylated. The formulation was concentrated 4-13-fold by adding 4-13-fold less 10% lactose continuous phase while keeping the other components of the formulation unchanged. The NPs were PEGylated by adding 8% Brij 700 during the preparation wherein 8% was the w/w ratio of Brij 700 to Miglyol 808.

3.2.3.2. Characterization of BTM NPs containing 2-Br-C16-DX

3.2.3.2.1. Particle size and zeta potential

Particle size and size distribution of NPs were determined using an N5 Submicron Particle Size Analyzer (Beckman). Five (5) µL of NPs was diluted with 1 mL of water to reach the intensity required by the instrument. Particle size was determined at 90°

light scattering at 25°C. The zeta potential of NPs was determined using the Zetasizer Nano Z (Malvern Instruments, Southborough, MA).

3.2.3.2.2. Drug entrapment efficiency

Drug entrapment efficiency was determined by SEC. 2-Br-C16-DX NPs were separated with the free drug by a Sepharose CL-4B column (15 cm). NPs were eluted using PBS in fractions 5-8 (1 mL/fraction, confirmed by dynamic light scattering intensity). Each fraction was evaporated to dryness in vacuo, resuspended in 1 mL ACN and analyzed by HPLC to determine the concentration of 2-Br-C16-DX in each fraction. The % drug entrapment efficiency was defined as $100\% \times \text{the ratio of the weight of drug detected in fractions 5-8 to the total drug weight detected.}$

3.2.3.2.3. Physicochemical stability of 2-Br-C16-DX NPs

The 2-Br-C16-DX NP suspension was stored at 4°C. At designated time points, the particle size was measured after the NP suspension being allowed to equilibrate to room temperature. The 2-Br-C16-DX concentration was determined by HPLC.

3.2.4. In-vitro drug release in mouse plasma

In-vitro release studies were performed in 100% BALB/c mouse plasma. Briefly, 100 μL of purified 2-Br-C16-DX NPs were spiked into 2 mL of mouse plasma. The release

mixture was incubated at 37°C in a water bath shaker. At designated time points from 0 hr to 8 hr, two aliquots of release mixture were removed. One aliquot (100 µL) was used to determine the total drug concentration by solid phase extraction (SPE) using Hybrid-SPE precipitate method. Briefly, one volume of release mixture was mixed with three volumes of 2% formic acid in ACN. Following vortex and centrifugation, the supernatant was applied to a Hybrid-SPE cartridge. The eluate was collected for HPLC analysis. Another aliquot (100 µL) was used to determine the drug remained in the NPs using the method described above. The % DX released at any time point was calculated as $100\% \times [(\text{Total drug detected} - \text{drug remaining in the NPs}) / \text{Total drug detected}]$.

3.2.5. 2-Br-C16-DX digestion

3.2.5.1. 2-Br-C16-DX digestion in fresh mouse plasma

The esterase digestion study was performed in fresh BALB/c mouse plasma. The 2-Br-C16-DX DMSO stock solution (5 mg/mL) or 2-Br-C16-DX NPs (0.5 mg/mL) was spiked into the plasma to make a final concentration of 10 µg/mL. As controls, 2-Br-C16-DX DMSO solution mixed with blank NPs or Brij 78 (1.7 mg/mL) and TPGS (0.8 mg/mL), was as well spiked into the plasma to make a final concentration of 10 µg/mL. The mixture was incubated at 37°C in a water bath shaker. At designated time points, 100 µL of digestion mixture was removed. The concentration of 2-Br-C16-DX was determined by Hybrid-SPE precipitate method as described above followed by

HPLC analysis. The % 2-Br-C16-DX remaining at any time point was calculated as $100\% \times \text{the ratio of remaining drug amount to the total drug spiked into this volume of plasma}$. The concentration of DX in the same sample was determined by LC/MS. The % 2-Br-C16-DX hydrolyzed to DX at any time point was calculated as $100\% \times [(\text{DX amount detected} \times 1124 / 807) / \text{the total drug spiked into this volume of plasma}]$.

3.2.5.2. 2-Br-C16-DX digestion in 4T1 tumor homogenate

The 4T1 solid tumor was collected from 4T1 xenografted mice after euthanasia. Three hundred (300) μL of PBS was added to every 100 mg of tumor tissues. Tumors were homogenized using Omni Bead Ruptor 24 homogenizer with 2.8 mm zirconium oxide beads (Omni International, Kennesaw, GA). The 2-Br-C16-DX DMSO stock solution (5 mg/mL) or 2-Br-C16-DX NPs (0.5 mg/mL) was spiked into the homogenate to make a final concentration of 10 $\mu\text{g/mL}$. The mixture was incubated at 37°C in a water bath shaker. At designated time points, 100 μL of homogenate was removed. The concentration of 2-Br-C16-DX was determined by Hybrid-SPE precipitate method as described above followed by HPLC analysis. The % 2-Br-C16-DX remaining at any time point was calculated as $100\% \times \text{the ratio of remaining drug amount to the total drug spiked into this volume of tumor homogenate}$. The concentration of DX in the same sample was determined by LC/MS. The % 2-Br-C16-DX hydrolyzed to DX at any time point was calculated as $100\% \times [(\text{DX amount detected} \times 1124 / 807) / \text{the total drug spiked into this volume of tumor homogenate}]$.

3.2.6. Evaluation of in-vitro cytotoxicity

The MTT assay was utilized to assess cytotoxicity of free 2-Br-C16-DX and the 2-Br-C16-DX NPs. Serial dilutions of free drugs or drug containing NPs were added to the DU-145 cells or 4T1 cells and incubated for 48 hr. The cells were then incubated with MTT solution for 4 hr and the formazan dyes were solubilized by DMSO. The absorbance was measured using the Synergy 2 Multi-Detection Microplate Reader at 570 nm, and the concentration of drug that inhibited cell survival by 50% (IC₅₀) was determined from cell survival plots.

3.2.7. In-vivo pharmacokinetics and biodistribution of 2-Br-C16-DX NPs

Female BALB/c mice were injected s.c. in the right interscapular region 1×10^6 4T1 cells suspended in 100 μ L of FBS-free RPMI-1640 medium. When the tumor volume reached 400 – 500 mm³, mice were randomly divided into two groups. The mice (n=3/time point) were injected via tail vein with Taxotere or 2-Br-C16-DX NPs, all at a DX dose of 10 mg/kg. At designated time points from 3 min to 96 hr, the mice were given an overdose of ketamine (100 mg/kg) and Domitor (0.5 mg/kg) for deep anesthesia prior to cardiac puncture to collect blood and a cervical dislocation was then performed to euthanize the mice. After euthanasia, organs (heart, liver, spleen, lung and

kidney) and tumor were collected and flash frozen in liquid nitrogen. For plasma separation, the blood collected in heparin-coated tubes was centrifuged at 12,300 rpm for 15 min. The obtained plasma was processed with Hybrid-SPE precipitate method as described above. For organs and tumor, 300 μ L of 2% formic acid in ACN was added to every 100 mg of tissues. Tissues were homogenized using Omni Bead Ruptor 24 homogenizer with 2.8 mm zirconium oxide beads. Following vortex and centrifugation, the supernatant was applied to a Hybrid-SPE cartridge. The eluate was collected for analysis. The concentrations of 2-Br-C16-DX in plasma and tissue extract were determined by HPLC, and the DX concentrations were quantified by LC/MS. Pharmacokinetic analysis and modeling was performed by WinNonlin (version 5.2.1; Pharsight Corp, Mountain View, CA).

3.2.8. Evaluation of maximum tolerated dose (MTD)

3.2.8.1. Single-dose MTD

Female BALB/c mice were randomly divided into four groups. The mice ($n = 8$) were injected via tail vein with test samples (100 mg conjugate/kg, 130 mg conjugate/kg and 150 mg conjugate/kg 2-Br-C16-DX NPs). The mice in the control group were not treated. All mice were monitored after injection. Body weight and body conditions were monitored daily for a week.

3.2.8.2. Multiple-dose MTD

Female BALB/c mice were randomly divided into five groups. The mice ($n = 5$) were injected via tail vein with test samples Q7d \times 3 (40 mg conjugate/kg, 70 mg conjugate/kg, 100 mg conjugate/kg and 130 mg conjugate/kg 2-Br-C16-DX NPs). The mice in the control group were not treated. All mice were monitored after injection. Body weight and body conditions were monitored daily for three weeks.

3.2.9. In-vivo antitumor efficacy

Female BALB/c mice were injected s.c. in the right interscapular region 1×10^6 4T1 cells suspended in 100 μ L of FBS-free RPMI-1640 medium. When the tumor volume reached 70 – 100 mm³, mice were randomly divided into multiple groups. For the first efficacy study, the mice ($n = 8$) were injected via tail vein with test samples twice per week (10 mg conjugate/kg 2-Br-C16-DX NPs, 10 mg DX/kg Taxotere, and 10 mg conjugate/kg 2-Br-C16-DX in Taxotere vehicle). For the second efficacy study, the mice ($n = 9$) were injected via tail vein with test samples Q5d \times 2 (130 mg conjugate/kg 2-Br-C16-DX NPs, 130 mg conjugate/kg equivalent blank NPs, 20 mg DX/kg Taxotere, and 10 mg conjugate/kg 2-Br-C16-DX in Taxotere vehicle). For the third efficacy study, the mice ($n = 9$) were injected via tail vein with test samples Q7d \times 2 (70 mg conjugate/kg 2-Br-C16-DX NPs, 70 mg conjugate/kg equivalent blank NPs, 20 mg DX/kg Taxotere, and 10 mg conjugate/kg 2-Br-C16-DX in Taxotere vehicle). The mice

in the naive group were not treated. Tumor volume was measured by caliper three times per week. Tumor volume was calculated as $\text{length} \times (\text{width})^2/2$. The body weight and body conditions were monitored as well. Tumor growth and mouse mortality were recorded until day 23. Percentage survival of each group was calculated and plotted for the third efficacy study.

3.2.10. Statistical analysis

Statistical comparisons were performed using analysis of variances (ANOVA) (©1992-2007 GraphPad Prism Software, Inc.). Results were considered significant at 95% confidence interval ($p < 0.05$).

4. Results

4.1. Synthesis and characterization of 2-Br-C16-DX

DX were modified to a more lipophilic prodrug 2-Br-C16-DX by a one-step esterification reaction with a 2-bromohexadecanoyl chain attached to the 2'-position of DX (Figure 4.1). The 2'-OH is the most reactive hydroxyl group among the multiple hydroxyl groups in DX molecule, followed by 7-OH and 10-OH.¹ The presence of bromine on the acyl chain made the carboxylic acid more reactive than its counterpart lack of bromine so that in addition to 2'-substitution, byproducts with 7- and

10-substitution were also formed. Pure 2'-monosubstituted DX conjugate was obtained after purification by preparative TLC and confirmed by TLC, NMR and mass spectrometry.

4.2. Preparation and characterization of 2-Br-C16-DX BTM NPs

The previously optimized BTM NPs were able to entrap 2-Br-C16-DX with an entrapment efficiency of $56.8 \pm 2.8\%$. The 2-Br-C16-DX NPs had a mean particle size of 210 ± 2.15 nm with a zeta potential of -5.52 ± 0.97 mV (Table 4.1). The 2-Br-C16-DX NPs were physically and chemically stable at 4°C upon long-term storage. The particle size slightly increased from 210 nm to 230 nm and 2-Br-C16-DX concentration in the NP suspension was unchanged for at least 5 months (Figure 4.2).

4.3. In-vitro drug release in mouse plasma

The release of 2-Br-C16-DX from NPs in 100% mouse plasma was studied using the “ex-vivo” method developed in previous studies. Similar to C18-DX and C22-DX lack of bromine, an initial 45% burst release was observed upon spiking into the mouse plasma with no additional release within 8 hr (Figure 4.3).

4.4. 2-Br-C16-DX digestion

In fresh mouse plasma, 10% of 2-Br-C16-DX was hydrolyzed to DX in 48 hr when it was spiked into plasma in DMSO solution (Figure 4.4). When entrapped in NPs, 45% of 2-Br-C16-DX was hydrolyzed to DX and 35% of 2-Br-C16-DX remained intact in 48 hr. The NP-encapsulation induced digestion was consistent with the other three DX conjugates lack of bromine. The digestion rate and extent of 2-Br-C16-DX was significantly higher than C18-DX and C22-DX as expected especially when being entrapped in NPs. The mass balance did not reach 100% for NP-encapsulated 2-Br-C16-DX after 48 hr incubation suggesting the presence of alternative transfer pathways. To further investigate the mechanism of NP-encapsulation induced digestion, free 2-Br-C16-DX was also incubated with blank BTM NPs or the same surfactant components in BTM NPs in fresh mouse plasma. The digestion profiles of these two controls were more comparable to that of free 2-Br-C16-DX rather than 2-Br-C16-DX NP, indicating that the drug has to be encapsulated in the NPs to be more rapidly hydrolyzed.

In 4T1 tumor homogenate, only 6% of NP-encapsulated 2-Br-C16-DX and 2% of free 2-Br-C16-DX were hydrolyzed to DX within 48 hr (Figure 4.5). However, the loss of conjugate in NPs in 48 hr was 100%, whereas 20% loss of parent drug was observed with free 2-Br-C16-DX. The recovery of total drug mass was about 82% and 6% for free conjugate and NP-encapsulated conjugate, respectively.

4.5. In-vitro cytotoxicity

The in-vitro cytotoxicity was evaluated in two cell lines human prostate cancer cell DU-145 and murine breast cancer cell 4T1. In DU-145 cells, free 2-Br-C16-DX was 16.4-fold less active than DX (Figure 4.6A). Compared to the three DX conjugates without bromine, the free 2-Br-C16-DX was more toxic than any of those conjugates. C12-DX and C18-DX NPs showed comparable IC₅₀ values with their free forms, and C22-DX NPs showed only vehicle-related toxicity for 48 hr incubation. In contrast, the cytotoxicity of 2-Br-C16-DX NPs increased 6.5-fold compared to free 2-Br-C16-DX, which was still 2.5-fold lower than DX.

In 4T1 cells, free 2-Br-C16-DX was 2.8-fold less potent than DX (Figure 4.6B). When entrapped in BTM NPs, the cytotoxicity increased 12.7-fold compared to free 2-Br-C16-DX. More impressively, the IC₅₀ value of 2-Br-C16-DX NP was 4.5-fold lower than that of free DX. It is the first time in these studies that a DX conjugate in any form had higher cytotoxicity than unmodified DX. The blank NPs did not show significant cytotoxicity in either cell lines (IC₅₀ was 1842 ± 287 nM in DU-145 and 2955 ± 435 nM in 4T1 in drug equivalent dose, respectively).

4.6. In-vivo pharmacokinetics and biodistribution of 2-Br-C16-DX NPs

The plasma concentration-time curves in mice receiving i.v. bolus injections of Taxotere and 2-Br-C16-DX NPs at a dose of 10 mg DX/kg are shown in Figure 4.7A.

Pharmacokinetic parameters obtained using a noncompartmental model of analysis are listed in Table 4.2. The $AUC_{0-\infty}$ value of NP-formulated 2-Br-C16-DX was about 100-fold higher than that of Taxotere. The DX concentration in plasma was below the lower limit of quantification after 8 hr, whereas 2-Br-C16-DX could be detected until 96 hr. The terminal half-life of NP-formulated 2-Br-C16-DX was 8.7-fold higher compared to that of Taxotere. The plasma concentrations of DX as an active metabolite hydrolyzed from 2-Br-C16-DX were determined and shown in Figure 4.7B. DX concentrations of Taxotere are also shown as a reference for comparison. The pharmacokinetic parameters of DX from 2-Br-C16-DX NP are also shown in Table 4.2. The DX from 2-Br-C16-DX NP was detectable until 24 hr and below the lower limit of quantification after that. 2-Br-C16-DX NP improved DX AUC 4.3-fold compared to Taxotere. The terminal half-life of DX from 2-Br-C16-DX NP was comparable with that of Taxotere but its MRT was 6.4-fold higher than that of Taxotere.

The biodistribution of 2-Br-C16-DX and DX in main organs and tumors after i.v. administration of 2-Br-C16-DX NP and Taxotere is presented in Figure 4.8. The concentrations of DX from Taxotere in all organs rapidly decreased with time except for in tumors (Figure 4.8B). The lack of time-dependent elimination in the tumor likely reflects the abnormal tumor vasculature and dysfunctional lymphatic drainage. The overall concentrations of 2-Br-C16-DX were significantly higher than DX in all organs and tumors. A significant accumulation of 2-Br-C16-DX in liver and spleen was observed after the administration of 2-Br-C16-DX NP (Figure 4.8A). The

2-Br-C16-DX concentration in liver and spleen increased in the first several hours indicating the slow uptake of NPs by RES. The tumor accumulation of 2-Br-C16-DX and DX was shown in Figure 4.9. The AUC_{0-96} of 2-Br-C16-DX was 10-fold higher compared to Taxotere in xenografted 4T1 solid tumors (Table 4.3). The DX from 2-Br-C16-DX NP in the tumor generally increased with time and the AUC_{0-96} was 1.5-fold higher than that of Taxotere. The AUC_{plasma} and AUC_{tumor} of Taxotere obtained in these studies are comparable with other reports in the literature.^{6,7}

4.7. MTD of 2-Br-C16-DX NPs

The tolerability of 2-Br-C16-DX NP was assessed by body weight change and body conditioning evaluation. The MTD was defined as the maximum dose that causes only minor signs of toxicity (e.g., weight loss, poor coat condition) and no mortality. After single i.v. bolus injection of 150 mg conjugate/kg 2-Br-C16-DX NP, 7/8 mice died 5 min post injection and 1/8 died after 24 hr indicating acute toxicity at this dose, likely hematologic toxicity. The body weight of the control group and groups receiving single injection of 100 mg conjugate/kg or 130 mg conjugate/kg 2-Br-C16-DX NP is shown in Figure 4.10A. Mice receiving 100 mg conjugate/kg dose gained about 2% body weight while mice receiving 130 mg conjugate/kg dose kept their body weight almost unchanged, suggesting that these doses were well tolerated. As a result, the single-dose MTD was identified as 130-150 mg conjugate/kg (equivalent 93-108 mg DX/kg). The

MTD of Taxotere has been reported in the literatures as 15-33 mg/kg.^{7,8} The MTD of 2-Br-C16-DX NP was about 5-fold higher than that of Taxotere.

Multiple-dose MTD was also evaluated because in preclinical efficacy studies and in clinical practice, repeated treatments are required. The multiple-dose MTD was assessed by treating BALB/c mice with 2-Br-C16-DX NP at a dose ranging from 40 to 130 mg conjugate/kg, once per week for three weeks. Figure 4.10B demonstrates the body weight change of all five groups in three weeks. After the second dose at day 7, mice in 100 mg conjugate/kg group and 130 mg conjugate/kg group continuously lost weight. Until day 18, 2/5 mice in 100 mg conjugate/kg group and 3/5 mice in 130 mg conjugate/kg group were observed over 20% body weight loss. In contrast, the mice receiving 70 mg conjugate/kg 2-Br-C16-DX NP kept their body weight unchanged during the experimental time frame, therefore the multiple-dose MTD was identified as 70 mg conjugate/kg (equivalent 50 mg DX/kg) for at least three treatments. The multiple-dose MTD was about 2.5-fold higher compared to Taxotere indicating that 2-Br-C16-DX NP can be administered at significantly higher doses.

4.8. In-vivo antitumor efficacy

The antitumor efficacy of 2-Br-C16-DX NP was evaluated in a 4T1 breast cancer xenograft mouse model. In the first study, mice were treated with a low dose of 2-Br-C16-DX NP and Taxotere with high dose frequency (10 mg DX or conjugate/kg,

twice a week). The greatest tumor growth inhibition was observed with 2-Br-C16-DX NP treatment group (Figure 4.11). Taxotere and free 2-Br-C16-DX also showed some antitumor effect as compared to naive group. A statistically significant difference of 2-Br-C16-DX NP with all other treatments was observed at day 13 and 15, with post-hoc least significant difference test.

In the second efficacy study, a single-dose MTD of 2-Br-C16-DX NP (130 mg conjugate/kg) and Taxotere (20 mg DX/kg) was administered. Due to the solubility limitation, the maximum formulatable dose of 2-Br-C16-DX in Taxotere vehicle (10 mg conjugate/kg) was adopted. Mice were treated with these doses every 5 days. Tumor volume increased with control, blank BTM NPs, free 2-Br-C16-DX and Taxotere administration (Figure 4.12). The tumor growth in the 2-Br-C16-DX NP treatment group was almost completely inhibited. Taxotere at this high dose also significantly inhibited tumor growth. A statistically significant difference of 2-Br-C16-DX NP with all other treatments was observed at as early as day 5 and continued to the end of the study, with post-hoc Tukey's test. However, the aggressive dose regimen caused evident toxicity in 2-Br-C16-DX NP treatment group. At day 12, a 20% of body weight loss was observed in 3/9 mice in 2-Br-C16-DX NP treatment group after only two doses. It should be noted that mice in Taxotere group also lost some body weight but not as significant as 2-Br-C16-DX NP group. The results of the second efficacy study demonstrated that dose adjustment for multiple treatments was warranted.

In the third efficacy study, multiple-dose MTD of 2-Br-C16-DX NP was administered and dose frequency was adjusted to Q7d. Tumor volume increased with control, blank BTM NPs, free 2-Br-C16-DX and Taxotere administration (Figure 4.13). The most significant tumor growth inhibition was observed with 2-Br-C16-DX NP treatment group. Antitumor effect of Taxotere was comparable with the second efficacy study. In the third efficacy study, a statistically significant difference of 2-Br-C16-DX NP with all other treatments was observed starting from day 7 and continued to the end of the study, with post-hoc Tukey's test. Figure 4.14 shows the Kaplan-Meier survival curves of mice until day 23. The 50% survival time of naive, blank BTM NP, free 2-Br-C16-DX and Taxotere groups was between 14 days and 19 days. All mice in naive, blank BTM NP, free 2-Br-C16-DX and Taxotere groups died within 21 days. In 2-Br-C16-DX NP treatment group, 100% survival through day 23 was observed.

5. Discussion

In the present studies, a lipophilic DX conjugate 2-Br-C16-DX was synthesized and characterized. The new conjugate was well entrapped and retained in the oil-filled NPs. The digestion kinetics of 2-Br-C16-DX was improved compared to the three DX-lipid conjugates which lacked bromine. The retention of the conjugate in the long-circulating NPs, along with its very different digestion kinetics, resulted in a significantly improved pharmacokinetic profile, blood exposure of DX and tumor accumulation,

which in turn led to superior antitumor efficacy.

In the previous chapter, three DX-lipid conjugates were synthesized to overcome the poor retention of DX in the BTM 808 NPs in aqueous phase and in biologically relevant medium. The >10-fold increase in the solubility of DX conjugates in Miglyol 808 compared to DX allowed for a significant increase in drug loading, entrapment and retention in plasma. However, as prodrugs, their digestion kinetics was not optimal. The hydrolysis of C12-DX was too rapid whereas the hydrolysis rate and extent of C18-DX and C22-DX were too low in mouse plasma bearing high esterase activity. To further optimize the hydrolysis kinetics while retain the good drug entrapment and retention, the DX conjugate was modified by choosing a lipid with chain length between 12 and 18, and with a bromine at the 2-position of the lipid chain. The new DX conjugate 2-Br-C16-DX was successfully encapsulated in the BTM NPs with comparable entrapment efficiency and very similar release profile in mouse plasma with the other DX-lipid conjugates. The ester bond is more susceptible to hydrolysis with an electron-withdrawing group at the 2-position. As expected, the hydrolysis profile of 2-Br-C16-DX fell in between C12-DX and C18-DX. In contrast to C12-DX, 60% of which was rapidly hydrolyzed to DX in 4 hr, or C18-DX, only 14% of which was hydrolyzed to DX in 48 hr, 2-Br-C16-DX was slowly hydrolyzed to DX to an extent of 45% in 48 hr. The slower but higher extent of hydrolysis is expected to benefit the sustained release of DX in-vivo and further improve the DX blood exposure.

Despite of the different digestion kinetics, a NP-encapsulation induced

digestion was also observed for 2-Br-C16-DX in-vitro. A hypothesis was proposed in the previous chapter to explain the phenomenon. It is speculated that the amphiphilic DX conjugate molecules locate on the surface of the oil-filled NPs with relatively hydrophilic head orienting toward the aqueous phase and the lipid tail anchoring in the oil core. The huge specific surface area of NPs makes DX conjugate readily accessible to enzymes including esterases in the aqueous phase to transfer DX conjugate to DX and others. On the contrary, free DX conjugate molecules, once spiked into plasma, tightly bind to the plasma proteins (e.g., albumin) leading to the shield of cleavage site. To rule out the possibility that some components in the BTM NPs synergistically accelerated the hydrolysis of DX conjugate, in the present studies, two control experiments were conducted. The blank BTM NPs or the same surfactant components in BTM NPs co-incubation with free 2-Br-C16-DX did not accelerate the hydrolysis of 2-Br-C16-DX indicating that the more rapid hydrolysis of NP-encapsulated 2-Br-C16-DX was not caused by the catalysis of NP ingredient(s). Furthermore, the results also rule out the possibility that the NP-encapsulation induced digestion was caused by a simple solubilization effect, since the surfactants with the same concentration in the NPs were also capable of solubilizing the conjugate. However, these surfactants also did not accelerate the digestion. These results further support the hypothesis described above.

The cytotoxicity of 2-Br-C16-DX was higher compared to all three DX-lipid conjugates without bromine in DU-145 cells after 48 hr incubation. The higher

cytotoxicity may be partly attributed to its sustained but high extent of hydrolysis to DX. It remains possible that intact 2-Br-C16-DX possesses cell growth inhibition activity by its own right. The cytotoxicity of 2-Br-C16-DX NP was 6.5-fold and 12.7-fold higher compared to free 2-Br-C16-DX in DU-145 and 4T1 cells, respectively. This effect could be explained by NP-encapsulation induced digestion of 2-Br-C16-DX in the medium or intracellularly, but there are other possibilities as well. The higher cytotoxicity of 2-Br-C16-DX NP may also be explained by increased cellular uptake and/or different cellular compartmental sequester facilitated by NP. These factors may also contribute to the higher cytotoxicity of 2-Br-C16-DX NP in the highly aggressive breast cancer cell 4T1 compared to unmodified free DX. The low sensitivity of 4T1 cells to DX is probably due to their extremely rapid proliferation as well as other intrinsic detoxification mechanisms (e.g., degradation of DX). Hence, the uptake of high drug payload NPs by endocytosis followed by sustained release of DX may play essential roles in the improved cytotoxicity of 2-Br-C16-DX NP in 4T1 cells.

In-vivo, NP-formulated 2-Br-C16-DX achieved 100-fold higher AUC compared to Taxotere. The remarkably high AUC, long terminal half-life and long MRT were attributed to the stable anchoring of 2-Br-C16-DX in the long-circulating NPs as predicted by the in-vitro release study. The elimination routes of 2-Br-C16-DX include: 1) uptake of drug containing NPs by RES, 2) release of conjugate followed by elimination as free drug, and 3) hydrolysis of the conjugate to DX. All NP-formulated conjugates shared the first elimination route while NP-formulated 2-Br-C16-DX also

had similar release profile with NP-formulated C18-DX and C22-DX. The significantly higher hydrolysis kinetics differentiated NP-formulated 2-Br-C16-DX from the other two conjugates. As a result, the pharmacokinetic profile of NP-formulated 2-Br-C16-DX fell in between NP-formulated C12-DX and C18-DX, which was consistent with their trend of the in-vitro hydrolysis rates. Due to the sustained and high extent of hydrolysis, the AUC of DX in the plasma after the administration of 2-Br-C16-DX NPs was not only over 4-fold higher than that of Taxotere, but also significantly higher than the other three conjugates. The 2-Br-C16-DX NPs served as a drug reservoir and released DX in a sustained manner as shown in Figure 4.7B. The high concentration and prolonged exposure of both 2-Br-C16-DX and DX from 2-Br-C16-DX NPs in the plasma were beneficial to their passive tumor accumulation via the EPR effect. The AUC_{tumor} of 2-Br-C16-DX was 10-fold greater than that of Taxotere. The AUC_{tumor} of DX from 2-Br-C16-DX NP was 1.5-fold greater than that of Taxotere. However, the overall ratio of AUC_{tumor} of DX from 2-Br-C16-DX NP to that of 2-Br-C16-DX was low in 96 hr. The DX in the tumor was from two potential routes: direct uptake of DX from the systemic circulation and cleavage from the 2-Br-C16-DX accumulated in the tumors. The clear ascending trend of DX with time in the tumor suggests that the in-situ hydrolysis dominated the DX tumor concentration. The low rate of hydrolysis in the tumor in-vivo is consistent with its in-vitro tumor homogenate hydrolysis, suggesting low esterase activity in 4T1 tumor. The non-specific esterase activity in various human malignant tumors has been studied by histochemical analysis.

It has been previously reported that the esterase activity in breast tumors is generally low.⁹ In contrast, esterase activity is highly elevated in some tumor types compared to their normal tissue of origin such as colon and rectum adenocarcinoma, and thyroid tumors. It is likely that these tumor types with high esterase activity would serve as better models for the ester prodrugs that mostly depend on the enzymatic conversion to their active forms to exert antitumor effects. The NP-formulated 2-Br-C16-DX showed a marked accumulation in liver and spleen and the accumulation was increasing during the first several hours of the study. It clearly indicated a slow uptake of drug containing NPs by the RES. Although PEGylation reduces RES clearance, a great accumulation in RES-related organs is unfortunately still a typical distribution pattern for most of the NPs.^{10,11}

Murine breast cancer 4T1 is a highly aggressive and metastatic tumor model. They can spontaneously metastasize to the lung, liver, lymph nodes and brain while the primary tumor grows in-situ after injected s.c. into BALB/c mice. The tumor growth and metastatic spread of 4T1 cells in BALB/c mice very closely mimic human breast cancer.^{12,13} The in-vivo efficacy study in mice bearing breast cancer 4T1 xenografts using low dose (10 mg DX or conjugate/kg) demonstrated a statistically significant tumor growth inhibition effect by 2-Br-C16-DX NP compared to the standard-of-care therapy, which was consistent with their superior plasma pharmacokinetics and tumor distribution. However, given the high aggressiveness of 4T1 tumor model, it is not surprising that the low dose regimen did not achieve optimal antitumor efficacy. Since

2-Br-C16-DX NP was much better tolerated than Taxotere as indicated by the MTD studies, higher doses can be given expecting to achieve maximum tumor inhibition. In the second efficacy study, the single-dose MTD of 2-Br-C16-DX NP almost completely inhibited the tumor growth. However, the single-dose MTD with a relatively high dosing frequency caused fatal toxicity in mice at the same time. The acceptable body condition scoring values and body weight after treatment with the blank NPs suggested that the toxicity was not caused by the delivery vehicle but an accumulative effect of 2-Br-C16-DX itself (data not shown). It is speculated that most of the systemic side effects are likely attributed to the DX released in the circulation due to the high esterase activity in mouse plasma. However, since human plasma esterase activity is much lower than mouse as shown in Chapter 3 and demonstrated by others,^{14,15} it can be anticipated that in humans or in esterase-deficient mice, 2-Br-C16-DX NP would be better tolerated than in BALB/c mice. DX as a potent cytotoxic agent, once released in the circulation, causes inevitable toxicity to normal cells especially rapidly proliferating cells. Therefore, a fine balance between tolerable adverse effects and as high as possible efficacy is critical when choosing a therapeutic dose. With the objective to better balance the toxicity and efficacy, a third efficacy study was performed. Although the tumor inhibition effect was not as outstanding as in the second study, the body conditions of NP-treatment group were well maintained suggesting that 70 mg conjugate/kg is an optimal dose for the repeated treatment of 2-Br-C16-DX NP. The tumor growth was significantly suppressed by only two doses of 2-Br-C16-DX NP and

the suppression effect continued to at least day 23. The long-lasting antitumor effect of 2-Br-C16-DX NP reflected its prolonged exposure in the circulation as well as in tumors. In contrast, in Taxotere treatment group, after the last treatment at day 7, tumor growth quickly resumed. The rapid tumor growth after the termination of the treatment caused 100% mortality in 21 days despite its antitumor efficacy during the treatment. The short antitumor effect of Taxotere was consistent with its short half-life in-vivo.

In conclusion, the 2-Br-C16-DX NP developed in these studies maintained the high drug entrapment and long drug retention in the NPs while improving the hydrolysis kinetics of the conjugate in-vitro. The 2-Br-C16-DX NP developed in these studies had long circulation in the blood, high accumulation in the tumor and low toxicity, which therefore led to superior antitumor efficacy and less systemic toxicity in-vivo. Collectively, these studies demonstrate that the oil-filled lipid NPs containing a DX-lipid conjugate with fine-tuned lipophilicity and activation kinetics successfully improved the therapeutic index of DX. The encouraging results of these studies suggest that the novel formulation holds great promise for further clinic development.

Table 4.1. Compositions and properties of 2-Br-C16-DX NPs

Miglyol 808 (mg/mL)	Brij 78 (mg/mL)	TPGS (mg/mL)	2-Br-C16-DX (mg/mL)	Temperature (°C)	Particle size (nm)	Zeta potential (mV)	% Entrapment efficiency
2.5	1.7	0.8	0.5	60	215.6 ± 2.15	-5.52 ± 0.97	56.8 ± 2.8

Table 4.2. Pharmacokinetic parameters of 2-Br-C16-DX and DX in mice after i.v. bolus administration of 2-Br-C16-DX NP and Taxotere

	Taxotere	NP-formulated 2-Br-C16-DX	DX from 2-Br-C16-DX NP
$t_{1/2}$ (hr)	4.04	35.3	5.62
AUC_{0-96} (h*mg/L)	2.36	230	10.1
$AUC_{0-\infty}$ (h*mg/L)	2.47	265	10.6
V_d (L/kg)	4.48	0.55	--
K_{el} (1/hr)	0.17	0.02	0.12
CL (L/hr/kg)	4.05	0.04	--
C_{max} (mg/L)	10.5	192	2.59
MRT (hr)	1.10	15.2	7.06

Table 4.3. Tumor accumulation of 2-Br-C16-DX and DX in mice after i.v. bolus administration of 2-Br-C16-DX NP and Taxotere

	Taxotere	NP-formulated 2-Br-C16-DX	DX from 2-Br-C16-DX NP
AUC ₀₋₉₆ (µg/g*h)	7.10	70.6	10.4

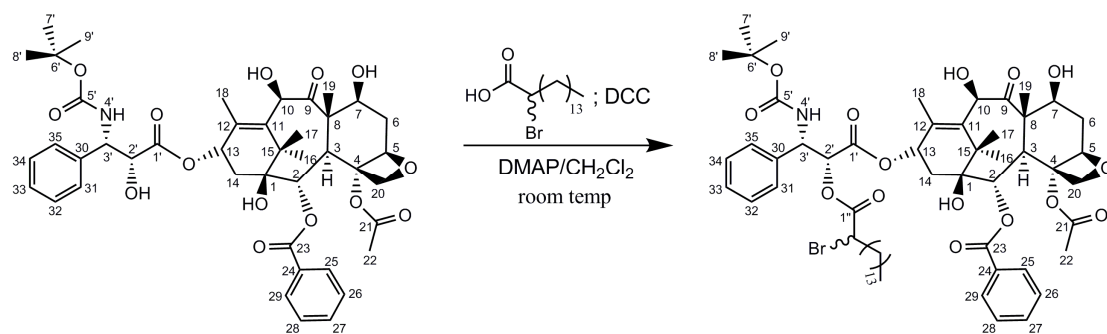


Figure 4.1. Synthesis of 2'-(2-bromohexadecanoyl)-docetaxel conjugate

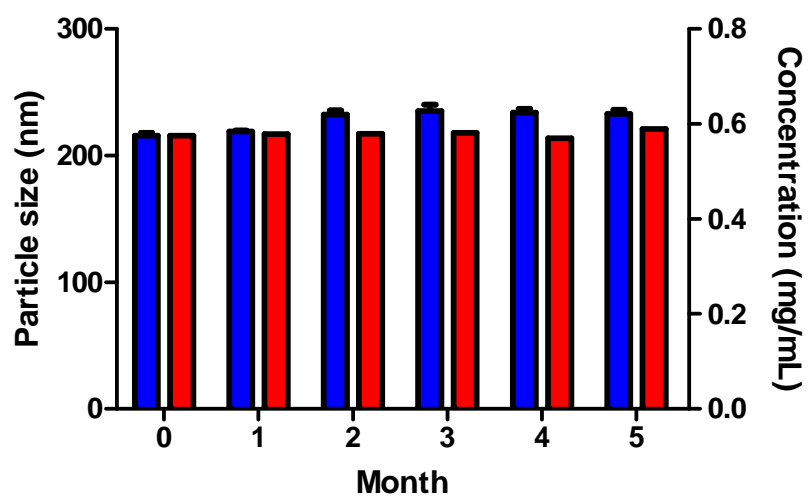


Figure 4.2. Physicochemical stability of 2-Br-C16-DX NPs stored at 4°C.

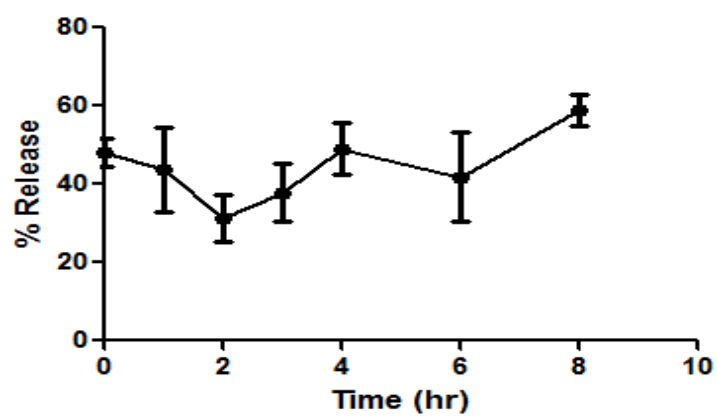
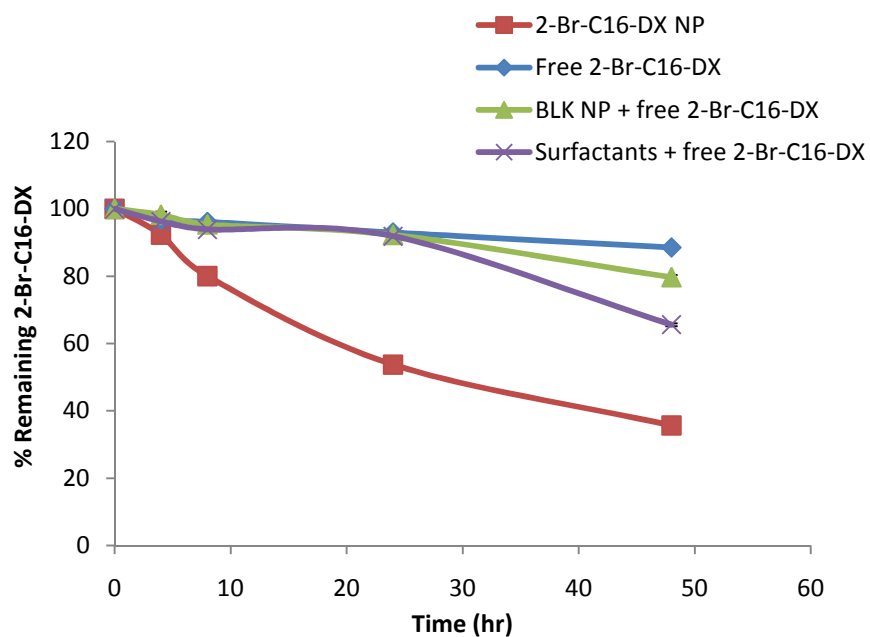


Figure 4.3. Release of 2-Br-C16-DX from BTM NPs in 100% mouse plasma at 37°C.

A



B

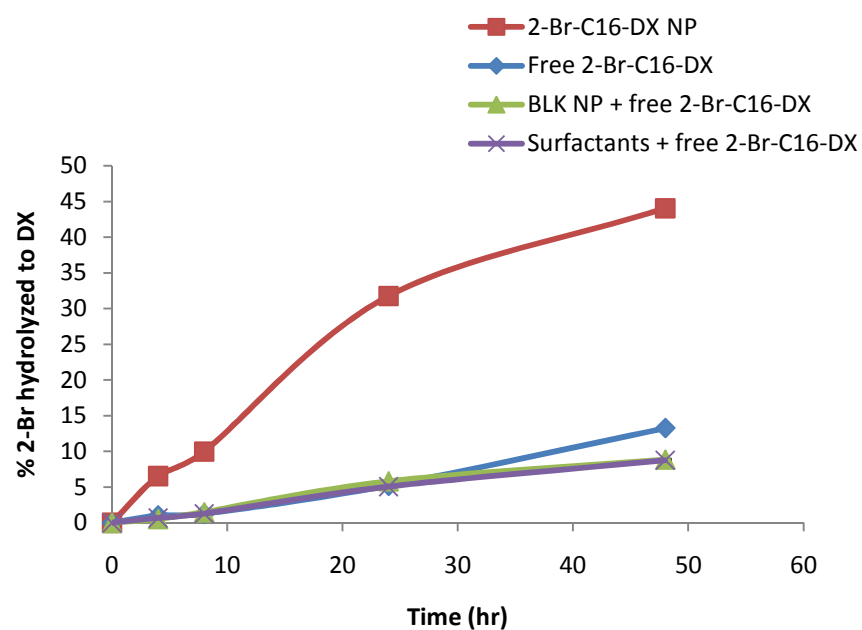
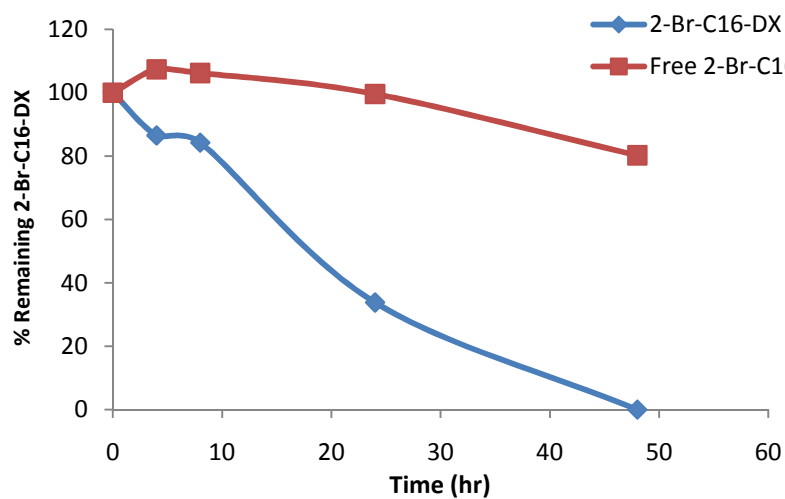


Figure 4.4. The digestion of 2-Br-C16-DX in fresh 100% mouse plasma at 37°C. (A) The loss of DX conjugates. (B) The formation of DX. Data are shown as mean \pm SD (n = 3).

A



B

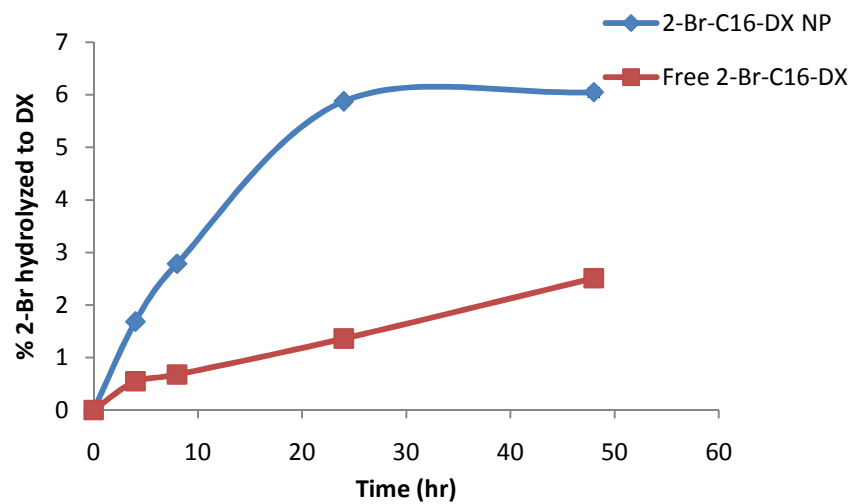
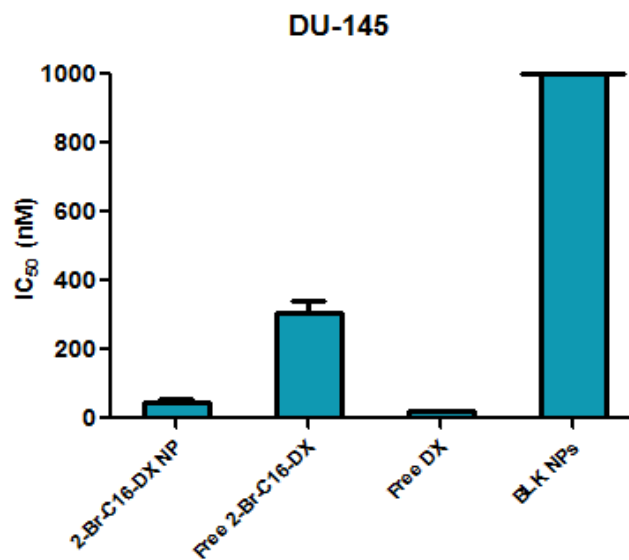


Figure 4.5. The digestion of 2-Br-C16-DX in 4T1 tumor homogenate at 37°C. (A) The loss of DX conjugates. (B) The formation of DX. Data are shown as mean \pm SD (n = 3).

A



B

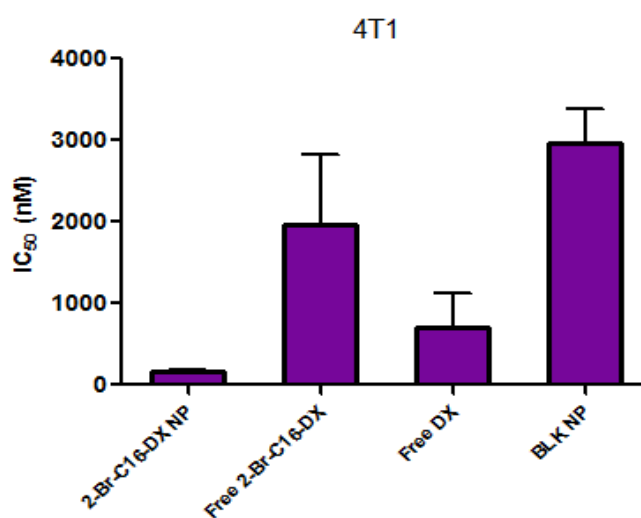
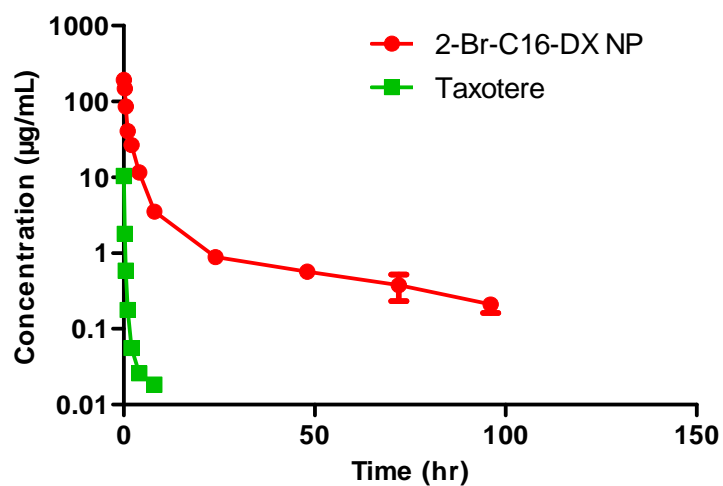


Figure 4.6. In-vitro cytotoxicity of free 2-Br-C16-DX and 2-Br-C16-DX NPs in (A) human prostate cancer cell DU-145 cells and (B) murine breast cancer cell 4T1 cells. Blank NPs were dosed at drug equivalent dose. Drug equivalent dose of NPs are calculated from the NP compositions.

A



B

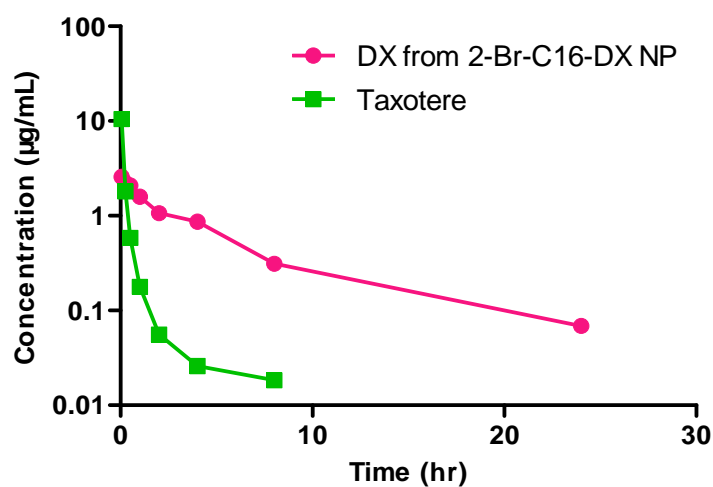
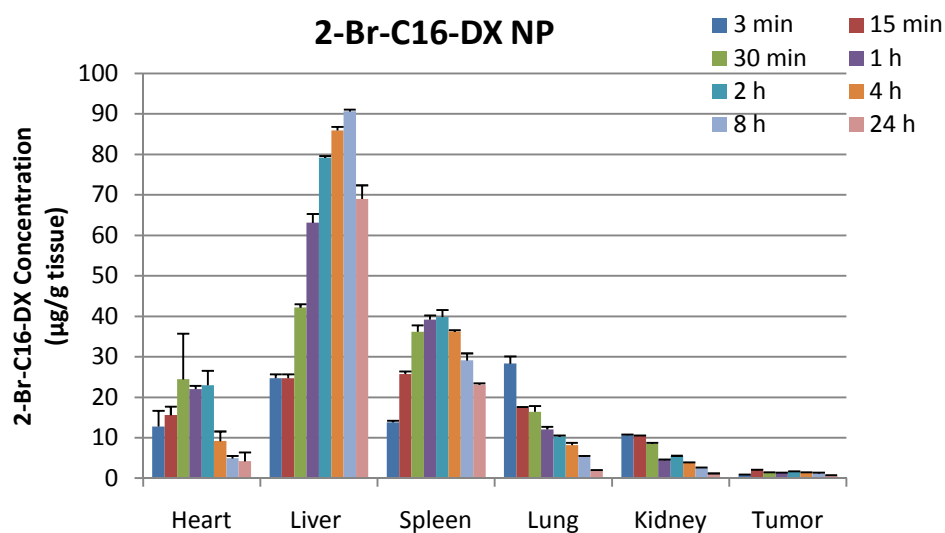


Figure 4.7. Plasma concentration-time curves for (A) DX and 2-Br-C16-DX after administration of Taxotere and 2-Br-C16-DX NPs (10 mg DX/kg), and (B) DX as an active metabolite from 2-Br-C16-DX NPs using Taxotere as a reference. Data are shown as mean \pm SD (n = 3).

A



B

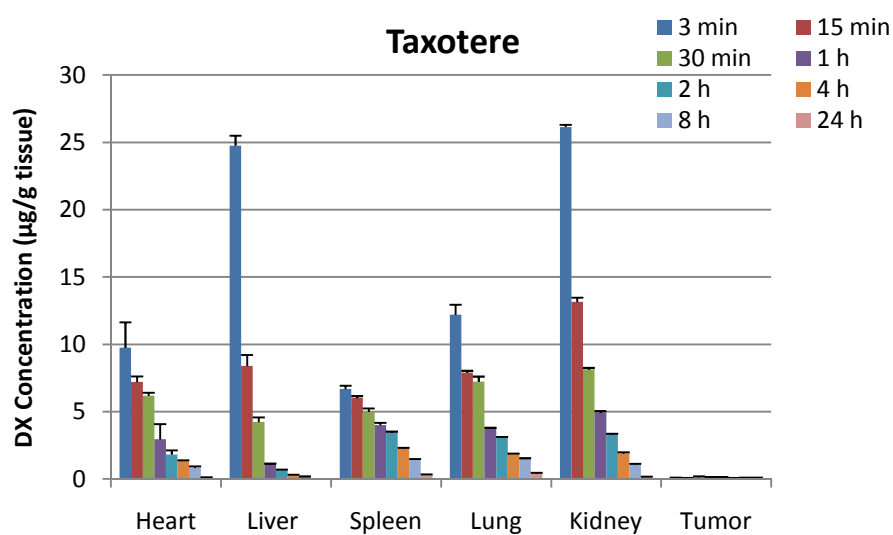
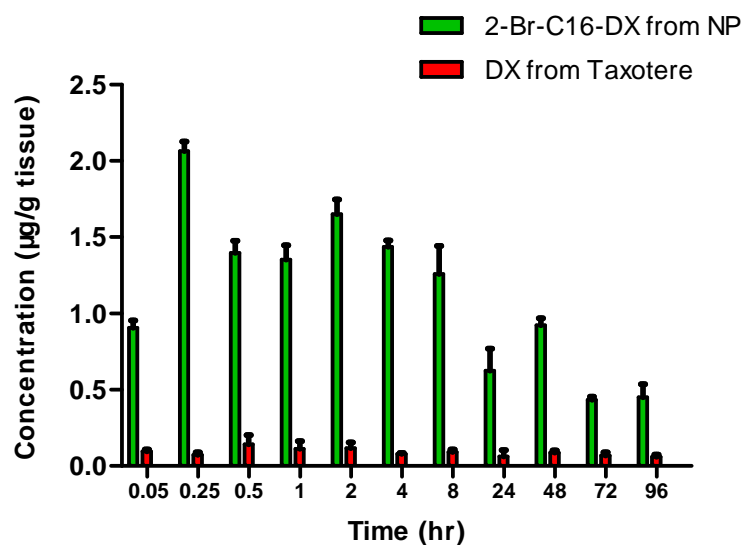


Figure 4.8. Biodistribution of (A) 2-Br-C16-DX and (B) DX in heart, liver, spleen, lung, kidney and tumor after i.v. administration of 2-Br-C16-DX NP and Taxotere (10 mg DX/kg). Data are shown as mean \pm SD (n = 3).

A



B

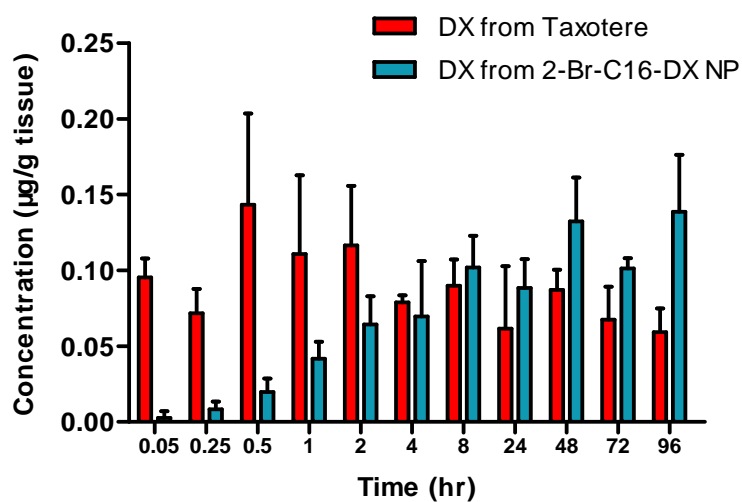
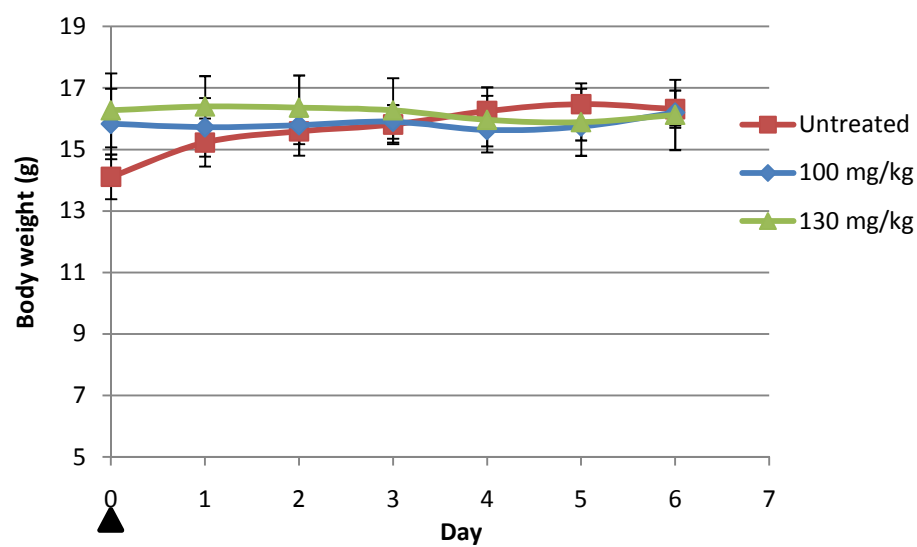


Figure 4.9. Tumor accumulation of (A) 2-Br-C16-DX from NPs and DX from Taxotere, and (B) DX as an active metabolite from 2-Br-C16-DX NPs after i.v. administration of 2-Br-C16-DX NP and Taxotere (10 mg DX/kg) using Taxotere as a reference. Data are shown as mean \pm SD (n = 3).

A



B

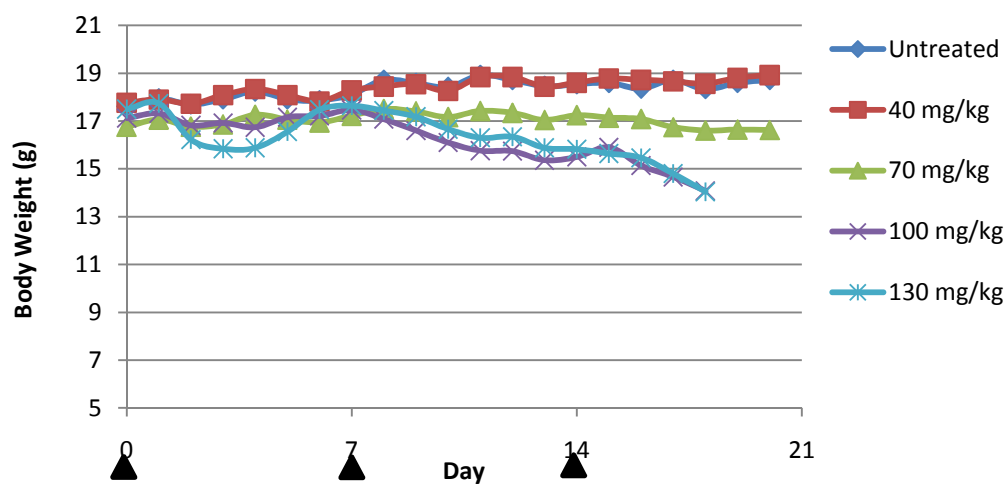


Figure 4.10. Body weight of mice after (A) single i.v. administration of 2-Br-C16-DX NPs, and (B) Q7d \times 3 i.v. administration of 2-Br-C16-DX NPs with different doses.

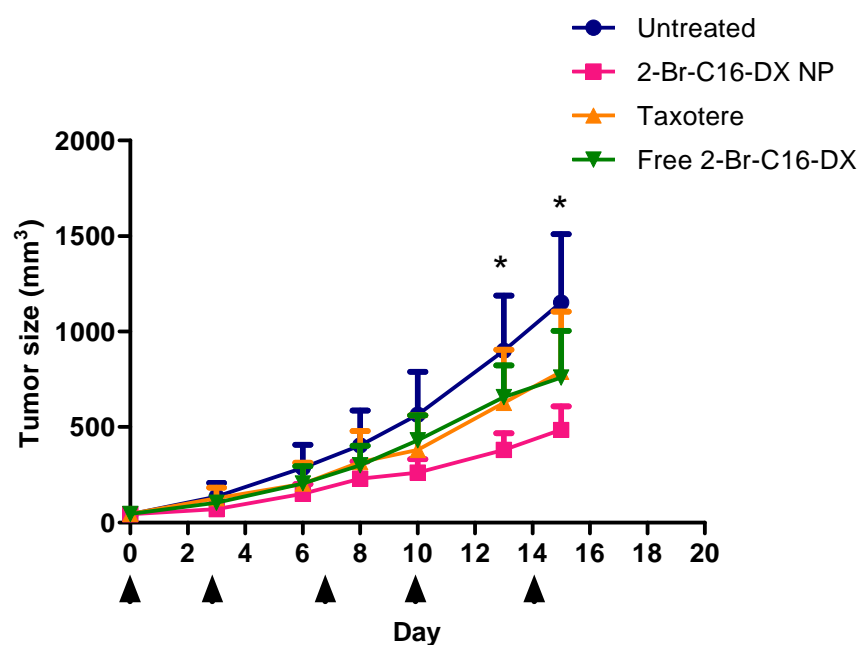


Figure 4.11. The first antitumor efficacy study. 4T1 xenografted female BALB/c mice bearing 70 – 100 mm³ tumor were treated i.v. with 10 mg/kg 2-Br-C16-DX NPs, 10 mg/kg Taxotere, or 10 mg/kg 2-Br-C16-DX in the Taxotere vehicle on day 0, 3, 7, 10, and 14. Data are shown as mean \pm SD (n = 8). * $p < 0.05$.

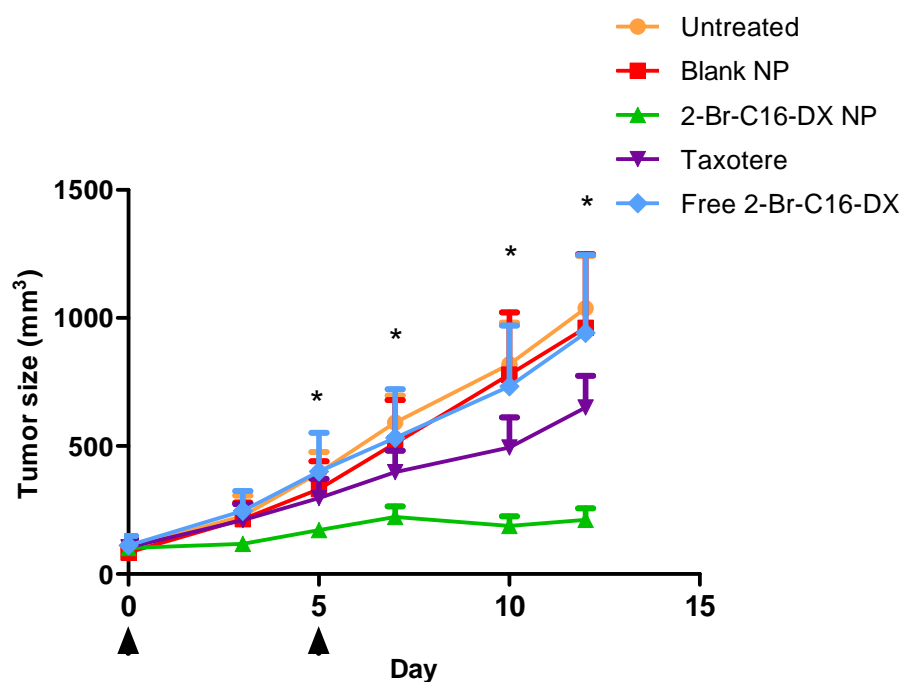


Figure 4.12. The second antitumor efficacy study. 4T1 xenografted female BALB/c mice bearing 70 – 100 mm³ tumor were treated i.v. with 130 mg/kg 2-Br-C16-DX NPs, 130 mg/kg equivalent blank NPs, 20 mg/kg Taxotere, or 10 mg/kg 2-Br-C16-DX in the Taxotere vehicle on day 0 and 5. Data are shown as mean \pm SD (n = 9). * $p < 0.05$.

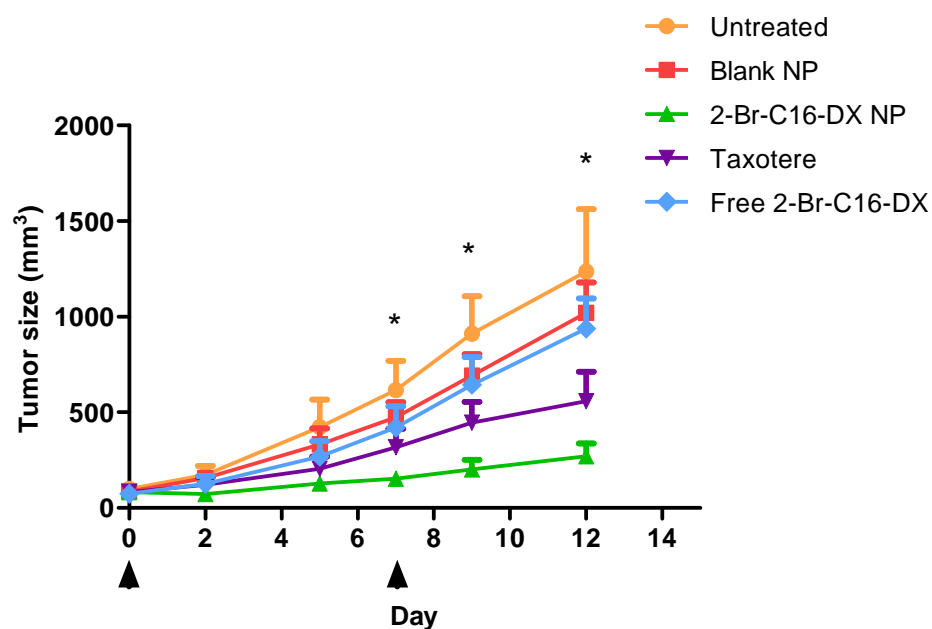


Figure 4.13. The third antitumor efficacy study. 4T1 xenografted female BALB/c mice bearing 70 – 100 mm³ tumor were treated i.v. with 70 mg/kg 2-Br-C16-DX NPs, 70 mg/kg equivalent blank NPs, 20 mg/kg Taxotere, or 10 mg/kg 2-Br-C16-DX in the Taxotere vehicle on day 0 and 7. Data are shown as mean \pm SD (n = 9). * $p < 0.05$.

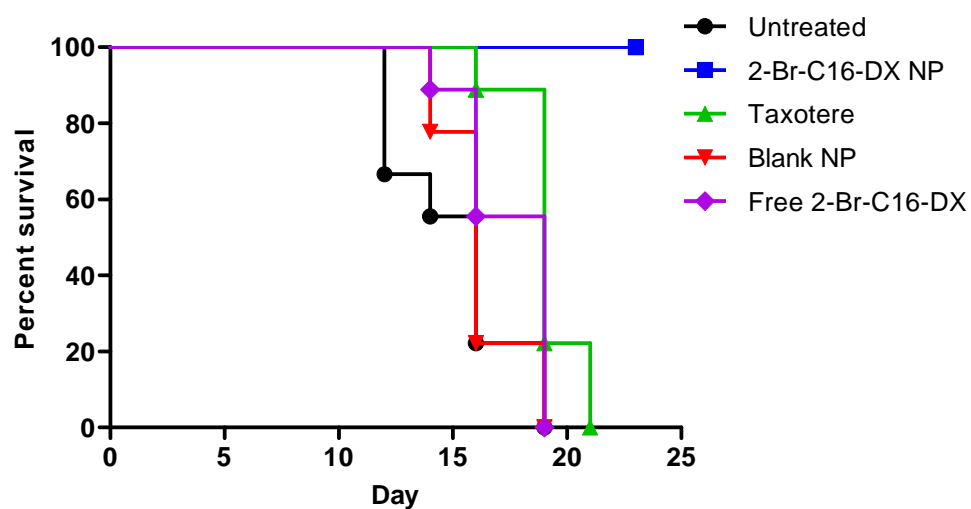


Figure 4.14. Kaplan-Meier survival curves of 4T1 xenografted female BALB/c mice treated with 70 mg/kg 2-Br-C16-DX NPs, 70 mg/kg equivalent blank NPs, 20 mg/kg Taxotere, or 10 mg/kg 2-Br-C16-DX in Taxotere vehicle (n=9) on day 0 and 7.

References

1. Huynh L, Leroux JC, Allen C. Enhancement of docetaxel solubility via conjugation of formulation-compatible moieties. *Org Biomol Chem*. Sep 7 2009;7(17):3437-3446.
2. Parness J, Kingston DG, Powell RG, Harracksingh C, Horwitz SB. Structure-activity study of cytotoxicity and microtubule assembly in vitro by taxol and related taxanes. *Biochem Biophys Res Commun*. Apr 14 1982;105(3):1082-1089.
3. Ali S, Ahmad I, Peters A, et al. Hydrolyzable hydrophobic taxanes: synthesis and anti-cancer activities. *Anticancer Drugs*. Feb 2001;12(2):117-128.
4. Ahmad I, Masters GR, Schupsky JJ, et al. Growth inhibition of a human ovarian tumor by a novel paclitaxel derivative in SCID mice. *Oncol Res*. 1999;11(6):273-280.
5. Dong XW, Mattingly CA, Tseng M, Cho M, Adams VR, Mumper RJ. Development of new lipid-based paclitaxel nanoparticles using sequential simplex optimization. *Eur J Pharm Biopharm*. May 2009;72(1):9-17.
6. van Tellingen O, Beijnen JH, Verweij J, Scherrenburg EJ, Nooijen WJ, Sparreboom A. Rapid esterase-sensitive breakdown of polysorbate 80 and its impact on the plasma pharmacokinetics of docetaxel and metabolites in mice. *Clin Cancer Res*. Oct 1999;5(10):2918-2924.
7. Zhigaltsev IV, Winters G, Srinivasulu M, et al. Development of a weak-base docetaxel derivative that can be loaded into lipid nanoparticles. *J Control Release*. Jun 15 2010;144(3):332-340.
8. Dykes DJ, Bissery MC, Harrison SD, Jr., Waud WR. Response of human tumor xenografts in athymic nude mice to docetaxel (RP 56976, Taxotere). *Invest New Drugs*. 1995;13(1):1-11.
9. Cohen RB, Nachlas MM, Seligman AM. Histochemical demonstration of esterase in malignant tumors. *Cancer Res*. Sep 1951;11(9):709-711.
10. Yang SC, Lu LF, Cai Y, Zhu JB, Liang BW, Yang CZ. Body distribution in mice of intravenously injected camptothecin solid lipid nanoparticles and targeting effect on brain. *J Control Release*. Jun 2 1999;59(3):299-307.
11. Harivardhan Reddy L, Sharma RK, Chuttani K, Mishra AK, Murthy RS. Influence of administration route on tumor uptake and biodistribution of

etoposide loaded solid lipid nanoparticles in Dalton's lymphoma tumor bearing mice. *J Control Release*. Jul 20 2005;105(3):185-198.

12. Aslakson CJ, Miller FR. Selective events in the metastatic process defined by analysis of the sequential dissemination of subpopulations of a mouse mammary tumor. *Cancer Res*. Mar 15 1992;52(6):1399-1405.
13. Pulaski BA, Terman DS, Khan S, Muller E, Ostrand-Rosenberg S. Cooperativity of Staphylococcal aureus enterotoxin B superantigen, major histocompatibility complex class II, and CD80 for immunotherapy of advanced spontaneous metastases in a clinically relevant postoperative mouse breast cancer model. *Cancer Res*. May 15 2000;60(10):2710-2715.
14. Xu Z, Chen L, Gu W, et al. The performance of docetaxel-loaded solid lipid nanoparticles targeted to hepatocellular carcinoma. *Biomaterials*. Jan 2009;30(2):226-232.
15. Li B, Sedlacek M, Manoharan I, et al. Butyrylcholinesterase, paraoxonase, and albumin esterase, but not carboxylesterase, are present in human plasma. *Biochem Pharmacol*. Nov 25 2005;70(11):1673-1684.

Chapter 5.

Summary and future directions

1. Summary

DX is one of the most potent anticancer drugs used in the clinical treatment of various cancers. Taxotere is currently the only commercial dosage form of DX on the market. Drawbacks associated with the formulation have been widely recognized and reported. The overall goal of this project was to develop a formulation that safely, effectively and selectively delivered DX to solid tumors utilizing state of the art nanotechnology. The developmental process generated three generations of formulation. The first generation was oil-filled NPs containing DX. The second generation was oil-filled NPs containing DX-lipid conjugates with different fatty acid chain lengths. The third generation was oil-filled NPs containing a bromoacyl DX conjugate 2-Br-C16-DX. The three generations of DX formulations were described in detail in Chapter 2, Chapter 3 and Chapter 4, respectively.

Generation 1

The focus of the studies in Chapter 2 was the development of oil-filled NP. The highlight of these studies was the methodology of studying the drug release in pure

mouse plasma. The formulation was based on the previously developed BTM 812 NPs for the delivery of PX. Liquid lipid Miglyols were firstly screened for their solvation ability for DX to select a lipid phase with the highest drug solubility. Miglyol 808 was identified as the Miglyol with the highest solvation ability for DX that was capable of forming NPs. Miglyol 808 was used as the oil phase to develop new BTM NPs by the guidance of sequential simplex optimization. The final optimized BTM 808 NPs successfully entrapped DX with 85% entrapment efficiency as determined by ultrafiltration. The formulation was physically stable at 4°C for at least three months. The oil-filled NPs containing DX showed similar cytotoxicity compared to free DX in sensitive DU-145 and PC-3 cells while in their resistant counterparts, the IC₅₀ values of DX NPs were 3-fold lower compared to free DX. These results confirmed our previous findings that the oil-filled BTM NPs could overcome P-gp-mediated resistance in-vitro. To better mimic in-vivo physiological environment and overcome the poor in-vitro/in-vivo correlation, a novel “ex-vivo” release method was developed to study the DX release from NPs in mouse plasma. To our knowledge, this is the first in-vitro release method in which NPs are spiked directly into 100% plasma samples. Despite the desirable formulation properties, DX was found to be very quickly released in mouse plasma. The re-characterization by SEC revealed that DX was not truly entrapped into the NPs during preparation. The different entrapment efficiencies suggest that depending on the formulation, different measurement methods may result in very different results. The first generation oil-filled NPs containing DX may not be

considered a successful formulation. However, the methodologies developed in these studies provided more meaningful guidance for the development of improved formulations with better drug retention.

Generation 2

To overcome the poor retention of DX in the oil-filled NPs in simple aqueous phase and in biologically relevant medium, three DX lipid conjugates (C12-DX, C18-DX and C22-DX) were synthesized and fully described in Chapter 3. The three conjugates showed >10-fold solubility increase in the liquid oil phase Miglyol 808 over DX. On the basis of previously developed BTM NPs, another experimental design orthogonal design was performed to further increase the drug entrapment efficiency in the NPs. The optimized formulation significantly reduced the surfactant concentration. The conjugates were successfully entrapped in the reduced-surfactant NPs with entrapment efficiencies about 50-60% as measured by SEC. The DX conjugates were well retained in the NPs not only during preparation in 10% lactose, but also in mouse plasma. In 100% mouse plasma, after the initial 45% burst of drug, C12-DX showed another 40% release within 8 hr, whereas C18-DX and C22-DX in NPs showed no additional release. In-vitro hydrolysis studies showed that the hydrolysis rate was C12-DX > C18-DX > C22-DX, which was predicted by their different steric hindrance. In-vivo, NP-formulated DX conjugates showed 8-450-fold higher AUC_{0-∞} values than that of Taxotere, demonstrating prolonged retention of DX conjugate in the blood. More

importantly, C12-DX and C18-DX improved DX $AUC_{0-\infty}$ over that of Taxotere. The prolonged exposure of DX from C18-DX demonstrated that C18-DX NPs served as a drug reservoir and released DX in a sustained manner. C18-DX NPs have the potential to exert higher in-vivo anticancer efficacy. The generation 2 formulation comprised of oil-filled NPs containing DX-lipid conjugates achieved stable drug retention and the consequent superior pharmacokinetic profiles. The highlight of this chapter is that the in-vitro release in mouse plasma and in-vitro hydrolysis well correlated with the in-vivo pharmacokinetic profiles of both DX conjugates and activated DX, indicating that the combination of these in-vitro assays could serve as a good predictor for the in-vivo pharmacokinetics. However, the DX conjugate with more desirable in-vivo pharmacokinetics (C18-DX) showed significantly lower cytotoxicity than DX in-vitro. The results suggested that the activation kinetics of DX lipid conjugate remains to be further tuned.

Generation 3

The generation 3 formulation focused on the modification of the entrapped prodrug. A bromoacyl DX conjugate 2-Br-C16-DX was synthesized to maintain the high drug loading, entrapment and retention in oil-filled lipid NPs while improve the hydrolysis kinetics. The conjugate was successfully entrapped in the previously optimized NPs with an entrapment efficiency of 56.8%. In-vitro release studies in 100% mouse plasma showed an initial 45% burst release with no additional release within 8 hr. The

entrapment efficiency and release profile were similar to those of C18-DX. In contrast, 45% of the new conjugate was hydrolyzed to DX by esterase in-vitro in 48 hr. Consistent with its more efficient hydrolysis, the conjugate showed comparable cytotoxicity with unmodified DX in DU-145 and 4T1 cells when encapsulated in NPs. In-vivo, the $AUC_{0-\infty}$ value of NP-formulated 2-Br-C16-DX was about 100-fold greater than that of Taxotere. 2-Br-C16-DX NP improved DX AUC 4.3-fold compared to Taxotere. More importantly, the high concentration and prolonged exposure of both 2-Br-C16-DX and DX from 2-Br-C16-DX NPs in circulation led to a 10-fold and 1.5-fold greater accumulation of 2-Br-C16-DX and DX in tumors compared to Taxotere, respectively. The 2-Br-C16-DX NPs were well tolerated in mice as compared to Taxotere. In mice bearing metastatic 4T1 tumors, 2-Br-C16-DX NPs showed marked anticancer efficacy as well as survival benefit over all controls. The highlight of the studies in this chapter is that the generation 3 formulation improved the overall therapeutic index of DX and was significantly more efficacious in the treatment of metastatic breast cancer relative to the standard-of-care Taxotere.

In conclusion, an injectable NP formulation was successfully developed for the delivery of DX by step-by-step and rationale development and optimization approach. The encouraging results of these studies suggest that the oil-filled NPs containing bromoacyl DX conjugate 2-Br-C16-DX hold great promise to be translated to clinical application and the approach may be extended to other tumor types. The strategy of

developing a hydrolyzable lipophilic prodrug may render an alternative approach for other therapeutic agents to be delivered in lipid-based NPs. In addition, the novel “ex-vivo” release method developed in these studies provides more predictive in-vitro guidance for the development of improved and more potent nano-formulations.

2. Future directions

The nano-formulations developed in the present studies have been proven to passively target solid tumors taking good advantage of the EPR effect and achieve high tumor accumulation. The next logical step would be incorporating active targeting into the formulation to actively target tumors and selectively kill cancer cells. Human epidermal growth factor receptor (EGFR), a transmembrane receptor, has emerged as an attractive target for targeted drug delivery. Overexpression of EGFR has been detected in one third of all solid tumors, in many of which EGFR expression characterizes a more advanced disease stage.¹ Our laboratory has successfully developed oil-filled NPs with surface-chelated nickel (Ni-NPs) using a Brij 78-NTA-Ni conjugate.² The surface of the Ni-NPs was decorated with a novel high affinity histidine ×6-tagged EGFR-binding Z domain (heptameric Z^{EGFR} domain) via his-tag-Ni affinity binding. The novel targeting ligand was generated by Liu et al. by fusing a heptamerization domain with an EGFR-binding Z domain of an affibody molecule. The EGFR-targeting NPs have shown enhanced internalization in EGFR-overexpressing A431 cells in-vitro. In-vivo studies showed an extensive localization (19% of the total

detected fluorescence) in tumor tissue and 2-fold increase of intracellular uptake with the targeted Ni-NPs. Our colleagues and collaborators are now working on a trimeric EGFR-binding ligand that is more stable with smaller size. Combining the EGFR-targeting NPs with the hydrolyzable, long-retention DX prodrug, higher anticancer efficacy is expected in the EGFR-overexpressing tumor models such as A431 and MDA-MB-468 tumors. Our preliminary studies have shown that the incorporation of trimeric EGFR-binding ligand did not alter the entrapment efficiency of 2-Br-C16-DX in the NPs. This formulation remains to be further optimized and fully characterized. With the concerns of in-vivo stability, alternatively, we can covalently attach cysteine-terminated EGFR-targeted Z domain to the NP surface using a Brij 78-maleimide reagent.

Despite the thorough characterization of the DX conjugate NPs in-vitro, many aspects of their in-vivo behaviors are not yet clear. First of all, the pharmacokinetics and biodistribution studies only quantified the total drug concentrations. It remains unknown that what fraction of the total drug represents released drug and what fraction is still retained in the NPs. The most commonly used method to study this is to radiolabel the NPs.³ The radioactivity-time curve represents the circulation of the delivery vehicles. A stable drug to NP ratio indicates stable drug retention in the delivery vehicles. Alternatively, a more direct approach is to differentiate the free drug with the NP-formulated drug. Zamboni et al. have developed a solid-phase separation method to physically separate liposome-encapsulated and released drug in mouse

plasma.^{4,5} Compared to the radiolabeling method, the development of this approach takes a lot more effort, and the method is often drug and formulation dependent. Not until we can differentiate the free drug with NP-formulated drug will it be clear about how the drug release in-vitro correlates with the in-vivo release profile of the NPs. Without the direct evidence showing the in-vivo release of NPs, the slow/no in-vitro release in plasma and high in-vivo AUC suggest that a slow in-vivo release is very likely. If it holds true that 2-Br-C16-DX as well as C18-DX and C22-DX are not further released from the NPs in-vivo after the burst, is it a favorable property or not? In the systemic circulation, “no release” is surely a good property for the drugs to take advantage of the long-circulating NPs and avoid systemic toxicity because the drug must be released to exert its pharmacological activity. Once located in the tumor site, at the cellular level, the integrity of drug-containing NP is also critical. For example, for NPs that overcome efflux pump mediated resistance, the endocytosis of high drug payload NPs is one of the mechanisms. For active targeting NPs, since the targeting ligands are on the NPs, the retention of drug in the NPs is apparently desirable. Collectively, generally speaking, “no release” before the cellular internalization is a favorable property. Given that “no release” is desirable, the burst release observed with the current formulations should be reduced or prevented by formulation optimization. Following this issue, many questions remain to be answered. How and where are the drugs released from the NPs in the cell? What is the ultimate intracellular fate of lipid NPs? How do NPs traffic intracellularly? What enzymes are responsible for the NP

breakdown and what are their kinetics? Further investigations will definitely help us to understand the NP behaviors on the cellular level.

Another issue associated with formulation remaining to be fully characterized and further improved is PEGylation. So far, a reliable approach to accurately quantify the PEG chain on the NP surface is still missing. In the development of Ni-NPs for active targeting, it was found that the incorporation of Brij 78-NTA-Ni in the NPs ($\sim 90\%$) was significantly higher than the incorporation of Brij 700-NTA-Ni ($\sim 50\%$).² The results suggest that a surfactant with a medium PEG chain (Brij 78) anchors better in the oil-filled BTM NPs probably due to its miscibility with Miglyol 808. On the contrary, surfactant with a relatively longer PEG chain (Brij 700) tends to participate into the aqueous phase due to its higher hydrophilicity. In the light of this hypothesis, Brij 78-PEG 750, a PEGylation agent with medium PEG chain was synthesized in our laboratory. To fully understand what PEG chain length and what PEG density are optimal for RES stealth, systematic studies are definitely needed in the future.

Prodrugs are an important drug delivery strategy. In addition to the delivery carrier, there remains opportunity to improve and optimize the prodrug approach. In Chapter 3, three DX conjugates were synthesized and compared. It was found that many physical/chemical properties of these conjugates are chain-length dependent. In Chapter 4, only one modified conjugate 2-Br-C16-DX was synthesized and investigated based on the previous findings. Although this modified conjugate showed

improved hydrolysis kinetics compared to the other three DX conjugates and marked in-vivo anticancer efficacy, it is premature to claim that 2-Br-C16-DX is the best of its kind. The acyl chain length and the electron-withdrawing group are two factors that can be further tuned. In addition, it remains unclear about whether the conjugates have their own antitumor activity and, if any, what then is the mechanism(s). Our colleague found that a PX-lipid conjugate C22-PX had appreciable microtubule-binding affinity, which is different from most of the reports in the literature.^{6,7} Besides the microtubule binding mechanism, other mechanisms if any remain to be investigated.

Choosing a suitable animal model plays essential roles in demonstrating the advantages of ester prodrug containing NPs and interpreting the preclinical results to the relevance of clinical applications. In the present studies, in-vitro and in-vivo results all indicated that 2-Br-C16-DX was highly cleaved in the plasma but not in the tumor tissues. In an ideal scenario, DX should not be released in the systemic circulation but only liberated in the targeted action site such as the tumor. However, mouse plasma bears high esterase activity while the esterase activity in the 4T1 breast cancer selected in these studies is probably low. This former limitation may be overcome, to some extent, by using a carboxylesterase-deficient mouse model to better mimic human plasma. On the other hand, the DX ester prodrug that mostly depends on the esterase-mediated activation may exert significantly enhanced anticancer activity in the high-esterase-activity tumor models such as colon tumors or thyroid tumors. Additional in-vivo efficacy studies will be carried out in more clinically relevant cancer models.

Currently, we have shown preliminary efficacy in an orthotopic non-small cell lung cancer (NSCLC) mouse model with 2-Br-C16-DX NPs. The orthotopic NSCLC model was established by directly injecting luciferase-expressing A549-luc-c8 cells (Caliper Life Sciences) into the left lung parenchyma of nude mice. In this model, 2-Br-C16-DX NPs administered i.v. at a dose of 70 mg/kg, Q7d \times 5 showed significantly lower luminescence level than 20 mg/kg standard-of-care Taxol and Taxotere. Survival benefit is expected in the future studies. The efficacy of 2-Br-C16-DX NPs will also be evaluated in genetically engineered mouse model (GEMM) developed in UNC Mouse Phase 1 Unit (MP1U) by collaboration. These studies will extend the application of oil-filled NPs containing DX prodrug to the treatment of various cancers.

References

1. Ritter CA, Arteaga CL. The epidermal growth factor receptor-tyrosine kinase: a promising therapeutic target in solid tumors. *Seminars in Oncology*. Feb 2003;30(1 Suppl 1):3-11.
2. Benhabbour SR LJ, Kim D, Jain A, Wadhwa S, Parrott MC, Liu R, Desimone J, Mumper RJ. In vitro and in vivo assessment of targeting lipid-based nanoparticles to the epidermal growth factor-receptor (EGFR) using a novel Heptameric Z(EGFR) domain. *J Control Release*. 2011.
3. Zhigaltsev IV, Winters G, Srinivasulu M, et al. Development of a weak-base docetaxel derivative that can be loaded into lipid nanoparticles. *J Control Release*. Jun 15 2010;144(3):332-340.
4. Zamboni WC, Strychor S, Joseph E, et al. Plasma, tumor, and tissue disposition of STEALTH liposomal CKD-602 (S-CKD602) and nonliposomal CKD-602 in mice bearing A375 human melanoma xenografts. *Clin Cancer Res*. Dec 1 2007;13(23):7217-7223.
5. Zamboni WC, Strychor S, Maruca L, et al. Pharmacokinetic study of pegylated liposomal CKD-602 (S-CKD602) in patients with advanced malignancies. *Clin Pharmacol Ther*. Nov 2009;86(5):519-526.
6. Ali S, Ahmad I, Peters A, et al. Hydrolyzable hydrophobic taxanes: synthesis and anti-cancer activities. *Anticancer Drugs*. Feb 2001;12(2):117-128.
7. Parness J, Kingston DG, Powell RG, Harracksingh C, Horwitz SB. Structure-activity study of cytotoxicity and microtubule assembly in vitro by taxol and related taxanes. *Biochem Biophys Res Commun*. Apr 14 1982;105(3):1082-1089.

Appendix.

SiRNA targeting using injectable nano-based delivery systems

Summary

The 2006 Nobel Prize in Physiology or Medicine was awarded to Andrew Fire and Craig Mello who demonstrated a fundamental control of gene expression called RNA interference. Since the first time siRNA was shown to knock down the expression of a target protein in mammal cells in 2001, a significant surge of interest has been focused on this promising area. This chapter will provide an overview of RNAi and siRNA, siRNA-based therapeutics, as well as review the current state-of-the-art of injectable siRNA nano-delivery systems and targeting strategies. The review will also discuss the chemical, physical, and biological barriers as well as ideal criteria for effective siRNA nano-based therapeutics.

L Feng, and RJ Mumper. “siRNA targeting using injectable nano-based delivery systems”, *Pharmaceutical Dosage Forms: Parenteral Medications*, Edited by Sandeep Nema and John D Ludwig. Vol 3: Regulations, Validation and the Future. Third Edition. Informa Healthcare. (2010) Chapter 6, 86-108.

I. Overview

1.1. RNAi Mechanisms and siRNA

Antisense is a ubiquitous and conserved phenomenon in cells. Antisense nucleotides suppress the gene expression through several distinct mechanisms, such as RNaseH-induced degradation of complementary mRNA through antisense oligonucleotides hybridizing to their target mRNA; sterical inhibition of mRNA translation or pre-translational splicing; cleavage of target mRNA by some ribozymes or deoxyribozymes due to their intrinsic catalytic activity; RNA induced silencing complex (RISC)-mediated degradation of target mRNA by double-stranded RNA (dsRNA) [1-3].

RNA interference, or RNAi is the antisense effect caused by RNA. Double-stranded RNAs (dsRNAs) are important regulators of gene expression in eukaryotic cells. Interfering dsRNAs cleave mRNA through several steps. First, the “DICER” enzyme and its co-factors cleaves dsRNA to 21-23 base-pair segments, which are called small interfering RNAs (siRNAs) and assists their loading onto the RISC. RISC removes the sense strand, uses the antisense strand as a guide to seek the complementary region in the mRNA and pairs the antisense strand to its target. RISC contains an important protein Argonaute 2 (Ago 2) which has an RNaseH-like domain carrying the activity of RNA cleavage. After cleavage, the resulting 5’ and 3’ fragments are subsequently subjected to full degradation by other nucleases [2-4]. Interfering

dsRNA can be either endogenously produced or exogenously provided. However, exogenous dsRNAs longer than 30 base pairs cause severe toxic responses in mammals which limit their applications [5]. In 2001, Elbashir and colleagues published a paper in *Nature* reporting the use of synthetic 19 base-pair duplexes siRNAs with 2 base 3' overhangs to mediate RNAi in mammalian cell culture systems [6]. Later, researchers extended this to recombinant DNA expressing similar short interfering RNA in order to have longer effect in cells. siRNA has quickly become one of the most powerful and indispensable tools in molecular biology.

1.2. Therapeutic Target and Applications

Since siRNA is a highly specific tool for target gene knockdown, it has been used in the field of molecular biology to understand gene function, as well as to identify and validate genes [7-11]. On the basis of knowledge of gene function, siRNA designed to target gene encoding disease-associated protein is currently under intensive investigation as a potent and specific therapeutic agent.

RNAi was found as an anti-viral defense in plant [12]. Thus siRNA as a treatment of human virus diseases may hold the greatest promise in the clinic. Recently, several groups have explored the therapeutic effects of RNAi on Hepatitis B virus (HBV) [13], Hepatitis C virus (HCV) [14], human immunodeficiency virus type 1 (HIV-1) [15-17], Herpes simplex virus 2 (HSV-2) [18], respiratory syncytial virus

(RSV) [19, 20], human papillomavirus (HPV) [21, 22] as well as others through inhibiting viral replication and production mechanisms. All the studies have yielded encouraging results. Another strategy is to inhibit the host proteins for pathogen invasion or signaling pathways that initiate the inflammatory response such as cell death receptor Fas [23-25] and Caspase 8 [26, 27].

A second therapeutic application for RNAi is the treatment of dominant genetic diseases. Autosomal dominant diseases caused by mutant gene encoding essential proteins can be treated by siRNA targeting the mutated alleles. Studies have demonstrated that many familial neurodegenerative diseases, such as Huntington's disease, spinobulbar muscular atrophy and slow channel congenital myasthenic syndrome (SCCMS) caused by the overexpression of mutated genes or CAG-repeat expansions that encode polyglutamine in the disease protein might be treated by siRNAs [28, 29]. Another example is the Cu, Zn superoxide dismutase (SOD1) gene in amyotrophic lateral sclerosis (ALS). Schwarz et al. reported that siRNA was specific enough to discriminate single nucleotide polymorphism. Many SOD1 mutations are single nucleotide mutations which makes siRNA a promising potential therapeutic strategy for the treatment of ALS [30].

Along with the intensive research in molecular biology on cancer, the involvement of more and more signaling pathways and oncogenic genes has been demonstrated, which in turn makes RNAi anticancer therapy possible. Oncogenic genes are often important for cell survival and growth when normally expressed and

strictly regulated. In addition, inhibitors of oncogenic proteins are not specific and often cause severe side effects. The high specificity of siRNA allows the selective knockdown of mutated oncogenes without influencing normal cells. Mutations of Ras are present in many cancers such as pancreatic cancers, colon cancers, leukemia, as well as others. In oncogenic K-RasV12, a point mutation results in a valine instead of a glycine in wild-type K-Ras. A viral siRNA transfection targeting this region strongly inhibited the expression of K-RasV12 and tumor formation in nude mice [31, 32]. Besides targeting oncogenes like Bcr-Abl [33], Bcl-2 [34], Survivin [35], some alternative strategies have also been investigated and have obtained success to some extent. Suppression of tumor angiogenesis by effectively silencing epidermal growth factor receptor gene (EGFR) and vascular endothelial growth factor receptors (VEGFR) inhibited the in-vivo growth of non-small lung cancer [36] and PC-3 prostate cancer cells [37], respectively. An RNAi approach also enhanced the effects of chemotherapy in resistant breast cancer cells due to the suppression of MDR1 [38, 39].

1.3. Delivery Barriers and Challenges

As a potential therapeutics of human diseases, siRNA needs to be efficiently delivered in-vivo. Before designing an effective delivery system for siRNA, it is crucial to understand the six main challenges and barriers of siRNA delivery.

First, siRNAs are vulnerable to nucleases in serum and tissues. Second, siRNA

would be rapidly cleared from circulation by renal excretion and reticuloendothelial system (RES) uptake especially delivered in a nanoparticulate formulation that was prone to RES uptake and elimination. Third, extravasation of siRNA across the endothelium and access to the target tissue is difficult due to its size and negative charge. Fourth, as hydrophilic, negatively charged macromolecules, siRNAs may have poor plasma membrane penetrating properties. Furthermore, if the siRNAs enter cells through endocytosis mechanism, another important barrier is endosomal escape. Eventually siRNA would end up in late endosome or lysosome and be digested if they could not be released to cytoplasm where its effect takes place. Finally, the persistence of siRNA effect is not permanent due to inability to reproduce itself.

1.4. Available Delivery Approaches

Both non-carrier and carrier strategies are available for in-vivo siRNA delivery. Aimed at overcoming individual delivery barriers, various non-carrier systems or methods have been developed. Chemical modifications have been applied to improve the nuclease stability of siRNA; for example, sulfur substitution for a non-bridging oxygen in the phosphodiester linkages [40]. Simple conjugation of siRNAs with ligands represents a large portion in this category. Cholesterol siRNA conjugation reduces renal excretion and increases circulation half-life by binding to plasma albumin. Long chain fatty acid conjugation of siRNA may facilitate the cellular uptake of siRNA

by receptor-mediated endocytosis [41]. A considerable effort has been devoted to cell penetrating peptide (CPP) conjugate investigation. These small polycationic peptides rich in arginine and lysine promote the cell penetrating of the coupled cargo, which could be siRNA or siRNA containing complexes. However, the mechanism of uptake and the delivery efficiency is still controversial. An intravenous injection of naked siRNA in massive volume through mouse tail vein has been performed to increase the transport of siRNA through capillary endothelial cells. This method is termed hydrodynamic injection and induces hepatic gene silencing [42]. Other non-carrier methods include topical application and the gene gun, among others. Generally, these methods are less efficient and/or practical than carrier strategies.

As for carrier strategies, these can be further divided into viral and non-viral carriers. To this point, viruses are still the most efficient vehicles for gene delivery. Due to their intrinsic nature and function, they can easily penetrate capillary membranes, cell membrane and even nuclear membranes to reach their destination. When the siRNA containing nucleic acid is inserted to the genetic DNA, it enables long-term expression thus has the ability to chronically suppress gene expression. However, the disadvantages are obvious and inevitable. For example, viral carriers have the difficulties of preparation and storage, immunogenicity, and potential carcinogenicity if they either suppress tumor suppressor genes or activate oncogenes. Hence, extensive attention has been attracted to the design and study of non-viral nano-scale siRNA delivery systems. Although this is a relatively novel area, a growing number of

achievements have been made in the recent years as will be discussed in detail.

1.5. Differences between siRNA and pDNA Delivery

As double-stranded nucleic acids, siRNA and double-stranded DNA (dsDNA) share many common properties. They have similar back-bone structure with the same negative charge to nucleotide ratio. They both can interact electrostatically with positively charged agents so that many delivery systems are designed based on this principle. Plasmid DNA (pDNA) has been investigated and delivered for at least two decades. Considering the similarity between siRNA and pDNA, applying the knowledge from pDNA delivery systems can facilitate rationale approaches to the delivery of siRNA. However, understanding the key differences between pDNA and siRNA is critical for designing the most efficient and safe siRNA delivery systems.

First, RNA is more sensitive to enzymatic degradation than DNA. The 5'-carbon sugar in RNA nucleotides is ribose instead of deoxyribose in DNA. This structure makes the RNA backbone more susceptible to spontaneous breakdown and hydrolysis by nucleases. Moreover, DNase and RNase are present in various environments both in-vitro and in-vivo. To avoid unexpected degradation during handling and preparation process, creating a DNase/RNase-free environment is of great importance. However, DNase inhibition can be easily achieved while RNase inhibition is much more difficult. In particular, RNase A is extremely stable in an aqueous

environment [43]. Chemical modifications have been performed to increase the stability of dsRNA, e.g. 2'-O-methyl modification, incorporation of locked nucleic acids (LNAs), phosphorothioate etc. [40]. The greater susceptibility of RNA highlights the critical need for a protective carrier to effectively deliver siRNA.

Second, the delivery destination or intracellular location needed for pDNA and siRNA action is quite different. Plasmid DNA requires delivery into the nucleus of the host cell where it can use the transcriptional machinery of the host cell to carry out its therapeutic effect. Unlike pDNA exerting its effect in the nucleus, the target of siRNA is its complementary mRNAs that has already been released from the nucleus after transcription. Therefore, siRNA only needs to be delivered to cytoplasm. For this reason, pDNA delivery often requires a nuclear localization mechanism such as the inclusion of a nuclear localization sequence or carriers that can carry their cargo to nucleus.

Third, due to their different action mechanisms, the duration of siRNA and pDNA effects differs as well. Naked siRNAs, unlike pDNA-expressed siRNAs, are not regenerated in cells. Thus, in rapidly dividing cells, the typical gene silencing duration is 3-7 days because of the dilution of the siRNAs below a certain level. In contrast, in slowly or non-dividing cells, the gene knockdown effect can last as long as 3 weeks depending on the stability and half-life of the suppressed protein [44]. The therapeutic effects with pDNAs not only depend on their own stability, but also the strength of their promoters if they are non-integrative. In comparison, it is well known that the

therapeutic effects of integrated DNA vectors could be long-term or even permanent. Hence, the contrast between the pDNA and siRNA requirements above highlight the fact that successful siRNA therapy will necessitate repeated treatment which makes selection of the carrier with low cytotoxicity and immunogenicity even more important for siRNA.

Another obvious difference between pDNA and siRNA is the molecular weight and size of the molecules. The pDNAs used in gene therapy are usually several kilobase pairs while siRNAs are only 21-23 bp. In pDNA delivery, it is often complexed and condensed to nanometric-sized particles directly with cationic agents. However, it is well known that many types of cationic condensing agents (polymers, lipids, etc.) often times lead to aggregation of the condensed particles. Due to its smaller size, siRNA is perhaps easier to complex with cationic condensing agents. However, these complexes with siRNA are often unstable and decomplex since the smaller siRNA is not condensed and the ionic interaction is much easier to compete off with counter-ions. RNA is somewhat stiffer than DNA. The persistence length, which is a basic mechanical property quantifying the stiffness of a long chain molecule, of dsDNA is 450-500 Å and that of double-stranded RNA is ~700 Å [45]. At 2.7 Å per base pair, the persistence length for RNA is 260 bp. So basically, 21-23 bp siRNA behaves as a rod and is not likely to be further condensed. Therefore, electrostatic interaction between siRNA and cationic agents could lead to a relatively uncontrolled interaction and forming complexes of large sizes and poor stability, and as a consequence incomplete

encapsulation [46].

Considering the differences discussed above, the strategy for the delivery of pDNA and siRNA should be interrogated carefully. One should not assume that a delivery system that works for pDNA could be simply transferred to siRNA delivery system before more thorough investigation is performed.

II. Ideal injectable nano-based systems for siRNA delivery

For an ideal injectable nano-based delivery system to efficiently deliver siRNA, no matter it is for topical or systemic administration, certain criteria must be met. For systemic injection of siRNA, additional criteria need to be considered.

Generally speaking, at the cellular level, a successful delivery vehicle must be formulated to have the following characteristics: (1) provide protection to siRNA against degradation in extracellular fluids; (2) facilitate efficient cellular uptake; (3) facilitate endosomal escape before the early endosome becomes late endosome or lysosomes in which the siRNA will be destroyed; (4) be able to readily release siRNA upon arrival at the cytosol where the RNAi effect takes place; (5) non-toxic to the cells; (6) be stable during storage and in the vehicle for administration solution i.e., chemically and physically stable.

For a systemically administered siRNA nano-carrier, there are some additional concerns: (1) provide protection to siRNA against degradation not only in the

extracellular fluids but also in the systemic circulation; (2) be stable in the systemic circulation with limited break-down and/or aggregation before it arrives at the target site; (3) be able to extravasate blood vessels and penetrate tissues to gain access to the target site; (4) maintain proper particle size and surface properties to avoid clearance and/or elimination via the kidneys and RES.

To further increase the efficiency of in-vivo siRNA delivery, target strategies are widely applied. As for targeted systemic nano-carrier, choosing a suitable target ligand is critical as well. First of all, the targeting should be specific enough, i.e. the expression of the receptor on the target cells should be highly specific, highly expressed, and not shed, among others. Second, the targeting ligand should have high affinity with the target receptor to ensure sufficient retention time as well as trigger cellular uptake via receptor mediated endocytosis instead of remaining bound to the receptor. Last but not least, the targeting ligand should be amenable to the required chemistries needed to attach the ligand to the nano-carrier, as well as have low or no immunogenicity.

III. Nano-based delivery systems

3.1. Complexes

RNA is a molecule consisting of a chain of nucleotide units. Each nucleotide is composed of a nitrogenous base, a ribose sugar, and a phosphate. RNA is a negatively-charged molecule due to the negative charge on phosphate groups at

physiological pH. siRNA molecules are double stranded RNA with 19-21 base pairs. Calculating the charge density gives about 3 negative charges per kilo-dalton (kD) molecular weight of siRNA.

To date, complexes of siRNA with various positively charged materials by electrostatic interaction represent the largest portion of active research. In this category, there are two major subgroups and some others.

3.1.1. Lipoplex

The most often referenced formulation in this group is cationic liposomes. When cationic liposomes are mixed with negatively charged siRNA, the organized bilayer structure of the liposome is altered by electrostatic interaction so that they are no longer referred to as liposomes, but have a new name of “lipoplexes”.

The DOTAP Liposomal Transfection Reagent is a commercially available liposome formulation of the monocationic lipid 1,2-Dioleoyl-3-Trimethylammonium-Propane (DOTAP) that can be used for the transfection of nucleic acids. Mixing the DOTAP reagent with the negatively charged siRNA results in a spontaneously formed stable complex that can be directly added to the tissue culture medium with or without serum. Commercially available DOTAP is not only used as an instrumental tool for in-vitro siRNA delivery to investigate gene functions in molecular biology, it has been used to deliver siRNA in mice to prove the

concept and feasibility of certain therapeutic ideas [47-50].

Dioleoyl-phosphatidylethanolamine (DOPE) is a neutral helper lipid usually used with DOTAP to formulate transfection reagent. It is generally believed that DOPE enhances transfection due to its tendency to form hexagonal phase structures at temperatures above 10°C which facilitates siRNA endosomal escape [51].

Based on this classical liposome formulation, targeting ligands have been included to deliver siRNA to specific tissues. For example, Chang et al. developed a tumor targeting immunoliposome that takes advantage of elevated transferrin receptor (TfR) levels on tumor cells to deliver pDNA, antisense oligonucleotides, imaging agent or siRNA [52-54]. The anti-transferrin receptor single-chain antibody fragment was incorporated into the liposomes and formed immunoliposomes. This intravenously administered immunoliposome delivered its cargo (which could be pDNA, antisense oligonucleotides, imaging agent or siRNA) specifically and efficiently to primary/metastatic tumors. In addition, a pH-sensitive histidine-lysine peptide (HoKC) was included in the complex to further increase the endosomal escape. In a recent report, the results showed increased potency of the liposome-HoKC complex and their ability of carrying anti-HER2 siRNA to target and sensitize tumor cells, silencing the target gene, and inhibiting tumor growth in-vivo [55]. Lima et al. associated transferrin instead of the TfR antibody to DOTAP/cholesterol liposome, another conventional cationic liposome, to target TfR expressing cells [56]. In-vitro experiments by the group showed enhanced gene knockdown activity of transferrin-associated liposome

compared to the conventional liposomes by anti-GFP siRNA. Besides tumor targeting, siRNA liposomes are targeted to other tissues and organs such as the liver. Kim and his colleagues formulated anti-HBV siRNA into a complex of DOTAP/Chol liposome and apolipoprotein A-I (apo A-I) [57]. Apolipoprotein is recognized by class B, type 1 scavenger receptor (SR-BI) which is predominantly expressed in the liver. When the liver-targeting formulation was injected intravenously into a HBV carrying mouse model, the viral protein expression was reduced to about 30% and its effect lasted up to 8 days upon a single treatment.

In addition to the commercially available lipids, some cationic lipids are also designed and synthesized to improve the transfection efficiency and reduce the cytotoxicity. It has been reported that an ether linkage containing cationic lipid, such as 1,2-dioleoyloxypropyl-3-trimethylammonium chloride (DOTMA), has higher in-vivo transfection efficiency than the corresponding ester analogue DOTAP [58]. Based on the structure-activity information, Chien et al. synthesized ether-linked cationic cardiolipin analogue (CCLA) where the phosphate groups of cardiolipin were replaced with quaternary ammonium groups as shown in Figure A.3 (a) [59].

Their report showed that the transfection efficiency of the luciferase reporter gene in mice was seven-fold higher than the commercially available DOTAP-based liposome and the CCLA-based liposome had lower toxicity than DOTAP transfection reagent. When the CCLA-based liposome was used to deliver the c-raf siRNA in mice bearing human breast cancer (MDA-MB-231) xenografts, the tumor growth was

inhibited 73% as compared to free siRNA treatment. For the same reason, many groups synthesized other cationic lipids to meet the needs of in-vitro and in-vivo delivery such as cationic cholesterol-based polyamine lipid N'-cholesteryloxycarbonyl-3,7-diazanonane-1,9-diamine (CDAN) [46], 2- (3- [bis- (3-amino- propyl)- amino]- propylamino)- N- ditetradecylcarbamoylethyl- acetamide (RPR209120) [60], MVL5 [61]. Their structures are shown in Figure A.3 (b-d). Positive charges could also be incorporated by adding aminoglycoside to the lipid. Desigaux et al. synthesized a series of cationic lipids (DOST, DOSK, DOSP, DOSN) bearing various aminoglycosides (tobramycin, kanamycinA, paromomycin and ethylthioneomycin B, respectively) linked to two dioleoyl chains by a succinyl spacer for specific interaction with siRNA [62].

Besides lipid-aided cellular delivery, some positively charged cell penetrating peptides (CPP) have been incorporated into conventional liposomes. In a study by Mudhakar et al., liposomes composed of egg phosphatidylcholine (EPC) and cholesterol were modified by direct conjugation of a novel peptide IRQRRRR (IRQ) to the surface of liposomes [63]. IRQ is a peptide ligand that targets skeletal muscle found by in-vivo phage display. Since the novel peptide IRQ is rich in arginine, it not only serves as a tissue-target moiety, but also triggers the cellular uptake via caveolar endocytosis.

An interesting concept called site-specific release is applied to liposomal siRNA targeting delivery as well. It is well known that under pathological conditions the

expressions of many proteins are altered including intracellular receptors and enzymes, as well as others. Most of the recent studies have focused on targeting modified receptors using either an antibody or a small molecular receptor substrate. However, changed expression of enzymes in the pathological tissue could also serve as a novel target by triggering site-specific release of therapeutic agent. For example, sPLA₂ is an enzyme upregulated in cancer and inflammatory tissues, but it is present at low levels in the blood circulation. Foged et al. formulated a liposome including lipid dipalmitoylphosphatidylglycerol (DPPG), which is favored by Human group IIA sPLA₂. They hypothesized that the liposome could site-specifically release siRNA in inflammatory tissue but not in the systemic circulation or other tissues [64]. Moreover, the hydrolysis products were thought to disturb the cellular membrane and facilitate the uptake of siRNA. Although their data showed that the sPLA₂ degradable liposomes did not silence EGFP expression in HeLa cells, they did show that the siRNA from the liposomal formulation was taken up by HeLa cells and that uptake was augmented by the addition of sPLA₂. The concept of site-specific release with no active targeting moieties opens an alternative avenue and deserves more attention.

3.1.2. Polyplex

Polymers, either natural or synthetic, represent another major group of complexing agents for siRNA delivery. The formulation of nucleic acids complexed

with polymers is generally called “polyplex” in this chapter even though in various literatures they are sometimes referred to as nanoparticles or micelles.

Cationic polymers, e.g. polyethylenimine (PEI), polypropylenimine (PPI), poly-L-lysine (PLL), polyallylamine (PAA), cationic dextran and chitosan are the most commonly used materials for siRNA complexation. Among them, PEI is the most widely used polymer for complexing with siRNA.

The native branched PEI (25 kDa) is a prototype polymeric transfection agent that has gained widespread use. Branched PEI contains primary, secondary and tertiary amines in the molar ratio of 1:2:1. The primary amines are mainly responsible for nucleic acid condensation while the secondary and tertiary amines provide buffering capacity and therefore facilitate endosomal escape via the so-called “proton sponge” effect. The transfection efficiency of PEI, along with its cytotoxicity, strongly depends on its molecular weight. Usually, high molecular weight PEI has higher transfection efficiency but with higher toxicity as well, while low molecular weight PEI has lower cytotoxicity with reduced transfection efficiency. To enhance the gene delivery efficiency and minimize cytotoxicity of PEI, there has been a great deal of effort focused on structurally modifying PEI. For example, Hua et al. cross-linked low molecular weight 800 Da PEI with short diacrylate linkages to form higher molecular weight PEI structures [65]. The modification combines the favorable low toxicity of low molecular weight PEI with the higher transfection efficiency of high molecular weight PEI. The biodegradable ester bonds are hydrolyzed under physiological

conditions within the cell after delivery and convert the cross-linked high molecular weight PEI into low toxic low molecular weight PEI. In a study of pDNA transfection, an optimal cross-linked PEI, EGDMA-PEI 800-4h (the product of conjugation of amino groups of 800-Da PEI to EGDMA for 4 h), resulted in a 9-fold increase in gene delivery efficiency in B16F10 cells and a 16-fold increase in 293T cells compared to commercially available 25 kDa PEI control. Later the modified PEI was used to deliver plasmid-encoded focal adhesion kinase-1 (FAK) siRNA in-vivo and prolonged the survival of the tumor-bearing mice [66]. To address the associated cytotoxicity with the use of PEI for siRNA delivery, Swami et al. cross-linked PEI with 1,4-butanediol diglycidyl ether (bisepoxide) [67]. The modification converted primary amines, which are believed to be the main source of cytotoxicity to secondary and secondary to tertiary amines. The system was found to deliver siRNA more efficiently into HEK cells as compared to native PEI 25 kDa with significantly reduced cytotoxicity.

Jere et al. conjugated low molecular weight PEI and PEG with biodegradable poly (β -amino ester) (PAE) [68]. The high repetitive PEI units are thought to result in high delivery efficiency while PEG units and the ester linkage facilitate more rapid intracellular siRNA release and lead to enhanced polymer degradation resulting in lower cytotoxicity. As a result, PAE as a carrier was found to be less toxic and 1.5-fold more effective than standard PEI 25 kDa. Several other PEI modifications have been investigated by Wagner et al. [69]. The groups performed a number of modifications including ethyl acrylate, acetylation of primary amines, or introduction of negatively

charged propionic acid or succinic acid groups to the PEI structure. All the conjugates led to reduced toxicity in comparison to the unmodified PEI. In particular, succinylation of PEI resulted in up to 10-fold lower toxicity in Neuro2A cells.

In order to facilitate release of siRNA in the cell, branches of PEI have been derivatized with ketal linkages [70]. Ketal linkages are acid-degradable under mild acidic pHs (e.g., pH 5.0) and facilitate the release of siRNA in the endosomal environment as shown in Figure A.4. The ketalized PEI complexed with siRNA into siRNA/PEI polyplexes with a particle size range of 80-200 nm showed enhanced delivery efficiency with reduced cytotoxicity.

One of the primary disadvantages of the use of positively-charged complexing agents is that they are prone to aggregation or disassociation in the blood when complexed to siRNA. Moreover, positively-charged complexing agents tend to interact with the negatively-charged proteins in the systemic circulation and are taken up by the RES system. To address this potential problem, PEG has been utilized to shield the surface of the complex which serves to provide enhanced stability. PEG has either been conjugated directly to siRNA or to the cationic polymer. For example, Kim et al. conjugated PEG to siRNA via a disulfide linkage which could then be cleaved in the reductive environment in endosomes and cytoplasm. The PEG-siRNA conjugate was then complexed with PEI to form a nanoparticle [71]. The resulting nanoparticle has an inner core comprised of siRNA/PEI surrounded by a hydrophilic PEG shell. This kind of structure is similar to amphiphilic lipidic micelle and could be spontaneously formed,

so it is called a self-assembled micelle even though the particle size is often not in the traditional micellar range. In-vivo imaging results from Kim et al. showed enhanced accumulation of micelles in the tumor region following intravenous injection. PEGylated siRNA has also been complexed with other cationic polymers such as poly-L-lysine (PLL) [72].

PEG has also been conjugated to the cationic polymer. For example, PEG derivatized diblock or triblock copolymers have been designed and synthesized by many groups. A recent publication reported the synthesis of a triblock polymer consisting of monomethoxy poly(ethylene glycol) (PEG), poly(3-caprolactone) (PCL) and poly(2-aminoethyl ethylene phosphate) (PPEEA) (Figure A.5) [73]. The polymers in an aqueous solution spontaneously formed positively charged micelles surrounded by PEG corona. siRNA was post-loaded into the formed micelles resulting in complexes with an average particle size from 98 to 125 nm depending on the nitrogen to phosphate (N/P) ratio.

Besides the linear copolymers, cationic graft comb-like copolymers were synthesized and used to deliver siRNA. Sato et al. prepared and evaluated a series of cationic comb-type copolymers (CCCs) consisting of a PLL backbone and PEG or dextran side chains [74]. The water soluble dextran side chains of the copolymer are in abundance (more than 70 wt. %) and the highly dense PEG brush reinforced the electronic interaction between copolymers and siRNA instead of hindering it. The most remarkable property of the CCC with higher side chain content (10 wt.% PLL and 90%

wt.% PEG) is that it increased circulation time of siRNA in mouse bloodstream by 100-fold [74]. Interestingly, even when the CCC was injected into mouse intravenously 20 min prior to the injection of siRNA, the CCC still increased the half-life of the post-injected siRNA by more than 60-fold suggesting that the CCC prefers interaction with siRNA to other anions existing in blood.

While some investigators increase the stability and systemic half-life of siRNA polyplexes by incorporating PEG, others provide protection to the polycation/siRNA complex with another layer of lipid coating. Kim et al. synthesized a water soluble lipopolymer (WSLP) by conjugating cholesteryl chloroformate to PEI 1.8 kDa through a hydrophobic lipid anchor [75]. The lipopolymer combined the advantages of both liposomes and cationic PEI. While the positively charged head group PEI complexed with siRNA and enhanced endosomal escape, the lipid coating on the complex further protected the complex from aggregation and RES clearance and increased the cell membrane permeability. The in-vivo data showed that WSLP/VEGF siRNA complexes reduced tumor volume by 55% at 21 days and by 65% at 28 days relative to control tumors.

While most of the approaches discussed so far increase the transfection efficiency of PEI by reducing its cytotoxicity or provide protection against systemic clearance to some extent, a novel approach is to directly attaching PEI with a membrane active peptide. Melittin (Mel) is the major bioactive component of the bee venom. Mel has been conjugated to PEGylated PEI or PLL [76]. To avoid its extracellular lytic

activity, the amines of Mel were modified with dimethylmaleic anhydride which was cleaved under acidic pH in the endosome and enhanced the endosomolytic activity of Mel. PEG-PEI-Mel and PEG-PLL-Mel showed 70% and more than 90% in-vitro luciferase gene knockdown, respectively.

To achieve targeted delivery, targeting moieties have been attached to PEI. PEI is usually PEGylated with ligands conjugated to the distal end of the PEG, while direct attachment of ligands to PEI is performed as well. Schiffelers et al. targeted tumor neovasculature expressing integrins by conjugating an Arg-Gly-Asp (RGD) peptide to 25 kDa PEI [77]. siRNA specific to vascular endothelial growth factor receptor-2 (VEGF R2) was complexed with the modified PEI at a N/P ratio of 2 to 6, resulting in the formation of polyplexes with average particle size of about 100 nm. The intravenous administration of these polyplexes to nude mice showed tissue-specific accumulation of PEI-PEG-RDG/siRNA. Related, Kim et al. utilized a similar approach to complex siRNA with PEI-PEG-folate [78]. Interestingly, their results showed that the delivery of siRNA led to the most pronounced gene silencing effect compared to the delivery of antisense oligodeoxynucleotide (AS-ODN) or siRNA expressing plasmid DNA. Another recently published paper reported on the using of hyaluronic acid (HA) as a ligand to target lymphatic vessel endothelial hyaluronan receptor-1 (LYVE-1) [79]. In-vitro data showed that increased siRNA uptake in HA receptor expressing cells but not in non-expressing cells, and that the gene silencing effect was inhibited by free HA in a concentration-dependent manner.

Compared to the relatively extensive investigation of PEIs and PLLs for siRNA delivery to date, studies on the use of other polymers is limited. Chitosan is one polymer being investigated for siRNA delivery. Although chitosan has been studied for more than a decade as delivery system for pDNA, there are only few studies using it as a carrier of siRNA. Chitosan is a copolymer of N-acetyl-D-glucosamine (GlcNAc) and D-glucosamine (GlcN) produced by the alkaline deacetylation of chitin. As a natural polymer, chitosan is considered to be biocompatible and non-toxic, although this depends on various physical-chemical properties such as purity, % deacetylation, and Mw, among others. The primary amines in the chitosan backbone become positively charged at the pH levels below the pKa of the primary amine (pKa 6.5) so that chitosan forms complex with siRNA with electrostatic interaction. Several studies of chitosan/siRNA complex have shown that the ability of the chitosan to deliver siRNA to cells is dependent on the weight ratio, Mw of chitosan, and the degree of deacetylation [80-83]. Similar to other complexes, chitosan/siRNA complexes can be formed by simple mixing and stirring process. Different from other synthetic polymers, the N/P ratios to prepare chitosan/siRNA are much higher. For example, Kjemis et al. used N/P ratio as high as 285, however, these high ratios reduced cell viability [80]. The in-vitro data showed that chitosan/siRNA complexes formed using high Mw (114 and 170 kDa) and deacetylation degree (84%) at N/P 150 were most stable with particle size about 200 nm [81]. The group showed that 80% enhanced green fluorescent protein (EGFP) gene silencing efficiency was obtained after 24 h in H1299 green cells in-vitro.

Effective in-vivo gene silencing was achieved in mice bronchiole epithelial cells (37% and 43% reduction of EGFP positive cells compared to scramble siRNA and untreated control, respectively) after nasal administration. However, the ability of the complexes to deliver siRNA systemically requires further investigation.

Thiamine pyrophosphate (TPP) has been used to form salts with chitosan to improve chitosan water solubility [83]. Chitosan is a weak base with pKa value of 6.2-7.0, thus of poor solubility at neutral to alkaline pH. TPP is a zwitterionic compound, which can increase the water solubility of chitosan due to the phosphate groups. On the other hand, the amine groups of TPP together with chitosan bind to negatively charged siRNAs to form complexes. The maximal EGFP gene silencing effect mediated by chitosan-TPP/siRNA was 70-73%. Another study by Katas et al. used sodium tripolyphosphate to ionically cross-link chitosan to form nanoparticles [82]. siRNA was either mixed with sodium tripolyphosphate, and then dripped into a chitosan salt solution, or adsorbed to preformed chitosan/tripolyphosphate particles. The particle size of chitosan/tripolyphosphate was 510 ± 22.9 nm and 276 ± 17.9 nm formed using chitosan glutamate 470 kDa and 160 kDa, respectively. The particle size of chitosan/tripolyphosphate was 709 ± 50.3 nm and 415 ± 44.6 nm formed using chitosan hydrochloride 270 kDa and 110 kDa, respectively.

Mixson et al. synthesized several branched peptide polymers composed of histidine and lysine (HK polymer) [84]. Figure A.6 shows the structure of a branched HK polymer with eight terminal branches and histidine-rich domains (H³K8b). An

integrin-binding ligand RGD was further added to increase the delivery efficiency of siRNA. Although the sizes of HK polymer/siRNA polyplexes were over 400 nm, the in-vitro delivery efficiency was significant. The complex of H³K8b and anti- β -galactosidase (β -gal) siRNA inhibited β -gal expression by more than 80% after 48 h in SVR-bag4 cells that stably expressed β -gal. The H³K8b/anti-luciferase siRNA complex inhibited more than 90% luciferase activity in MDA-MB-435 cells which were cotransfected with a luciferase expression plasmid.

3.1.3. Others

In addition to the two larger families of cationic complexing reagents, lipids and polymers, there are several other molecules that have been proposed to make nano-based siRNA delivery systems.

Positively charged natural proteins are a pool of convenient reagents in terms of their potential to complex and deliver siRNA. In a broad sense, protein is also a group of polymers. To date, atelocollagen is the only protein used alone to delivery siRNA both in-vitro and in-vivo [85]. Atelocollagen is a highly purified decomposition product of type I collagen derived from dermis of cattle with a molecular weight of 300 kDa. The amino acid sequence at both N- and C-terminal of a collagen called telopeptide is the main source of the immunogenicity. Therefore, atelocollagen lack of telopeptides, obtained by pepsin treatment, is low in immunogenicity. It is a rod-like molecule with a

length of 300 nm and a diameter of 1.5 nm. Atelocollagen, which is positively charged, interacts with the negatively charged siRNA to form an atelocollagen/siRNA complex with a diameter of 100-300 nm. An interesting property of atelocollagen is that it is soluble at a lower temperature but solidifies at a temperature over 30°C. Therefore, the atelocollagen/siRNA complexes were prepared and stored at 4°C. Once introduced into animals, the complex becomes solidified and releases siRNA in a controlled manner for a period of time due to the biodegradable nature of atelocollagen. Direct intratumoral injection of human HST-1/FGF-4 (fibroblast growth factor) siRNA complexed with atelocollagen resulting in about 12-fold and 8-fold tumor growth inhibition compared to atelocollagen alone and control siRNA, respectively, in an orthotopic xenograft of a human non-seminomatous germ cell tumor at 21 days after treatment.

Based on the barriers that must be overcome to deliver siRNA, some innovative carriers have been synthesized to fulfill multiple functions in one system. 1,4,7-triazanonylimino-bis [N-(oleic-yl-cysteinyl-histinyl)-1-aminoethyl] propionamide] (THCO) (Figure A.7) and (1-aminoethyl) imino-bis [N-(oleic-yl-cysteinyl-histinyl)-1-aminoethyl]propionamide] (EHCO) are two molecules containing a protonatable amines head group of different pK_as, two cysteine residues and two 8-heptadecenyl tails [86, 87]. They form stable complexes with siRNA through charge and hydrophobic interaction. The protonatable amino head group consists of primary, secondary and tertiary amines having different pK_as (the pK_a values of primary, secondary and tertiary amines are approximately 6.5, 7.0 and 6.0, respectively),

which is similar to branched PEI. Thus, these molecules not only complex siRNA, but also facilitate endosomal escape. The dithiol groups in the molecules can be polymerized by forming disulfide bonds to further provide stability to the formed siRNA complex. The disulfide bonds may be reduced in the endosome and cytoplasm resulting in the dissociation and release of siRNA. The multifunctional compounds mediated 40-88% silencing of luciferase expression with 100 nM siRNA in U87-luc cells.

Additionally, there are some interesting carriers that are quite unique in terms of geometry and other physical-chemical properties. For example, a cone-shaped macrocyclic octaamine as shown in Figure A.8 has been proposed by Aoyama et al. [88]. The novel carrier has four long alkyl chains and eight amino groups on the opposite side of the calix[4]resorcarene macrocycle. What makes the macrocyclic octaamine different from other cationic lipids or polymers is that being a small and single molecule (Mw 1740), the compound unimolecularly presents a positive charge cluster motif with a well-defined geometry. Like amphiphilic micelle-forming polymers, the macrocyclic octaamine itself may form small micelle-like particles, with hydrophilic amino groups outside and lipophilic chain inside as illustrated in Figure A.8. As a result, the cone-shaped macrocyclic octaamine formed complexes with siRNA in compact size of ~10 nm. Although the in-vitro delivery of macrocyclic octaamine/siRNA complex occurred with 90-95% knockdown of luciferase expression in HeLa, HepG2 and HEK293 cells at 48 h, its in-vivo performance remains to be

investigated.

The KALA peptide (WEAK LAKA LAKA LAKH LAKA LAKA LKAC EA) is a well-known cationic, amphiphilic and fusogenic peptide, which has been popularly studied as an endosomal escaping peptide complexing with various nucleic acids. However, it was reported that KALA/siRNA complexes did not show sufficient gene silencing effect in the presence of serum proteins. In a recent study, two cysteine residuals were added to both terminals of KALA [89]. The cysteine-KALA-cysteine peptide (CWEAK LAKA LAKA LAKH LAKA LAKA LKAC) self-crosslinked through reducible di-sulfide linkage. The crosslinked KALA (cl-KALA) formed more stable and compact complexes with siRNA. To further improve the colloidal stability, siRNA was modified with PEG. According to a previous report of the same group, direct PEG conjugation to siRNA could form more stable complexes than those by PEG modified cationic polymers [71]. Although cl-KALA/siRNA and cl-KALA/siRNA-PEG only showed 23.6% and 47% knockdown of GFP expression in MDA-MB-435-GFP cells at the N/P ratio of 64, the data showed their potential as a nano-based delivery system for siRNA.

3.2. Nanoparticles

In a broad sense, all particles in the nano-scale range are called nanoparticles. However, in this chapter, nanoparticles are differentiated from nanocomplexes by their

more organized structures, i.e., well defined shell and core structures.

Huang et al. has developed a targeted nanoparticle formulation for siRNA systemic delivery to metastatic tumors overexpressing the sigma receptor [90, 91]. The core of the nanoparticle is a complex of siRNA, calf thymus DNA and protamine, a highly positively charged peptide. The shell of the nanoparticle is a reorganized liposome structure consisting of DOTAP and cholesterol (1:1 molar ratio) (Figure A.9). Thus, the nanoparticle is referred to as “LPD”, or Liposome-Polycation-DNA. The nanoparticles are formed spontaneously by mixing the core complexes with pre-formed cationic liposomes. To create a sterically-stabilized particle and for subsequent targeting, DSPE-PEG₂₀₀₀ (1,2- distearoyl-sn- glycerol-3- phosphoethanolamine-N-[methoxy(polyethylene glycol)₂₀₀₀]) or DSPE-PEG-anisamide was post-inserted into the preformed LPD. The in-vitro results showed that the delivery efficiency of the targeted nanoparticles was 4-7-fold higher than the non-targeted nanoparticles. The in-vivo tissue distribution results suggested that LPD surface-modified by PEG delivered a therapeutic dose to the tumor and avoided substantial accumulation in the liver with either targeted or untargeted LPD. These results suggest that the tumor accumulation of LPD with particle size around 100 nm is primarily due to the EPR (enhanced permeability and retention) effect as compared to targeting. After a single i.v. injection of 150 µg/kg anti-luciferase siRNA, 70-80% luciferase activity was silenced in a metastatic mouse tumor model. To avoid potential immunogenicity and inflammatory responses with calf thymus DNA, the calf thymus DNA has also been

replaced with hyaluronic acid to produce LPH (Liposome-Polycation-Hyaluronic acid) nanoparticles [92]. The results showed that while the gene silencing effect of LPH nanoparticles is comparable to LPD nanoparticles, the immunotoxicity of LPH is much lower.

A similar structure to LPH has also been reported by Peer et al. to develop leukocyte-directed nanoparticles to deliver anti-Cyclin D1 siRNA [93]. The pre-formed liposome is composed of phosphatidylcholine (PC), dipalmitoylphosphatidylethanolamine (DPPE), and cholesterol (Chol). High molecular weight hyaluronan (850 kDa), was attached to the outer surface of the liposomes by covalent linkage to DPPE to provide steric stabilization. The resulting nanoparticles were equipped with targeting function through covalently conjugating to the hyaluronan a monoclonal antibody FIB504 against $\beta 7$ integrins which are highly expressed in gut mononuclear leukocytes. Anti-Cyclin D1 siRNA loaded nanoparticles were formed by rehydrating lyophilized liposomes with water containing protamine-condensed siRNA. In an experimentally induced colitis mouse model, the $\beta 7$ integrins targeted nanoparticles knocked down the Cyclin D1 expression to the normal level and ameliorated the colitis score.

An organic-inorganic hybrid nanoparticle was developed by Kataoka et al. [94, 95]. The organic-inorganic shell-core structure is a core composed of nanocrystals of siRNA/CaP (calcium phosphate) complexes surrounded by a hydrophilic shell of a PEG-PAA block copolymer (polyethylene glycol-aspartic acid). Due to its potential

biocompatibility, CaP is widely applied in various biomedical applications. Its binding affinity to a variety of molecules including proteins, nucleic acid and small molecule drugs makes it a potential controlled release material. However, one of the difficulties in using CaP to form nanoparticles is the relatively rapid crystallization rate of CaP. In the absence of other materials, the growth of siRNA/CaP complex crystals is rapid and precipitates are formed within minutes after mixing siRNA and CaP solutions. However, in the presence of a PEG-polycarboxylate block copolymer, such as PEG-PAA, the rapid crystal growth is controlled or even prevented through the absorption of the PAA segment of PEG-PAA on the formed crystal surface. The resulting complex nanoparticles have diameters ranging from 100 to 300 nm depending on the PEG-PAA and CaP concentrations. Moreover, the CaP core dissociates in the intracellular environment with lower calcium concentration as compared to the extracellular fluids, allowing the controlled release of siRNA from the core matrix. However, since the complex nanoparticles lack the ability to escape the endosomes, in-vitro gene knockdown experiments are performed by pretreatment of the cells with chloroquine, a well known adjuvant to provide endosomal escape. Although the in-vitro luciferase expression was silenced by the siRNA/CaP/PEG-PAA nanoparticles to about 40% in 293 cells, the requirement of chloroquine makes this formulation less practical for siRNA delivery. To facilitate endosomal escape provided by the nanoparticle itself, PAA was replaced with polymethacrylic acid (PMA), another polyanion that undergoes a conformational change at pH 4-6 to expose a more hydrophobic structure that is able

to interact with the endosomal membrane and disturb its structure. As a result, the luciferase activity was inhibited to 20% in 293 cells using as low of a siRNA concentration of 25 nM without the use of chloroquine.

Davis et al. designed a modular-delivery vehicle that utilizes an inclusion complex for targeted delivery of siRNA [96]. The inclusion complex was comprised of siRNA and a synthesized cyclodextrin-containing polycation (CDP) that provided two functions. One, the polycation contains 2 mol of positive charge per CDP monomer, which complexes with negatively charged siRNA and self assembles to nanoparticles. Two, the cyclodextrin motifs on the surface of the nanoparticle serve as a “loading dock” to incorporate PEGs and target ligands. PEG molecules containing adamantane (AD) on the proximal end and either methoxy (AD-PEG) or a targeting ligand such as transferrin (AD-PEG-Tf) on the distal end was mixed with CDP at a 1:1 AD-PEG/ β -CD (mol/mol) ratio in water. AD-PEG or AD-PEG-Tf was attached to the polymer via inclusion complex formation between adamantane and the β -CD motifs on the polycation backbone. A calculation of the stoichiometry of each particle estimated that a 70 nm particle contained about 2000 siRNA molecules and around 100 AD-PEG-Tf molecules. Thus, each CDP nanoparticle could theoretically deliver a large payload of siRNA with a large ratio of siRNA to targeting ligand (20:1). The functional efficiency of CDP nanoparticles was demonstrated through knockdown of luciferase reporter protein expression. HeLa cells treated with CDP nanoparticles containing both pGL-3 plasmid DNA expressing firefly luciferase and siRNA against luciferase showed 50%

lower expression of luciferase than cells that received either the plasmid alone or the plasmid plus control siRNA.

While most of the nanoparticle designs tend to entrap or hide siRNA in the nanoparticle core thus providing siRNA protection against degradation, a few groups have attempted to adsorb siRNA on the surface of solid nanoparticles. For example, Kim et al. developed cationic solid lipid nanoparticles consisting of natural components of protein-free low-density lipoprotein (LDL) to deliver siRNA [97]. LDLs are natural nano-carriers abundant in the bloodstream, transporting lipids, cholesterol, proteins and hydrophobic drugs throughout systemic circulation. Solid lipid nanoparticles, mimicking natural LDL, have been shown to be very stable and behave similarly to native LDL when injected into the bloodstream. The solid lipid nanoparticles were comprised of 45% (w/w) cholesteryl ester, 3% (w/w) triglyceride, 10% (w/w) cholesterol, 14% (w/w) DOPE, and 28% (w/w) 3 β -[N-(N', N'- dimethylaminoethane)-carbamoyl]- cholesterol (DC-chol). The function of the cationic DC-chol was to make the surface of the nanoparticles positively-charged with a zeta potential of about +40 mV. siRNA was conjugated to PEG via a disulfide linkage and anchored onto the surface of cationic solid lipid nanoparticles through charge interaction. Under an optimal weight ratio of DC-chol and siRNA-PEG conjugate, the LDL-like nanoparticles silenced the expression of green fluorescent protein (GFP) and VEGF to 40% and showed much less cytotoxicity than PEI 25k in MDAMB435 cells. Although work with the LDP-like particles has only progressed to in-vitro studies, it is expected

that the LDL-like nanoparticle may be useful for in-vivo tumor targeting delivery of siRNA since elevated levels of low density lipoprotein receptor (LDLR) are reported in various cancer cells such as myeloid leukemic cells, colon, kidney, and brain tumor cells.

Finally, like DOTAP liposomes, nanoparticles for nucleic acid delivery including siRNA are also patented and commercially available for the purpose of scientific research. Bioalliance (Paris, France) patented a chitosan-coated poly-isohexylcyanoacrylate (PIHCA) nanoparticle in 2004. The nanoparticle was directly utilized by Pille et al. to deliver anti-RhoA (Ras homologous A) siRNA in mice and to prove the therapeutic potential of the strategy to treat aggressive breast cancers [98].

3.3. Nanocapsules

Nanocapsules are structurally similar to nanoparticles except for having a liquid-filled core instead of a solid core. To date, there are just a few publications on the use of nanocapsules as siRNA delivery carriers. The following will discuss two such nanocapsules that have novel properties as potential siRNA delivery systems.

Ideally, to entrap siRNA in the internal core of a nanocapsule, the core should be aqueous to accommodate the hydrophilic siRNA. The preparation of nanocapsules usually involves the preparation of an emulsion. An oil-in-water emulsion is unable to

encapsulate the hydrophilic siRNA alone. In addition, a water-in-oil emulsion leads to nanocapsules suspended in an oil phase which may not be desirable for intravenous administration or would have to be removed prior to injection. To facilitate the formulation of siRNA in a nanocapsule, Couvreur et al. developed a nanocapsule with an aqueous core that also could suspend in an aqueous vehicle [99]. A water-in-oil nanoemulsion was first prepared by adding an aqueous phase containing siRNA to an oil phase comprised of Miglyol and Span 80. Then, isobutylcyanoacrylate (IBCA) monomer was added to the nanoemulsion under mechanical stirring. When IBCA polymerized, it formed a shell structure surrounding the aqueous core containing entrapped siRNA. Later, the oil phase and surfactant were removed by ultracentrifugation. The resulting pellet was resuspended in water to produce a nanosuspension with a particle size of 350 ± 100 nm. In-vitro studies in NIH/3T3 cells stably transfected with human EWS-Fli1 gene showed that siRNA against EWS-Fli1 oncogene delivered in the nanocapsules inhibited the EWS-Fli1 mRNA level to 40%. When tested in-vivo in xenograft mice bearing EWS-Fli1-expressing tumors, the nanocapsules were found to inhibit 80% of the tumor growth after intratumoral injection when compared with the saline treated control mice. This is the first study reporting on the use of aqueous core nanocapsules for the delivery of siRNA with resulting efficacy in-vivo.

To facilitate endosomal escape and release siRNA to the cytosol where RNAi events take place, various endosomal escaping agents have been utilized such as

fusogenic lipids and peptides, polymers exerting proton-sponge effect etc. A novel endosomal breaking formulation called thermo-sensitive hydrogel nanocapsules were developed by Park et al. [100]. The thermo-sensitive Pluronic F-127/PEI 2K nanocapsules were synthesized by interfacial crosslinking reaction between pre-activated Pluronic F-127 and low Mw PEI 2K at the oil-in-water interface. The resulting Pluronic/PEI 2K nanocapsules had an interior structure filled with aqueous fluid surrounded by a crosslinked Pluronic/PEI 2K shell. Most pluronic copolymers have the critical micelle temperature (CMT) ranging from 25 to 40°C. Above the CMT, the pluronic co-polymers self-assemble to form a spherical micellar structure by dehydration of the poly-(propylene oxide) (PPO) moieties within the structure. The average particle size of Pluronic/PEI 2K nanocapsules was 118.9 ± 15.3 nm at 37 °C and 412.3 ± 83.2 at 15°C, respectively. According to the temperature-dependent property of pluronic, the collapse of the nanocapsules with increasing temperature is primarily caused by enhanced hydrophobic interactions between the PPO blocks in the Pluronic F-127 copolymers. PEG conjugated siRNA was anchored to the surface of Pluronic/PEI 2K nanocapsules through charge interaction. In in-vitro cell transfection experiments, 3 h after the cells treated with the nanoparticles at 37°C, 15 min of 15°C cold shock was given to the cells. The increased particle size under 15°C caused a 41.7-fold volume change which disrupts the endosomal membrane by physical strength. With cold shock treatment, the expression of GFP in HeLa cells and VEGF in PC-3 cells was reduced to 37.3% and 3.2%, respectively.

3.4. Dendrimers

Polycationic dendrimers such as poly-(amidoamine) (PAMAM) dendrimers have long been used to deliver DNA. Recent studies have shown that PAMAM may also serve as siRNA delivery carriers [101]. PAMAM dendrimers contain primary amine groups on the surface and tertiary amine groups in the internal architecture. The primary amines bind siRNA, while the tertiary amines act as a proton-sponge and facilitate the endosomal release of siRNA into the cytoplasm. The siRNA-PAMAM complexes are very stable which could only be dissociated under very strong ionic strength conditions. PAMAM dendrimers are termed as G_n with n denoting dendrimer generation number. As the generation number increases, the number of terminal amines increases. Thus, similar to DNA-PAMAM affinities, an increase in PAMAM generation leads to stronger interactions between the dendrimer and the siRNA. Zhou et al. showed that GL3Luc siRNA- G_7 complex reduced the expression of luciferase to 20% in A549Luc cells in-vitro [102]. To lower the cytotoxicity of G_7 PAMAM dendrimers while maintaining the siRNA binding affinity, surface PAMAM-NH₂ was acetylated with acetic anhydride, and internal PAMAM-OH was quaternized with methyl iodide [103]. Both modifications generate neutral outer surface with internal positive charges. It was found that the modifications did not interfere with the binding ability but significantly decrease the cytotoxicity of G_7 PAMAM dendrimers. An effort was also

made to further increase the cellular uptake of siRNA-PAMAM complex by conjugating the cell penetrating peptide, Tat; however, the conjugation of Tat did not improve the efficiency of the dendrimer [104].

The terminal groups of G₃ PAMAM dendrimer was partially conjugated with α -cyclodextrin (α -CDE) to deliver siRNA [105]. CDE, at high concentration, disturbs the cellular membrane components such as phospholipids and cholesterol, leading to increased membrane permeability. Moreover, the α -CDE has low cytotoxicity even at high charge ratio of α -CDE/nucleic acid. Thus, the G₃ PAMAM dendrimer/ α -CDE conjugate was developed to reduce the cytotoxicity and increase the delivery efficiency for nucleic acids. A pilot study showed that siRNA against pGL3 luciferase delivered by G₃ PAMAM dendrimer / α -CDE conjugate suppressed the luciferase gene expression level in-vitro by about 50% in NIH3T3-luc cells.

Dendritic poly(L-lysine) generation 6 (KG₆) was used to deliver several siRNAs by Okitsu et al. [106]. KG₆ was used in combination with the amphiphilic weak-base peptide Endo-Porter (EP), which is a commercially available cellular delivery reagent available from Gene-Tools. Neither KG₆ nor EP could efficiently deliver GAPDH siRNA when KG₆ or EP was used alone. However, when KG₆/EP was used together, GAPDH was efficiently knocked down at both protein levels and mRNA levels in H4IIEC3 cells.

3.5. Other novel carriers

In addition to the traditional siRNA delivery carriers discussed above, there are several highly innovative new strategies that are being developed and tested as potential delivery systems for siRNA.

Quantum dots (QD) are a nano-scaled semiconductor inorganic material that has provided greatly enhanced capabilities for medical imaging and diagnostics. Gao et al. developed a class of dual-functional nanoparticle for both siRNA delivery and imaging based on the use of QDs [107]. Highly luminescent QDs were first synthesized and encapsulated in the poly-(maleic anhydride-alt-1-tetradecene) bearing surface carboxylic acid groups. The carboxylic acid groups were then partially converted to tertiary amines. It was found that by balancing the ratio of the carboxylic acid and tertiary amine moieties, the proton-sponge effect could be precisely controlled. The resulting polymer coated QDs were suitable for siRNA binding, penetrating the cell, and for providing a mechanism for endosomal escape (Figure A.10). In comparison to cationic lipids and polymer-based siRNA delivery systems, the QD-based nanoparticles have much smaller size and more uniform size distribution. QDs with core size of 6 nm yielded polymer coated dots with sizes of 13 nm and 17 nm before and after siRNA binding, respectively. The QD nanoparticles efficiently delivered siRNA against cyclophilin B in a human breast cancer cell line and led to nearly complete suppression of cyclophilin B expression, which was superior to three most commonly used transfection reagents (LipofectamineTM, TransIT-TKOTM, and JetPEITM). Another

advantage of the QD-siRNA particles is that they provide simultaneous delivery of siRNA with imaging allowing for real-time tracking and intracellular localization of QDs during delivery.

Guo et al. have also engineered protein- and lipid-free multifunctional RNA nanoparticles to deliver siRNA and combine targeted therapy and imaging in a natural modality, pRNA (packing RNA), by utilizing RNA nanotechnology [108]. pRNA is a vital component of molecular motor which uses ATP as energy to package DNA into the procapsid during the replication of linear dsDNA viruses. The 117-nucleotide pRNA monomer contains two functional domains: the intermolecular-interacting domain and the double-stranded helical DNA packaging domain. The intermolecular-interacting domain contains left and right loops like two arms that interlock with other pRNA monomers via base-pairing to form dimer, trimer, or hexamers with size of 10-30 nm. Figure A.11 shows the structure of a pRNA trimer. According to their study, the replacement of pRNA helical region with siRNA, or connection of the RNA aptamer, or connection of other chemical components did not interfere with the folding and trimering of the pRNA as long as the two strands are paired, nor the function of siRNA and other connected moieties. Therefore, they tried to replace the helical region with small RNA fragments and connect RNA aptamer or other chemical components to this region to engineer a variety of chimeric pRNAs. The pRNA trimers with size of about 20 nm are extremely compact and versatile nanoparticles and of lots of advantages. For example, as shown in Figure A.11, a trimeric complex composed of pRNA/aptamer

(CD4), pRNA/siRNA (BIM), and pRNA/FITC could target CD4 positive cells and simultaneously deliver siRNA against proapoptosis factor BIM and imaging molecule FITC to these cells. In addition, more than one siRNA could be constructed to the pRNA nanoparticles to inhibit the expression of multiple oncogenes. RNA aptamers, comparing to antibodies and phage-displaying peptides, have very low immunogenicity. Furthermore, the size, shape, stoichiometry and the functions of the final product are highly controllable.

IV. Future Perspective

The promise of siRNA applications as a powerful therapeutic agent relies on a successful delivery vehicle. In part II, a series of criteria of an “ideal” nano-based siRNA delivery system were addressed and can be summarized as: efficient, specific and safe. From part III, it is obvious that a great deal of efforts has been devoted to pursuing the “ideal” nano-based systems for siRNA delivery and the field is developing rapidly. However, all current-reported formulations have recognizable gaps.

The delivery efficiency depends on many factors. First, the structures of carrier materials are critical. Currently, although there are some general rules to design and synthesize siRNA complexing agents (for example, the presence of positive charges), the investigation of structure-efficiency relationship is still under a trial-and-error mode. In the future, when large amount of compounds have been studied, database could be

built, and thus computer simulation and modeling would be performed to rationally design the delivery agent and to predict binding and assembly with siRNA.

Particle size is another factor controlling the in-vivo efficiency of siRNA nanoparticles. Nanoparticles with a broad range of particle size (from 20 nm up to about 800 nm) have been reported in the literature to deliver siRNA in-vitro. However, since most of the studies have stopped at in-vitro experiments, the in-vivo efficacy of the siRNA nanoparticles remains a question so that the optimal particle size that facilitates cellular uptake, tissue penetration and minimizes systemic clearance is not fully understood yet.

In addition to particle size and size distribution, other properties such as shape, mechanical properties, and surface texture and morphology are also important factors affecting siRNA delivery efficiency of nanoparticles both in-vitro and in-vivo. While chemical modifications of carrier materials are the major strategy to increase the efficiency of siRNA delivery nowadays, the influence of physical properties of the nano-formulation has been underestimated. Together with particle size, these physical properties and their influence on the nanoparticle behavior in circulation, tissue distribution, cell penetration, and cellular trafficking require more attention.

The specificity of siRNA delivery primarily depends on the selection of a target and ligand, both of which would benefit from progress and advances in other fields. The advances in molecular biology would help find more specifically expressed target such as receptors, integrins or enzymes in pathological tissues as well as more specific

and high affinity ligand via, for example, in-vivo phage display.

Years ago, the incorporation of PEG in various nano-formulations dramatically decreased their non-specific RES clearance and increased their circulation half-life. As the non-specific RES clearance decreases, the accumulation of nanoparticles in target organ or tissue increases. Hence, to increase the delivery specificity, active targeting using a targeting ligand is preferred; however, improved delivery by passive targeting may also have therapeutic potential and utility.

In terms of the safety of nano-based siRNA delivery system, on one hand, efforts need to be given to further decrease the cytotoxicity of carrier materials and to look for less immunogenic targeting ligands. On the other hand, the toxicity of different formulations is mostly identified and/or estimated by in-vitro experiments. However, cytotoxicity is often cell-type dependent. Thus, the field also is in need of improved, predictive, in-vitro models to more accurately reflect the in-vivo environment.

There is no doubt that delivering siRNA safely and efficiently is a challenging task. The field is in need of a breakthrough.

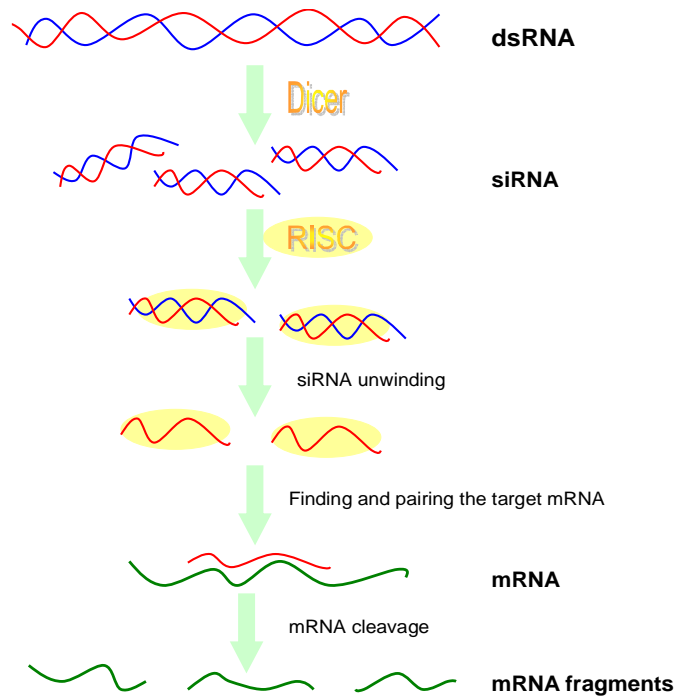


Figure A.1. Mechanism of RNA interference

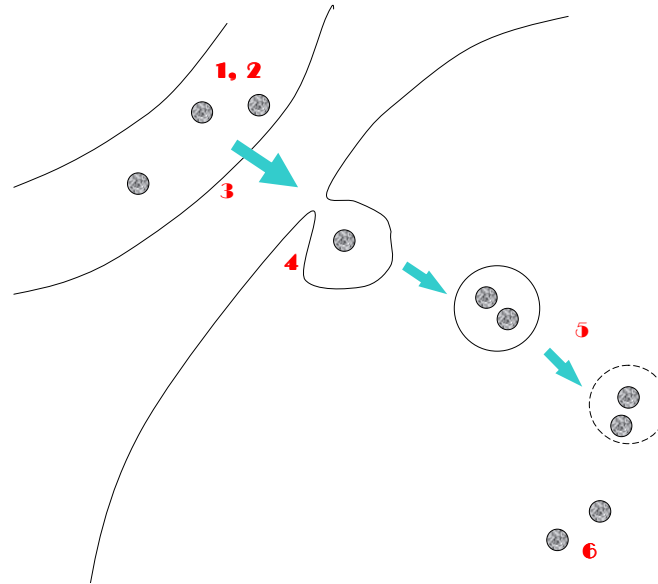


Figure A.2. Challenges for siRNA delivery. The barriers include (1) susceptibility in the blood circulation and tissues after injection, (2) rapid clearance by renal excretion and RES uptake, (3) extravasation across the endothelium and to the target tissue (4) penetration through the cell membrane, (5) endosomal escape, and (6) transient persistence in cells

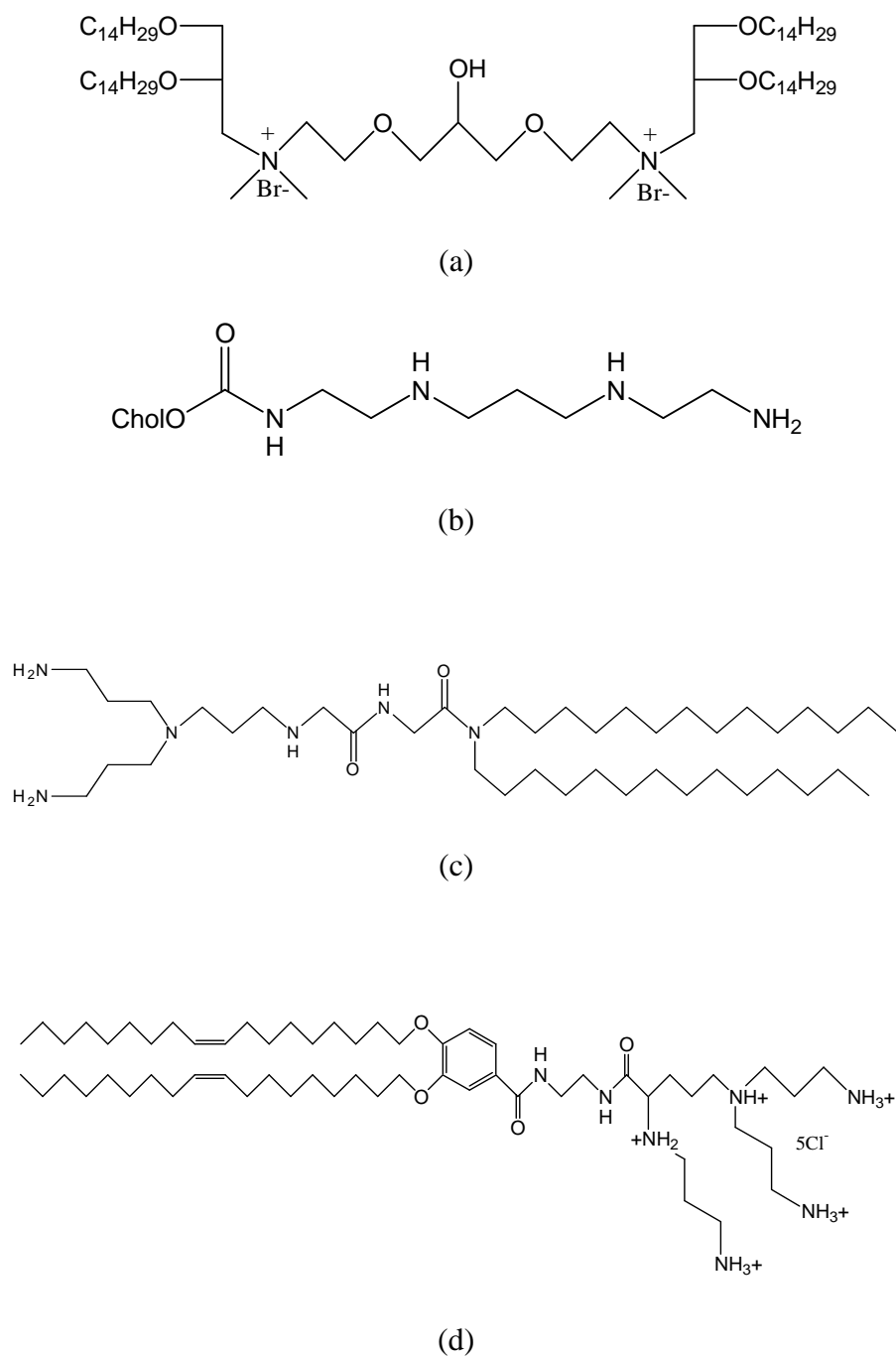


Figure A.3. Structures of (a) CCLA, (b) CDAN, (c) RPR209120, and (d) MVL5

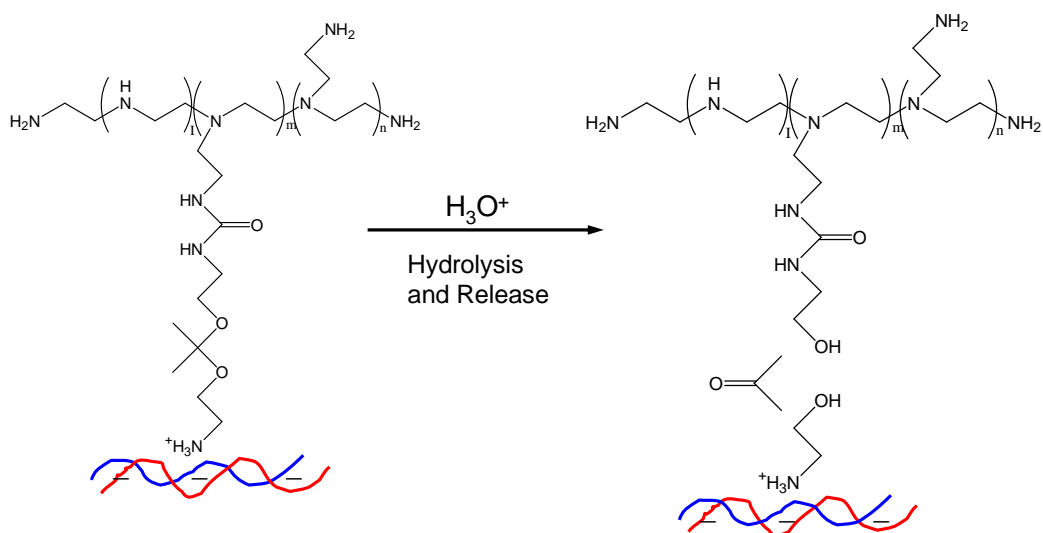


Figure A.4. Dissociation of nucleic acids from ketalized PEI upon hydrolysis.
Figure adapted from Shim et al. (2008)

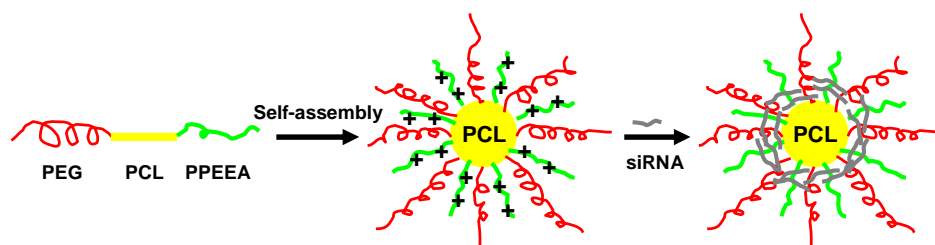


Figure A.5. Self-assembling of cationic micellar nanoparticles and loading of siRNA. Figure adapted from Sun et al. (2008)

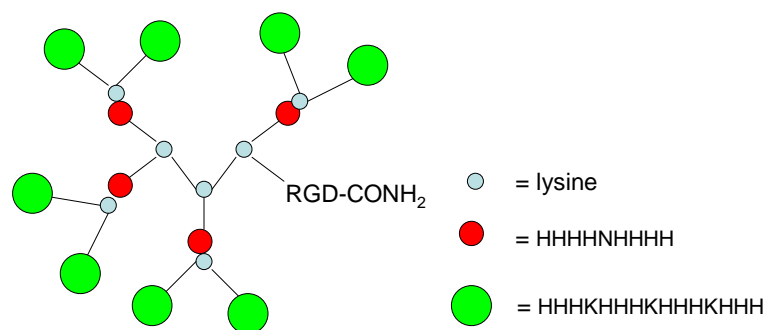


Figure A.6. Schematic structure of H3K8b polymer.

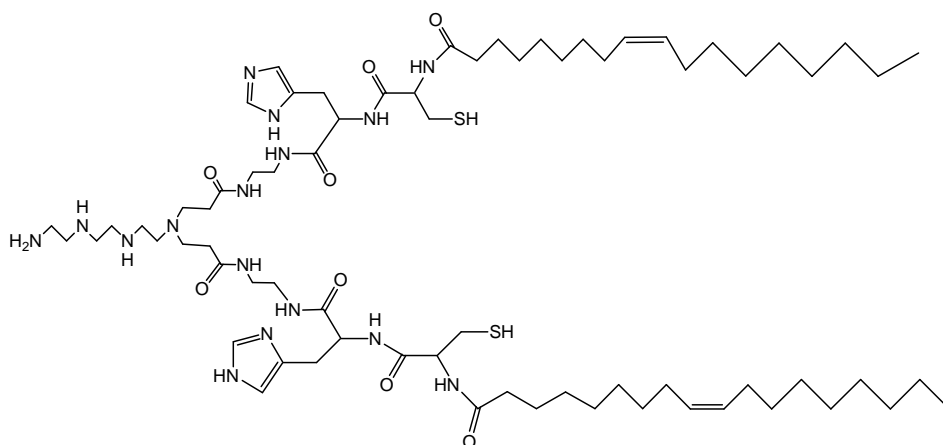


Figure A.7. Structure of THCO

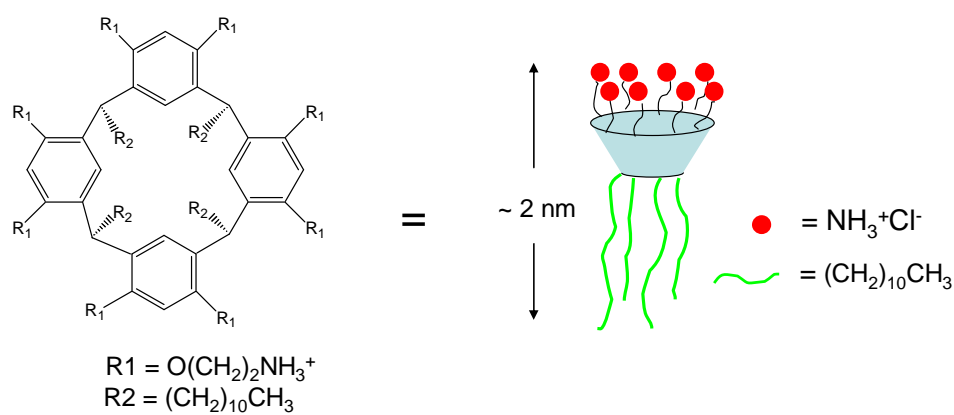


Figure A.8. Cone-shaped structure of macrocyclic octaamine. Figure adapted from Matsui et al. (2006)

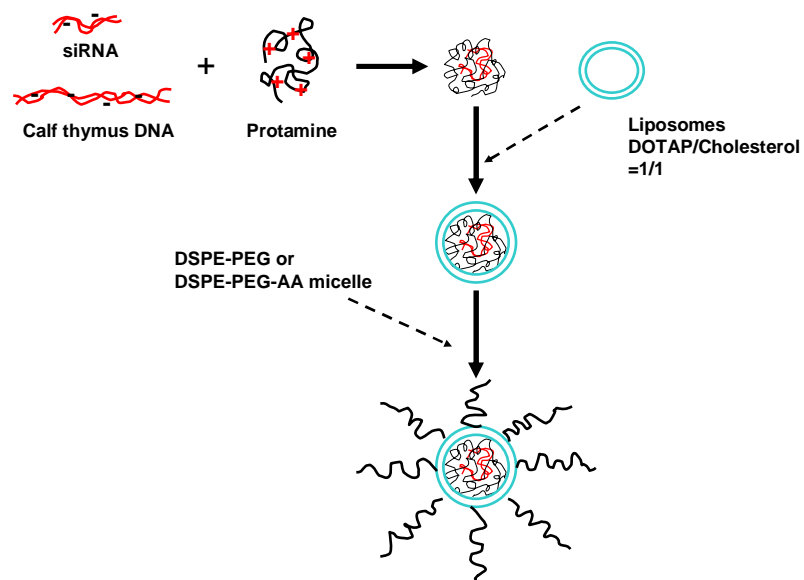


Figure A.9. Preparation of PEGylated LPD. Figure adapted from Li et al. (2006)

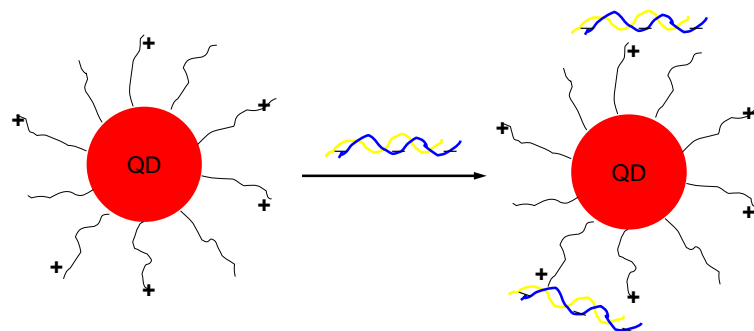


Figure A.10. Adsorption of siRNA onto surface-modified QDs.

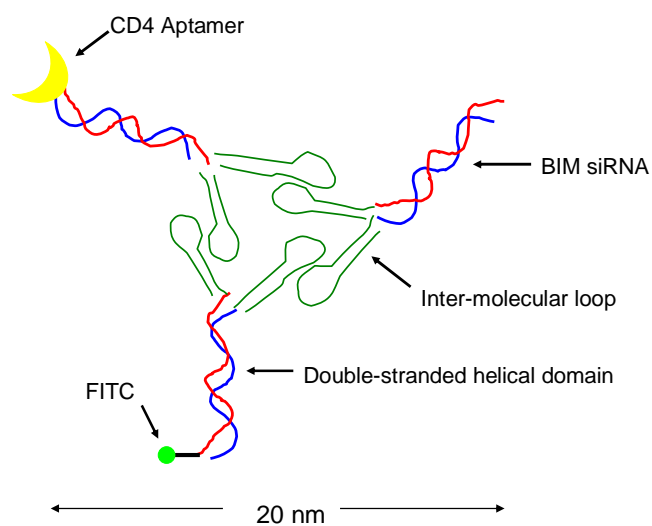


Figure A.11. Schematic structure of engineering pRNA nanoparticle containing siRNA, aptamer and fluorescent label.

References

1. Meister, G. and T. Tuschl, *Mechanisms of gene silencing by double-stranded RNA*. Nature, 2004. **431**(7006): p. 343-9.
2. Hannon, G.J., *RNA interference*. Nature, 2002. **418**(6894): p. 244-51.
3. Valencia-Sanchez, M.A., et al., *Control of translation and mRNA degradation by miRNAs and siRNAs*. Genes Dev, 2006. **20**(5): p. 515-24.
4. Ameres, S.L., J. Martinez, and R. Schroeder, *Molecular basis for target RNA recognition and cleavage by human RISC*. Cell, 2007. **130**(1): p. 101-12.
5. Reynolds, A., et al., *Induction of the interferon response by siRNA is cell type- and duplex length-dependent*. Rna, 2006. **12**(6): p. 988-93.
6. Elbashir, S.M., et al., *Duplexes of 21-nucleotide RNAs mediate RNA interference in cultured mammalian cells*. Nature, 2001. **411**(6836): p. 494-8.
7. Gurney, A.M. and E. Hunter, *The use of small interfering RNA to elucidate the activity and function of ion channel genes in an intact tissue*. J Pharmacol Toxicol Methods, 2005. **51**(3): p. 253-62.
8. Zaffaroni, N., M. Pennati, and M. Folini, *Validation of telomerase and survivin as anticancer therapeutic targets using ribozymes and small-interfering RNAs*. Methods Mol Biol, 2007. **361**: p. 239-63.
9. Morgan-Lappe, S.E., et al., *Identification of Ras-related nuclear protein, targeting protein for xenopus kinesin-like protein 2, and stearyl-CoA desaturase 1 as promising cancer targets from an RNAi-based screen*. Cancer Res, 2007. **67**(9): p. 4390-8.
10. Tyner, J.W., et al., *RNAi screening of the tyrosine kinome identifies therapeutic targets in acute myeloid leukemia*. Blood, 2008. **111**(4): p. 2238-45.
11. Gust, T.C., et al., *RNA interference-mediated gene silencing in murine T cells: in vitro and in vivo validation of proinflammatory target genes*. Cell Commun Signal, 2008. **6**: p. 3.
12. Vance, V. and H. Vaucheret, *RNA silencing in plants--defense and counterdefense*. Science, 2001. **292**(5525): p. 2277-80.
13. McCaffrey, A.P., et al., *Inhibition of hepatitis B virus in mice by RNA interference*. Nat Biotechnol, 2003. **21**(6): p. 639-44.
14. McCaffrey, A.P., et al., *RNA interference in adult mice*. Nature, 2002.

418(6893): p. 38-9.

15. Song, E., et al., *Antibody mediated in vivo delivery of small interfering RNAs via cell-surface receptors*. Nat Biotechnol, 2005. **23**(6): p. 709-17.
16. Park, W.S., et al., *Specific HIV-1 env gene silencing by small interfering RNAs in human peripheral blood mononuclear cells*. Gene Ther, 2003. **10**(24): p. 2046-50.
17. Novina, C.D., et al., *siRNA-directed inhibition of HIV-1 infection*. Nat Med, 2002. **8**(7): p. 681-6.
18. Palliser, D., et al., *An siRNA-based microbicide protects mice from lethal herpes simplex virus 2 infection*. Nature, 2006. **439**(7072): p. 89-94.
19. Bitko, V., et al., *Inhibition of respiratory viruses by nasally administered siRNA*. Nat Med, 2005. **11**(1): p. 50-5.
20. Zhang, W., et al., *Inhibition of respiratory syncytial virus infection with intranasal siRNA nanoparticles targeting the viral NS1 gene*. Nat Med, 2005. **11**(1): p. 56-62.
21. Jiang, M. and J. Milner, *Selective silencing of viral gene expression in HPV-positive human cervical carcinoma cells treated with siRNA, a primer of RNA interference*. Oncogene, 2002. **21**(39): p. 6041-8.
22. Yoshinouchi, M., et al., *In vitro and in vivo growth suppression of human papillomavirus 16-positive cervical cancer cells by E6 siRNA*. Mol Ther, 2003. **8**(5): p. 762-8.
23. Song, E., et al., *RNA interference targeting Fas protects mice from fulminant hepatitis*. Nat Med, 2003. **9**(3): p. 347-51.
24. Wang, J., et al., *Fas siRNA reduces apoptotic cell death of allogeneic-transplanted hepatocytes in mouse spleen*. Transplant Proc, 2003. **35**(4): p. 1594-5.
25. Perl, M., et al., *Silencing of Fas, but not caspase-8, in lung epithelial cells ameliorates pulmonary apoptosis, inflammation, and neutrophil influx after hemorrhagic shock and sepsis*. Am J Pathol, 2005. **167**(6): p. 1545-59.
26. Zender, L., et al., *Caspase 8 small interfering RNA prevents acute liver failure in mice*. Proc Natl Acad Sci U S A, 2003. **100**(13): p. 7797-802.
27. Wesche-Soldato, D.E., et al., *In vivo delivery of caspase-8 or Fas siRNA improves the survival of septic mice*. Blood, 2005. **106**(7): p. 2295-301.

28. Caplen, N.J., et al., *Rescue of polyglutamine-mediated cytotoxicity by double-stranded RNA-mediated RNA interference*. Hum Mol Genet, 2002. **11**(2): p. 175-84.
29. Miller, V.M., et al., *Allele-specific silencing of dominant disease genes*. Proc Natl Acad Sci U S A, 2003. **100**(12): p. 7195-200.
30. Schwarz, D.S., et al., *Designing siRNA that distinguish between genes that differ by a single nucleotide*. PLoS Genet, 2006. **2**(9): p. e140.
31. Brummelkamp, T.R., R. Bernards, and R. Agami, *A system for stable expression of short interfering RNAs in mammalian cells*. Science, 2002. **296**(5567): p. 550-3.
32. Brummelkamp, T.R., R. Bernards, and R. Agami, *Stable suppression of tumorigenicity by virus-mediated RNA interference*. Cancer Cell, 2002. **2**(3): p. 243-7.
33. Wohlbold, L., et al., *All common p210 and p190 Bcr-abl variants can be targeted by RNA interference*. Leukemia, 2005. **19**(2): p. 290-2.
34. Manka, D., Z. Spicer, and D.E. Millhorn, *Bcl-2/adenovirus E1B 19 kDa interacting protein-3 knockdown enables growth of breast cancer metastases in the lung, liver, and bone*. Cancer Res, 2005. **65**(24): p. 11689-93.
35. Kami, K., et al., *Downregulation of survivin by siRNA diminishes radioresistance of pancreatic cancer cells*. Surgery, 2005. **138**(2): p. 299-305.
36. Zhang, M., et al., *Silencing the epidermal growth factor receptor gene with RNAi may be developed as a potential therapy for non small cell lung cancer*. Genet Vaccines Ther, 2005. **3**: p. 5.
37. Takei, Y., et al., *A small interfering RNA targeting vascular endothelial growth factor as cancer therapeutics*. Cancer Res, 2004. **64**(10): p. 3365-70.
38. Wu, H., W.N. Hait, and J.M. Yang, *Small interfering RNA-induced suppression of MDR1 (P-glycoprotein) restores sensitivity to multidrug-resistant cancer cells*. Cancer Res, 2003. **63**(7): p. 1515-9.
39. Stierle, V., A. Laigle, and B. Jolles, *Modulation of MDR1 gene expression in multidrug resistant MCF7 cells by low concentrations of small interfering RNAs*. Biochem Pharmacol, 2005. **70**(10): p. 1424-30.
40. Manoharan, M., *RNA interference and chemically modified small interfering RNAs*. Curr Opin Chem Biol, 2004. **8**(6): p. 570-9.
41. Wolfrum, C., et al., *Mechanisms and optimization of in vivo delivery of*

- lipophilic siRNAs*. Nat Biotechnol, 2007. **25**(10): p. 1149-57.
42. Lewis, D.L. and J.A. Wolff, *Systemic siRNA delivery via hydrodynamic intravascular injection*. Adv Drug Deliv Rev, 2007. **59**(2-3): p. 115-23.
 43. Maruyama, T., et al., *Inhibitory effects of gold(III) ions on ribonuclease and deoxyribonuclease*. J Inorg Biochem, 2007. **101**(1): p. 180-6.
 44. Bartlett, D.W. and M.E. Davis, *Insights into the kinetics of siRNA-mediated gene silencing from live-cell and live-animal bioluminescent imaging*. Nucleic Acids Res, 2006. **34**(1): p. 322-33.
 45. Kebbekus, P., D.E. Draper, and P. Hagerman, *Persistence length of RNA*. Biochemistry, 1995. **34**(13): p. 4354-7.
 46. Spagnou, S., A.D. Miller, and M. Keller, *Lipidic carriers of siRNA: differences in the formulation, cellular uptake, and delivery with plasmid DNA*. Biochemistry, 2004. **43**(42): p. 13348-56.
 47. Kornek, M., et al., *1,2-dioleoyl-3-trimethylammonium-propane (DOTAP)-formulated, immune-stimulatory vascular endothelial growth factor a small interfering RNA (siRNA) increases antitumoral efficacy in murine orthotopic hepatocellular carcinoma with liver fibrosis*. Mol Med, 2008. **14**(7-8): p. 365-73.
 48. Cardoso, A.L., et al., *Tf-lipoplexes for neuronal siRNA delivery: A promising system to mediate gene silencing in the CNS*. J Control Release, 2008.
 49. Sioud, M. and D.R. Sorensen, *Cationic liposome-mediated delivery of siRNAs in adult mice*. Biochem Biophys Res Commun, 2003. **312**(4): p. 1220-5.
 50. Sorensen, D.R., M. Leirdal, and M. Sioud, *Gene silencing by systemic delivery of synthetic siRNAs in adult mice*. J Mol Biol, 2003. **327**(4): p. 761-6.
 51. Zhang, Y., *Cationic Liposome-Mediated Gene Delivery*. Cambridge Healthtech Institute's 4th Annual Meeting, 1997(1997. Oct 12-14).
 52. Xu, L., et al., *Systemic p53 gene therapy of cancer with immunolipoplexes targeted by anti-transferrin receptor scFv*. Mol Med, 2001. **7**(10): p. 723-34.
 53. Xu, L., et al., *Systemic tumor-targeted gene delivery by anti-transferrin receptor scFv-immunoliposomes*. Mol Cancer Ther, 2002. **1**(5): p. 337-46.
 54. Pirollo, K.F., et al., *A tumor-targeted nanodelivery system to improve early MRI detection of cancer*. Mol Imaging, 2006. **5**(1): p. 41-52.
 55. Pirollo, K.F., et al., *Materializing the potential of small interfering RNA via a*

- tumor-targeting nanodelivery system*. Cancer Res, 2007. **67**(7): p. 2938-43.
56. Cardoso, A.L., et al., *siRNA delivery by a transferrin-associated lipid-based vector: a non-viral strategy to mediate gene silencing*. J Gene Med, 2007. **9**(3): p. 170-83.
 57. Kim, S.I., et al., *Systemic and specific delivery of small interfering RNAs to the liver mediated by apolipoprotein A-I*. Mol Ther, 2007. **15**(6): p. 1145-52.
 58. Song, Y.K., et al., *Characterization of cationic liposome-mediated gene transfer in vivo by intravenous administration*. Hum Gene Ther, 1997. **8**(13): p. 1585-94.
 59. Chien, P.Y., et al., *Novel cationic cardiolipin analogue-based liposome for efficient DNA and small interfering RNA delivery in vitro and in vivo*. Cancer Gene Ther, 2005. **12**(3): p. 321-8.
 60. Khoury, M., et al., *Efficient new cationic liposome formulation for systemic delivery of small interfering RNA silencing tumor necrosis factor alpha in experimental arthritis*. Arthritis Rheum, 2006. **54**(6): p. 1867-77.
 61. Bouxsein, N.F., et al., *Structure and gene silencing activities of monovalent and pentavalent cationic lipid vectors complexed with siRNA*. Biochemistry, 2007. **46**(16): p. 4785-92.
 62. Desigaux, L., et al., *Self-assembled lamellar complexes of siRNA with lipidic aminoglycoside derivatives promote efficient siRNA delivery and interference*. Proc Natl Acad Sci U S A, 2007. **104**(42): p. 16534-9.
 63. Mudhakhir, D., et al., *A novel IRQ ligand-modified nano-carrier targeted to a unique pathway of caveolar endocytic pathway*. J Control Release, 2008. **125**(2): p. 164-73.
 64. Foged, C., H.M. Nielsen, and S. Frokjaer, *Liposomes for phospholipase A2 triggered siRNA release: preparation and in vitro test*. Int J Pharm, 2007. **331**(2): p. 160-6.
 65. Dong, W., et al., *Cross-linked polyethylenimine as potential DNA vector for gene delivery with high efficiency and low cytotoxicity*. Acta Biochim Biophys Sin (Shanghai), 2006. **38**(11): p. 780-7.
 66. Li, S., et al., *Polyethylenimine-complexed plasmid particles targeting focal adhesion kinase function as melanoma tumor therapeutics*. Mol Ther, 2007. **15**(3): p. 515-23.
 67. Swami, A., et al., *A unique and highly efficient non-viral DNA/siRNA delivery system based on PEI-bisepoxide nanoparticles*. Biochem Biophys Res

Commun, 2007. **362**(4): p. 835-41.

68. Jere, D., et al., *Poly(beta-amino ester) as a carrier for si/shRNA delivery in lung cancer cells*. Biomaterials, 2008. **29**(16): p. 2535-47.
69. Zintchenko, A., et al., *Simple modifications of branched PEI lead to highly efficient siRNA carriers with low toxicity*. Bioconjug Chem, 2008. **19**(7): p. 1448-55.
70. Shim, M.S. and Y.J. Kwon, *Controlled delivery of plasmid DNA and siRNA to intracellular targets using ketalized polyethylenimine*. Biomacromolecules, 2008. **9**(2): p. 444-55.
71. Kim, S.H., et al., *Local and systemic delivery of VEGF siRNA using polyelectrolyte complex micelles for effective treatment of cancer*. J Control Release, 2008. **129**(2): p. 107-16.
72. Oishi, M., et al., *Lactosylated poly(ethylene glycol)-siRNA conjugate through acid-labile beta-thiopropionate linkage to construct pH-sensitive polyion complex micelles achieving enhanced gene silencing in hepatoma cells*. J Am Chem Soc, 2005. **127**(6): p. 1624-5.
73. Sun, T.M., et al., *Self-assembled biodegradable micellar nanoparticles of amphiphilic and cationic block copolymer for siRNA delivery*. Biomaterials, 2008. **29**(32): p. 4348-55.
74. Sato, A., et al., *Polymer brush-stabilized polyplex for a siRNA carrier with long circulatory half-life*. J Control Release, 2007. **122**(3): p. 209-16.
75. Kim, W.J., et al., *Efficient siRNA delivery using water soluble lipopolymer for anti-angiogenic gene therapy*. J Control Release, 2007. **118**(3): p. 357-63.
76. Meyer, M., et al., *Breathing life into polycations: functionalization with pH-responsive endosomolytic peptides and polyethylene glycol enables siRNA delivery*. J Am Chem Soc, 2008. **130**(11): p. 3272-3.
77. Schiffelers, R.M., et al., *Cancer siRNA therapy by tumor selective delivery with ligand-targeted sterically stabilized nanoparticle*. Nucleic Acids Res, 2004. **32**(19): p. e149.
78. Hwa Kim, S., et al., *Target-specific gene silencing by siRNA plasmid DNA complexed with folate-modified poly(ethylenimine)*. J Control Release, 2005. **104**(1): p. 223-32.
79. Jiang, G., et al., *Hyaluronic acid-polyethyleneimine conjugate for target specific intracellular delivery of siRNA*. Biopolymers, 2008. **89**(7): p. 635-42.

80. Howard, K.A., et al., *RNA interference in vitro and in vivo using a novel chitosan/siRNA nanoparticle system*. Mol Ther, 2006. **14**(4): p. 476-84.
81. Liu, X., et al., *The influence of polymeric properties on chitosan/siRNA nanoparticle formulation and gene silencing*. Biomaterials, 2007. **28**(6): p. 1280-8.
82. Katas, H. and H.O. Alpar, *Development and characterisation of chitosan nanoparticles for siRNA delivery*. J Control Release, 2006. **115**(2): p. 216-25.
83. Rojanarata, T., et al., *Chitosan-thiamine pyrophosphate as a novel carrier for siRNA delivery*. Pharm Res, 2008. **25**(12): p. 2807-14.
84. Leng, Q., et al., *Highly branched HK peptides are effective carriers of siRNA*. J Gene Med, 2005. **7**(7): p. 977-86.
85. Minakuchi, Y., et al., *Atelocollagen-mediated synthetic small interfering RNA delivery for effective gene silencing in vitro and in vivo*. Nucleic Acids Res, 2004. **32**(13): p. e109.
86. Wang, X.L., et al., *A multifunctional and reversibly polymerizable carrier for efficient siRNA delivery*. Biomaterials, 2008. **29**(1): p. 15-22.
87. Wang, X.L., et al., *Novel polymerizable surfactants with pH-sensitive amphiphilicity and cell membrane disruption for efficient siRNA delivery*. Bioconjug Chem, 2007. **18**(6): p. 2169-77.
88. Matsui, K., et al., *RNAi silencing of exogenous and endogenous reporter genes using a macrocyclic octamine as a "compact" siRNA carrier. Studies on the nonsilenced residual activity*. Bioconjug Chem, 2006. **17**(1): p. 132-8.
89. Mok, H. and T.G. Park, *Self-crosslinked and reducible fusogenic peptides for intracellular delivery of siRNA*. Biopolymers, 2008. **89**(10): p. 881-8.
90. Li, S.D. and L. Huang, *Surface-modified LPD nanoparticles for tumor targeting*. Ann N Y Acad Sci, 2006. **1082**: p. 1-8.
91. Li, S.D. and L. Huang, *Targeted delivery of antisense oligodeoxynucleotide and small interference RNA into lung cancer cells*. Mol Pharm, 2006. **3**(5): p. 579-88.
92. Chono, S., et al., *An efficient and low immunostimulatory nanoparticle formulation for systemic siRNA delivery to the tumor*. J Control Release, 2008. **131**(1): p. 64-9.
93. Peer, D., et al., *Systemic leukocyte-directed siRNA delivery revealing cyclin D1 as an anti-inflammatory target*. Science, 2008. **319**(5863): p. 627-30.

94. Kakizawa, Y., et al., *Organic-inorganic hybrid-nanocarrier of siRNA constructing through the self-assembly of calcium phosphate and PEG-based block animer*. J Control Release, 2006. **111**(3): p. 368-70.
95. Kakizawa, Y., S. Furukawa, and K. Kataoka, *Block copolymer-coated calcium phosphate nanoparticles sensing intracellular environment for oligodeoxynucleotide and siRNA delivery*. J Control Release, 2004. **97**(2): p. 345-56.
96. Bartlett, D.W. and M.E. Davis, *Physicochemical and biological characterization of targeted, nucleic acid-containing nanoparticles*. Bioconjug Chem, 2007. **18**(2): p. 456-68.
97. Kim, H.R., et al., *Cationic solid lipid nanoparticles reconstituted from low density lipoprotein components for delivery of siRNA*. Mol Pharm, 2008. **5**(4): p. 622-31.
98. Pille, J.Y., et al., *Intravenous delivery of anti-RhoA small interfering RNA loaded in nanoparticles of chitosan in mice: safety and efficacy in xenografted aggressive breast cancer*. Hum Gene Ther, 2006. **17**(10): p. 1019-26.
99. Toub, N., et al., *Efficacy of siRNA nanocapsules targeted against the EWS-Flt1 oncogene in Ewing sarcoma*. Pharm Res, 2006. **23**(5): p. 892-900.
100. Lee, S.H., et al., *Thermally sensitive cationic polymer nanocapsules for specific cytosolic delivery and efficient gene silencing of siRNA: swelling induced physical disruption of endosome by cold shock*. J Control Release, 2008. **125**(1): p. 25-32.
101. Shen, X.C., et al., *Importance of size-to-charge ratio in construction of stable and uniform nanoscale RNA/dendrimer complexes*. Org Biomol Chem, 2007. **5**(22): p. 3674-81.
102. Zhou, J., et al., *PAMAM dendrimers for efficient siRNA delivery and potent gene silencing*. Chem Commun (Camb), 2006(22): p. 2362-4.
103. Patil, M.L., et al., *Surface-modified and internally cationic polyamidoamine dendrimers for efficient siRNA delivery*. Bioconjug Chem, 2008. **19**(7): p. 1396-403.
104. Kang, H., et al., *Tat-conjugated PAMAM dendrimers as delivery agents for antisense and siRNA oligonucleotides*. Pharm Res, 2005. **22**(12): p. 2099-106.
105. Tsutsumi, T., et al., *Evaluation of polyamidoamine dendrimer/alpha-cyclodextrin conjugate (generation 3, G3) as a novel carrier for small interfering RNA (siRNA)*. J Control Release, 2007. **119**(3): p. 349-59.

106. Inoue, Y., et al., *Efficient delivery of siRNA using dendritic poly(L-lysine) for loss-of-function analysis*. J Control Release, 2008. **126**(1): p. 59-66.
107. Yezhelyev, M.V., et al., *Proton-sponge coated quantum dots for siRNA delivery and intracellular imaging*. J Am Chem Soc, 2008. **130**(28): p. 9006-12.
108. Khaled, A., et al., *Controllable self-assembly of nanoparticles for specific delivery of multiple therapeutic molecules to cancer cells using RNA nanotechnology*. Nano Lett, 2005. **5**(9): p. 1797-808.